

Synthetic biology meets liposome-based drug delivery

Soler Canton, Alicia

DOI

[10.4233/uuid:b46cc724-c6cf-4282-b3ba-3817e8bebf87](https://doi.org/10.4233/uuid:b46cc724-c6cf-4282-b3ba-3817e8bebf87)

Publication date

2019

Document Version

Final published version

Citation (APA)

Soler Canton, A. (2019). *Synthetic biology meets liposome-based drug delivery*. [Dissertation (TU Delft), Delft University of Technology]. <https://doi.org/10.4233/uuid:b46cc724-c6cf-4282-b3ba-3817e8bebf87>

Important note

To cite this publication, please use the final published version (if applicable).
Please check the document version above.

Copyright

Other than for strictly personal use, it is not permitted to download, forward or distribute the text or part of it, without the consent of the author(s) and/or copyright holder(s), unless the work is under an open content license such as Creative Commons.

Takedown policy

Please contact us and provide details if you believe this document breaches copyrights.
We will remove access to the work immediately and investigate your claim.

SYNTHETIC BIOLOGY MEETS LIPOSOME-BASED DRUG DELIVERY

SYNTHETIC BIOLOGY MEETS LIPOSOME-BASED DRUG DELIVERY

Dissertation

for the purpose of obtaining the degree of doctor
at Delft University of Technology
by the authority of the Rector Magnificus prof.dr.ir. T.H.J.J. van der Hagen
chair of the Board for Doctorates
to be defended publicly
on Monday 7th October 2019 at 12:30

by

Alicia SOLER CANTÓN

Master of Science in Molecular Biotechnology,
Wageningen University, The Netherlands
born in Xátiva, Spain.

This dissertation has been approved by the promotors.

Composition of the doctoral committee:

Rector Magnificus,	chairperson
Dr. C.J.A. Danelon	Delft University of Technology, promotor
Prof. dr. M. Dogterom	Delft University of Technology, promotor

Independent members:

Prof. dr. Ir. Pascale Daran-Lapujade	Delft University of Technology
Dr. S. Bonnet	Leiden University
Dr. H. Hulleman	VU University Medical Center
Prof. dr. E. Mastrobattista	Utrecht University
Prof. dr. ir. S. Tans	Delft University of Technology, reserve member



Keywords: synthetic biology, liposomes, gene therapy, RNA, therapeutic nanofactories, light activation, single vesicle analysis

Printed by: Ridderprint

Cover by: Roland Punt & Alicia Soler Cantón

Copyright © 2019 A. Soler Cantón

Casimir PhD series, Delft-Leiden 2019-35

ISBN 978-90-8593-418-9

An electronic copy of this dissertation is available at

<http://repository.tudelft.nl/>

To four extraordinary human beings:

Luisi, Yayi, Lolo & María

CONTENTS

1. Introduction	1
1.1 In vivo synthetic biology.....	1
1.2 Vesicle bioreactors for the production of genetically-encoded therapeutic drugs.....	2
1.3 Liposomes as drug delivery devices.....	2
1.4 Liposomal RNA-based gene therapy.....	6
1.5 The importance of single-vesicle characterization for the development of precise drug-delivery systems	9
1.6 The importance of precise drug biodistribution	9
1.7 Thesis outline	11
1.8 References.....	12
2. Exploring the therapeutic potential of RNA-producing fed-vesicle bioreactors.....	15
2.1 Introduction	16
2.1.1 Vesicle bioreactors for the production of genetically-encoded therapeutic drugs	16
2.1.2 Envisioning a novel fed-vesicle bioreactor for the production and delivery of therapeutic RNA	17
2.1.3 Liposome immobilization as a platform for high-throughput RNA-loaded single-vesicle characterization.....	18
2.1.4 Spinach RNA aptamer as a reporter of transcription	19
2.2 Materials and Methods	21
2.2.1 Preparation of a Spinach-encoding DNA template	21
2.2.2 Kinetic measurement of the T7-Spinach(221) DNA transcription in bulk.....	22
2.2.3 Preparation of lipid-coated beads.....	22
2.2.4 Spinach transcription inside α -hemolysin fed-vesicle bioreactors	22
2.2.5 Preparation of Spinach-containing liposomes through in-vesicle transcription.....	23
2.2.6 Preparation of Spinach RNA pre-loaded liposomes.....	23
2.2.7 Liposome sample preparation for background correction	24
2.2.8 Fluorescence microscopy imaging of liposomes	24
2.2.9 Analysis of Spinach content in α -hemolysin fed-vesicle reactors	25
2.2.10 Image processing for improved analysis of Spinach content in liposomes	25
2.3 Results	25
2.3.1 A low fraction of SUVs is expected to be transcriptionally active	25
2.3.2 All RNA pre-loaded liposomes are expected to encapsulate Spinach RNA molecules.....	27
2.3.3. Spinach RNA is successfully produced with a T7 in vitro transcription system in both commercial and homemade buffers.....	28
2.3.4. α -Hemolysin does not enhance in-vesicle Spinach transcription.....	29

2.3.5 In-vesicle transcription does not lead to liposomes with higher RNA content in comparison with RNA pre-loaded liposomes.....	30
2.4 Discussion.....	34
2.5 Conclusions.....	36
2.6 Supplementary information.....	37
2.7 Acknowledgements.....	37
2.8 References.....	38
3. Developing an optogenetic switch for the spatiotemporal control of therapeutic RNA production in small vesicles.....	43
3.1 Introduction.....	44
3.1.1 Light-activated production of gene-encoded therapeutic molecules in liposomes.....	44
3.1.2 In-situ drug synthesis in nanocarriers nourished by their surrounding environment.....	46
3.1.3. Adapting the T7 LA-DNA technology for triggered in-situ production of therapeutic siRNA in liposomes.....	47
3.2 Material and methods.....	48
3.2.1 Amino T7 oligo conjugation to PC biotin.....	48
3.2.2 HPLC examination of the amino T7-PC biotin oligo.....	48
3.2.3 HPLC purification of the amino T7-PC biotin oligo.....	49
3.2.3 Preparation of a Spinach-encoding DNA template.....	49
3.2.4 PCR of Spinach-encoding DNA with the amino T7-PC biotin oligo.....	49
3.2.5 LA-Spinach DNA formation through binding of tetravalent NeutrAvidin.....	50
3.2.6 UV photocleavage of LA-Spinach DNA in bulk solution.....	50
3.2.7 Transcription of the LA-Spinach DNA.....	50
3.2.8 Bulk transcription measurements by spectrofluorometry.....	50
3.2.9 Light-triggered transcription inside liposomes.....	51
3.3 Results.....	53
3.3.1 An LA-Spinach DNA can be successfully assembled.....	53
3.3.2 Photocleavage of LA-Spinach DNA leads to a four-fold increase on Spinach RNA production.....	55
3.3.3 Triggered in-vesicle transcription from the LA-Spinach DNA shows no advantage over unirradiated liposomes.....	57
3.3.4 HPLC purification of the LA-Spinach DNA.....	58
3.3.5 Characterization of the transcription ability of the HPLC-purified LA-Spinach DNA....	59
3.4 Discussion.....	62
3.5 Conclusions.....	66
3.6 Acknowledgements.....	66
3.7 References.....	67

4. A platform for the production of therapeutic SHRNA inside cell-targeting vesicles	71
4.1 Introduction	72
4.1.1 RNA interference (RNAi).....	72
4.1.2 RNAi mechanisms.....	72
4.1.3 Harnessing the RNAi natural process for therapy	73
4.1.4 Folate as a ligand for liposomal targeted delivery	75
4.1.5 The logistics of the endosomal system and the endosomal escape problem	76
4.1.6 Cell penetrating peptides (CPPs) to trigger endosomal escape.....	78
4.1.7 Vesicle bioreactors for the exonuclease production of therapeutic SHRNA inside mammalian cells	79
4.2 Materials and Methods	80
4.2.1 Materials	80
4.2.2 SHRNA sequence design	80
4.2.3 ssDNA oligos hybridization to form linear dsDNA templates for SHRNA production...	81
4.2.4 Bulk SHRNA production.....	82
4.2.5 Denaturing Urea Polyacrylamide Gel Electrophoresis (Urea PAGE).....	82
4.2.6 Cell culture	82
4.2.7 Calcium phosphate transfection.....	82
4.2.8 Lipofectamine transfection.....	83
4.2.9 Electroporation transfection	83
4.2.10 Dual luciferase assay.....	83
4.2.11 RNA isolation from cells and relative quantification by RT-qPCR.....	83
4.2.12 Preparation of lipid-coated beads	84
4.2.13 Extrusion.....	84
4.2.14 Production of liposomes.....	84
4.2.15 Association of liposomes with cells.....	85
4.2.16 Colocalization of liposomes with lysosomes.....	85
4.2.17 SHRNA release assay with azido acid melittin (A-A melittin).....	85
4.2.18 SHRNA transcription in fed-vesicle bioreactors.....	86
4.2.19 Confocal microscopy and image analysis.....	86
4.3 Results	87
4.3.1 Design and synthesis of SHRNA from a linear DNA template using T7 RNA polymerase	87
4.3.2 In vitro study of SHRNA cleavage with purified human Dicer enzyme	89
4.3.3 SHRNA transcribed in vitro suppress gene expression in mammalian cells.....	90
4.3.4 Folate-targeted liposomes are selectively uptaken by KB cells	90
4.3.5. In vitro transcribed SHRNA can silence luciferase in lipofectamine transfected HeLa cells, but not in KB cells	93
4.3.6 Poor MEN1 mRNA expression limits its use as readout of gene silencing.....	95

4.3.7 Folate-targeted liposomes follow the endo-lysosomal pathway and conclude trapped in lysosomes	96
4.3.8 Folate-labelled SUVs are not sensitive to azido-acid melittin (A-A melittin).....	99
4.3.9 SHRNA production in folate-labelled fed-liposomes.....	101
4.4 Discussion.....	103
4.4.1 Possible improvements on SHRNA design.....	103
4.4.2 Possible improvements on the characterization of folate-targeted delivery.....	104
4.4.3 Alternatives for improved DNA transfection of KB cells.....	105
4.4.4 Endogenous targets high higher mRNA expression than MEN1 should be used as model to report silencing via RT-qPCR.....	107
4.4.5 Membrane conjugation of pH-responsive CPPs will be key for successful endosomal escape.....	107
4.4.6 Non-fed vesicle bioreactors as more promising systems for in situ RNA production....	108
4.5 Conclusions	109
4.6 Supplementary information	110
4.7 Acknowledgements	111
4.8 References.....	112
5. Development and single-particle characterization of a liposomal delivery system for the chemotherapeutic compound SN-38	121
5.1 introduction	122
5.2 material and methods.....	124
5.2.1 Materials	124
5.2.2 Formation of SN-38-containing lipid films	124
5.2.3 Formation of folate-containing lipid films.....	125
5.2.4 Liposomal SN-38 production.....	125
5.2.5 Preparation of folate-labeled liposomes	125
5.2.6 Dynamic light scattering.....	125
5.2.7 Size exclusion chromatography	126
5.2.8 Fluorescence spectroscopy	126
5.2.9 Preparation of chambered coverslips.....	126
5.2.10 Fluorescence confocal microscopy.....	127
5.2.11 High performance liquid chromatography.....	127
5.2.12 pH dependence assays.....	127
5.2.13 Release experiments	128
5.2.14 Liposome-mediated stability assays	128
5.2.15 Complexation of SN-38 with SBE- β -CD.....	129
5.2.16 Quantitation of SN-38	129
5.2.17 Preparation of SN-38-SBE- β -CD-lipid nanoparticles	130

5.2.18 Cell culture	130
5.2.19 Fluorescence imaging of KB cells	130
5.2.20 Cell viability assay.....	130
5.3 results	131
5.3.1 Liposome production by swelling of SN-38-loaded lipid films supported on glass beads.....	131
5.3.2 SN-38 is rapidly released from folate-HSCP liposomes	132
5.3.3 Complexation of SN-38 with SBE- β -CD increases the drug solubility	135
5.3.4 Entrapment of SN-38-SBE- β -CD complexes into liposomes leads to the formation of stable SN-38-SBE- β -CD-lipid nanoparticles.....	136
5.3.5 SN-38-SBE- β -CD-lipid nanoparticles can interact with cancer cells	138
5.4 discussion.....	140
5.5 conclusions	143
5.6 Supplementary information	144
5.7 Acknowledgements	147
5.8 references	148
Summary.....	152
Samenvatting.....	155
Aknowledgements.....	159
Curriculum vitae	163
List of publications.....	165

1.

INTRODUCTION

Synthetic biology is an emerging and rapidly expanding field of research focused on the assembly of novel biological systems with novel functionalities for different applications. These systems are frequently genetic circuits constructed with elements from different organisms, capable of acting as natural biological networks. One of the most exciting applications of synthetic biology is its use to bring solutions for biomedical challenges. Though this research area is still in its infancy, translational medicine is already witnessing the first steps towards the development of therapies based on synthetic biology. New synthetic biology-based approaches in the field of gene therapy, cell therapy, immunotherapy, tissue engineering, regenerative medicine, vaccine development or antibiotic resistance are emerging and impacting the way we will treat cancer, infectious and immunological diseases, or metabolic disorders [1, 2].

1.1 IN VIVO SYNTHETIC BIOLOGY

Hitherto, most projects on therapeutic synthetic biology have focused their attention on the assembly and engineering of genetic circuits or other biological modules *in vivo* into cells or unicellular organisms [3, 4]. Remarkable examples in the field of cancer therapy are the engineering of bacteria and viruses to specifically invade and kill cancer cells (Fig. 1a-1b), or the engineering of lymphocyte T cells to express a synthetic receptor (chimeric antigen receptor, CAR) that binds specific tumor antigens presented on the surface of the tumor cell. Different engineered bacteria or bacteriophages are also being developed for the disruption of bacterial and viral infections, and a diverse spectrum of interactive genetic circuits capable of performing therapeutic function in a controlled manner are being engineered in cells to restore healthy metabolism in metabolic disorders (Fig. 1c) [1].

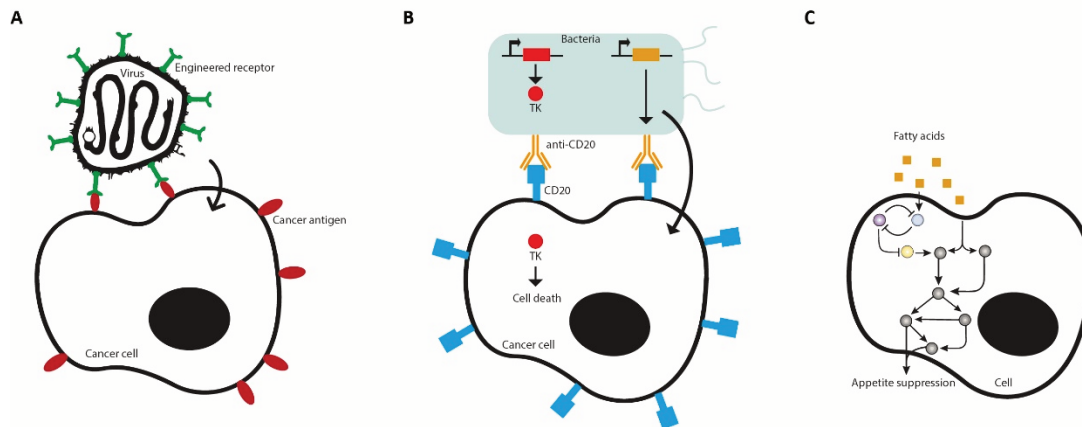


Fig. 1. Schematic examples of *in vivo* synthetic biology in therapeutics. A) Oncolytic virotherapy: Virus engineered to bind specific cancer antigens; B) Anticancer bacteria: Bacteria engineered to infect tumor cells through specific surface antibody expression and produce a pro-drug converting enzyme (thymidine kinase, TK); C) Treatment of diet-induced obesity: Gene circuits are engineered in cells such that the presence or absence of fatty acid is constantly sensed and trigger transcription activators or repressors, respectively, ultimately leading to the regulation of fatty acid levels in blood, adapted from [1].

1.2 VESICLE BIOREACTORS FOR THE PRODUCTION OF GENETICALLY-ENCODED THERAPEUTIC DRUGS

In certain cases, the complexity of living cells can challenge *in vivo* engineering. Cell-free synthetic biology (or *in vitro* synthetic biology), an emerging branch of synthetic biology, makes use of cell-free gene expression systems to create biological networks that function without the use of living cells [5]. More than a decade ago, the convergence of *in vitro* synthetic biology, cell-free gene expression systems and liposome technology gave rise to the creation of artificial vesicle bioreactors that can synthesize genetically-encoded molecules [6, 7]. Though the primary motivation of these studies was the assembly of a semi-synthetic cell, the application of this technology for different therapeutic purposes has been envisioned [8]. Examples of this are the creation of antigen-producing liposomes as novel vaccination system [9], the development of bioreactor liposomes suited for remotely controlled in-situ mRNA [10] or protein [11] production *in vivo*, or the assembly of a PCR-based nanofactory for gene delivery [12].

1.3 LIPOSOMES AS DRUG DELIVERY DEVICES

Liposomes are spherical vesicles consisting of one or more lipid bilayers surrounding an aqueous solution (Fig. 2). Liposomes are mainly composed by phospholipids, which are the major component of most biological cell membranes. Phospholipids are a class of lipids with amphipathic nature, consisting in a hydrophilic head and a hydrophobic tail, and are divided in two main groups: glycerophospholipids and sphingolipids [13]. The hydrophilic moiety comprises a polar head group containing a phosphate, which is negatively charged at neutral

pH [13, 14], while the hydrophobic tails are composed by two fatty acid chains. For this reason, when dissolved in an aqueous solution, these molecules are able to pack into sheets, forming a membrane bilayer, where the hydrophilic head interacts with water and the hydrophobic tails interact with each other [13], forming a liposome. Depending on the lipid composition and on the method used to produce them, liposomes can exist with different sizes, lamellarity states and charges [15].

As drug delivery systems, liposomes offer important advantages in comparison to other drug delivery vehicles. First, because liposomes are mostly composed of natural phospholipids and cholesterol, they are more biocompatible and biodegradable than other delivery devices, inherently inducing low toxicity [16, 17]. At the level of clinical manufacturing, liposome production is easy and scalable. Moreover, thanks to their structure, liposomes can encapsulate hydrophilic compounds in their core, hydrophobic compounds inside their phospholipid bilayer and amphipatic compounds at the interface between the phospholipid bilayer and the aqueous phase [15, 18]. Thus, liposomes are able to deliver a broad variety of therapeutic compounds, making them probably the most versatile type within all delivery nanocarriers [17]. Further broadening their versatility is the fact that generally therapeutically relevant physico-chemical properties in a delivery carrier such as charge, fluidity and permeability, can be precisely tuned in liposomes through modifications on the molar ratio of their constituent lipids [19].

In addition, liposomes can be actively targeted to specific tissues through ligand-mediated targeting. For this, different targeting ligands such as vitamins, proteins, peptides, antibodies, carbohydrates or glycoproteins can be attached to the surface of liposomes to target specifically tissues whose cells overexpress a specific cell membrane receptor. Active targeted delivery can lead to improved therapeutic efficacy and reduced systemic toxicity [16, 17].

Importantly, the stability and circulation time of liposomes *in vivo* can be significantly extended by coating their surface with hydrophilic polymers such as linear polyethylene glycol (PEG). Liposome PEGylation can inhibit liposome aggregation and unspecific interactions with serum lipoproteins preventing their premature clearance *in vivo* by the reticuloendothelial system (RES) [17, 20].

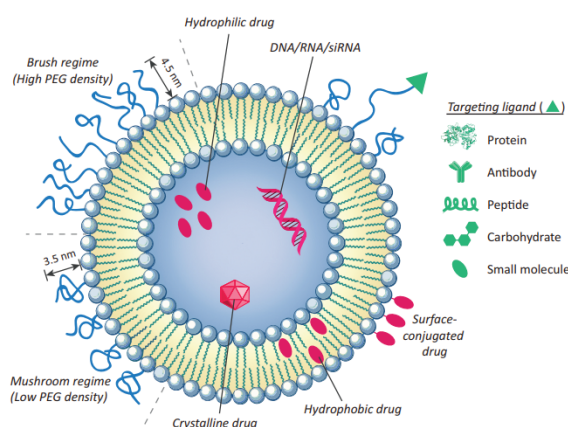


Fig. 2. Schematic of a liposome and the relevant structural elements in liposomal drug delivery, taken from [17].

It is probably for all these reasons that liposome-based drugs are the most successful drug delivery systems ever developed with more than fifteen approved drugs [16]. Liposomes entered the market for the first time in 1995, when Doxil, a PEGylated liposomal doxorubicin formulation, was approved by the Food and Drug Administration (FDA). Since then, fourteen other liposome-based drugs have arrived to the market (see Table 1) and others are undergoing different phases of clinical investigation [21]. As seen in Table 1, currently FDA-approved liposomal drugs entrap so called “small molecules” with chemotherapeutic (doxorubicin, daunorubicin, cytarabine, mifamurtide, vincristine, irinotecan), antibiotic (amphotericin B), photosensitizing (verteporphin) and pain relief (morphine sulfate, bupivacaine) function, inactivated virus particles or viral membrane proteins. However, during the last decade, liposomes have been extensively investigated as delivery vehicles of nucleic acids for gene therapy in the clinic [18].

Table 1. FDA-approved liposome-based drugs, taken from [21].

SN	Clinical Products (Approval Year)	Administration	Active Agent	Lipid/Lipid:Drug Molar Ratio	Indication	Company
1.	Doxil [®] (1995)	i.v.	Doxorubicin	HSPC:Cholesterol:PEG 2000-DSPE (56:39:5 molar ratio)	Ovarian, breast cancer, Kaposi's sarcoma	Sequus Pharmaceuticals
2.	DaunoXome [®] (1996)	i.v.	Daunorubicin	DSPC and Cholesterol (2:1 molar ratio)	AIDS-related Kaposi's sarcoma	NeXstar Pharmaceuticals
3.	Depocyt [®] (1999)	Spinal	Cytarabine/Ara-C	DOPC, DPPG, Cholesterol and Triolein	Neoplastic meningitis	SkyPharma Inc.
4.	Myocet [®] (2000)	i.v.	Doxorubicin	EPC:Cholesterol (55:45 molar ratio)	Combination therapy with cyclophosphamide in metastatic breast cancer	Elan Pharmaceuticals
5.	Mepact [®] (2004)	i.v.	Mifamurtide	DOPS:POPC (3:7 molar ratio)	High-grade, resectable, non-metastatic osteosarcoma	Takeda Pharmaceutical Limited
6.	Marqibo [®] (2012)	i.v.	Vincristine	SM:Cholesterol (60:40 molar ratio)	Acute lymphoblastic leukaemia	Talon Therapeutics, Inc.
7.	Onivyde [™] (2015)	i.v.	Irinotecan	DSPC:MPEG-2000:DSPE (3:2:0.015 molar ratio)	Combination therapy with fluorouracil and leucovorin in metastatic adenocarcinoma of the pancreas	Merrimack Pharmaceuticals Inc.
8.	Abelcet [®] (1995)	i.v.	Amphotericin B	DMPC:DMPG (7:3 molar ratio)	Invasive severe fungal infections	Sigma-Tau Pharmaceuticals
9.	Ambisome [®] (1997)	i.v.	Amphotericin B	HSPC:DSPG:Cholesterol:Amphotericin B (2:0.8:1:0.4 molar ratio)	Presumed fungal infections	Astellas Pharma
10.	Amphotec [®] (1996)	i.v.	Amphotericin B	Cholesteryl sulphate:Amphotericin B (1:1 molar ratio)	Severe fungal infections	Ben Venue Laboratories Inc.
11.	Visudyne [®] (2000)	i.v.	Verteporphin	Verteporphin:DMPC and EPG (1:8 molar ratio)	Choroidal neovascularisation	Novartis
12.	DepoDur [™] (2004)	Epidural	Morphine sulfate	DOPC, DPPG, Cholesterol and Triolein	Pain management	SkyPharma Inc.
13.	Exparel [®] (2011)	i.v.	Bupivacaine	DEPC, DPPG, Cholesterol and Tricaprylin	Pain management	Pacira Pharmaceuticals, Inc.
14.	Epaxal [®] (1993)	i.m.	Inactivated hepatitis A virus (strain RGSB)	DOPC:DOPE (75:25 molar ratio)	Hepatitis A	Crucell, Berna Biotech
15.	Inflexal [®] V (1997)	i.m.	Inactivated hemagglutinine of Influenza virus strains A and B	DOPC:DOPE (75:25 molar ratio)	Influenza	Crucell, Berna Biotech

i.v. (intravenous); i.m. (intramuscular); HSPC (hydrogenated soy phosphatidylcholine); PEG (polyethylene glycol); DSPE (distearoyl-sn-glycero-phosphoethanolamine); DSPC (distearoylphosphatidylcholine); DOPC (dioleoylphosphatidylcholine); DPPG (dipalmitoylphosphatidylglycerol); EPC (egg phosphatidylcholine); DOPS (dioleoylphosphatidylserine); POPC (palmitoyloleoylphosphatidylcholine); SM (sphingomyelin); MPEG (methoxy polyethylene glycol); DMPC (dimyristoyl phosphatidylcholine); DMPG (dimyristoyl phosphatidylglycerol); DSPG (distearoylphosphatidylglycerol); DEPC (dierucoylphosphatidylcholine); DOPE (dioleoyl-sn-glycero-phosphoethanolamine).

1.4 LIPOSOMAL RNA-BASED GENE THERAPY

Gene therapy is the introduction of genetic material into cells to treat pathological conditions through the modulation of gene-expression. Apart from DNA, different RNA molecules including microRNA (miRNA), small interfering RNA (siRNA), short interfering RNA (shRNA), messenger RNA (mRNA) and single-stranded antisense oligonucleotides (ASOs) are used for this purpose [18]. Compared to DNA, RNA therapy has the advantages of not requiring entrance into the nucleus or transcription to exert their function, and thus, the chance of genomic integration of the delivered molecule can be considered negligible [22].

Hitherto, most RNA-based drugs that have achieved the clinical trial stage are based on RNAi therapy (see Table 2). RNAi has demonstrated huge therapeutic potential through exhaustive *in vitro* and *in vivo* studies [23]. Importantly, in August 2018, the first RNAi-based drug was approved for the treatment of a disease [24]. Named Patisiran, this drug consists of a dsRNA siRNA entrapped in a lipid-nanoparticle for systemic delivery to hepatocytes in the liver [25], aimed to treat a rare hereditary disease named transthyretin amyloidosis. The approval of this drug marks the end of a long struggle to prove the therapeutic power of siRNA in the clinic [24], and opens the door of future gene therapy to RNA-based drugs. For its part, mRNA-based gene therapy is still in its infancy compared to RNAi, but the delivery barriers they encounter are very similar to those faced by RNAi and it does not require its integration into the endogenous RNAi machinery to exert its effect. Progresses in this field are promising, which is currently in expansion [18].

Table 2. Selection of ongoing clinical trials of siRNA-based drugs, adapted from [26].

Compound	Application route	Formulation/ modification	Target	Indication	Company	Clinical status
Bevasiranib	Intravitreal	—	VEGF	Age-related macular degeneration	Opko Health Inc.	Phase III, ⁷⁷ terminated
AGN-745 (Sirna027)	Intravitreal	—	VEGF	Age-related macular degeneration	Allergan/Sirna	Phase II, ^{73,75} terminated
ALN-RSV01	Inhalation	—	RSV nucleocapsid gene	RSV infection after lung transplantation	Alnylam Pharmaceuticals	Phase II, ^{73,75} completed
RX1109	Intradermal	Asymmetric siRNA with phosphorothioates and lipophilic ligands	Connective tissue growth factor	Dermal scarring after surgery	RXi Pharmaceuticals	Phase II ^{73,75}
QPI-1002	Intravenous	Modified siRNA (alternating 2'-O-Me)	p53	Delayed graft function and acute kidney injury	Quark Pharmaceuticals/ Novartis	Phase II ^{73,75}
CALAA-01	Intravenous	RONDEL™ (cyclodextrin-based formulation with PEG and transferrin)	M ₂ subunit of ribonucleotide reductase	Solid tumors	Arrowhead Research Corporation	Phase I, ^{68,71} completed
ALN-TTRsc	Subcutaneous	GalNAc conjugate	TTR	TTR amyloidosis (FAC)	Alnylam Pharmaceuticals	Phase II ^{73,75}
ARC-520	Intravenous	Dynamic polyconjugate (co-injection with siRNA)	Coagulation factor 7	Hepatitis B	Arrowhead Research Corporation	Phase II ^{73,75}
siRNA-EphA2-DOPC	Intravenous	Liposome (DOPC)	EPHA2	Advanced cancers	MD Anderson Cancer Center	Phase II ^{73,75}
TD101	Intradermal injection/ microneedle	Modified siRNA ("Accell": 2'-O-Me, cholesterol, phosphorothioates)	Keratin 6a	Pachyonychia congenita	Trans Derm	Phase I, ^{68,71} completed
Atu027	Intravenous	Atuplex® (liposome) with AtuRNA® (2'-O-Me)	Protein kinase N3	Advanced solid cancer	Silence Therapeutics	Phase II ^{73,75}
Atu111	Intravenous	DACC lipoplex	Angiopoietin-2	Lung indications	Silence Therapeutics	Phase II ^{73,75}
PF-655	Intravitreal	AtuRNA® (2'-O-Me)	RTP801	Diabetic macular edema/age-related macular degeneration	Quark Pharmaceuticals/ Pfizer	Phase II ^{73,75}
QPI-1007	Intravitreal	Modified siRNA (alternating 2'-O-Me)	Caspase 2	Optic nerve atrophy and non-arteritic ischemic optic neuropathy	Quark Pharmaceuticals	Phase I/IIa ^{68,71,73,75}
siG12D LODER	Intratumoral	LODER™ (PLGA matrix)	Mutant K-Ras G12D	Pancreatic ductal adenocarcinoma	Silenseed	Phase I/II ^{68,71,73,75}
TKM-PLK1	Hepatic intraarterial/ intravenous	SNALP	PLK1	Liver cancer	Tekmira Pharmaceuticals	Phase I/II ^{68,71,73,75}
ND-L02-S0201	Intravenous	Vitamin A-coupled lipid nanoparticles	HSP47	Fibrosis	Nitto Denko Corporation	Phase I ^{68,71}
DCR-MYC	Intravenous	Lipid nanoparticles (EnCore)	MYC	Hepatocellular carcinoma	Dicerna Pharmaceuticals	Phase I ^{68,71}

Abbreviations: siRNA, small interfering RNA; PEG, polyethyleneglycol; SNALP, stable nucleic acid lipid particle; TTR, transthyretin; FAP, familial amyloid polyneuropathy; FAC, familial amyloid cardiomyopathy; DOPC, 1,2-dioleoyl-sn-glycero-3-phosphocholine; DACC, D-alanyl-D-alanine carboxypeptidase.

Due to their negative charge, large size and hydrophilicity, RNA molecules encounter different biological barriers during their systemic delivery and cell entry. Prior to arriving to their site of action in the body, RNA molecules are faced with serum endonucleases, the immune system, non-specific interactions with proteins or non-target cells and renal clearance. Following, extravasation through the blood vessels, cellular internalization and endosomal escape are necessary for their successful delivery [18].

Liposomes have been long investigated as delivery vehicles for nucleic acids to overcome these barriers (Fig. 2) [18]. In fact, liposomes are probably the most frequently investigated for RNAi-based drugs, owing to all the advantages mentioned above (section 1.3) and to the extensive

track record of liposome usage in the clinic [23]. Hence, several liposomal RNAi-based formulations are going through clinical trials (see Table 2).

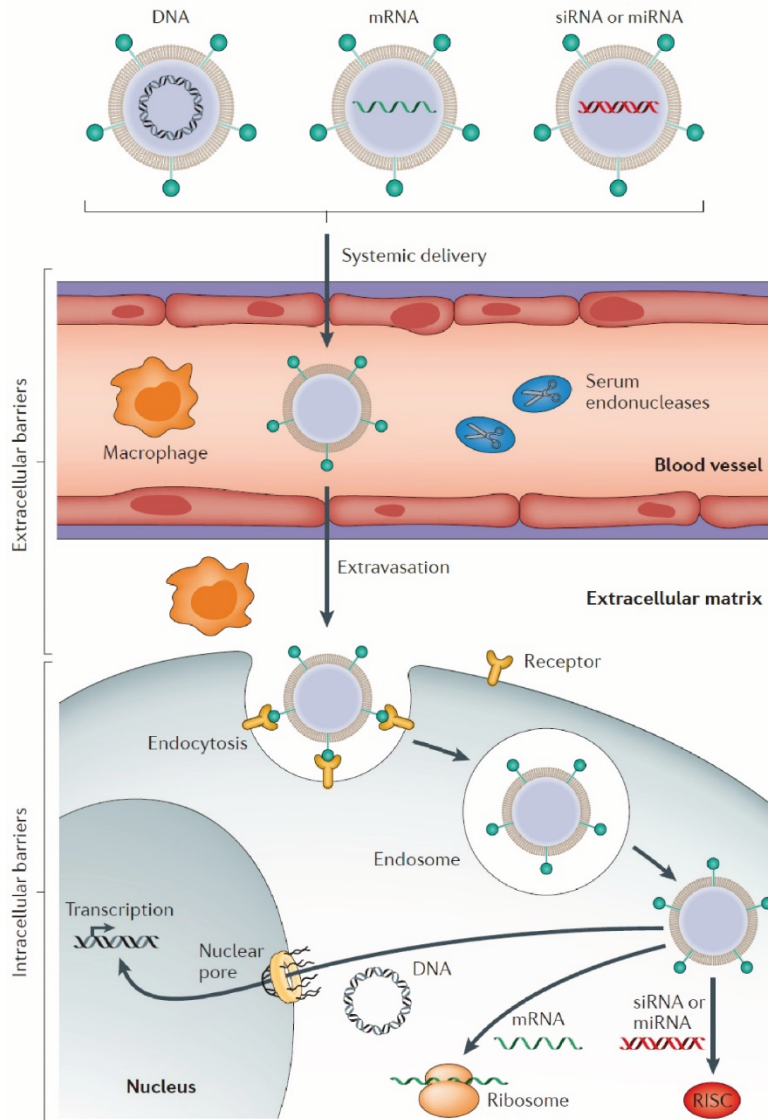


Fig. 3. Barriers to successful liposomal delivery of nucleic acids in vivo. After entrance into the circulatory system, liposomes need to protect nucleic acids from degradation by serum endonucleases, escape detection by the immune system, avoid renal clearance and nonspecific interactions (for this, polyethylene glycol, i.e. PEG, is added to the liposome's surface). Additionally, liposomes have to extravasate from the bloodstream to reach their target tissues. Last, liposomes must mediate cell entry and endosomal escape (through specific elements such as cell-perforating peptides, CPPs). To exert its function, DNA must be transported to the nucleus. Conversely, RNAi and mRNA should be respectively loaded into the RNA-induced silencing complex (RISC) or the translation machinery in the cytoplasm to exert their activity. Taken from [27].

For successful drug delivery, liposomes also have to confront different barriers in vivo (see Fig. 3). For a long time, cationic liposomes were the standard delivery vehicles for RNA [23]. When produced by conventional means, cationic lipids were used for efficient RNA entrapment, that was mediated by the association of the nucleic acids with lipids [16]. However, cationic lipids are toxic. Moreover, the use of cationic lipids results sometimes in the formation of RNA/lipid

complexes, i.e. lipoplexes, instead of liposomes. In the other hand, negatively charged liposomes are quickly cleared from blood circulation. Consequently, there is a high interest on the development of liposomes with reduced cationic charges or solely composed by non-ionic lipids. However, reducing cationic charges may reduce the encapsulation efficiency of liposomes produced through conventional methods. An hypothetical vesicle-fed bioreactor could, on the other hand, allow high encapsulation efficiencies in nearly neutrally charged liposomes [23], since one of the well established formulations that have allowed RNA and protein synthesis in fed-vesicle bioreactors were composed by nearly 80% of the non-ionic DMPC or DOPC [28]. This potential advantage of vesicle bioreactors has already been claimed by Lee et al. [29]. The authors developed a PCR-based nanofactory for the delivery of plasmid DNA with a liposome formulation composed solely of neutral lipids (DPPC:CHOL:DOPE-Rhod = 13:6:1). In vivo delivery of the amplified genes inside their vesicle bioreactor showed gene expression without toxicity.

1.5 THE IMPORTANCE OF SINGLE-VESICLE CHARACTERIZATION FOR THE DEVELOPMENT OF PRECISE DRUG-DELIVERY SYSTEMS

In spite of their long history of investigation, encapsulation efficiency (the ratio of therapeutic molecule inside the delivery vehicle relative to the total drug amount in the loading solution), a key parameter for the development of a drug delivery system, is generally investigated as a bulk property and measured accordingly as the average content of all nanoparticles in the preparation [30, 31]. However, this parameter is strongly affected by a compendium of different features associated to liposomes, such as the charge, rigidity or hydrophobicity of their surface, morphological characteristics such as shape, size or lamellarity, the vesicle preparation method or the inherent properties of the drug [30]. Thus, liposomes are intrinsically highly heterogeneous nanoparticles, exhibiting different physical and chemical properties even when prepared under the same conditions (size, lipid composition, encapsulation efficiency, charges) [32]. As a consequence, vesicle's drug content is entangled to heterogeneity in liposome preparations, and averaging methods lead to a loss of information that can be essential to understand the effects of the drug delivery system under development [33]. Frequently, electron microscopy is used to study the drug content inside individual vesicles, but this technique only allows the characterization of a minute fraction of the liposome preparation. Of particular interest is the use of techniques that enable high-throughput characterization of the drug content inside individual vesicles.

1.6 THE IMPORTANCE OF PRECISE DRUG BIODISTRIBUTION

Liposomal drug delivery systems have critically evolved over the past five decades, enabling the targeted delivery of genes and small drug molecules [34]. However, in spite of these advances, there have been few bench-to-bedside successful applications. One of the limitations to the

development of successful therapeutic liposome formulations is their observed membrane leakiness and premature drug release upon administration [35]. Controlling the bio-distribution of a therapeutic drug is essential to minimize toxic side effects and enhance the efficiency of the treatment [36]. Ensuring drugs arrive to their target destination is of particular importance for highly localized diseases [37]. To tackle this problem, the creation of targeting delivery systems with stimuli-responsive ability can improve the biodistribution profile of a drug and allow its delivery on demand [35].

1.7 THESIS OUTLINE

This work contributes to the convergence of the fields of synthetic biology and biomedicine, presenting different possible applications of vesicle bioreactors for the improvement of current RNA-based gene delivery systems. Herein, we give a brief description of each chapter in this thesis:

- **In Chapter 2**, we provide a method for the high-throughput characterization of RNA content in liposome preparations at the single vesicle level. For this, the Spinach RNA aptamer was used as fluorescent RNA reporter. Moreover, the loading potential of fed-vesicle bioreactors are compared to those of conventionally produced liposomes.
- **In Chapter 3**, we intended to implement a light sensitive switch for remote spatiotemporal control of gene expression in liposomes. This work gives important steps towards the development of a remotely activated therapeutic RNA delivery system.
- **In Chapter 4**, we created a platform for the in vitro production of shRNA inside folate-labelled vesicle bioreactors. Moreover, we studied the specificity of folate-mediated targeted delivery of our vesicle bioreactors to cells in vitro. This platform was devised for the future ex vivo production of targeted liposomes that are highly loaded with shRNA (Chapter 2) or for the spatiotemporally triggered production of therapeutic RNA in vivo (Chapter 3).
- **In Chapter 5**, we developed a new liposomal drug delivery system for the chemotherapeutic compound SN-38. SN-38-in-cyclodextrin-in-folate-labelled lipid nanoparticles were created, and their heterogeneity was characterized at high-throughput by fluorescence microscopy. Additionally, the therapeutic effect of these nanoparticles was studied in vitro in human cells.

Together, these efforts demonstrate the prominence of compositional heterogeneity of biomolecule-loaded small unilamellar vesicles and stress the importance of single-vesicle characterization to optimize the formulations of liposome-based drug delivery systems.

1.8 REFERENCES

- [1] Z. Abil, X. Xiong, and H. Zhao, “Synthetic biology for therapeutic applications,” *Mol. Pharm.*, vol. 12, no. 2, pp. 322–331, 2015.
- [2] W. C. Ruder, T. Lu, and J. J. Collins, “Synthetic biology moving into the clinic.,” *Science*, vol. 333, pp. 1248–1252, 2011.
- [3] C. E. Hodgman and M. C. Jewett, “Cell-free synthetic biology: Thinking outside the cell,” *Metab. Eng.*, vol. 14, no. 3, pp. 261–269, 2012.
- [4] A. S. Khalil and J. J. Collins, “Synthetic biology: applications come of age.,” *Nat. Rev. Genet.*, vol. 11, pp. 367–379, 2010.
- [5] Y. Lu, “Cell-free synthetic biology: Engineering in an open world,” *Synth. Syst. Biotechnol.*, vol. 2, no. 1, pp. 23–27, 2017.
- [6] V. Noireaux and A. Libchaber, “A vesicle bioreactor as a step toward an artificial cell assembly.,” *Proc. Natl. Acad. Sci. U. S. A.*, vol. 101, no. 51, pp. 17669–74, Dec. 2004.
- [7] S. M. Nomura, K. Tsumoto, T. Hamada, K. Akiyoshi, Y. Nakatani, and K. Yoshikawa, “Gene expression within cell-sized lipid vesicles.,” *Chembiochem*, vol. 4, no. 11, pp. 1172–5, Nov. 2003.
- [8] P. R. Leduc *et al.*, “Towards an in vivo biologically inspired nanofactory,” *Nat. Nanotechnol.*, vol. 2, no. 1, pp. 3–7, 2007.
- [9] M. Amidi, M. de Raad, D. J. a Crommelin, W. E. Hennink, and E. Mastrobattista, “Antigen-expressing immunostimulatory liposomes as a genetically programmable synthetic vaccine,” *Syst. Synth. Biol.*, vol. 5, no. 1, pp. 21–31, 2011.
- [10] V. Chan, S. K. Novakowski, S. Law, C. Klein-Bosgoed, and C. J. Kastrup, “Controlled Transcription of Exogenous mRNA in Platelets Using Protocells,” *Angew. Chemie - Int. Ed.*, vol. 54, no. 46, pp. 13590–13593, 2015.
- [11] A. Schroeder *et al.*, “Remotely Activated Protein-Producing Nanoparticles,” *Nano Lett*, vol. 12, pp. 2685–2689, 2012.
- [12] S. Lee *et al.*, “DNA amplification in neutral liposomes for safe and efficient gene delivery,” *ACS Nano*, vol. 8, no. 5, pp. 4257–4267, 2014.
- [13] D. L. Nelson, M. M. Cox, and A. L. Lehninger, *Lehninger principles of biochemistry*. 2013.
- [14] M. R. Mozafari, “Nanoliposomes: Preparation and Analysis,” in *Liposomes: Methods and Protocols, Volume 1: Pharmaceutical Nanocarriers*, V. Weissig, Ed. Totowa, NJ: Humana Press, 2010, pp. 29–50.
- [15] H. I. Chang and M. K. Yeh, “Clinical development of liposome-based drugs: Formulation, characterization, and therapeutic efficacy,” *Int. J. Nanomedicine*, vol. 7, pp. 49–60, 2012.

- [16] T. M. Allen and P. R. Cullis, "Liposomal drug delivery systems: From concept to clinical applications," *Adv. Drug Deliv. Rev.*, vol. 65, no. 1, pp. 36–48, 2013.
- [17] G. T. Noble, J. F. Stefanick, J. D. Ashley, T. Kiziltepe, and B. Bilgicer, "Ligand-targeted liposome design: Challenges and fundamental considerations," *Trends Biotechnol.*, vol. 32, no. 1, pp. 32–45, 2014.
- [18] H. Yin, R. L. Kanasty, A. a. Eltoukhy, A. J. Vegas, J. R. Dorkin, and D. G. Anderson, "Non-viral vectors for gene-based therapy.," *Nat. Rev. Genet.*, vol. 15, no. 8, pp. 541–555, Jul. 2014.
- [19] Y. Malam, M. Loizidou, and A. M. Seifalian, "Liposomes and nanoparticles: nanosized vehicles for drug delivery in cancer," *Trends Pharmacol. Sci.*, vol. 30, no. 11, pp. 592–599, 2009.
- [20] G. Bozzuto and A. Molinari, "Liposomes as nanomedical devices," *Int. J. Nanomedicine*, vol. 10, pp. 975–999, 2015.
- [21] U. Bulbake, S. Doppalapudi, N. Kommineni, and W. Khan, "Liposomal formulations in clinical use: An updated review," *Pharmaceutics*, vol. 9, no. 2, pp. 1–33, 2017.
- [22] R. S. McIvor, "Therapeutic delivery of mRNA: The medium is the message," *Mol. Ther.*, vol. 19, no. 5, pp. 822–823, 2011.
- [23] H. Yi Xue, P. Guo, W.-C. Wen, and H. Lun Wong, "Lipid-Based Nanocarriers for RNA Delivery," *Curr. Pharm. Des.*, vol. 21, pp. 3140–3147, 2015.
- [24] H. Ledford, "Gene-silencing technology gets first drug approval after 20-year wait," *Nature*, vol. 560, no. 7718, pp. 291–292, 2018.
- [25] C. Sheridan, "With Alnylam's amyloidosis success, RNAi approval hopes soar," *Nat. Biotechnol.*, vol. 35, no. 11, pp. 995–997, 2017.
- [26] M. Rizk and Ş. Tüzmen, "Update on the clinical utility of an RNA interference-based treatment: Focus on Patisiran," *Pharmgenomics. Pers. Med.*, vol. 10, pp. 267–278, 2017.
- [27] H. Yin, R. L. Kanasty, A. a. Eltoukhy, A. J. Vegas, J. R. Dorkin, and D. G. Anderson, "Non-viral vectors for gene-based therapy," *Nat. Rev. Genet.*, vol. 15, no. 8, pp. 541–555, 2014.
- [28] Z. Nourian, W. Roelofsen, and C. Danelon, "Triggered gene expression in fed-vesicle microreactors with a multifunctional membrane," *Angew. Chemie - Int. Ed.*, vol. 51, no. 13, 2012.
- [29] S. Lee *et al.*, "DNA Amplification in Neutral Liposomes for Safe and Efficient Gene Delivery," no. 5, pp. 4257–4267, 2014.
- [30] B. Sun and D. T. Chiu, "Determination of the encapsulation efficiency of individual vesicles using single-vesicle photolysis and confocal single-molecule detection," *Anal. Chem.*, vol. 77, no. 9, pp. 2770–2776, 2005.

- [31] K. A. Edwards and A. J. Baeumner, "Analysis of liposomes," *Talanta*, vol. 68, no. 5, pp. 1432–1441, 2006.
- [32] C. Chen, S. Zhu, T. Huang, S. Wang, and X. Yan, "Analytical techniques for single-liposome characterization," *Analytical Methods*. 2013.
- [33] B. Lohse, P. Y. Bolinger, and D. Stamou, "Encapsulation efficiency measured on single small unilamellar vesicles," *J. Am. Chem. Soc.*, vol. 130, no. 44, pp. 14372–14373, 2008.
- [34] V. P. Torchilin, "Multifunctional nanocarriers," *Adv. Drug Deliv. Rev.*, vol. 64, no. SUPPL., pp. 302–315, 2012.
- [35] B. S. Pattni, V. V. Chupin, and V. P. Torchilin, "New Developments in Liposomal Drug Delivery," *Chem. Rev.*, p. 150526165100008, 2015.
- [36] S. Szunerits, F. Teodorescu, and R. Boukherroub, "Electrochemically triggered release of drugs," *Eur. Polym. J.*, vol. 83, pp. 467–477, 2016.
- [37] P. R. Leduc *et al.*, "Towards an in vivo biologically inspired nanofactory," vol. 2, no. January, pp. 3–7, 2007.

2.

EXPLORING THE THERAPEUTIC POTENTIAL OF RNA-PRODUCING FED-VESICLE BIOREACTORS

Decades after the concept was proposed, gene therapy has finally emerged as a promising approach for the treatment of numerous diseases. RNA-based gene therapy in particular, offers a safer and easier delivery approach compared to DNA-based therapy. Lipid vesicles called liposomes are the most investigated vehicles for the delivery of therapeutic RNA. However, encapsulation efficiency, a key parameter in the development of any delivery system, is generally measured as the average drug content in liposome preparations. In this work, we provide a method for the characterization of RNA content in liposome samples at the single vesicle level. An RNA aptamer-fluorogen complex called Spinach, was used as model system to report liposomal RNA content by fluorescence microscopy. The loading potential of fed-vesicle bioreactors, where RNA is internally produced from a DNA template, is compared to that of conventional RNA encapsulation in liposomes. The results show that direct entrapment of pre-synthesized RNA provides a higher fraction of RNA-loaded liposomes. Additionally, we show for the first time how biotin-based vesicle immobilization can be conveniently applied to study liposomal gene delivery systems by high-throughput fluorescence imaging of single vesicles. Although we did not achieve the implementation of a highly-RNA producing fed-vesicle bioreactor, we propose several recommendations to improve our technology and achieve this goal.

2.1 INTRODUCTION

2.1.1 VESICLE BIOREACTORS FOR THE PRODUCTION OF GENETICALLY-ENCODED THERAPEUTIC DRUGS

Protein-producing fed-vesicle bioreactors (Fig. 1) consist of a cell-free transcription/translation system surrounded by a semi-permeable lipid membrane that enables the entrance of small feeding molecules from the surrounding environment into the vesicle's lumen while keeping the macromolecules needed for gene expression inside [1, 2]. This selective permeability is generally induced through the induction of small membrane breaks by applying high external osmotic pressure (Fig. 1a), or through the creation of nanopores (Fig. 1b). Transcription is usually carried out by the bacteriophage T7 RNA polymerase, that is chosen due to the simplicity of this protein (a ~100 kDa monomer) [3] and its high processivity [4]. Meanwhile, the translation machinery is generally derived from *Escherichia coli* [5–7].

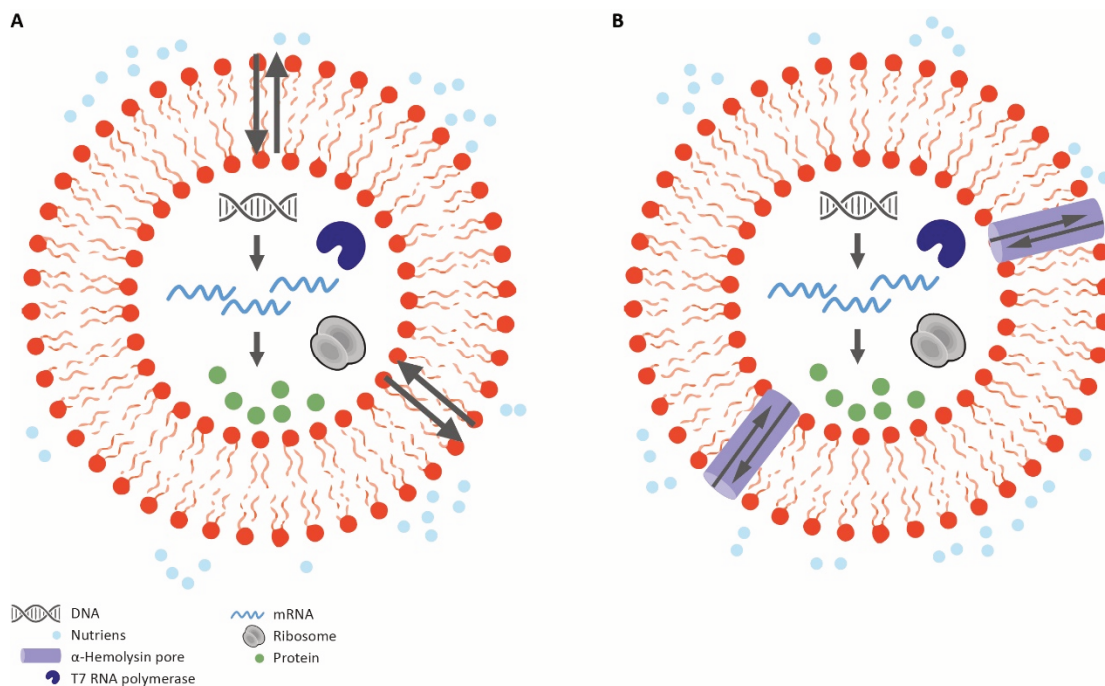


Fig. 1. Approaches to the creation of gene-expressing fed-vesicle bioreactors. Nutrients (rNTPs, amino acids) are provided through the creation of A) membrane defects by creating an osmotic pressure across the vesicle membrane or B) through the incorporation of membrane nanopores.

Remarkably, single-vesicle studies on fed-vesicle bioreactors of micrometer size range have shown that, under certain conditions, protein synthesis can be more efficient and longer when taking place inside vesicles compared to bulk solution [1, 2, 8]. In the work of Noireaux & Libchaber [1], the production of the fluorescent protein GFP in vesicles was prolonged for several hours in comparison to bulk solution when the nutrients necessary for transcription and translation were externally supplied and introduced through membrane defect generation provoked by osmotic pressure. These effects were greatly enhanced when α -hemolysin pores

nanopores were incorporated to the lipid membranes, which increased membrane permeability to the feeding solution. α -hemolysin is a water soluble monomer composed of 293 amino acids synthesized by the bacteria *Staphylococcus Aureus* [9]. Upon binding into a lipid bilayer, α -hemolysin assembles into an heptameric nanopore of 2.6 nm in diameter that allows the penetration of molecules smaller than 3 kDa. This size allows ribonucleotides (rNTPs) and amino acids to diffuse into the liposomes, while the macromolecules necessary for transcription and translation remain trapped in the vesicle's lumen.

2.1.2 ENVISIONING A NOVEL FED-VESICLE BIOREACTOR FOR THE PRODUCTION AND DELIVERY OF THERAPEUTIC RNA

In the context of therapeutics, exploiting the potential of such fed-vesicle bioreactors could be very valuable for the development of efficiently loaded liposomal delivery systems. Inspired by this idea, we envisioned the assembly of a therapeutic fed-vesicle that could act as both drug-producing bioreactor and drug delivery vehicle. Following compartmentalized drug synthesis, the fraction of vesicle-bioreactors with desired drug content could be sorted through high-throughput single vesicle analysis to achieve a sample of highly and precisely-loaded therapeutic liposomes for targeted delivery (see Fig. 2). In this regard, fluorescence-activated cell sorting (FACS) has been successful in sorting GFP-synthesizing cell-sized bioreactors [10].

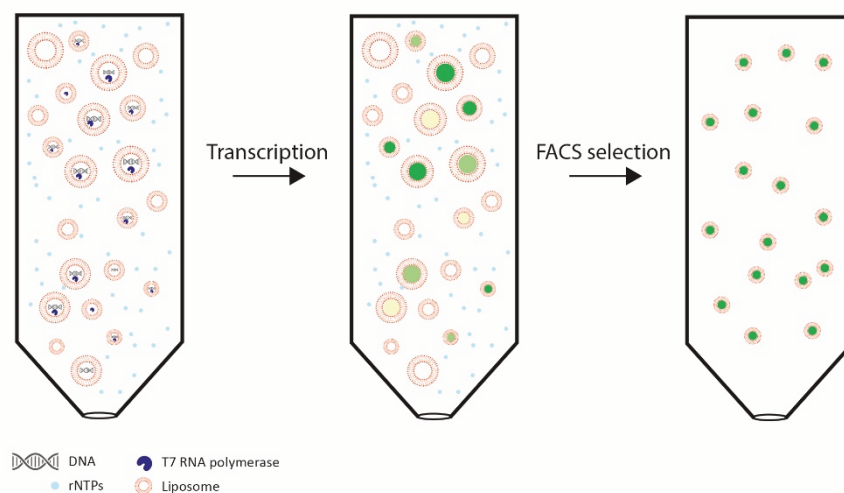


Fig. 2. Workflow in the production of an improved liposomal formulation for RNA delivery. First, transcription is carried out in a reaction of fed-vesicle bioreactors. As a result, vesicle bioreactors with different RNA concentrations are obtained (represented as green tones of varying intensities). RNA-containing vesicles with the desired size and RNA content are sorted by FACS, leading to the final liposomal formulation. Sorting will require the lighting of therapeutic molecule with a fluorescence reporter.

In order to be delivered *in vivo*, the size of the vesicles composing such therapeutic nanofactory is restricted. Liposomes used for systemic drug delivery *in vivo* typically feature sizes between 80 and 150 nm in diameter, since they provide the longest circulation life-times, minimizing their removal from circulation by the liver and the spleen. While liposomes smaller than 80 nm

are mainly removed from circulation by the liver, those larger than 250 nm are predominantly uptaken by the spleen [11].

It is known that enzymatic reactions inside liposomes are significantly influenced by the size of the vesicles [10]. For the production of a protein, the presence of a large number of components inside the vesicles is required. However, as liposome size decreases, the fraction of liposomes encapsulating all the needed components does as well, limiting the implementation of therapeutic-sized bioreactors for the production and delivery of protein drugs.

On the other hand, RNA production in a fed-vesicle solely requires the encapsulation of a DNA template and a T7 RNA polymerase. Thus, the fraction of liposomes encapsulating these elements may be less severely affected. Consequently, the development of therapeutic-sized bioreactors for the production and delivery of therapeutic RNA for gene-based therapy may be less limited than for the production of therapeutic proteins.

2.1.3 LIPOSOME IMMOBILIZATION AS A PLATFORM FOR HIGH-THROUGHPUT RNA-LOADED SINGLE-VESICLE CHARACTERIZATION

Immobilization of lipid vesicles through molecular linkers onto solid supports is an extremely valuable and convenient technique that allows the high-throughput characterization of vesicle preparations and the study of diverse biological processes taking place at lipid membranes at the single vesicle level [12] through fluorescence microscopy. In particular, the use of Streptavidin as a molecular linker, first pioneered by Stamou and co-workers [13], allows immobilization of small unilamellar vesicles without major morphological changes when the number of molecular tethers is kept low.

For this, biotinylated bovine serum albumin (BSA-biotin) is first attached to the solid support, and subsequently functionalized with streptavidin (Fig. 3). In turn, the external surface of lipid vesicles is tethered with biotin through the addition of biotinylated lipids in their formulation. Thanks to the high affinity of the linkage between biotin and streptavidin ($KD \sim 10^{-15}$) [14], vesicles become irreversibly locked onto the surface [13].

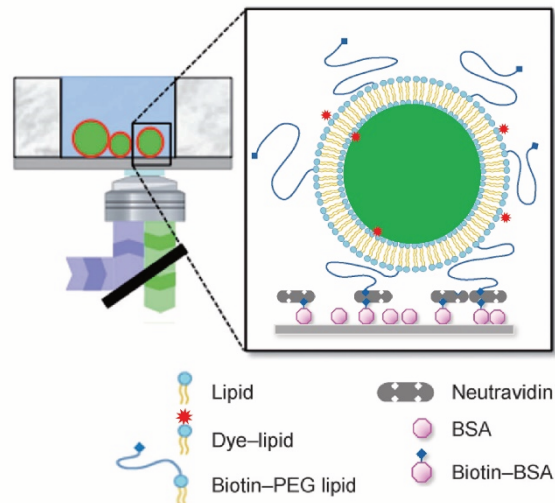


Fig. 3. Surface immobilization of biotinylated liposomes on a functionalized microscope coverslip through biotin-neutravidin binds. Adapted from [2].

This type of vesicle immobilization has been employed to study diverse processes, such as protein-vesicle interactions and the effect of membrane curvature over such interactions [15–18], enzymatic reactions triggered in the vesicle’s lumen [2, 19–22], and the encapsulation efficiency in single vesicles [23].

Using this technique, Lohse et al. [23] investigated the encapsulation efficiency of a fluorescent dye inside unilamellar vesicles ranging in size between 100 and 400 nm. These vesicles were produced through one of the most standard vesicle production procedures (dry-lipid-film rehydration, extrusion and freeze-thaw). Surprisingly, the encapsulation efficiency of the fluorescent dye was inversely proportional to the vesicle’s diameter. Moreover, a large number of empty vesicles similarly spread through the whole range of vesicle sizes was found. In agreement with this result, a single-vesicle electron microscopy study from Luisi et al. [24] on the encapsulation of a protein in vesicle with sizes ranging between 50 and 300 nm, showed again that the smallest vesicles reached the highest encapsulation efficiencies, and found that protein entrapment follows a dual behavior, characterized by many empty vesicles and some extremely crowded vesicles. Altogether, these studies further highlight the importance of an exhaustive characterization of the heterogeneity of encapsulation for the improvement for liposome-based drug delivery systems.

2.1.4 SPINACH RNA APTAMER AS A REPORTER OF TRANSCRIPTION

In this work we intended to adapt the described liposome immobilization method to report the vesicle-to-vesicle heterogeneity on RNA content and DNA transcription inside SUV preparations at the single vesicle level in a high-throughput manner. To achieve this, the use of a genetically encoded fluorescent probe was chosen. Spinach, an RNA aptamer that binds to and activates the fluorescence of a small fluorophore called 3,5-difluoro-4-hydroxybenzylidene imidazolinone (DFHBI) [25] (Fig. 4a), has recently been used in our lab to report gene

expression inside immobilized giant unilamellar vesicles (GUVs) by fluorescence microscopy [20]. Similar results have been obtained using DFHBI-1T [21], a DFHBI analog with a 1,1,1-trifluoroethyl substituent characterized by increased brightness and improved compatibility with common fluorescence microscopy filter thanks to its GFP-like fluorescence properties (Ex-Max 482/Em-max 505 nm)[26](Fig. 4b). In the current study, a DNA template encoding the Spinach sequence, preceded by a T7 promoter, was used to study the RNA-content of conventionally produced liposomes in comparison to in situ RNA production in fed-vesicle bioreactors.

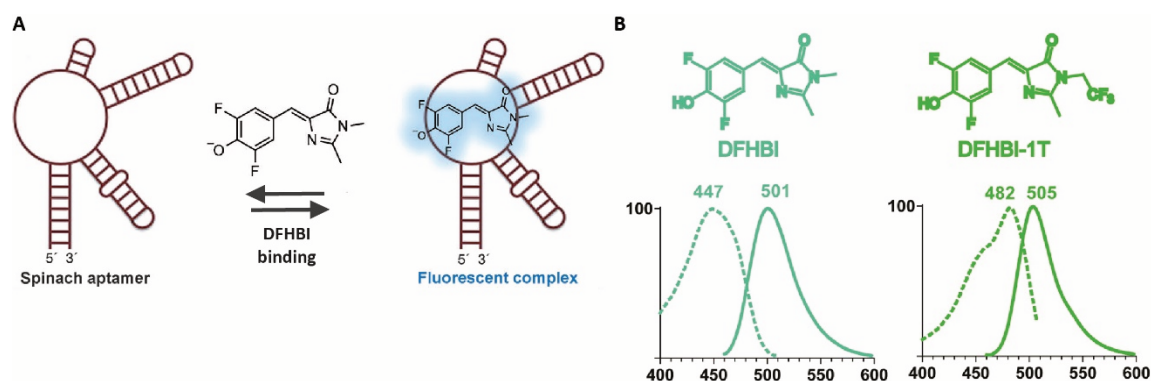


Fig. 4. The Spinach RNA aptamer and the fluorophores DFHBI and DFHBI-1T. A) When Spinach binds DFHBI, the complex Spinach-DFHBI becomes fluorescent. Adapted from van Nies et al. [20]. B) Spectra of excitation/emission from DFHBI and DFHBI-1T. Taken from [26].

In this work, we hypothesized that RNA synthesis inside therapeutic-sized fed-vesicle bioreactors (SUV, 200 nm in diameter, Fig. 5a) could be more efficient than in bulk solution (Fig. 5b). The semi-permeable membrane of a fed-vesicle bioreactor may allow access to an “unlimited” pool of rNTPs present in the liposome’s surroundings, what may lead to a fraction of transcriptionally active fed-vesicles that could potentially produce more RNA molecules per liposome than when pre-synthesized RNA is encapsulated in liposomes, assuming that enzyme activity and DNA stability are not limiting factors. Additionally, confinement of biochemical reactions in small volumes is known to alter the kinetics of enzymatic reactions in cells and in liposomes [27]. In fact, encapsulation seems to facilitate transcription and translation in liposomes [8, 28], what may further enhance the number of RNA molecules achieved per liposome in the fed-vesicle bioreactors.

Moreover, we wished to investigate the RNA content and vesicle-to-vesicle heterogeneity resulting from these two different production methods in a quantitative manner. In combination with a sorting approach to select liposomes with a specific size and RNA concentration, such efficient therapeutic bioreactors could set the basis of the development of well-characterized and highly-loaded liposome delivery systems.

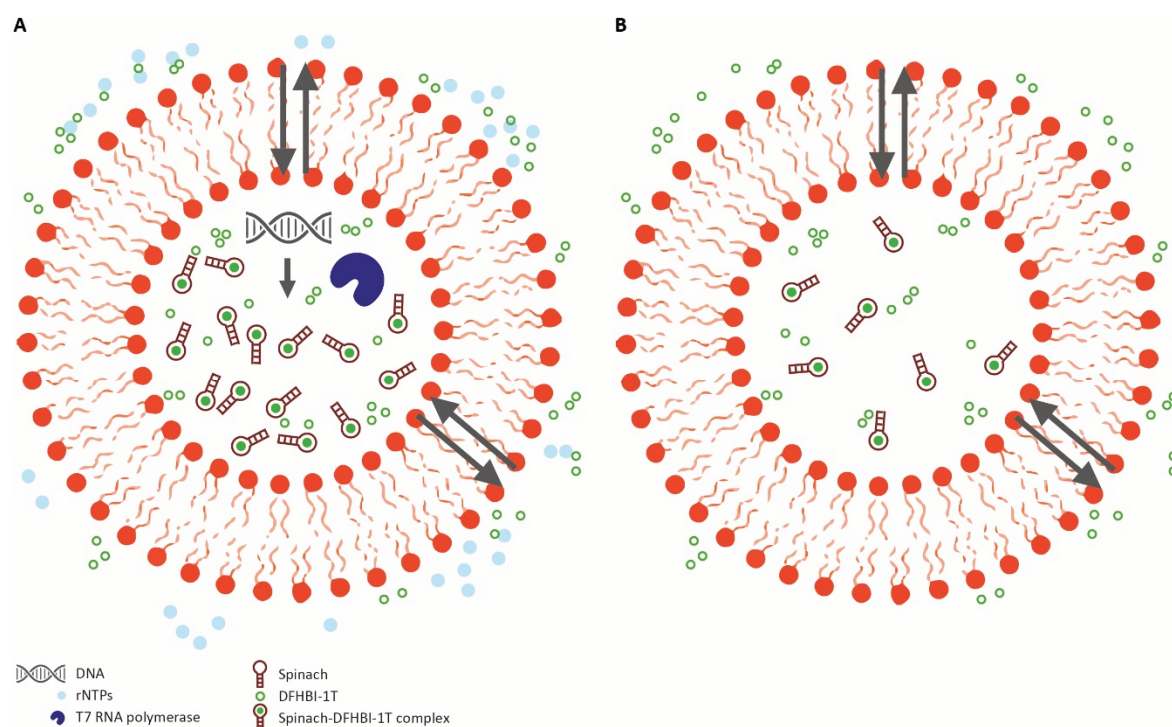


Fig. 5. Transcription in A) fed-vesicle bioreactors versus B) conventionally produced RNA pre-loaded liposomes. In B), RNA is produced in bulk gene expression reactions prior entrapment inside liposomes.

2.2 MATERIALS AND METHODS

2.2.1 PREPARATION OF A SPINACH-ENCODING DNA TEMPLATE

A linear DNA template encoding meYFP-Spinach was used to isolate the Spinach aptamer DNA sequence flanked by a T7-promoter and terminator sequences with the forward and reverse primers CHD367 and CHD91, respectively (Table 1). The PCR reaction mix consisted of 0.1 ng/ μ l of meYFP-Spinach, 0.2 μ M Fw CHD367, 0.2 μ M Fw 91CHD, 0.02 U/ μ l of Phusion[®] High-fidelity DNA polymerase (NEB) and 5X Phusion HF buffer (NEB) adjusted to 800- μ l with MiliQ water. The PCR was run with the following thermal cycles: 95 $^{\circ}$ C for 3 min, 30x (95 $^{\circ}$ C for 30 sec, 52.5 $^{\circ}$ C for 30 sec and 72 $^{\circ}$ C for 1 min 15 sec) and 72 $^{\circ}$ C for 5 min. 5 μ l of reaction product were loaded with a 6x DNA loading buffer (Promega) in a 1.2% agarose gel in TAE buffer using a 50-bp DNA ladder (NEB). The rest of the reaction product was purified with the Wizzard PCR-clean up System (Promega). This construct was named T7-Spinach(221) DNA.

Table 1. DNA primers for the amplification of a T7-Spinach(221) DNA.

DNA name	Sequence (5' - 3')	Description
CHD367	GAAATTAATACGACTCACTATAGGGAGAAAGCTTCCCGGGAAAGTATATATGAG	FW Spinach - T7 promoter
CHD91	AAAAAACCCCTCAAGACCCGTTTAGAGG	RV Spinach - T7 terminator

2.2.2 KINETIC MEASUREMENT OF THE T7-SPINACH(221) DNA TRANSCRIPTION IN BULK

A 20- μ l transcription reaction containing 80 nM of T7-Spinach(221) DNA, 2 μ l of T7 RNA polymerase, 8 mM ATP, 8 mM UTP, 8 mM GTP, 8 mM CTP (rNTPs and T7 RNA polymerase; RiboMAX Large Scale RNA Production System-T7, Promega), 20 μ M DFHBI and 4 μ l of transcription buffer (5x), was prepared in ice and transferred to a 20- μ l cuvette (Hellma). Following, the cuvette was mounted in the temperature-controlled holder of a fluorescence spectrophotometer (Cary Eclipse, Varian). Real-time monitoring of Spinach production at 37 °C was recorded every 30 sec with 460/502 nm excitation/emission wavelengths. Two transcription buffers were compared, the T7 transcription buffer from the commercial kit RiboMAX Large Scale RNA Production System-T7 (Promega) and a homemade transcription buffer with identical composition as the commercial buffer. The 5x homemade T7 transcription buffer consisted of 400 mM HEPES-KOH (pH 7.5), 120 mM MgCl₂, 10 mM Spermidine and 200 mM DTT.

2.2.3 PREPARATION OF LIPID-COATED BEADS

To prepare the lipid-coated beads used in the experiment testing α -hemolysin fed-bioreactors, a mixture of chloroform-dissolved lipids consisting of DPMC (66.5 mol%), DMPG (16.6 mol%), Cholesterol (16.6 mol%), DHPE-TexasRed (0.2 mol%) and DSPE-PEG(2000)-biotin (0.1 mol%) for a total mass of 2 mg, was prepared in a 25-ml round-bottom glass flask. All lipids were purchased from Avanti Polar Lipids, except the DHPE-TexasRed membrane dye that was from Invitrogen. Prior to the evaporation of the organic solvent, 1.5 g of 212-300- μ m acid-washed glass beads (Sigma-Aldrich) were added to the lipid mixture in order to increase the surface area where the lipid film would form and achieve a higher encapsulation efficiency [29]. The organic solvent was removed by overnight rotary evaporation at 300 mbar and 100 rpm. The dried lipid-coated beads were stored under argon at -20 °C and desiccated for at least 20 min before use. Each lipid-pipetting tip was washed three times with chloroform, and the washing volumes were added to the mixture.

In all other experiments, the molar percentages in the lipid formulation were slightly modified and consisted of DPMC (66.2 mol%), DMPG (16.6 mol%), Cholesterol (16.6 mol%), DHPE-TexasRed (0.45 mol%) and DSPE-PEG(2000)-biotin (0.2 mol%). When this formulation was used, solvent evaporation was performed at 100 rpm with the following steps in the rotavapor: 500 mbar for 30 min, 200 mbar for 30 min, 20 mbar for 1 h.

2.2.4 SPINACH TRANSCRIPTION INSIDE α -HEMOLYSIN FED-VESICLE BIOREACTORS

A 200- μ l pre-transcription reaction consisting of 70 nM T7-Spinach(221) DNA, 22.6 μ l T7 RNA polymerase and transcription buffer (RiboMAX™ Large Scale RNA Production System-T7 kit from Promega) was prepared, and incubated for 20 min at room temperature to induce the

formation of DNA-polymerase complexes. Then, 73 mg of lipid-coated beads were incubated with the pre-transcription reaction for 2 h at 30 °C and gentle manual swirling every 15 min, to obtain a final lipid concentration of 0.5 mg/ml. The resulting liposome solution was extruded to produce small unilamellar vesicles. Extrusion was performed by 13 passages with a 0.2- μ m filter membranes (Avanti Polar Lipids) and two 10-mm filter supports (Whatmann) on a mini-extruder (Avanti Polar Lipids), obtaining a theoretical liposome concentration of 2 nM. Prior to each extrusion, the assembled extruder was pre-washed with transcription buffer 1X and pre-heated to 40 °C ($>T_m$ of lipids).

Unencapsulated DNA was removed by addition of 0.05 U/ μ l DNase (1 U/ μ l, RQ1, Promega) followed by an incubation step at 37 °C for 20 min. DNA transcription took place inside liposomes by addition of 5 mM rNTPs, 0.9 μ M purified α -hemolysin (Sigma), and 60 μ M DFHBI-1T to the liposome samples, followed by an incubation step of 3 h at 37 °C.

2.2.5 PREPARATION OF SPINACH-CONTAINING LIPOSOMES THROUGH IN-VESICLE TRANSCRIPTION

A 200- μ l pre-transcription reaction consisting of 70 nM T7-Spinach(221), 4 μ l of 10-20 U/ μ L T7 RNA Polymerase (Promega) and homemade T7 transcription buffer was prepared, and incubated for 20 min at room temperature to induce the formation of DNA-polymerase complexes. Following, 75 mg of lipid-coated beads were swelled with the pre-transcription reaction for 2 h at 37 °C and gentle manual swirling every 15 min. The resulting liposome solution was extruded to produce small unilamellar vesicles (see 2.2.4).

Unencapsulated DNA was removed by addition of 0.05 U/ μ l DNase (1 U/ μ l, RQ1, Promega) followed by an incubation step for 20 min at 37 °C. DNA transcription was triggered inside liposomes by addition of 5 mM rNTPs, followed by an incubation step for 3 h at 37 °C. Unencapsulated RNA that might have been produced outside liposomes due to incomplete DNA degradation was removed by addition of 0.25-0.5 U/ μ l RNase ONE™ Ribonuclease (5-10 U/ μ l, Promega) followed by an incubation step for 20 min at 37 °C.

2.2.6 PREPARATION OF SPINACH RNA PRE-LOADED LIPOSOMES

A 200- μ l transcription reaction consisting of 70 nM T7-Spinach(221) DNA, 4 μ l of 10-20 U/ μ l T7 RNA Polymerase (Promega), 5 mM rNTPs (Promega RiboMax™ Large Scale RNA Production System-T7 kit) and homemade T7 transcription buffer was prepared, and incubated for 3 h at 37 °C to induce Spinach RNA production. Next, 75 mg of lipid beads were incubated with the transcription reaction for 2 h at 37 °C and gentle manual swirling every 15 min. The resulting liposome solution was subjected to 10 freeze-thaw cycles in order to enhance encapsulation efficiency [23]. Each freeze-thaw cycle consisted of 10 sec freezing in liquid nitrogen and 2 min defrosting in a water bath at 45 °C. Freeze-thawed liposomes were downsized by extrusion to produce SUVs, as described in section 2.2.4. Unencapsulated RNA

was removed by addition of 0.25-0.5 U/ μ l of RNase ONE™ Ribonuclease (5-10 U/ μ l, Promega) followed by an incubation step for 20 min at 37 °C.

2.2.7 LIPOSOME SAMPLE PREPARATION FOR BACKGROUND CORRECTION

A liposome sample was prepared to correct for the DFHBI-1T background fluorescence that did not originate from the Spinach-DFHBI-1T complex. This liposome sample was prepared following the same procedure as in section 2.2.6, but MiliQ water was added instead of T7 RNA polymerase to avoid Spinach RNA production.

2.2.8 FLUORESCENCE MICROSCOPY IMAGING OF LIPOSOMES

Custom-made glass chambers (Fig. 6) were prepared for fluorescence imaging of immobilized liposomes. In the experiment with α -hemolysin fed-vesicle bioreactors, 10 μ l of liposome sample were transferred to a custom-made imaging chamber. In the other experiments, the liposome solution was diluted 10x in transcription buffer containing 60 μ M DFHBI-1T and 3 μ l of this dilution were transferred to the imaging chamber.

Prior to sample addition, the glass coverslip inside the imaging chamber was functionalized with BSA-biotin and NeutrAvidin (Thermo Fisher Scientific) for liposome immobilization. Briefly, chambers were incubated with 10 μ l of 1 mg/ml BSA-biotin (Thermo Fisher Scientific) and 10 μ l of 1 mg/ml NeutrAvidin for 5 min at room temperature. Chambered coverslips were washed three times with MiliQ water after each incubation. Prior to liposome immobilization, the functionalized chambers were pre-washed two times with MQ and one time with 60 μ M DFHBI-1T in transcription buffer. After sample addition, the chamber was sealed and used for imaging immobilized liposomes with a Nikon A1+ laser scanning confocal microscope with a 100x oil immersion objective, using the 488 nm (DFHBI-1T) and 561 nm (Texas Red) laser lines with appropriate emission filters.

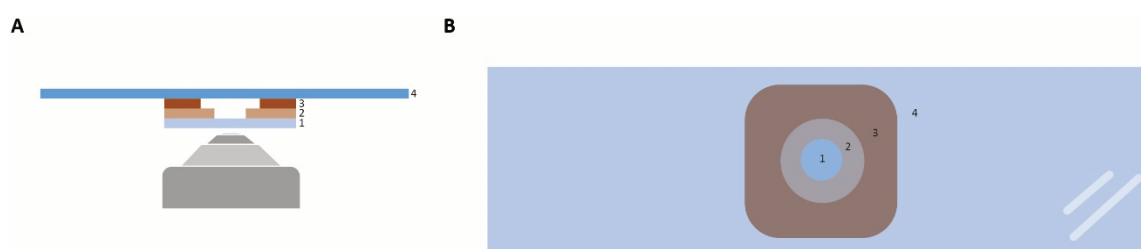


Fig. 6. A) Front-view and B) top view of custom-made chambered coverslips for liposome immobilization and visualization by fluorescence microscopy. A 18 mm x 18 mm silicon spacer (Press-to-seal silicone sheet, Life technologies) with a 5-mm spherical hole (2) was sealed to a clean coverslip (18 mm x 18 mm, Menzel-Gläser) (1). A silicon spacer with a larger hole was sealed on top the first silicone spacer (3). After sample addition, the chamber was sealed with a glass coverslide (76 x 26 mm, Menzel-Gläser) (4).

2.2.9 ANALYSIS OF SPINACH CONTENT IN α -HEMOLYSIN FED-VESICLE REACTORS

In experiments testing α -hemolysin fed-vesicle bioreactors, ImageJ (National Institute of Health) was used to create a semi-automatic macro to analyze Spinach and Texas Red intensities per liposome. Briefly, images composed of 6 x 6 fields of view were cropped into 36 individual images, and analyzed separately. To find all the liposomes in an image, the Texas red channel was used. For this, the Spinach and the Texas Red channels were split (Image > Color > Split Channels). A Gaussian blur with a radius of 2 pixels was applied on the Texas Red channel (Process > Filters > Gaussian Blur). To reduce the background noise, an automatic threshold (Image > Adjust > Threshold) was set to obtain a binary image. The regions of interest (ROI) were found by analyzing particles (Analyze > Analyze Particles). The size used ranges from 5 to 25 pixels units. The Areas, Min and Max gray values, Mean gray values, and Standard deviations of the Spinach and Texas Red values from all selected ROIs were measured and saved into Excel files.

2.2.10 IMAGE PROCESSING FOR IMPROVED ANALYSIS OF SPINACH CONTENT IN LIPOSOMES

In all other experiments, a MATLAB (MathWorks) code with improved features was used for quantitative analysis of the microscopy images (see Results). In this method, a Laplacian of Gaussian filter (LoG) was applied prior to image binarization and SUV selection (5-25 pixels), which is known to improve edge detection in images [30]. Additionally, we intended to improve background correction by applying a median filter, a smoothing technique known to reduce noise from images while preserving edges better than the Gaussian Blur under moderate noise levels, that was employed in Fig. 9 [31]. Last, the integrated Spinach fluorescence intensity inside each liposome was calculated by fitting the fluorescence intensity profile with a two-dimensional Gaussian function, as described for other SUVs [32] and other diffraction limited particles [33].

2.3 RESULTS

2.3.1 A LOW FRACTION OF SUVs IS EXPECTED TO BE TRANSCRIPTIONALLY ACTIVE

Prior to testing our hypothesis experimentally, we carried out some calculations to predict the fractions of RNA-containing liposomes in both fed-vesicle bioreactors and RNA pre-loaded liposomes.

For a liposome to be transcriptionally active, at least one DNA molecule and one RNA polymerase molecule should be co-encapsulated. A theoretical estimation allowed us to determine the expected fraction of Spinach expressing liposomes, considering the following assumptions:

- The distribution of DNA and RNA polymerase molecules within liposomes is random, this is, it follows a Poisson distribution:

$$P(X = k) = \frac{\lambda^k}{k!} e^{-\lambda} \quad (2.1)$$

where k is the number of DNA molecules encapsulated, and λ is the expectation value.

- Since the concentration of RNA polymerase was given in U/ μ l, it was assumed to be present in a saturating concentration. Therefore, the probability of RNA polymerase encapsulation by a liposome was set equal to 1.

In this hypothetical scenario, the probability of finding non-expressing or expressing liposomes depended on the number of DNA molecules encapsulated, which in turn depended on the bulk DNA concentration (C_{DNA}) and the volume of the liposome's lumen ($V_{liposome}$), which is that of a sphere:

$$V_{liposome} = \frac{4}{3}\pi r^3 \quad (2.2)$$

The expected value (λ) of the Poisson distribution was thus given by:

$$\lambda_{DNA} = C_{DNA} \cdot N_A \cdot V_{liposome} \quad (2.3)$$

where N_A is the Avogadro constant.

The resulting Poisson distribution formula was:

$$P_{DNA}(X = k) = \frac{(C_{DNA} \cdot N_A \cdot V_{liposome})^k}{k!} e^{-(C_{DNA} \cdot N_A \cdot V_{liposome})} \quad (2.4)$$

The probability of finding non-expressing liposomes was determined for 200-nm liposomes at a DNA concentration of 70 nM, and for 800-nm liposomes at a DNA concentration of 60 nM:

$$P_{800\text{ nm}}(X = 0) = e^{-(60 \cdot 10^{-9} \cdot 6.022 \cdot 10^{23} \cdot \frac{4}{3}\pi (400 \cdot 100^{-9})^3 \cdot 1000)} = 0.00621\% \quad (2.5)$$

$$P_{200\text{ nm}}(X = 0) = e^{-(70 \cdot 10^{-9} \cdot 6.022 \cdot 10^{23} \cdot \frac{4}{3}\pi (100 \cdot 100^{-9})^3 \cdot 1000)} = 83.81\% \quad (2.6)$$

Therefore, the probability of finding expressing liposomes is 100% at a concentration of 60 nM in 800-nm liposomes, while it is ~16% at a concentration of 70 nM in 200-nm liposomes. As shown in Fig. 7a, most 800-nm liposomes would encapsulate 5 to 15 DNA molecules. In comparison, most of the transcriptionally active 200-nm liposomes would encapsulate a single DNA molecule (Fig. 7b).

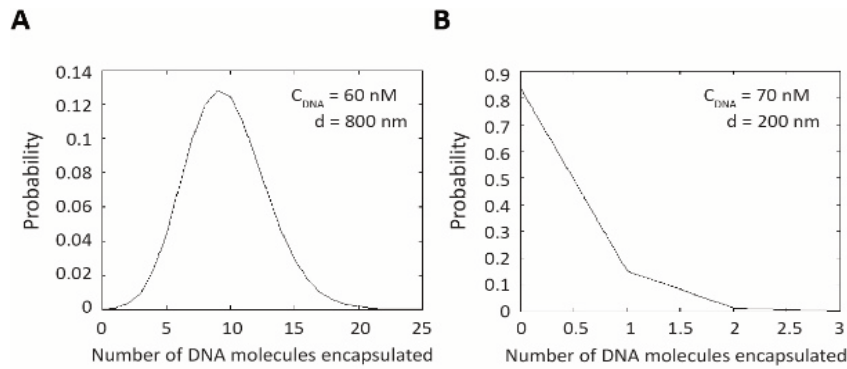


Fig. 7. Probabilities of encapsulating a specific number of DNA molecules A) at a DNA concentration of 60 nM and a liposome diameter of 800 nm; B) at a DNA concentration of 70 nM and a liposome diameter of 200 nm. The probability values of encapsulating one or two DNA molecules are 14.8% and 1.31% respectively in 200-nm liposomes. Together, they sum ~16% of the total fraction of liposomes, and 99.5% of the total fraction of transcriptionally active liposomes (91.4% one molecule; 6.7% two molecules).

2.3.2 ALL RNA PRE-LOADED LIPOSOMES ARE EXPECTED TO ENCAPSULATE SPINACH RNA MOLECULES

To determine the theoretical fraction of liposomes encapsulating pre-synthesized Spinach RNA, we first estimated the concentration of Spinach RNA produced in the transcription reactions. Considering that the final concentration of each rNTP in the transcription reaction is 5 mM, we determined the number of molecules of each nucleotide present in the reaction:

$$200 \cdot 10^{-6} L \cdot 5 \text{ mM} = 1 \mu\text{mol of each rNTP} \quad (2.7)$$

$$1 \cdot 10^{-6} \text{ mol} \cdot 6.022 \cdot 10^{23} \text{ mol}^{-1} = 6.022 \cdot 10^{17} \text{ molecules of each rNTP} \quad (2.8)$$

Considering the number of each nucleotide present in the Spinach RNA molecule (see Fig. S1), the nucleotide present in higher number is guanine (G), having 65 rGTPs, while the number of rUTP, rATP and rCTP are 49, 47 and 39, respectively. Considering rGTP the limiting factor in the transcription reaction, as it will be the first nucleotide to be depleted, the number of Spinach RNA molecules produced in 200 μ l of transcription reaction should be:

$$\frac{6.022 \cdot 10^{17} \text{ rGTP molecules in the reaction}}{65 \text{ rGTP molecules in Spinach RNA}} = 9.26 \cdot 10^{15} \text{ RNA molecules} \quad (2.9)$$

Therefore, the molar concentration of Spinach RNA produced should be:

$$\frac{9.26 \cdot 10^{15} \text{ RNA molecules}}{6.022 \cdot 10^{23} \text{ mol}^{-1} \cdot 200 \cdot 10^{-6} L} = 0.76 \cdot 10^{-4} M = 76 \mu M \quad (2.10)$$

Then, the probability of finding empty 200-nm liposomes was estimated assuming a Poisson distribution of the Spinach RNA molecules within the liposomes and the swelling solution:

$$P_{RNA}(X = k) = \frac{(C_{RNA} \cdot N_A \cdot V_{liposome})^k}{k!} e^{-(C_{RNA} \cdot N_A \cdot V_{liposome})} \quad (2.11)$$

Where C_{RNA} is the concentration of Spinach RNA.

$$P_{RNA}(X = 0) = e^{-(76 \cdot 10^{-6} \cdot 6.022 \cdot 10^{23} \cdot \frac{4}{3} \pi (100 \cdot 10^{-9})^3 \cdot 1000)} = 3.2 \cdot 10^{-10} \% = 0 \% \quad (2.12)$$

Therefore, the expected fraction of liposomes containing Spinach in the pre-synthesized sample is one. However, we hypothesize transcriptionally active fed-vesicles could potentially produce more RNA molecules per liposome because NTPs are continuously supplied from the environment and their exhaustion is unlikely given the large reservoir.

2.3.3. SPINACH RNA IS SUCCESSFULLY PRODUCED WITH A T7 IN VITRO TRANSCRIPTION SYSTEM IN BOTH COMMERCIAL AND HOMEMADE BUFFERS

In order to create a DNA template encoding a Spinach RNA aptamer, the Spinach DNA sequence was isolated by PCR from the fusion DNA construct encoding meYFP-Spinach. To make the aptamer transcribable by the T7 RNA polymerase, an overhanging Fw primer incorporating the T7 promoter sequence and a Rv primer encompassing the T7 terminator were used (Fig. 8a). As seen in Fig. 8b, a band corresponding in size to the expected amplified T7-Spinach(221) DNA fragment was obtained on an agarose gel. Next, the transcriptional ability of this construct was tested using a commercial T7 transcription buffer and a homemade T7 transcription buffer. As seen in Fig. 8c, similar Spinach RNA levels were produced from this construct with both buffers.

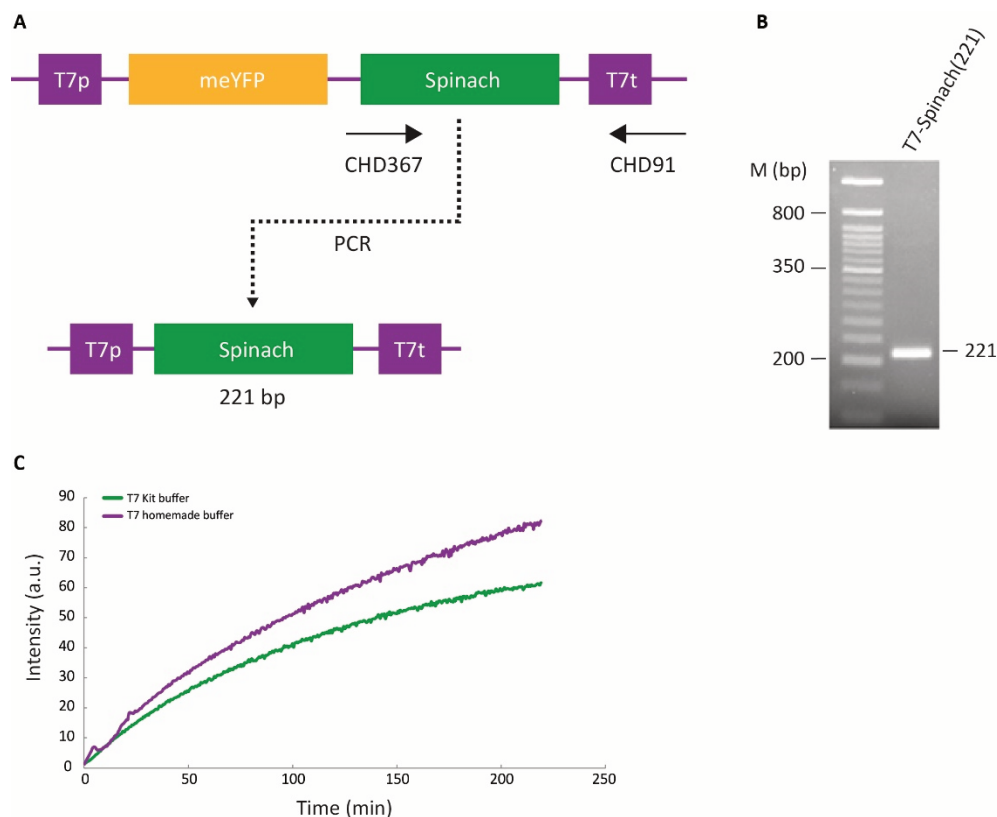


Fig. 8. A) DNA template encoding T7p-meYFP-Spinach-T7t and the isolated PCR product T7-Spinach(221) using primers CHD367 and CHD91 to isolate the Spinach aptamer encoding sequence. B) PCR amplification of T7-Spinach(221) DNA. M: DNA ladder. C) Time traces of Spinach fluorescence produced from T7-Spinach(221) (70 nM) with commercial T7 transcription buffer or homemade T7 transcription buffer.

2.3.4. α -HEMOLYSIN DOES NOT ENHANCE IN-VESICLE SPINACH TRANSCRIPTION.

First, the in-vesicle transcription of Spinach RNA inside SUVs in the presence of the membrane pore-forming protein α -hemolysin was investigated (Fig. 9). For this, liposomes co-encapsulating Spinach-encoding DNA and T7 RNA polymerase, were externally supplied with rNTPs and α -hemolysin, and incubated for three 3 h to trigger DNA transcription. Then, the Spinach and membrane dye fluorescence intensities of individual immobilized SUVs were analyzed at the single vesicle level by fluorescence microscopy (Fig. 9a-9b). Liposomes appeared as discrete diffraction-limited spots with a size lower than 1 μm and RNA-containing liposomes were identified as those where DFHBI-1T and membrane dye signal colocalized. As can be observed in Fig. 9a, Spinach RNA was successfully transcribed inside a small fraction of liposomes in the presence of α -hemolysin, in qualitative agreement with our theoretical calculations. Surprisingly, similar results were obtained for liposomes incubated in the absence of the pore-forming protein (Fig. 9a-9b), indicating that the vesicles were readily permeable for NTPs in its absence. Importantly, in both samples, about ~70% of the liposomes contained Spinach fluorescence intensities higher than the background signal (>200 a.u.) (Fig. 9d), suggesting a much larger fraction of RNA-expressing liposomes than theoretically expected. These results prompted us to study the potential of RNA-producing fed vesicle bioreactors in the absence of α -hemolysin.

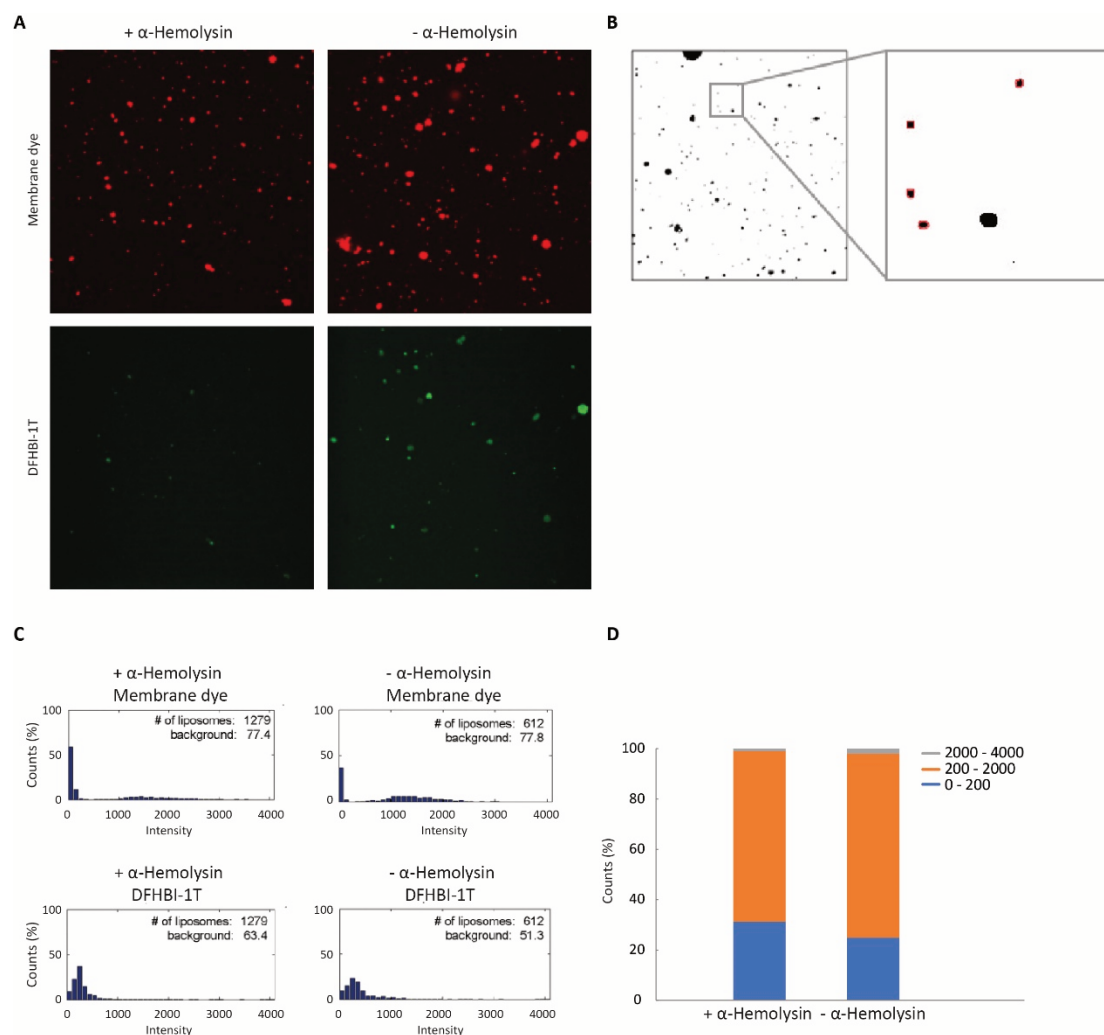


Fig. 9. Analysis of Spinach DNA transcription inside SUVs. A) Representative images of fluorescence confocal microscopy from SUVs incubated with or without α -hemolysin. Individual vesicles were tethered through a biotin-Neutravidin linker to a BSA-biotin passivated glass. B) Representative image of liposome selection in one field view using the membrane dye channel. Vesicles with sizes between 5 and 25 pixels were selected as SUVs (marked in red) for fluorescence intensity analysis. C) Histograms of membrane dye and Spinach fluorescence intensities from selected liposomes. D) Stacked bar charts of Spinach fluorescence intensities analyzed in the presence or absence of α -hemolysin.

2.3.5 IN-VESICLE TRANSCRIPTION DOES NOT LEAD TO LIPOSOMES WITH HIGHER RNA CONTENT IN COMPARISON WITH RNA PRE-LOADED LIPOSOMES

As described in Introduction 2.1, we hypothesized that a fed-vesicle bioreactor co-encapsulating a DNA template and an RNA polymerase, could, when continuously supplied with NTPs, reach a higher internal RNA concentration than that obtained inside liposomes by conventional RNA encapsulation. To investigate this hypothesis, the Spinach RNA content of both fed-vesicle bioreactors and RNA pre-loaded liposomes was analyzed at the single vesicle level by fluorescence microscopy. As shown in Fig. 10a, it is clear that conventional RNA encapsulation results in a higher fraction of RNA-containing liposomes than in-vesicle transcription (Fig. 10b), in agreement with theoretical predictions (see 2.3.1 and 2.3.2).

However, whereas 100% of the RNA pre-loaded liposomes are expected to contain Spinach RNA, evaluation of microscopy images shows that less than 50% of the liposomes exhibit Spinach fluorescence. Accordingly, from simple visual inspection of the microscopy images, the fraction of RNA-containing fed-vesicle bioreactors is considerably lower than the 16% theoretically expected. Aiming at an accurate quantitative characterization, we developed a MATLAB code that improves liposome selection and counting (see 2.2.10).

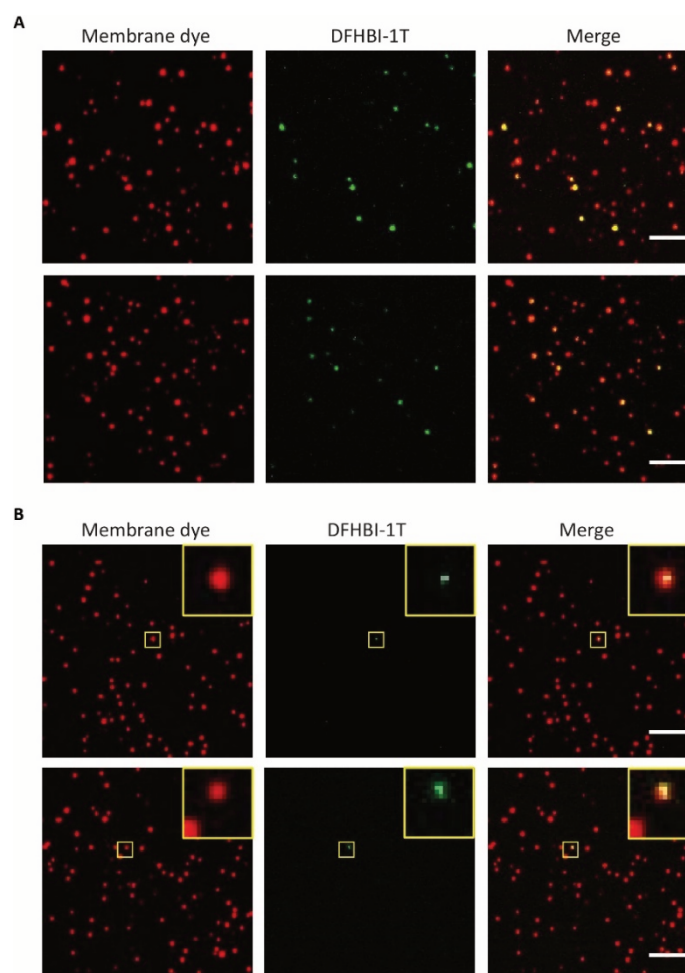


Fig. 10. Fluorescence confocal microscopy image of Spinach RNA in A) RNA pre-loaded liposomes and B) fed-vesicle bioreactors entrapping the T7-Spinach(221) DNA construct (scale bar: 5 μm).

To find optimal settings with respect to DFHBI-1T images, three 488-nm laser power values were used (Fig. 11a). The best acquisition setting was found to be LP10, as it offers the best compromise between signal-to-noise ratio, while minimizing the number of DFHBI-1T-saturating liposomes.

For each sample, liposome selection originated from multiple images. To discard large differences between images from a given sample due to focus variation during image acquisition, all liposomes from each field of view used for quantification were given a specific color. The scatterplots in Fig. 11b-11c verify that, in both types of sample, the scatterplots generated from different fields of view were identical.

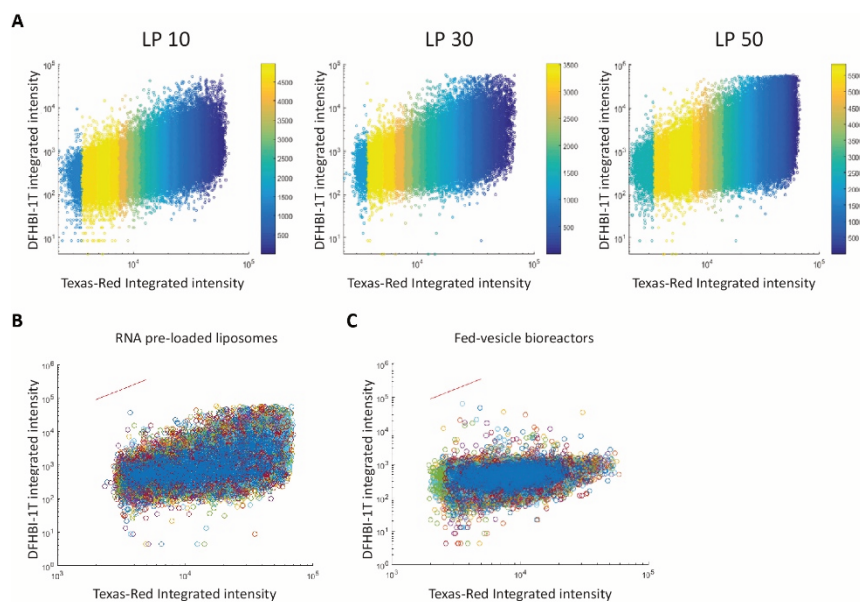


Fig. 11. A) Scatterplot representation of the membrane dye and DFHBI-1T fluorescence intensities obtained for three different DFHBI-1T laser powers (10, 30 and 50) for all selected liposomes in a sample of RNA pre-loaded liposomes; B) RNA pre-loaded liposomes (LP10) C) fed-vesicle bioreactors (LP10).

The distribution of membrane dye integrated intensities was similar in both samples encompassing nearly two orders of magnitude. In contrast, the distribution of DFHBI-1T integrated intensities covered a range of almost four orders of magnitude in RNA pre-loaded liposomes (Fig. 11b), but only two in fed-vesicle bioreactors (Fig. 11c), further indicating that higher Spinach concentrations are reached when pre-synthesized RNA is encapsulated in contrast to our prediction.

Following, we investigated the fraction of RNA-containing liposomes. To examine whether the fraction of RNA-loaded liposomes could be overestimated due to non-specific fluorescence in the DFHBI-1T channel, we performed a series of control experiments. Liposomes were prepared in the absence of RNA polymerase to avoid RNA production, allowing us to characterize the fluorescence signal that does not originate from the Spinach-DFHBI-1T complex. As shown in Fig. 12a-12b, a similarly large apparent fraction of RNA-containing liposomes was obtained in these liposomes in comparison with both types of sample, demonstrating that background signal actually dominates.

While no specific signal could be measured in samples with in-vesicle produced RNA, the DFHBI-1T fluorescence histogram for the RNA pre-loaded liposome samples exhibits a long-tail to higher intensity values that we attribute to encapsulated Spinach RNA. To determine the actual fraction of RNA-loaded liposomes, a Gaussian fit (red line) was applied to the histogram from liposomes where no RNA was produced. The resulting $\mu+2\sigma$ value was used as the threshold between empty liposomes and RNA-containing liposomes in both types of liposome samples, reducing the probability of mistakenly classifying an empty liposome as an RNA-containing liposome to less than 2.5%.

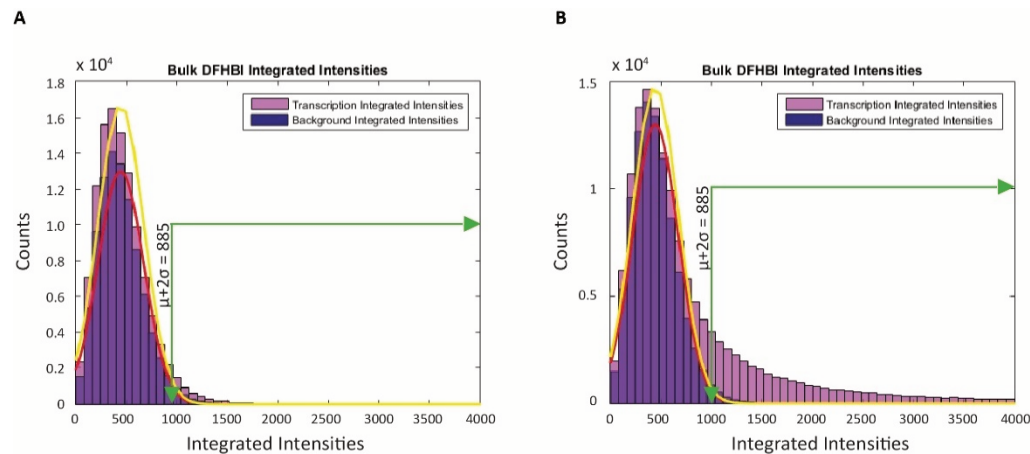


Fig. 12. Histograms of DFHBI-1T integrated fluorescence intensities in A) fed-vesicle bioreactors or B) RNA pre-loaded liposomes with a background liposome sample (bin size of 83.5 a.u.). The Gaussian fits of each histogram are shown with a red line for background liposomes and with a yellow line for fed-vesicle bioreactors and RNA pre-loaded liposomes.

After applying this threshold to all analyzed liposomes, we were able to determine the percentages of Spinach-containing liposomes in both RNA pre-loaded liposomes and fed-vesicle bioreactor samples. As indicated in Fig. 13a-13b, about ~35% of RNA pre-loaded liposomes contained Spinach RNA, while only ~2% of fed-vesicle bioreactors did.

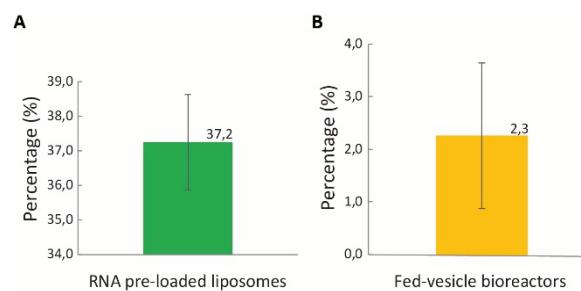


Fig. 13. Percentages of A) RNA pre-loaded liposomes (LP10) or B) fed-vesicle bioreactors (LP10) containing Spinach RNA determined after background correction. Error bars indicate the averages of three independent experiments.

Finally, we determined the fraction of liposomes containing high Spinach RNA concentrations with respect to the total amount of liposomes detected. For one pixel, we chose an arbitrary threshold at 3000 a.u. fluorescence integrated intensities (Fig. 14a-14b), and found that 6% of RNA pre-loaded liposomes contain high Spinach RNA concentrations while only a negligible percentage of fed-vesicle bioreactors do. Altogether, these results reject our working hypothesis, in which we envisioned that fed-vesicle bioreactors could achieve higher Spinach RNA concentrations compared to liposomes prepared by conventional RNA encapsulation.

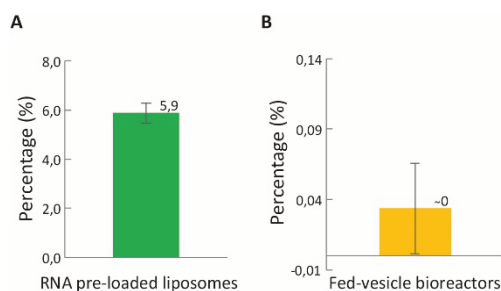


Fig. 14. Fraction of A) RNA pre-loaded liposomes (LP10) or B) fed-vesicle bioreactors (LP10) with high Spinach RNA content determined after background correction. Error bars indicate the averages of three independent experiments.

2.4 DISCUSSION

With the purpose of assembling a high-yielding RNA-producing fed-vesicle bioreactor, we intended to incorporate α -hemolysin pores to our membrane to enable efficient supply of NTPs provided in the external medium (Fig. 9). Our results suggest that, contrary to our expectations, the lipid membrane was permeable to rNTPs in the absence of nanopores (Fig. 9b), in non-osmotically stressing conditions and at a temperature (37 °C) far above the phase transition temperature of the lipids (DMPC = 23 °C, DMPG = 24 °C). Several factors might have been responsible for this unexpected membrane permeability.

First, incorporation of cholesterol in the lipid bilayer is known to influence membrane fluidity, increasing it at temperatures under the T_m , and decreasing it at temperatures over the T_m , thus abolishing the sharp phase transition temperature of the bilayer [34, 35]. Because our lipid formulation contains ~16 mol% of cholesterol, liposomes might be permeable to rNTPs even at temperatures above 23 °C. In this context, perhaps a small temperature decrease provoked by the addition of rNTPs to trigger transcription, might have shortly lowered the temperature a few degrees, inducing a very brief period of membrane permeability enabling diffusion of rNTPs into the liposome's lumen. To address this point, the T_m of fed-vesicle bioreactors should be determined, for instance using a calcein efflux assay or by calorimetry.

A second possible cause for intrinsic membrane permeability is an osmotic pressure. If particularly high concentrations of RNA polymerase or DNA occur in some liposomes [24, 36], the higher internal osmolarity may generate transient defects in the membrane.

Another factor that may have made the liposomes permeable to rNTPs is the presence of hydrophobic mismatch in the lipid bilayer. Hydrophobic mismatch is generally defined as the mismatch arising from the difference in the length of the hydrophobic segments from a transmembrane protein with respect to the lipid bilayer it spans. Consequently, both the peptide and the membrane suffer structural changes, including membrane deformation [37]. Though the effects of hydrophobic mismatches between two lipids of different length on bilayer permeability have been less characterized than the influence on membrane deformation, we

hypothesize that defects may arise making the lipid bilayer permeable to rNTPs. Though the largest fraction of lipids in the formulations used for this study consisted of short C14 chain phospholipids (DMPC, DMPG), a small fraction of C18 chain phospholipids (DSPE-PEG(2000)-biotin) and C16 phospholipids (DHPE-TexasRed) was present in the lipid formulation. This small fraction might have been enough to induce a certain level of membrane permeability through hydrophobic mismatch. Additionally, membrane curvature is known to generate lipid-packing defects [38]. Together with hydrophobic mismatches, these packing defects inherent to highly curved membranes may have enhanced membrane permeability. Importantly, the fact that most lipids in the composition have short C14 acyl chains may have contributed to the occurrence of the higher membrane permeability compared for instance with full C16 or C18 bilayers.

Moreover, our results suggest that α -hemolysin incorporation did not further enhance the permeability of liposomes (Fig. 9d). However, in this study, the formation of α -hemolysin pores was not confirmed. α -hemolysin can form membrane pores at extraordinarily low concentrations. Moreover, these pores are stable and do not induce membrane destabilization [1, 9]. Thus, the high molar excess of α -hemolysin with respect to the liposomes (~450 fold), was assumed to conclude on optimal pore formation.

Importantly, the formation of α -hemolysin pores depends on the lipid composition of the membrane [39], where choline-containing phospholipids are necessary for the establishment of the protein-membrane interaction and cholesterol facilitates the interaction. In this work, the choline-containing phospholipid DMPC represents ~66% of the total molar percentage, while cholesterol represents ~16%. Thus, according to the mentioned study, our lipid formulation should be favorable for the optimal formation of α -hemolysin pores. However, other factors related to the properties of our liposomes may have impeded the formation of α -hemolysin pores. A recent study in GUVs of various sizes (1-10 μm diameter), demonstrated that α -hemolysin nanopore assembly is curvature-dependent, decreasing as membrane curvature increases [40]. Thus, it is reasonable to hypothesize that the high membrane curvature of the fed-SUV reactors may have hampered the formation of α -hemolysin pores. Finally, a possible inhibitory effect may result from membrane pegylation.

Altogether, confirming the formation of α -hemolysin pores onto the membrane of our fed-vesicle bioreactors is of most importance. For this, the α -hemolysin protein can be fused through its C-terminus to the reporter protein eGFP, to visualize and quantify pore formation in the liposomes by fluorescence microscopy, as already done by Noireaux & Libchaber [1]. Further, to confirm that incorporation of α -hemolysin into the membrane leads for the formation of functional nanopores, fluorescence leakage assays can be performed using membrane-impermeable fluorescent probes that are smaller than α -hemolysin's pore size. Calcein (622 Da), a dye that self-quenches at high concentrations, has been successfully used for this purpose [41, 42]. An alternative scenario is to consider that the limiting factor for

transcription is not the amount of rNTPs but the activity of the T7 RNA polymerase or the stability of DNA. Hence, improving permeability would not increase the yield of RNA production.

The results from this study show that, unlike our initial hypothesis, transcription in fed-vesicle bioreactors (Fig. 14b) does not yield liposomes with enriched RNA concentrations compared to RNA pre-loaded liposomes (Fig. 14a). Further investigations are required to determine what step in the whole process is limiting: partial inactivation of components, diffusion of rNTPs across the membrane, amount of DNA:RNA polymerase complexes in liposomes or accumulation of pyrophosphate, that can inhibit transcription at the elongation step [43].

Moreover, low percentages of RNA-containing liposomes are found for RNA pre-loaded liposomes (Fig. 13a) and fed-vesicle bioreactors (Fig. 13b) compared to predicted values assuming a Poisson distribution. Several factors may contribute to this deviation. First, RNA encapsulation might not follow a classical statistic Poisson distribution. Instead, anomalous encapsulation may occur, such as spontaneous crowding observed by Lohse et al. [23] and Luisi et al. [24]. The same crowding effect might govern the encapsulation of DNA and T7 RNA polymerase in fed-vesicle bioreactors. Moreover, RNA encapsulation in the case of RNA pre-loaded liposomes and DNA encapsulation in that of fed-vesicle bioreactors might have been partially inhibited due to the presence of negatively charged lipids (DMPG) [27]. In this regard, the implementation of a completely neutral liposome composition could be evaluated to improve RNA or DNA encapsulation. Neutral formulations already known to allow in vesicle gene expression should be evaluated such as DPPC:CHOL:DOPE-Rhod (13:6:1 molar ratio) [44] or complete DOPC [29] should be evaluated. Moreover, the investigation of RNA expression in liposomes composed by DOPC:DOPE (75:25 molar ratio) could be considered, since this formulation is used in two out of the fifteen liposome formulations currently marketed, that encapsulate inactivated viral antigens [45].

Until recently, flow cytometry systems could not characterize vesicles with a diameter <300 nm [46]. However, a novel flow-cytometry-based set-up developed by Hoen et al. [47], allows detection of fluorescent nanoparticles of 100 nm and 200 nm in diameter. Using this system, we were able to detect empty fluorescently labelled liposomes of 200 nm and 800 nm in diameter (data not shown). In combination with sorting, this flow-cytometry system could allow us to develop a homogeneous drug delivery system based on highly RNA-loaded liposomes.

2.5 CONCLUSIONS

In conclusion, we have given the first steps towards the assembly of highly yielding RNA-producing liposomes. Different aspects need to be further characterized to address the limitations of our current formulation in order to achieve this. Alternative lipid formulations should be explored. Neutral lipid formulations should be a priority. The use of α -hemolysin in future formulations should be re-considered, and confirming nanopore formation in each

formulation should be the first key step before discarding its use. Further, our method for single vesicle analysis shows that liposome encapsulation is highly heterogenous and remarks the importance of high-throughput single-vesicle characterization within preparations. Key improvements can be made on this method that allow the precise size determination of all analyzed vesicles, and the automatic background subtraction during image analysis based on the findings from this study. This method should be used to study how RNA content and liposome volume relate to each other. The outcomes from this study may allow us to better understand the processes behind the heterogeneity in RNA content observed, confirming whether RNA encapsulation follows a Poisson distribution, and whether a confinement effect or a crowding effect take place in these preparations. Finally, a sorting platform should be implemented for the selection of highly yielding RNA-producing liposomes.

2.6 SUPPLEMENTARY INFORMATION

```
GGGAGAAAGCUUCCCGGGAAAGUAUAUAUGAGUAAAGAUUAUCGACGCAACUGA
AUGAAAUGGUGAAGGACGGGUCCAGGUGUGGCUGCUUCGGCAGUGCAGCUUGU
UGAGUAGAGUGUGAGCUCCGUAACUAGUCGCGUCGAUAUCCCCGGGCUAGCAU
AACCCCUUGGGGCCUCUAAACGGGUCU UGAGGGGUUUUUUG
```

Fig. S1. RNA sequence (5' → 3') of Spinach RNA aptamer transcribed from the DNA template T7-Spinach(221).

2.7 ACKNOWLEDGEMENTS

We thank Gabriella Tany and Robin van Albada for their contribution to this project. Thank you Anne for implementing our the Matlab codes used to analyze immobilized liposome samples. Thanks Pauline for useful discussions and kind advices concerning Spinach. Thank you Jeremy, for your kind help with confocal microscopy.

2.8 REFERENCES

- [1] V. Noireaux and A. Libchaber, "A vesicle bioreactor as a step toward an artificial cell assembly.," *Proceedings of the National Academy of Sciences of the United States of America*, vol. 101, no. 51, pp. 17669–74, Dec. 2004.
- [2] Z. Nourian, W. Roelofsen, and C. Danelon, "Triggered Gene Expression in Fed-Vesicle Microreactors with a Multifunctional Membrane," *Angew. Chem. Int. Ed*, vol. 51, pp. 3114–3118, Jan. 2012.
- [3] M. Chamberlin and J. Ring, "Characterization of T7-specific ribonucleic acid polymerase," *The Journal of biological chemistry*, vol. 248, no. March 25, pp. 2235–2244, 1973.
- [4] F. W. Studier and A. B. Moffatt, "Use of bacteriophage T7 RNA polymerase to direct selective high-level expression of cloned genes," *J. Mol. Biol.*, vol. 189, pp. 113–130, 1985.
- [5] C. Chiarabelli, P. Stano, and P. L. Luisi, "Chemical synthetic biology: A mini-review," *Frontiers in Microbiology*, vol. 4, no. SEP, pp. 1–7, 2013.
- [6] Y. Shimizu *et al.*, "Cell-free translation reconstituted with purified components.," *Nature biotechnology*, vol. 19, no. 8, pp. 751–5, Aug. 2001.
- [7] D. A. Chambers and G. Zubay, "The Stimulatory Effect of Cyclic Adenosine 3'5'-monophosphate on DNA-Directed Synthesis of -galactosidase in a Cell-Free System," *Proceedings of the National Academy of Sciences*, vol. 63, no. 1, pp. 118–122, 1969.
- [8] S. M. Nomura, K. Tsumoto, T. Hamada, K. Akiyoshi, Y. Nakatani, and K. Yoshikawa, "Gene expression within cell-sized lipid vesicles.," *Chembiochem*, vol. 4, no. 11, pp. 1172–5, Nov. 2003.
- [9] L. Song, M. R. Hobaugh, C. Shustak, S. Cheley, H. Bayley, and J. E. Gouaux, "Structure of staphylococcal alpha-hemolysin, a heptameric transmembrane pore," *Science*, vol. 274, no. December, pp. 1859–1865, 1996.
- [10] T. Sunami, K. Sato, T. Matsuura, K. Tsukada, I. Urabe, and T. Yomo, "Femtoliter compartment in liposomes for in vitro selection of proteins," *Analytical Biochemistry*, vol. 357, no. 1, pp. 128–136, 2006.
- [11] R. Van Der Meel, M. H. a. M. Fens, P. Vader, W. W. Van Solinge, O. Eniola-Adefeso, and R. M. Schiffelers, "Extracellular vesicles as drug delivery systems: Lessons from the liposome field," *Journal of Controlled Release*, vol. 195, pp. 72–85, 2014.
- [12] S. M. Christensen and D. G. Stamou, "Sensing-applications of surface-based single vesicle arrays," *Sensors*, vol. 10, no. 12, pp. 11352–11368, 2010.
- [13] D. Stamou, C. Duschl, E. Delamarche, and H. Vogel, "Self-Assembled Microarrays of Attoliter Molecular Vessels," *Angewandte Chemie - International Edition*, vol. 42, no. 45, pp. 5580–5583, 2003.

- [14] M. González, C. E. Argaraña, and G. D. Fidelio, “Extremely high thermal stability of streptavidin and avidin upon biotin binding,” *Biomolecular Engineering*, vol. 16, no. 1–4, pp. 67–72, 1999.
- [15] S. R. Tabaei, M. Rabe, V. P. Zhdanov, N. J. Cho, and F. Höök, “Single vesicle analysis reveals nanoscale membrane curvature selective pore formation in lipid membranes by an antiviral α -helical peptide,” *Nano Letters*, vol. 12, no. 11, pp. 5719–5725, 2012.
- [16] A. Tonnesen, S. M. Christensen, V. Tkach, and D. Stamou, “Geometrical Membrane Curvature as an Allosteric Regulator of Membrane Protein Structure and Function,” *Biophysical Journal*, vol. 106, no. 1, pp. 201–209, 2014.
- [17] M. B. Jensen *et al.*, “Membrane curvature sensing by amphipathic helices: A single liposome study using α -synuclein and annexin B12,” *Journal of Biological Chemistry*, vol. 286, no. 49, pp. 42603–42614, 2011.
- [18] V. K. Bhatia *et al.*, “Amphipathic motifs in BAR domains are essential for membrane curvature sensing,” *EMBO Journal*, vol. 28, no. 21, pp. 3303–3314, 2009.
- [19] Z. Nourian and C. Danelon, “Linking genotype and phenotype in protein synthesizing liposomes with external supply of resources,” *ACS Synthetic Biology*, vol. 2, no. 4, 2013.
- [20] P. van Nies *et al.*, “Unbiased tracking of the progression of mRNA and protein synthesis in bulk and in liposome-confined reactions,” *ChemBioChem: a European journal of chemical biology*, vol. 14, no. 15, pp. 1963–6, Oct. 2013.
- [21] P. Van Nies, A. S. Canton, Z. Nourian, and C. Danelon, *Monitoring mRNA and protein levels in bulk and in model vesicle-based artificial cells*, vol. 550. 2015.
- [22] P. Y. Bolinger, D. Stamou, and H. Vogel, “An integrated self-assembled nanofluidic system for controlled biological chemistries,” *Angewandte Chemie - International Edition*, vol. 47, no. 30, pp. 5544–5549, 2008.
- [23] B. Lohse, P. Y. Bolinger, and D. Stamou, “Encapsulation efficiency measured on single small unilamellar vesicles,” *Journal of the American Chemical Society*, vol. 130, no. 44, pp. 14372–14373, 2008.
- [24] P. L. Luisi, M. Allegretti, T. P. De Souza, F. Steiniger, A. Fahr, and P. Stano, “Spontaneous protein crowding in liposomes: A new vista for the origin of cellular metabolism,” *ChemBioChem*, vol. 11, no. 14, pp. 1989–1992, 2010.
- [25] J. S. Paige, K. Y. Wu, and S. R. Jaffrey, “RNA mimics of green fluorescent protein,” *Science (New York, N.Y.)*, vol. 333, no. 6042, pp. 642–6, Jul. 2011.
- [26] W. Song, R. L. Strack, N. Svensen, and S. R. Jaffrey, “Plug-and-Play Fluorophores Extend the Spectral Properties of Spinach,” *Journal of the American Chemical Society*, vol. 136, no. 4, pp. 1198–201, Jan. 2014.
- [27] T. Sunami, K. Hosoda, H. Suzuki, T. Matsuura, and T. Yomo, “Cellular compartment

- model for exploring the effect of the lipidic membrane on the kinetics of encapsulated biochemical reactions.,” *Langmuir : the ACS journal of surfaces and colloids*, vol. 26, pp. 8544–8551, 2010.
- [28] H. T. Bui, H. Umakoshi, K. X. Ngo, M. Nishida, T. Shimanouchi, and R. Kuboi, “Liposome membrane itself can affect gene expression in the Escherichia coli cell-free translation system,” *Langmuir*, vol. 24, no. 19, pp. 10537–10542, 2008.
- [29] Z. Nourian, W. Roelofsen, and C. Danelon, “Triggered gene expression in fed-vesicle microreactors with a multifunctional membrane,” *Angewandte Chemie - International Edition*, vol. 51, no. 13, 2012.
- [30] Dewald Esterhuizen, “Laplacian of Gaussian | Software by Default,” 2018-05-11, 2013. [Online]. Available: <https://softwarebydefault.com/tag/laplacian-of-gaussian/>. [Accessed: 30-Dec-2018].
- [31] E. Arias-Castro and D. L. Donoho, “Does median filtering truly preserve edges better than linear filtering?,” *Annals of Statistics*, vol. 37, no. 3, pp. 1172–1206, 2009.
- [32] S. Veshaguri *et al.*, “Direct observation of proton pumping by a eukaryotic P-type ATPase,” *Science*, vol. 351, no. 6280, pp. 1469–1473, 2016.
- [33] S. M. Anthony and S. Granick, “Image analysis with rapid and accurate two-dimensional Gaussian fitting,” *Langmuir*, vol. 25, no. 14, pp. 8152–8160, 2009.
- [34] M. Bloom, E. Evans, and O. G. Mouritsen, “Physical Properties of Fluid Lipid-Bilayer Component of Cell Membrane: a Perspective,” *Quarterly Reviews of Biophysics*, vol. 24, no. 3, pp. 293–397, 1991.
- [35] D. Papahadjopoulos, K. Jacobson, and T. Isac, “Phase transitions in phospholipid vesicles,” *Biochimica et biophysica acta*, vol. 311, pp. 330–348, 1973.
- [36] T. P. de Souza, A. Fahr, P. L. Luisi, and P. Stano, “Spontaneous Encapsulation and Concentration of Biological Macromolecules in Liposomes: An Intriguing Phenomenon and Its Relevance in Origins of Life.,” *Journal of molecular evolution*, pp. 179–192, Nov. 2014.
- [37] A. J. De Jesus and T. W. Allen, “The determinants of hydrophobic mismatch response for transmembrane helices,” *Biochimica et Biophysica Acta - Biomembranes*, vol. 1828, no. 2, pp. 851–863, 2013.
- [38] J. Bigay and B. Antonny, “Curvature, Lipid Packing, and Electrostatics of Membrane Organelles: Defining Cellular Territories in Determining Specificity,” *Developmental Cell*, vol. 23, no. 5, pp. 886–895, 2012.
- [39] M. Watanabe, T. Tomita, and T. Yasuda, “Membrane-damaging action of staphylococcal alpha-toxin on phospholipid-cholesterol liposomes,” *BBA - Biomembranes*, vol. 898, no. 3, pp. 257–265, 1987.

- [40] S. Fujii, T. Matsuura, and T. Yomo, "In vitro directed evolution of alpha-hemolysin by liposome display," *Biophysics*, vol. 11, no. 0, pp. 67–72, 2015.
- [41] C. L. Bashford *et al.*, "Pore Formation by *S. aureus* α -toxin in Liposomes and Planar Lipid Bilayers: Effects of Nonelectrolytes," *Membrane biology*, vol. 150, pp. 37–45, 1996.
- [42] G. Menestrina, C. L. Bashford, and C. A. Pasternak, "Pore-forming toxins: Experiments with *S. aureus* α -toxin, *C. perfringens* θ -toxin and *E. coli* haemolysin in lipid bilayers, liposomes and intact cells," *Toxicon*, vol. 28, no. 5, pp. 477–491, 1990.
- [43] K. H. Seifart, P. P. Juhasz, and B. J. Benecke, "A Protein Factor from Rat-Liver Tissue Enhancing the Transcription of Native Templates by Homologous RNA Polymerase B," *European Journal of Biochemistry*, vol. 33, no. 1, pp. 181–191, 1973.
- [44] S. Lee *et al.*, "DNA Amplification in Neutral Liposomes for Safe and Efficient Gene Delivery," no. 5, pp. 4257–4267, 2014.
- [45] U. Bulbake, S. Doppalapudi, N. Kommineni, and W. Khan, "Liposomal formulations in clinical use: An updated review," *Pharmaceutics*, vol. 9, no. 2, pp. 1–33, 2017.
- [46] H. B. Steen, "Flow cytometer for measurement of the light scattering of viral and other submicroscopic particles," *Cytometry*, vol. 57A, no. 2, pp. 94–99, 2004.
- [47] E. N. M. N. T. Hoen *et al.*, "Quantitative and qualitative flow cytometric analysis of nanosized cell-derived membrane vesicles," *Nanomedicine: Nanotechnology, Biology, and Medicine*, vol. 8, no. 5, pp. 712–720, 2012.

3.

DEVELOPING AN OPTOGENETIC SWITCH FOR THE SPATIOTEMPORAL CONTROL OF THERAPEUTIC RNA PRODUCTION IN SMALL VESICLES

Despite the remarkable advances in targeted liposomal delivery systems during the last decades, the precise biodistribution of a therapeutic molecule is still limited by factors such as premature drug release or degradation. The implementation of delivery systems with stimuli-responsive ability can improve the biodistribution profile of a drug and even allow its delivery on demand. Optogenetic tools are particularly interesting due to their non-invasive nature and their high spatiotemporal precision. Here, the assembly of a light-inducible RNA-producing vesicle bioreactor was attempted. A light-activated T7 promoter (LA-T7) based on a photocleavable linker between chemically modified nucleotides in the promoter region and a bulky protein that inhibits the docking of the T7 RNA polymerase, was prepared and characterized by high-performance liquid chromatography. The LA-T7 promoter was incorporated into a Spinach-encoding DNA template (LA-Spinach DNA). Light-inducible Spinach RNA production was demonstrated in bulk by monitoring the Spinach fluorescence. However, leaky expression in the off state impeded the realization of light-activated Spinach RNA production in vesicle bioreactors. The remaining steps for the assembly of a fully repressed LA-Spinach are described in this work. Moreover, the potentials of alternative optogenetic systems to control the production and delivery of therapeutic RNA molecules are discussed.

3.1 INTRODUCTION

An ideal drug delivery system could be defined as that in which a drug agent is: (i) encapsulated in a delivery carrier; (ii) introduced into the human body with minimal distress; (iii) transported to a targeted location avoiding harm to the neighboring tissue or organs; and (iv) released only at the targeted site with a controlled concentration-time delivery profile [1].

Regarding the latter, the implementation of targeting devices with stimuli-responsive capability can enable on-demand drug delivery [2]. Two main types of triggered drug release from liposomes have been explored [2, 3]: physiology-dependent triggers such as pH [4] or enzymes [5], and external-stimuli dependent triggers such as light [6, 7], heat [8], magnetism [9] and ultrasound [10, 11].

Physiology-based drug release strategies are highly affected by the heterogeneity of cells, tissue types, and microenvironments. Remotely controlled delivery systems, on the contrary, have the merit of being unaffected by these factors, thus overcoming these limitations [12]. Among these, light has emerged during the last decade as external regulator for biological systems due to its precise spatiotemporal resolution and minimal invasiveness [13].

3.1.1 LIGHT-ACTIVATED PRODUCTION OF GENE-ENCODED THERAPEUTIC MOLECULES IN LIPOSOMES

A further innovation for the creation of an on-demand delivery system involves merging the fields of synthetic biology and drug delivery to create a therapeutic nanofactory that synthesizes a drug in-situ in the patient's body as a response to a physiological or an external stimulus from inert precursors.

We, in particular, were interested in the assembly of a nanofactory with light-regulated production of gene-encoded therapeutic molecules, such as siRNA. Different optogenetic systems have been developed during the last years to control different cellular processes. Two main engineering approaches for the construction of an optically regulated gene or "optogen" have been used: one based on chemical modifications, the other on photoresponsive proteins. The earlier relies on the chemical incorporation of small light-sensitive moieties such as UV-responsive nitrobenzyl groups to a molecular element essential for gene expression.

Several studies have reported strategies for the development of light-triggered gene-expressing liposomes [14–16]. These systems were engineered using chemical modifications as optogenetic tool onto the bacteriophage T7 expression system.

In 2012, Schroeder et al. [14] developed liposomes controllably triggered by light to synthesize proteins. For this, liposomes with sizes between 170 nm and 15 μm were filled with a circular DNA caged by a photolabile protecting group and the cellular machinery responsible for transcription and translation. DNA strands were caged by phosphate esterification with 1-(4,5-

dimethoxy-2-nitrophenyl) diazoethane (DMNPE) and uncaged with UV irradiation at 365 nm, enabling transcription and subsequent protein synthesis (Fig. 1).

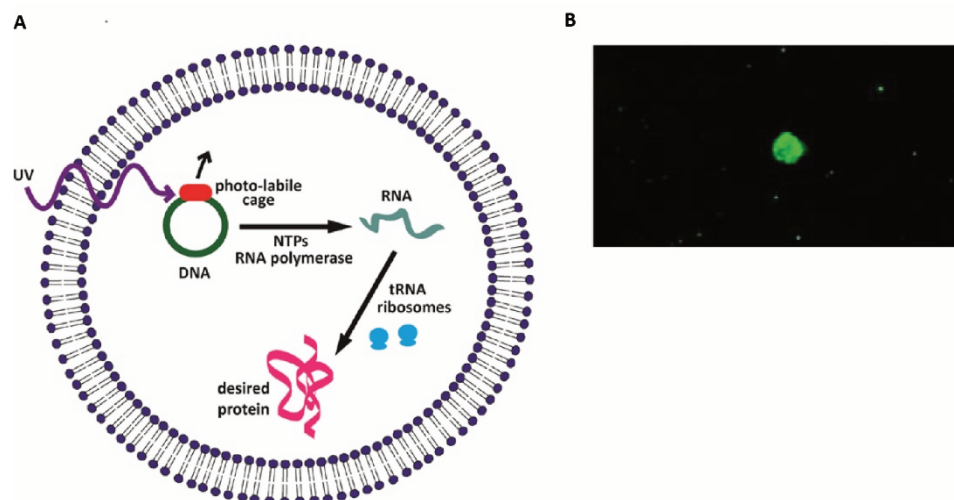


Fig. 1. Protein synthesizing particles. A) Scheme of a liposome loaded with an in vitro transcription and translation machinery. DNA, tRNA, ribosomes, amino acids, rNTPs and ions were encapsulated. B) Confocal image of light-triggered GFP-expression inside a vesicle, taken from [14].

A similar strategy was adopted by Chan et al. [15]. They developed light-inducible mRNA-synthesizing liposomes with an average size of 220 nm, by encapsulating a linear DNA and all the components for RNA production, where one of the ribonucleotides, ATP, was photocaged by esterification of the terminal phosphate with a blocking group. As in Schroeder et al. [14], UV illumination at 360 nm photolysed the caging group and rendered ATP available for DNA transcription. This study demonstrated the light-triggered in-situ transcription of an mRNA inside liposomes internalized by anucleated cells (platelets) (Fig. 2).

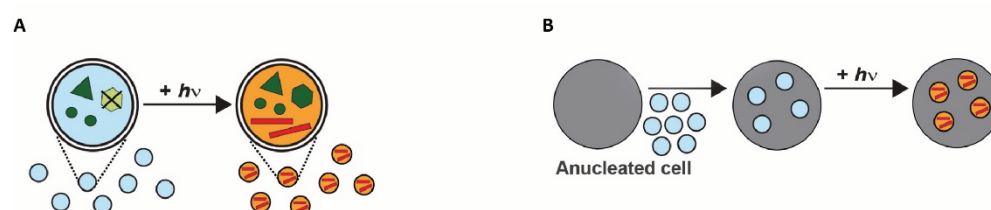


Fig. 2. A) Transcriptional components (dark green), including caged-ATP (light green), were encapsulated inside liposomes (light blue and orange). Upon irradiation, liposomes synthesized RNA (red lines). B) RNA-expressing liposomes allow transcription in anucleated cells [15].

An alternative strategy was adopted by Booth et al. [16], who developed a light-activated (LA) T7 DNA promoter to control gene expression of a fluorescent protein inside water in oil droplets around 100 μm in diameter (Fig. 3). The promoter was designed in such a manner that it could be placed upstream of any gene of interest. For its construction, seven C6-aminodT-modified nucleotides were incorporated across a single-stranded (ss) T7 promoter DNA

sequence (Fig. 3a). The amino-modified bases were then covalently attached to small biotin molecules modified with a photocleavable (PC) 2-nitrobenzyl ester linker. The position of the amine modifications was designed such that when the modified promoter would be used as primer for PCR amplification of a gene of interest, the PC-biotin moieties would protrude from the major groove at the T7 polymerase binding site. After PCR amplification, the creation of the LA-DNA was accomplished by attaching each biotin in the T7 promoter of the double-stranded DNA PCR product to a single monovalent streptavidin protein, which has a high affinity for biotin ($K_D \sim 10^{-14}$ M), similar to that of wild-type streptavidin ($K_D \sim 10^{-15}$ M) [17, 18]. Thanks to its large size, streptavidin acts as sterical blocker of the modified promoter, preventing RNA polymerase from binding and inhibiting transcription. Low-energy 365-nm ultraviolet (UV) irradiation allowed rapid and efficient cleavage of the 2-nitrobenzyl PC-linker, enabling access of RNA polymerase to the promoter and consequent activation of protein expression (Fig. 3b). Importantly, this promoter had a tightly regulated off-state, with negligible RNA transcription and protein expression prior to UV activation (Fig. 3c).

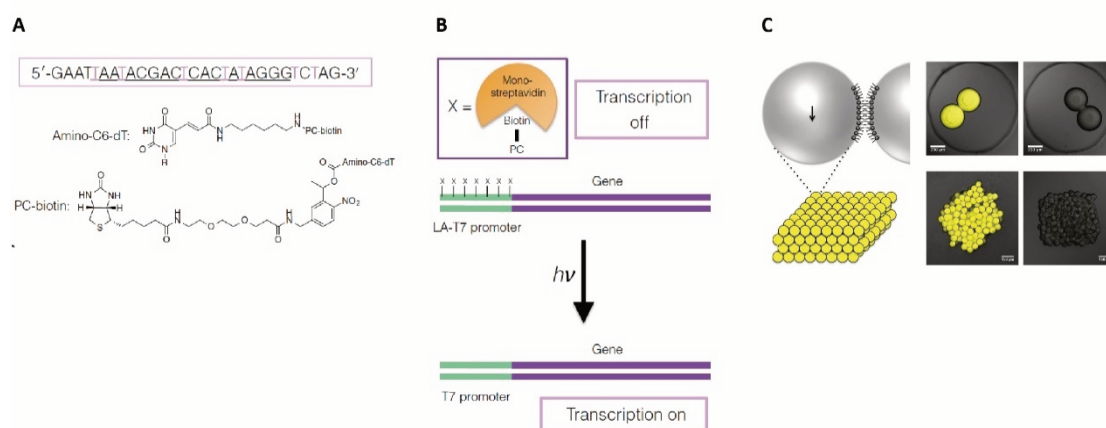


Fig. 3. Scheme of the construction of the T7 light-activated promoter. A) Amino modified T7 promoter sequence with amino-C6-dT modifications (pink) and chemical structures of the amino-C6-dT and PC-biotin groups. B) Mechanism of the LA-T7 technology. C) Light-activated expression of LA-mVenus protein in water-in-oil droplets. Taken from [16].

3.1.2 IN-SITU DRUG SYNTHESIS IN NANOCARRIERS NOURISHED BY THEIR SURROUNDING ENVIRONMENT

The ability of liposomes to interact with their environment and exchange nutrients by diffusion is an important step in the development of future therapeutic nanocarriers.

A recent study from Krinsky et al. [19] showed how therapeutic proteins can be produced inside micron-sized (median 2 μ m) liposomes that source nucleotides and amino acids from their outer environment in cell-free reactions (Fig. 4a-4b). Further, they demonstrated that liposomes with the same lipid composition, but encapsulating the whole machinery and nutrients for in vitro transcription and translation (IVTT), produced therapeutic proteins in-

situ in cultured cancer cells (Fig. 4c) and inside tumors in vivo. Their next step should be achieving in-vesicle protein production in-situ in cultured cells and in vivo using the external environment as sole nutrient supplier.

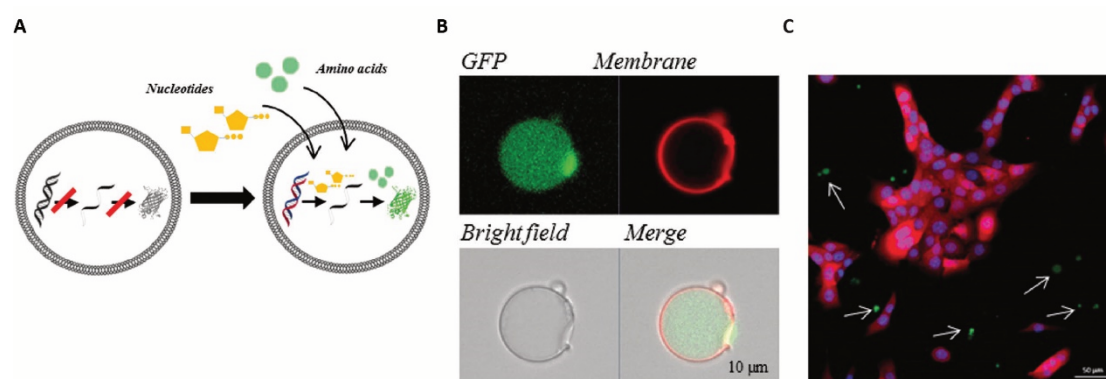


Fig. 4. A) Scheme and B) confocal microscopy images of in-vesicle cell-free expression of GFP, sourcing amino acids and nucleotides from their surrounding environment. C) Confocal microscopy image of the therapeutic *Pseudomonas* exotoxin A (PE)-producing liposomes in 4T1 breast cancer cells expressing a reporter mCherry gene, taken from [19]. PE-producing particles encapsulated the whole in vitro transcription and translation machinery (IVTT), and were kept in ice to avoid the start of protein expression until their addition to cells.

In the future, systems that can source nutrients from their surrounding environment could prolong the production of therapeutic compounds in situ. More importantly, such ability is a milestone for the development of on-demand nanoparticles, capable of controlled production and direct administration to the disease site when and where their function is required. Such platforms hold also potential for the development of personalized therapeutics.

3.1.3. ADAPTING THE T7 LA-DNA TECHNOLOGY FOR TRIGGERED IN-SITU PRODUCTION OF THERAPEUTIC SIRNA IN LIPOSOMES

We set out to adapt the T7 LA-DNA technology described above for the engineering of a remotely-activated 200-nm liposome bioreactor that produces therapeutic RNA sourcing nutrients by diffusion from its environment. As a proof of principle, we implemented the Spinach technology used in Chapter 2 with the LA-T7 promoter, allowing us to report light-triggered transcription through fluorescence. For this, the modified promoter was incorporated upstream of a Spinach DNA construct, encoding the Spinach RNA aptamer that is able to bind DFHBI-1T (Fig. 5). Tetravalent NeutrAvidin was used instead of monovalent streptavidin for the assembly of the caged DNA.

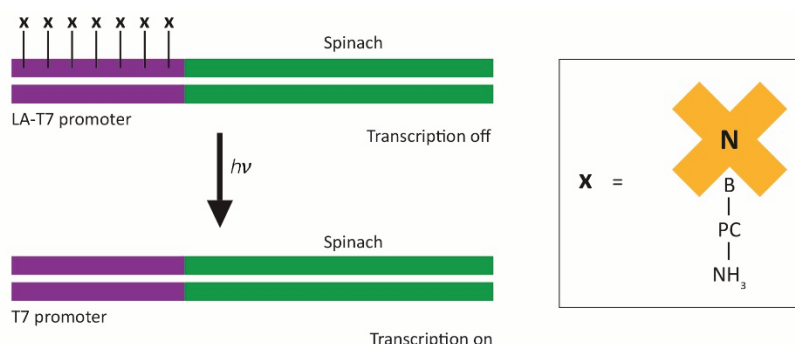


Fig. 5. Scheme of the construction of the LA-Spinach DNA construct. T7 RNA polymerase is blocked by tetravalent NeutrAvidin on the promoter. UV photocleavage of the biotin moiety allows the binding of T7 RNA polymerase for production of the Spinach RNA aptamer. $h\nu$ = light.

3.2 MATERIAL AND METHODS

3.2.1 AMINO T7 OLIGO CONJUGATION TO PC BIOTIN

All conjugation steps were performed in darkness as described by Booth et al. [16]. Briefly, amino T7 oligo (5 μ l, 100 μ M; ATDBio) (Table 1) was added to PC biotin (25 μ l, 10 mM in DMF) with 100 mM NaHCO₃ in a total volume of 50 μ l DMF in a 0.5-ml Protein LoBind tube (Eppendorf). The reaction mixture was kept at room temperature, vortexed and centrifuged every 15 min for 1 h and subsequently incubated at 4 °C overnight. Tris-HCl (350 μ l, 10 mM, pH 8.0) was added to stop the reaction. The product was purified with a 3-kDa Amicon Ultra column by washing the column four times with 450 μ l of 10 mM Tris-HCl (pH 8.0) according to the manufacturer's protocol. The Amicon-purified product was named amino T7-PC biotin. As negative control, the same procedure was carried out in parallel in the absence of PC biotin.

Table 1. Sequence of the amino T7 DNA oligo.

DNA name	Sequence (5' - 3')	Modification
T7-amino modified promoter	GAATXAA X ACGACXCACXAXAGGGXCXAG	X = C6-amino-dT

3.2.2 HPLC EXAMINATION OF THE AMINO T7-PC BIOTIN OLIGO

The efficiency of the conjugation reaction and of the purification of the modified T7 oligo were analyzed with high-performance liquid chromatography (HPLC, Agilent 1260 Infinity Quaternary LC). 3 μ l of amino T7-PC Biotin were separated on a Waters CSH 130 C18 column (100x2.1mm, 2.1 μ m) with a flow speed of 0.45 ml/min. Eluting buffers were buffer A (25 mM ammonium acetate, pH 7) and buffer B (acetonitrile) with a gradient of 0 min, 0% B; 3 min, 28% B; 11 min, 29% B; 12 min, 80% B; 13 min, 80% B; 14 min, 100% B; 19 min, 100% B. Peaks were measured by absorbance at 260 nm. When a steeper gradient was used, the gradient was modified as follows: 0 min, 0% B; 3 min, 28% B; 11 min, 35% B; 12 min, 80% B; 13 min, 80% B; 14 min, 100% B; 19 min, 100% B.

3.2.3 HPLC PURIFICATION OF THE AMINO T7-PC BIOTIN OLIGO

Further purification of the amino T7-PC biotin oligo was performed by HPLC on a Waters CSH 130 C18 column (150x10 mm, 5 μ m) with a flow speed of 5 ml/min. Eluting buffers were buffer A (25 mM ammonium acetate, pH 7) and buffer B (acetonitrile) with a gradient of 0 min, 0% B; 3 min, 28% B; 11 min, 29% B; 12 min, 80% B; 13 min, 80% B; 14 min, 100% B; 19 min, 100% B. Peaks were measured by absorbance at 260 nm. The peak corresponding to the T7 oligo was collected from different fractions in light-safe microcentrifuge tubes. Fraction volumes were 1 ml/fraction, 0.5 ml/fraction and 0.25 ml/fraction for the first, second and third purification, respectively. Injection volume was 100 μ l for the first purification and 40 μ l for the second and third purification.

All collected fractions were immediately frozen in liquid nitrogen and lyophilized overnight. Lyophilized fractions were re-dissolved in 50 μ l Tris-HCl 10 mM, vigorously vortexed, and spun at 13200 rpm for 10 min to remove excess salt. The re-dissolved DNA was further purified with the Wizzard PCR-clean up System (Promega). Alternatively, lyophilized fractions were either stored at -80 $^{\circ}$ C until use or re-dissolved in 50 μ l Tris-HCl 10 mM.

3.2.3 PREPARATION OF A SPINACH-ENCODING DNA TEMPLATE

A linear DNA template encoding meYFP-Spinach was used to isolate the Spinach aptamer DNA sequence flanked by a T7-promoter and terminator sequence with the forward and reverse primers CHD91 and CHD658, respectively (Table 2), creating the linear DNA construct T7-Spinach(224). The reaction product was analyzed with a 1.2% agarose gel in TAE buffer using a 50-bp DNA ladder (NEB) and further purified with the Wizzard PCR-clean up System (Promega).

Table 2. DNA primers for the amplification of a T7-Spinach(224) compatible with the T7-amino oligo.

DNA name	Sequence (5' - 3')	Modification
CHD658	GAATTAATACGACTCACTATAGGGTCTAGAAAGCTTCCCGGGAAAGTA	FW Spinach - T7 promoter
CHD91	AAAAAACCCTCAAGACCCGTTTAGAGG	RV Spinach - T7 terminator

3.2.4 PCR OF SPINACH-ENCODING DNA WITH THE AMINO T7-PC BIOTIN OLIGO

The amino T7-PC biotin primer was directly used as forward primer for the amplification of T7-Spinach(224). Briefly, 2 μ l of a 10x dilution of the amino T7-PC biotin oligo were mixed with 10 μ l Phusion HF buffer (5x), 1 μ l dNTPs (10 mM stock), 1.25 μ l reverse primer CHD91 (10 μ M stock; table 2), 0.5 μ l of 2 U/ μ l Phusion[®]HF DNA polymerase (Thermo Fisher Scientific) and 2 μ l of DNA T7-Spinach(224) DNA (10 ng/ μ l) in a total volume of 50 μ l. The PCR was run with the following thermal cycles: 95 $^{\circ}$ C for 3 min, 30x (95 $^{\circ}$ C for 30 sec, 52.5 $^{\circ}$ C for 30 sec and 72 $^{\circ}$ C for 1 min 15 sec) and 72 $^{\circ}$ C for 5 min. The reaction product was analyzed with a 1.2% (w/v) agarose gel in TAE buffer using a 1kb DNA Ladder (Promega) and purified with the Wizzard PCR-clean up System (Promega). This DNA construct was named biotin Spinach

DNA. As negative control, Amicon-purified amine-only T7 oligo was used to amplify the T7-Spinach(224) DNA. This DNA construct was named amine-only Spinach DNA. When the HPLC-purified T7-PC biotin oligo was used for amplification, 1.5 ng/ μ l of this oligo were added to the PCR reaction.

3.2.5 LA-SPINACH DNA FORMATION THROUGH BINDING OF TETRAVALENT NEUTRAVIDIN

To create the LA-Spinach DNA, tetravalent NeutrAvidin (Sigma Aldrich) was bound to the T7-amino-PC biotin Spinach DNA PCR product. Briefly, biotin Spinach DNA or the same DNA construct assembled with the HPLC-purified promoter was incubated with a 50x molar excess of tetravalent NeutrAvidin in 10 mM Tris-HCl (pH 8.0) in Protein LoBind tubes for 3 h at room temperature and overnight at 4 °C. As negative control, amine-only Spinach DNA was incubated in parallel with tetravalent NeutrAvidin.

3.2.6 UV PHOTOCLEAVAGE OF LA-SPINACH DNA IN BULK SOLUTION

UV photocleavage of LA-Spinach DNA was carried out by using a UV lamp (365 nm, Professionele 36 watt UV Tunnellamp). 4 μ l of 100 nM LA-Spinach DNA were held in darkness or under the UV lamp at a distance of 3 cm for 0 sec, 10 sec, 30 sec, 45 sec, 60 sec, 90 sec, 2 min, 5 min, 15 min, 22 min or 30 min, with UV directly illuminating the solution in the open tubes. As negative controls, the same procedure was performed with the amine-only Spinach DNA, the neutravidin-incubated amine-only DNA or biotin Spinach DNA. Photocleavage reaction products were analyzed with a 1.2% (w/v) agarose gel in TAE buffer using a 1kb DNA Ladder (Promega).

3.2.7 TRANSCRIPTION OF THE LA-SPINACH DNA

Briefly, 10 or 50 nM of LA-Spinach DNA were transcribed in a mixture containing 0.55 μ l 10-20 U/ μ l T7 RNA polymerase (Promega), 2.75 mM ribonucleotide triphosphate (rNTPs; RiboMAX Large Scale RNA Production System-T7, Promega), transcription buffer and 60 μ M DFHBI-1T (Lucerna, Inc) in a final volume of 20 μ l. As negative control, the neutravidin-incubated amine-only Spinach DNA, amine-only Spinach DNA or biotin Spinach DNA were transcribed. Solutions were kept on ice until transcription was started.

3.2.8 BULK TRANSCRIPTION MEASUREMENTS BY SPECTROFLUOROMETRY

Real-time monitoring of Spinach production through fluorescence was carried out on a CLARIOstar Microplate reader (BMG LABTECH'S). Briefly, 20 μ l of the transcription reactions were pipetted into a 384-well glass bottom microplate (Greiner Bio One). Real-time monitoring of Spinach production at 37 °C was recorded every 30 sec with 482/505 nm excitation/emission wavelengths.

3.2.9 LIGHT-TRIGGERED TRANSCRIPTION INSIDE LIPOSOMES

To prepare lipid-coated beads, a mixture of chloroform-dissolved lipids consisting of DPMC (66.2 mol%), DMPG (16.6 mol%), Cholesterol (16.6 mol%), DSPE-PEG(2000)-biotin (0.5 mol%), DHPE-TexasRed (0.2 mol%) and DSPE-PEG(5000)-Folate (0.1 mol%) for a total mass of 1 mg, was assembled in a 25-ml round-bottom glass flask. All lipids were purchased at Avanti Polar Lipids, except the DHPE-TexasRed membrane dye that was from Invitrogen. 0.75 g of 212-300- μm acid-washed glass beads (Sigma-Aldrich) were added to the lipid mixture, and the organic solvent was removed by overnight rotary evaporation at 400 mbar. The dried lipid-coated beads were stored under argon at $-20\text{ }^{\circ}\text{C}$ and desiccated for at least 20 min or flushed with argon for 30 sec before use. Each lipid-pipetting tip was washed three times with chloroform, and the washing volumes were added to the mixture.

A 100- μl pre-transcription reaction consisting of 10 nM LA-Spinach DNA, 4 μl of 10-20 U/ μl T7 RNA polymerase (P207B, Promega), 60 μM DFHBI-1T and transcription buffer (P207B, Promega) was assembled. When large unilamellar vesicles (LUVs) were produced, 34 mg of lipid-coated beads were swelled with 100 μl of pre-transcription reaction overnight at $37\text{ }^{\circ}\text{C}$ and the resulting liposome samples were downsized by 13 extrusion passages with a 0.8- μm filter membrane (Avanti Polar Lipids) and two 10 mm filter supports (Whatmann) on a mini-extruder (Avanti Polar Lipids). When small unilamellar vesicles (SUVs) were produced, swelling was performed for 2 h at $37\text{ }^{\circ}\text{C}$ and gentle manual swirling every 15 min, and a 0.2- μm (Avanti Polar Lipids) filter membrane was used for extrusion. Prior to each extrusion, the assembled extruder was pre-washed with 60 μM DFHBI-1T in transcription buffer.

Unencapsulated DNA was removed by addition of 1 μl of 1U/ μl DNase (RQ1, Promega) followed by an incubation step at $37\text{ }^{\circ}\text{C}$ for 20 min. Photocleavage of the LA-Spinach DNA encapsulated in the extruded liposomes was performed by 5 min UV irradiation as for the bulk solutions. DNA transcription took place by addition of 5 mM rNTPs to the liposome samples, followed by an incubation step for 3 h at $37\text{ }^{\circ}\text{C}$. Spinach RNA produced outside liposomes was removed by addition of 0.5 U/ μL of 10 U/ μl RNaseONE (Promega) followed by an incubation step for 20 min at $37\text{ }^{\circ}\text{C}$.

The liposome solution was diluted 20x in 60 μM DFHBI-1T in transcription buffer and 4-10 μl of sample were transferred to a custom-made imaging chamber. A glass coverslip was functionalized with BSA-biotin (Thermo Fisher Scientific) and NeutrAvidin for liposome immobilization. Briefly, chambers were incubated with 10 μl of 1 mg/ml BSA-biotin and 10 μl of 1 mg/ml NeutrAvidin for 5 min at room temperature. Chambered coverslips were washed three times with MiliQ water after each incubation. Prior to liposome immobilization, the functionalized chambers were pre-washed with transcription buffer (1x) containing 60 μM DFHBI-1T. In order to avoid sample evaporation during imaging, the 7-mm hole was filled with 15 μl MiliQ water. After sample addition, chambered coverslips were sealed with a 1 mm thick silicone spacer (Press-to-seal silicone sheet, Life technologies) and a coverslip, as shown

in Fig. 6. The sample of immobilized liposomes was imaged with a Nikon A1+ laser scanning confocal microscope with a 100x oil immersion objective, using the 488 nm (DFHBI-1T) and 561 nm (Texas Red) laser lines with appropriate emission filters. Microscopy images were analyzed with MATLAB (MathWorks). As negative control, the same procedure was followed with amine-only Spinach DNA. Aside from the UV photocleavage step, all steps in this procedure were performed in darkness.

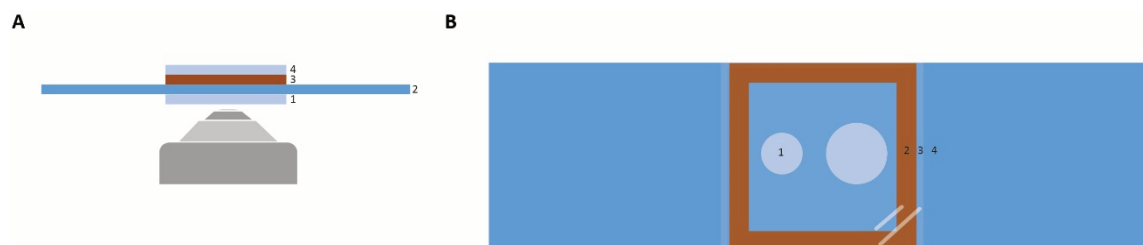


Fig. 6. A) Front-view and B) top view of custom-made chambered coverslips for liposome immobilization and visualization by fluorescence microscopy. Two spherical holes with diameters 5 mm and 7 mm were drilled onto a coverslide (76 x 26 mm, Menzel-Gläser) (2) with a Sand Blaster. After briefly washing the chambers with MiliQ water, coverslips were consecutively sonicated with 2% Hellmanex and MiliQ water for 10 min and washed with 100% ethanol. Dried coverslips were plasma cleaned on a Harrick Plasma PDC-002. In parallel, coverslips (24x60 mm, Menzel-Gläser) were consecutively sonicated with 2% Hellmanex and MiliQ water for 10 min and washed with 100% ethanol. A drop of Norland optical adhesive (NOA 81, Ultraviolet curing) was applied to the surroundings of the perforated holes on a single side of the coverslips, and a clean coverslip was immediately sealed on top by 5 min irradiation with a 365-nm light with a Promed UVL 36 lamp (1). Newly formed chambered coverslips were incubated for 48 h at 55 °C. Dried chambered coverslips were consecutively sonicated with 2% Hellmanex and MiliQ water for 10 min, washed with 100% ethanol, and stored in clean Petri dishes until usage. After sample addition, chambered coverslips were sealed with a 1 mm thick silicone spacer (Press-to-seal silicone sheet, Life technologies) (3) and a coverslip (4).

3.3 RESULTS

3.3.1 AN LA-SPINACH DNA CAN BE SUCCESSFULLY ASSEMBLED

In order to create a DNA template encoding a Spinach RNA aptamer, the Spinach DNA sequence was isolated by PCR from the fusion DNA construct encoding meYFP-Spinach. To make the aptamer transcribable by T7 RNA polymerase, an overhanging Fw primer incorporating the T7 promoter sequence and a Rv primer encompassing the T7 terminator were used (Fig. 7a). As seen on Fig. 7b, a band corresponding in size to the expected amplified T7-Spinach(224) DNA fragment was obtained.

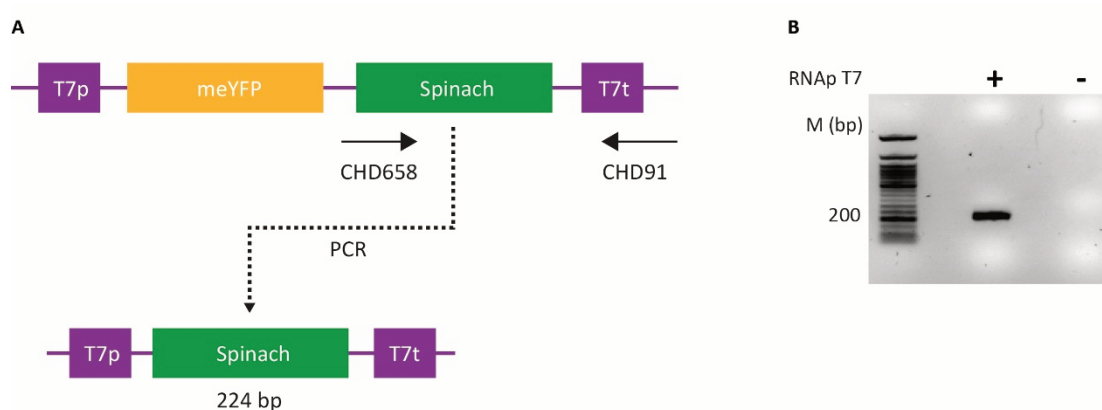


Fig. 7. A) DNA template encoding T7p-meYFP-Spinach-T7t and the isolated PCR product CHD658/91 using primers CHD658 and CHD91 to isolate the Spinach aptamer encoding sequence. B) PCR amplification of T7p-Spinach-T7t; M: DNA ladder.

To create a LA-T7 promoter, the amino-C6-dt modified bases from the amino T7 oligo were coupled to PC biotin groups, as described by Booth et al. [16]. HPLC analysis of the reaction products revealed a single peak for the unmodified amino T7 DNA primer at retention time 4 min (Fig. 8a). Alongside, the HPLC profile of the conjugated promoter showed several peaks eluting at retention times between 4 and 7.9 min (Fig. 8b), indicating that PC-biotin conjugation led to different degrees of modifications. The peak with retention time 7.9 min was assumed to correspond to the T7 amino primer species incorporating the PC-biotin in all seven amino-C6-dT modified bases. This species represented ~44% of the total amino T7 primer present in the sample. All intermediate species between the unconjugated and the fully conjugated T7 amino primer are associated to partial modifications, where PC-biotin was incorporated in one to seven C6-amino groups. A 3% of T7 amino DNA remained fully unmodified. Similar results were obtained in repeated conjugations (data not shown).

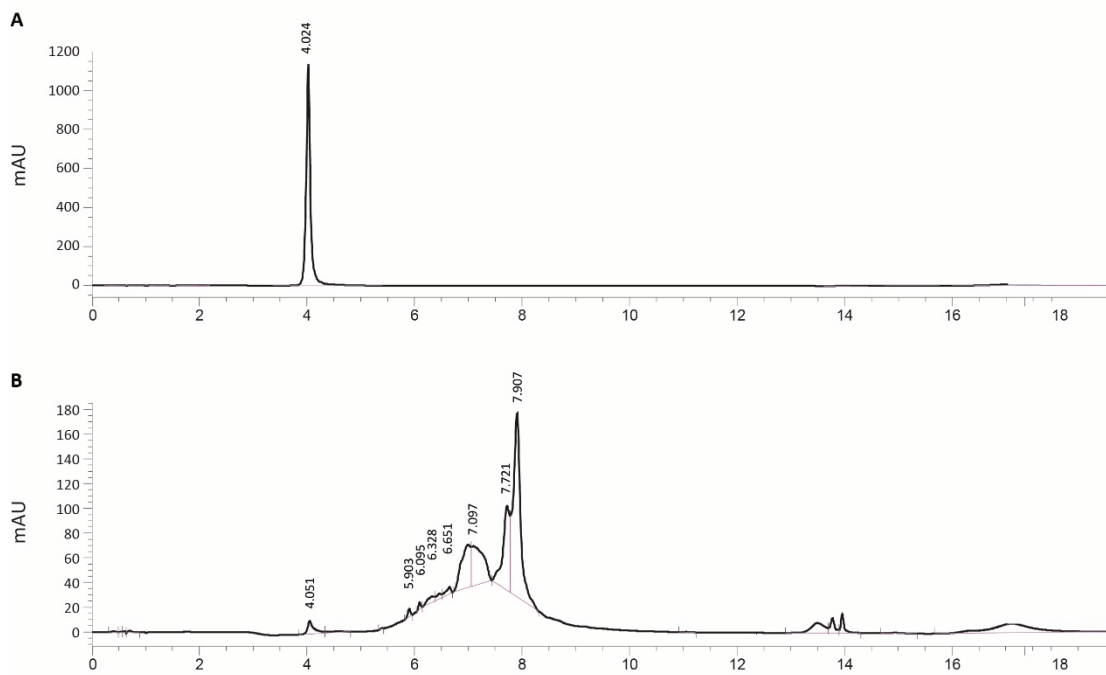


Fig. 8. HPLC chromatogram of A) amino T7 oligo; B) the reaction product of PC-biotin conjugation to the amino T7 oligo.

The conjugated oligo, amino T7-PC biotin, was used as forward primer to create a light-activated Spinach DNA sequence by PCR. In agreement with the results from Booth et al. [16], the product of amplification showed a mobility shift compared to the DNA product obtained by amplification with unmodified amino T7 oligo (Fig. 9). This shift is attributed to a structural re-arrangement of the DNA molecule due to its labelling to biotin. Band intensity analysis indicated that the upper band represented 41% of the amplified DNA. This result agreed with the 44% of fully modified oligo found by HPLC, further indicating that the higher band on gel at 0.6 kb corresponds to DNA with a fully biotinylated promoter. PCR amplification with the conjugated oligo resulted in lower amplification yield, indicating that the presence of biotin partially hinders DNA amplification.

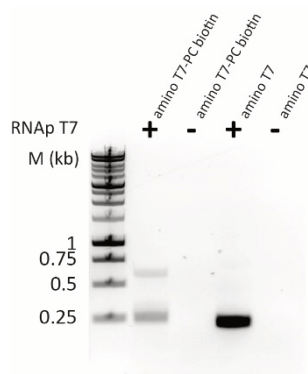


Fig. 9. PCR amplification of Spinach-encoding DNA with the amino T7-PC biotin oligo. M: DNA ladder.

3.3.2 PHOTOCLEAVAGE OF LA-SPINACH DNA LEADS TO A FOUR-FOLD INCREASE ON SPINACH RNA PRODUCTION

After coupling the PCR-amplified products to NeutrAvidin, their transcription kinetics after UV irradiation for different time intervals between 0 and 30 sec were investigated (Fig. 10).

To assess the possible DNA damage provoked by these irradiation intervals, their effect over amine-only DNA transcription was tested. Similar RNA levels were produced from this construct in all conditions, suggesting that these irradiation intervals did not harm the DNA (Fig. 10a). Moreover, similar transcription levels were observed when amine-only DNA was pre-incubated with (Fig. 10b) or without NeutrAvidin (Fig. 9a) indicating that, as expected, in the absence of biotin, NeutrAvidin does not bind the DNA and does not interfere with transcription.

RNA was produced from LA-Spinach DNA in all conditions (Fig. 10c). Full repression of transcription in the unirradiated sample did not occur. However, a 1.4 and a 2.5-fold increase on transcription was achieved after 10 and 30 sec irradiations compared to the unirradiated control, suggesting that UV successfully liberated at least a fraction of the DNA molecules. Moreover, no significant differences in transcription levels were observed between the different irradiation intervals when the DNA was not coupled to NeutrAvidin (biotin Spinach DNA, Fig. 10d). These results indicated that the promoter biotinylation alone does not hamper RNA transcription and therefore, the bounded NeutrAvidin is the only responsible for the partial repression of transcription observed in Fig. 10c.

Importantly, though the DNA concentrations in all transcription reactions was theoretically the same, the transcription levels reached on unirradiated amine-only DNA samples were on average 5.5 ± 0.4 times and $9.8 \pm$ times higher than those obtained from unirradiated biotin Spinach DNA and LA-Spinach DNA, respectively. These unexpected differences suggest that the DNA concentration of LA-Spinach DNA and biotin Spinach DNA were overestimated prior to the preparation of the transcription reactions.

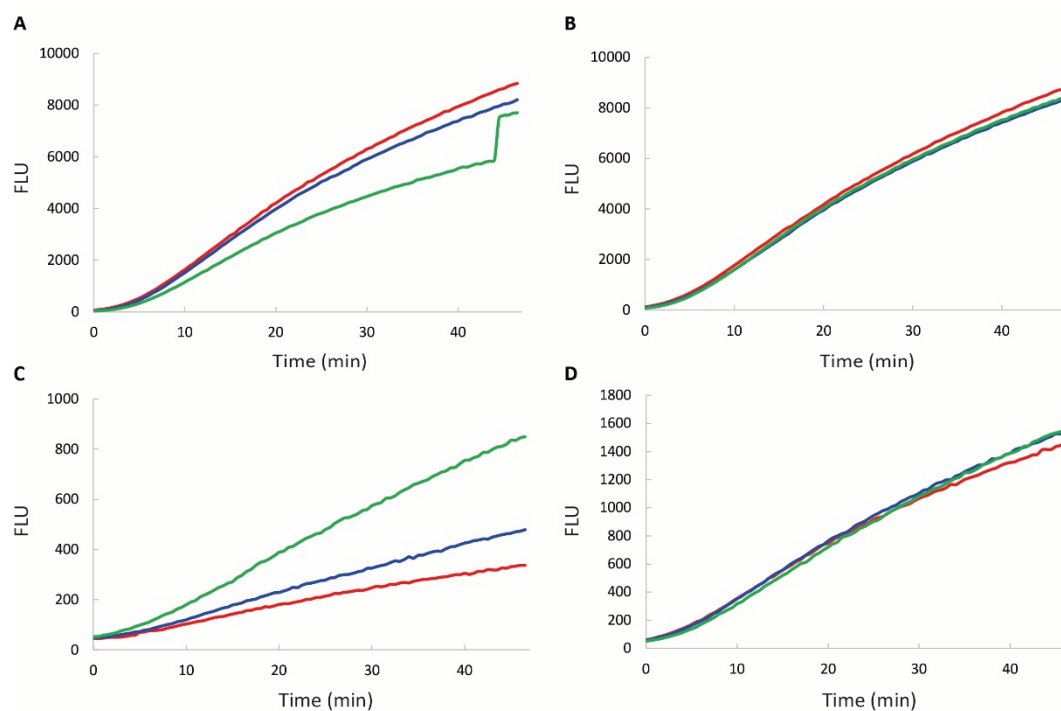


Fig. 10. Time traces of Spinach fluorescence produced from A) amine-only Spinach DNA, B) neutravidin-incubated amine-only Spinach DNA, C) LA-Spinach DNA and D) biotin Spinach DNA constructs after UV irradiation for 0 (red), 10 (blue) or 30 (green) sec.

To find the duration of UV irradiation necessary to reach maximum de-caging of the LA-Spinach DNA, we investigated the Spinach transcription levels obtained when using longer irradiation intervals up to 30 min (Fig. 11).

To control DNA damage, the same conditions were tested for non-caged DNA (amine-only Spinach DNA). The yields of Spinach RNA produced from this construct were similar for all illumination intervals, indicating UV irradiation did not harm the DNA even after a 30 min interval (Fig. 11a-11b).

As shown in Fig. 11c, the final levels of Spinach RNA produced from LA-Spinach DNA increased linearly with the duration of UV irradiation between 0 and 2 min ($y = 477,02x + 332,02$; $R^2 = 0,9904$). When the DNA was irradiated for 5 min, a 4.3-fold increase on transcription levels was observed (Fig. 11d). Extending this interval from 5 to 30 min, improved transcription levels only by a 1.2-fold (Fig. 11e). 5 min was chosen as key irradiation interval between transcription efficiency and DNA stability for further experiments.

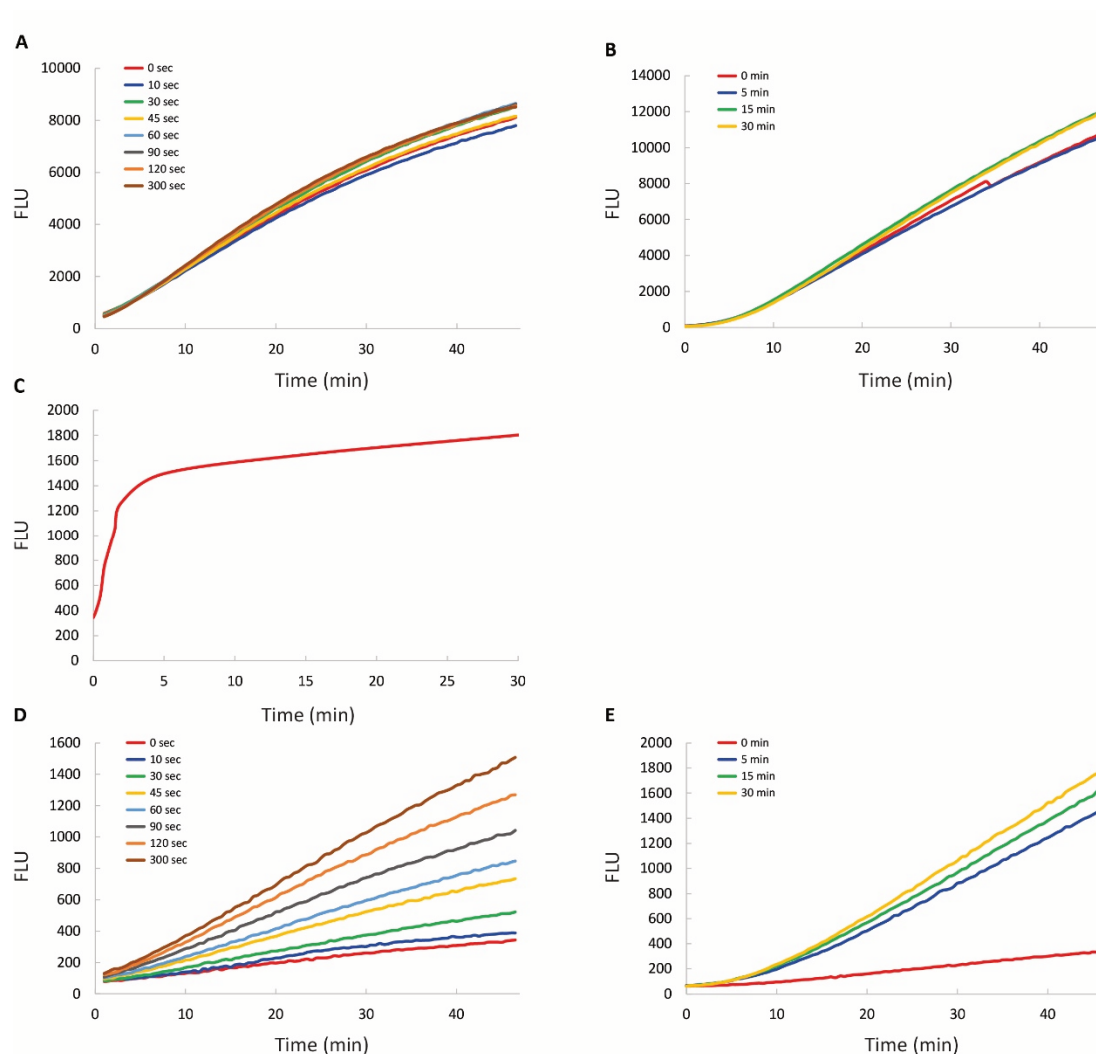


Fig. 11. A) Time traces of Spinach fluorescence produced from the amine-only Spinach DNA for UV irradiation intervals between 0 and 5 min. B) Time traces of Spinach fluorescence produced from the amine-only Spinach DNA for UV irradiation intervals between 0 and 30 min. C) Spinach RNA fluorescence as a function of the duration of UV irradiation measured after 46.5 min of transcription. D) Time traces of Spinach fluorescence produced from the LA-Spinach DNA for UV irradiation intervals between 0 and 5 min. E) Time traces of Spinach fluorescence produced from the LA-Spinach DNA for UV irradiation intervals between 0 and 30 min.

3.3.3 TRIGGERED IN-VESICLE TRANSCRIPTION FROM THE LA-SPINACH DNA SHOWS NO ADVANTAGE OVER UNIRRADIATED LIPOSOMES

To create an in-situ light-regulated therapeutic nanofactory, the LA-Spinach DNA construct and T7 RNA polymerase were co-encapsulated in liposomes and externally fed by rNTPs. In view of the results obtained in bulk (Fig. 11), we hypothesized that upon light stimulation, liposomes could have a higher fraction of transcriptionally active liposomes or that higher Spinach fluorescence could be measured in some vesicles compared to a non-irradiated sample. In-vesicle Spinach transcription was studied in LUVs and SUVs. Liposomes were produced, imaged (Fig. 12a) and their Spinach fluorescence analyzed (Fig. 12b). As shown in Fig. 12c, no significant differences were observed between the samples where the DNA was irradiated for 5 min and the negative control for both liposome sizes. Regarding the transcription levels, the

average Spinach fluorescence intensity were 178 and 239 a.u. respectively for irradiated and non-irradiated LUVs. Thus, even the non-irradiated liposomes showed a 25% higher average fluorescence signal compared to the irradiated sample. These values were 147 and 157 a.u. for SUVs.

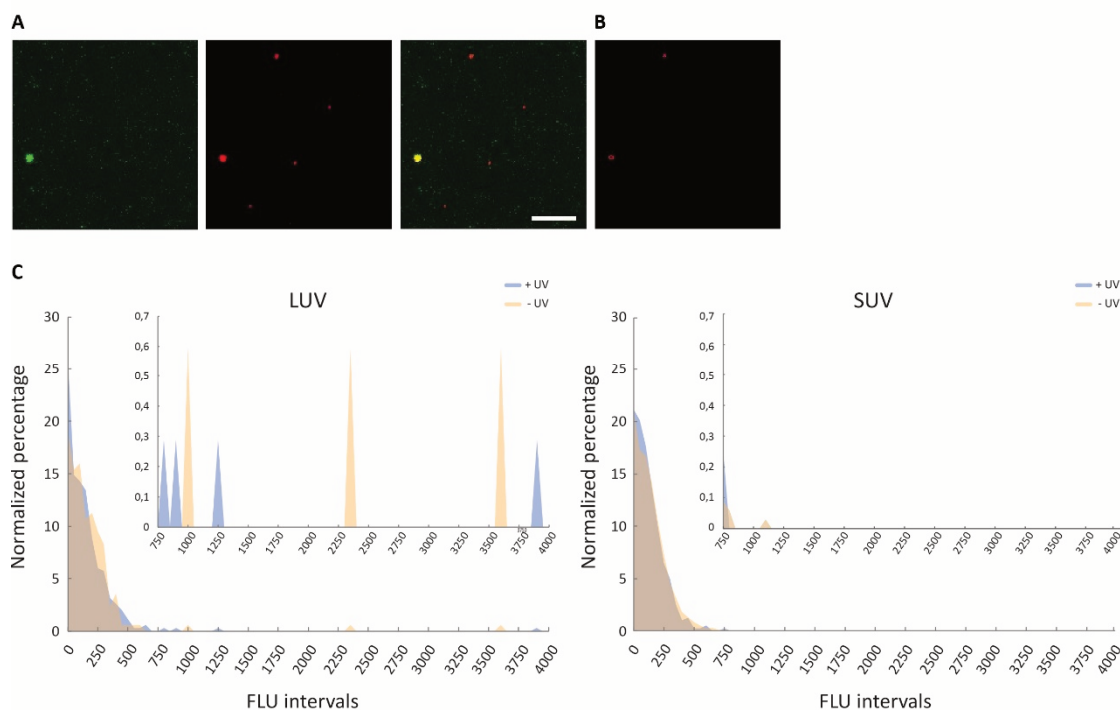


Fig. 12. Analysis of light-induced Spinach RNA transcription inside liposomes entrapping the LA-Spinach DNA construct. A) Fluorescence confocal microscopy image of LUVs, tethered through a biotin-NeutrAvidin linker to a BSA-biotin passivated glass (scale bar: 10 μm). B) Liposome selection in one field of liposomes. C) Normalized percentage of DFHBI-1T integrated intensities in selected liposomes.

3.3.4 HPLC PURIFICATION OF THE LA-SPINACH DNA

To create a DNA construct that allows the total off-state regulation of Spinach DNA transcription, we isolated the fraction of oligo containing all seven biotin modifications. For this, a new biotin-conjugated T7 oligo was assembled (Fig. 13a). After Amicon-column pre-purification, the biotin-conjugated T7 oligo was subjected to consecutive rounds of HPLC-purification, to isolate the peak eluting at 8 min. During purification, all modified T7 oligo species eluted together as one single peak at elution time 4.7 min (Fig. 13b). The shift on the elution time compared to the analytical column was due to the wider diameter of the purification column. Analytical HPLC after a first purification round showed that most of the partially modified T7 oligos could be separated from the fully modified oligo in the fractions F1 and F2, respectively (Fig. 13c). Fraction F2 contained two overlapping peaks at 7.93 and 8.08 min. At this point of the purification process, the earlier eluting peak at 7.93 was assumed to contain a partially modified T7 oligo. Thus, two additional rounds of purification were performed to isolate the last eluting peak at 8.08 min. Each peak was fractionated in at least three independent fractions and their volumes were lowered from 1 ml/fraction in the first

purification, to 0.5 ml/fraction and 0.25 ml/fraction in the second and third purifications. After the third purification round, two twin overlapping peaks with equal height were found at 7.7 and 7.9 min (Fig. 13d). The same fraction analysed applying a steeper gradient resembling the HPLC method used by Booth et al. [16], showed a single narrower peak eluting at 6.6 min (Fig. 13e). This result, together with the fact that peak fractionation was intensive through three consecutive purifications, suggested that the two peaks observed in Fig. 13d are most likely the same component, splitted in two twin peaks due to reasons inherent to sample preparation or the HPLC method in use. Importantly, substantial sample loss was observed at each purification round. Consequently, no further purifications were carried out.

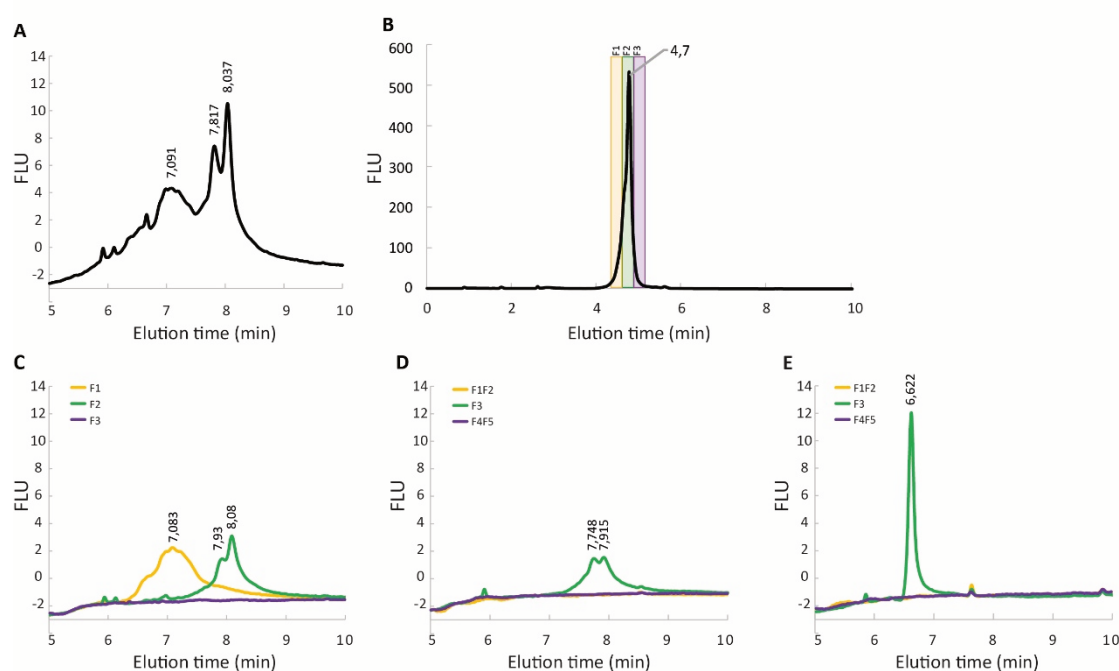


Fig. 13. A) HPLC analysis of amino T7-PC biotin oligo. B) 1st HPLC purification of fully biotinylated amino T7-PC biotin oligo. Target fractions F1, F2 and F3 were collected in the indicated intervals. C) HPLC analysis of fractions from 1st purification. D) HPLC analysis of fractions from 3rd purification. E) HPLC analysis of fractions from 3rd purification with steeper HPLC gradient.

3.3.5 CHARACTERIZATION OF THE TRANSCRIPTION ABILITY OF THE HPLC-PURIFIED LA-SPINACH DNA

Following HPLC-purification, the amino T7-PC biotin oligo was re-purified through a PCR clean up column and used as Fw primer for the amplification of T7-Spinach(224) DNA. As seen on Fig. 14a, PCR amplification produced one upper thick band at around 0.70 kb, corresponding to the DNA containing the fully biotinylated T7 promoter. Surprisingly, three additional faint bands were found at sizes 0.25, 0.30 and 0.5 kb. While the band at 0.5 kb could correspond to the twin peak found by HPLC at 7.7 min, the source of the lower bands is unclear. The lowest band, appearing at 0.25 kb, had the size of the fully unmodified DNA.

After binding this PCR product to tetravalent NeutrAvidin, we studied the cleavage of the PC group from the resulting HP-LA-Spinach DNA through a band shift assay (Fig. 14b). Based on the results from Booth et al. [16], we expected to observe biotin photocleavage as a gel shift, where HP-LA-Spinach DNA and biotin Spinach DNA would be reduced to the same apparent mass as the amine-only T7 Spinach DNA. Unexpectedly, no shift on the DNA band patterns were observed after irradiating HP-LA-Spinach-DNA for 5 min with respect to the non-irradiated DNA. This result suggested that no photocleavage of the biotin moiety took place upon irradiation. As well, no gel shift was observed on the DNA when this was not bound to NeutraVidin, discarding a relation between failed photocleavage and this protein.

To further address this, we carried out light-activated transcription from these DNA templates (Fig. 14c). As expected from the result obtained on gel, no Spinach RNA was produced from the HP-LA-Spinach DNA after irradiation. Surprisingly, however, no Spinach transcription was observed when the DNA template was not bound to NeutraVidin. Based on the results obtained with the non-HPLC-purified biotinylated DNA, where DNA transcription was not hampered by the biotin moieties, we expected to observe transcription in this sample, whether irradiated or not. Altogether, these results suggested that other factors apart from poor photocleavage inhibited transcription from the DNA templates assembled with an HPLC-purified promoter.

We prepared transcription reactions by increasing the irradiation period to 22 min (Fig. 14d) and the final DNA concentration by 5-fold (Fig. 14e). Extending the UV irradiation interval to 22 min did not seem to favor photocleavage on gel (Fig. 14d). Spinach fluorescence after 73 min was higher on the irradiated sample compared to the non-irradiated one (Fig. 14e). However, this difference was considered negligible since it remained within the regular variability of measurements and the signal to noise ratio was low.

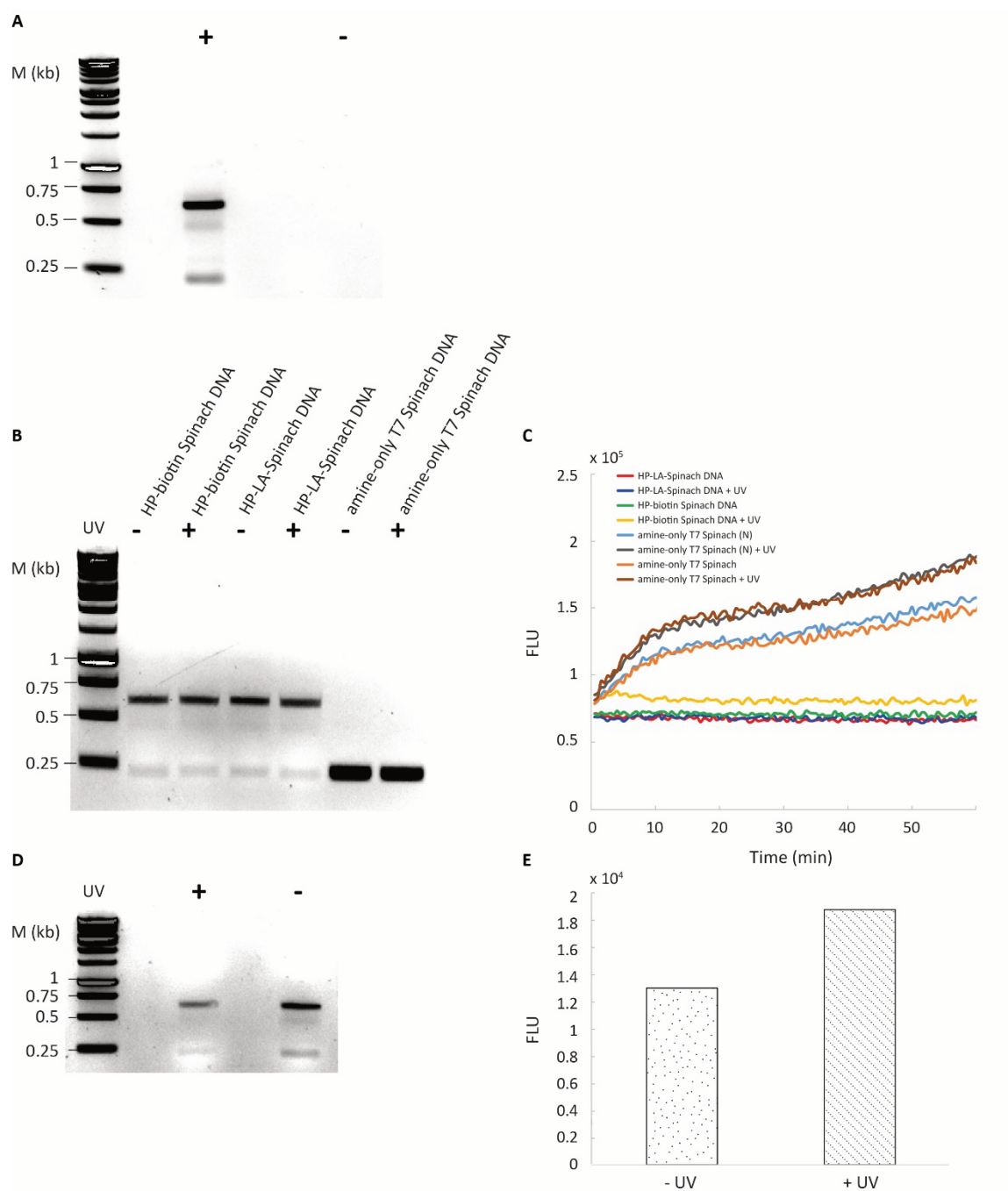


Fig. 14. A) PCR amplification of biotin Spinach DNA with HPLC-purified oligo. B) Photocleavage of HP-LA-Spinach DNA, biotin Spinach DNA and amine-only T7 Spinach DNA after 5 min UV irradiation. C) Time traces of Spinach fluorescence produced from HP-LA-Spinach DNA after UV irradiation for 5 min. D) Photocleavage of HP-LA-Spinach DNA after 5 min UV irradiation. E) Spinach fluorescence intensity after 73 min of bulk RNA transcription of 50 nM Spinach HP-LA-Spinach DNA irradiated for 22 min with UV. M: DNA ladder.

3.4 DISCUSSION

Light can allow precise spatiotemporal control of biological systems [13]. In the field of therapeutic nanocarriers, the use of light has been heavily investigated mainly for remote control of drug release [12]. Going one step forward, a few studies have reported the development light-controlled drug synthesis inside nanocarriers (see Introduction). In this work, we set out to implement the LA-DNA technology developed by Booth et al. [16] onto the liposome nanofactory presented in Chapter 2. Our ultimate goal is to create a liposome nanofactory whose therapeutic RNA synthesis is externally controlled by light.

HPLC purification of the LA-T7 promoter was not necessary to prove its regulatory power over Spinach DNA transcription (see Fig. 10-11). Although RNA production was partially regulated by UV illumination in bulk, such an effect was not observed when Spinach production was carried out in-vesicle (Fig. 11). Several factors may explain these different experimental outcomes. A sample of LA-Spinach DNA assembled with a non-HPLC purified LA-T7 promoter is composed by a mixture of caged and uncaged DNA molecules. Accordingly, the type of LA-Spinach DNA species that are encapsulated in liposomes is arbitrary, altering the proportions of the different DNA species in-vesicle in comparison to bulk. In addition, vesicles need to co-encapsulate both DNA and RNA polymerase to be transcriptionally active. The formation of transcription pre-initiation DNA-polymerase complexes prior to and during swelling, is hampered when the promoter is caged (not sterically accessible), which may bias the proportion of transcriptionally active liposomes towards those uncaged Spinach DNA species. In line with these considerations, we concluded that light regulation of RNA-expression cannot be efficiently achieved in-vesicle unless the LA-T7 promoter is fully repressed.

Our results show that a single HPLC-purification would suffice to isolate an LA-T7 promoter that, upon Neutravidin binding, fully represses transcription in the off state. The two peaks observed through the three consecutive purifications (Fig. 13c-13d), appeared as a single peak when the HPLC method of Booth et al. [16] was reproduced (Fig. 13e), indicating that their purified T7-oligo would likely show the same HPLC profile if it had been run with our protocol. Thus, whether the two peaks observed on our purifications corresponded to a single, fully biotinylated, T7-oligo species, or to a mixture of two different species, composed by T7-oligos with six or seven biotin modifications, using the first purification product would have very likely enabled the successful assembly of a fully repressed LA-T7 promoter. The minimum number of biotin modifications necessary to assemble a fully repressed promoter was not shown in Booth's study. Possibly, seven biotin modifications are not necessary to achieve full promoter repression.

Additionally, PC-biotin photocleavage and transcription appeared to be inhibited, even when NeutrAvidin was not coupled to the biotin groups (Fig. 14). After each purification step, the DNA was frozen in liquid nitrogen and lyophilized overnight to be re-dissolved and purified

again. This intensive manipulation carried out through the three HPLC purification cycles rendered, perhaps, the DNA molecules inactive.

A single HPLC-purification would have possibly avoided the great DNA loss and inactivation experienced in this study. Thus, in the next step, LA-Spinach DNA should be assembled with a one-time HPLC-purified T7 oligo. Nevertheless, the photocleavage and transcribability of this DNA should be first characterized via gel shift assay and bulk transcription prior to performing in-vesicle experiments.

Moreover, the illumination interval to achieve maximum DNA de-caging should be determined once again, since it might be different to the one found for the LA-Spinach DNA assembled with a non-HPLC purified LA-T7 promoter in this study (Fig. 11c).

In Booth's work, monovalent streptavidin was used instead of the wild type tetravalent streptavidin, avoiding crosslinking between different DNA molecules. Though we believe that such crosslinking should not alter photocleavage efficiency or the transcribability of de-caged DNA molecules, future studies should attempt to produce and purify monovalent streptavidin following the procedure described in the work of Howarth et al. [17].

Definitely, we are close to achieve the assembly of a fully repressed LA-Spinach DNA, which will allow us to demonstrate that DNA transcription inside nanometric vesicles can be controlled through light using the LA-T7 promoter technology. Once this step is achieved, the LA-T7 technology should be implemented onto therapeutic shRNA-encoding DNA templates (Chapter 4).

The therapeutic potential of this system for the creation of an in-situ light-regulated liposome nanofactory, is, however, limited by the irreversible nature of biotin photocleavage, which impedes the dynamic control of gene expression. When implemented in vivo, such shRNA liposome nanofactory would only allow a one-time irreversible activation of RNA production. Thus, the implementation of a reversible ON and OFF light-inducible transcription system would be of great therapeutic value.

The impressive evolution of tools in optogenetics during the last five years open great possibilities for this implementation [20]. For the creation of reversible T7 light-regulated gene switches, the use of engineered systems based on photoresponsive proteins has been proposed. A possible strategy to create a nanofactory with a reversible switch, is the use of a light-responsive T7 RNA polymerase, as the one engineered by Baumschlager et al. [13], denominated Opto-T7RNAP. It consists of a T7 RNA polymerase split in two domains, C-terminal (T7_{CT}) and N-terminal (T7_{NT}), fused to blue light-responsive heterodimerizers called positive magnet (pMag) and negative magnet (nMag) (see Fig. 15). pMag and nMag are two engineered variants of the Light-oxygen-voltage (LOV) photoreceptor Vivid (VVD) from the filamentous fungus *Neurospora crassa*. Upon blue light-irradiation (460 nm), these VVD variants use electrostatic interactions to prevent homodimerization (repulsion) and selectively

induce heterodimerization (attraction) (Fig. 15a), leading to the reconstitution of the functional polymerase [21] (Fig. 15b). This photoreceptor-based photoswitch allowed a high expression strength, with an inducible range of more than 300-fold, and low leakiness (<2% of total expression). In the absence of blue-light, Opto-T7RNAP returned to the inactive state within minutes, allowing precise dynamic control of gene expression.

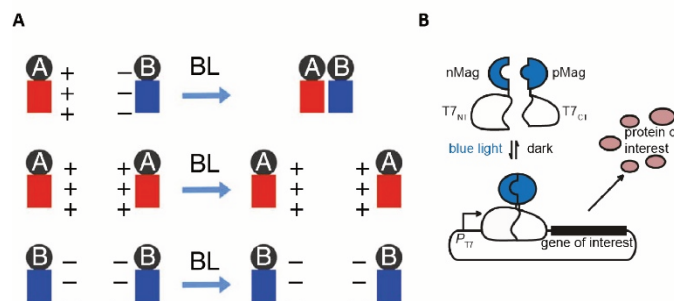


Fig. 15. Mode of function of the blue light-inducible Opto-T7RNAP. A) Interactions between Magnets. Upon blue-light irradiation, pMag (red) and nMag (blue) form heterodimers, taken from [21]. B) Light-dependent gene expression Opto-T7RNAP system. Opto-T7RNAP activity was measured through mCherry reporter fluorescence, taken from [13].

A shared limitation of the LA-T7 and the Opto-T7RNAP systems for their implementation as transcription trigger *in vivo* is the high energy wavelength with which they function. To induce PC-biotin photocleavage, a light wavelength of 365 nm is required, whereas the Opto-T7RNAP system is triggered with blue light at 460 nm. These high energy wavelengths propagate poorly through organs. Maximum penetration depth of light is ~1 mm at 365 nm and ~2 mm at 460 nm in skin tissue. Ranges of near-to-infrared (NIR) wavelengths between 650 and 1000 nm allow maximum tissue penetration (~5 mm), thanks to the reduced light absorption by tissues and decreased light scattering. Also, at this wavelength range, photodamage is minimized. For this reason, NIR wavelength is known as the “phototherapeutic window” [22]. Therefore, shifting the wavelength of light activation towards this region of the spectrum would be most beneficial [23].

A unique class of photoreceptors, called phytochromes, has the ability to absorb far-red or NIR light. Phytochromes use heme-derived tetrapyrrole compounds as light-sensing chromophores [24]. In 2013, Müller et al. [25] developed the first NIR light responsive system for spatiotemporal control of gene expression in mammalian cells, using the photoreceptor phytochrome B (PhyB) and the phytochrome-interacting factor 6 (PIF6) from *Arabidopsis thaliana*. As seen on Fig. 16a, this system was reversibly switched between ON- and OFF-states with short light pulses at 660 or 740 nm. Very recently, a different NIR optogenetic system for gene transcription regulation in mammalian cells was developed by Redchuk et al. [24]. This light-sensing system was based on the optogenetic pair from *Rhodospseudomonas palustris* formed by a bacterial phytochrome (BphP1) and Q-PAS1, an engineered variant of its original

protein partner PpsR2. As shown in Fig. 16b, transcription was light-controlled and reversibly activated by wavelengths between 740-780 nm [26].

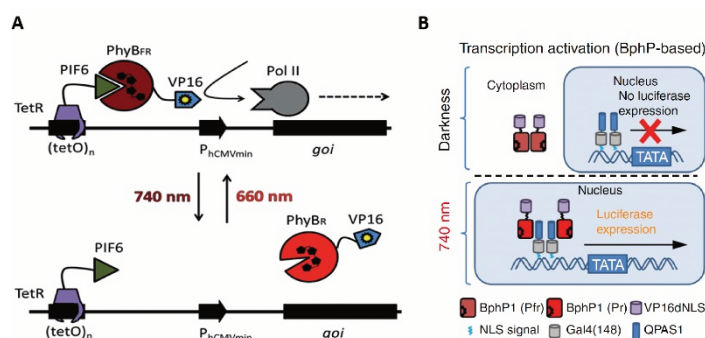


Fig. 16. Mode of function of two different NIR-light-inducible gene expression systems for mammalian transcription machinery. A) Plant-derived optogenetic pair: Illumination at 660 nm converts the PhyB into the biologically active FR form (PhyBfr) and induces heterodimerization with PIF6 that binds the TetOn operator site via TetR. The PhyB-fused VP16 domain recruits the polymerase II transcription initiation complex, that induces phCMV promoter activation and activates transcription by mammalian RNA polymerase II. Illumination at 740 nm, converts PhyB into the biologically inactive R form (PhyBr), terminating the interaction with PIF6, and thus inactivating the promoter and silencing transcription, taken from [25]. B) Bacteria-derived optogenetic pair: in the dark, BphP1 is in the inactive Pfr state in the cytoplasm and Q-PAS1 is bound to the upstream activation sequence (UAS) in the nucleus. NIR light irradiation (740 nm) converts BphP1 to its active Pr state, which travels to the nucleus and binds Q-PAS1. The complex BphP1-Q-PAS1 acts as transactivator of gene expression and transcription is carried out by mammalian RNA polymerase II, taken from [27].

NIR photocontrol of gene expression has also been achieved in *E. coli* [28]. For this, a bacterial phytochrome with diguanylate cyclase activity was engineered (BphS), which converts GTP into *c*-di-GMP upon NIR light irradiation. This photocontrol module regulated gene expression via a *c*-di-GMP-responsive transcription factor in *E. coli* (Fig. 17).

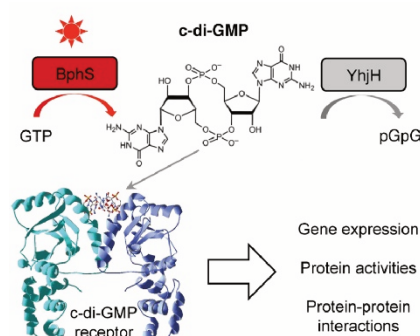


Fig. 17. Mode of function of an NIR-light-inducible gene expression system in *E. coli*, taken from [28].

Among the phytochromes available in nature, optogenetic tools based on bacterial phytochromes are particularly suited for use in mammalian cells, tissues and whole animals. The main reason behind this is that bacterial phytochromes use biliverdin (BV) as chromophore, which is naturally available in all mammalian cells and tissues, though levels vary depending on the type of cell and tissue. Plant-derived phytochromes like PhyB, in comparison, use chromophores that are not available in eukaryotic cells (phycocyanobilin), thus requiring

exogenous delivery. Moreover, bacterial phytochromes are activated by NIR light at 740 nm, that penetrates deep into mammalian tissues. Instead, plant-derived PhyB, is activated with light at 660 nm, which has poorer tissue penetration [27].

Hitherto, NIR light-control of gene expression systems have been developed for the mammalian (Fig. 15) and the bacterial transcription machineries (Fig. 16). To our knowledge, no NIR gene switch system has been implemented for the T7 RNA polymerase transcription system.

Since its discovery five decades ago, the T7 RNA polymerase transcription system has been adopted with success as a robust RNA and protein expression tool in various hosts, including prokaryotic, eukaryotic and cell-free systems. Recently, this system has become an essential component in synthetic biology [29]. Due to these reasons, the implementation of the T7 RNA polymerase transcription system with an NIR optogenetic tool for light regulated expression will be a very valuable tool in the fields of synthetic biology, synthetic tissue engineering and regenerative medicine.

In the future, bacterial phytochrome-based optogenetic pairs such as the one described in Fig. 15b could be adapted for the regulation of gene expression systems that use the bacteriophage T7 RNA polymerase. Such adaptation would enable the implementation of our liposome nanofactory with light-regulated production of therapeutic RNA *in vivo*.

3.5 CONCLUSIONS

The objective of this work was to develop the first light-regulated RNA-producing nanofactory in therapeutically sized fed-vesicle bioreactors that can source nutrients from their environment *in-situ*. Though the LA-T7 technology chosen has limited therapeutic potential, its implementation for the assembly of a light-regulated therapeutic RNA liposome nanofactory is, nonetheless, of great value to prove that RNA production can be precisely controlled by light in time and space in mammalian cells. In this study, the assembly of a fully repressed LA-Spinach DNA was nearly achieved, and the few remaining steps for this accomplishment have been described. On the whole, the development of different optogenetic tools will foster the progress of biomedicine due to their noninvasiveness and precise spatiotemporal resolution.

3.6 ACKNOWLEDGEMENTS

We thank Niels van den Broek for his help with implementing an HPLC detection and purification method for the light-activated Spinach construct.

3.7 REFERENCES

- [1] P. R. Leduc *et al.*, “Towards an in vivo biologically inspired nanofactory,” *Nature Nanotechnology*, vol. 2, no. 1, pp. 3–7, 2007.
- [2] B. S. Pattni, V. V. Chupin, and V. P. Torchilin, “New Developments in Liposomal Drug Delivery,” *Chemical Reviews*, p. 150526165100008, 2015.
- [3] S. Bibi, E. Lattmann, A. R. Mohammed, and Y. Perrie, “Trigger release liposome systems: Local and remote controlled delivery?,” *Journal of Microencapsulation*, vol. 29, no. 3, pp. 262–276, 2012.
- [4] M. B. Yatvin, W. Kreutz, B. A. Horwitz, and M. Shinitzky, “pH-sensitive liposomes: Possible clinical implications,” *Science*, vol. 210, no. 4475, pp. 1253–1255, 1980.
- [5] T. Hesketh, S. Payne, and J. Humphrey, “Complement and phospholipase C lysis of lipid membranes,” *Immunology*, vol. 5, pp. 705–711, 1972.
- [6] D. H. Thompson, O. V. Gerasimov, J. J. Wheeler, Y. Rui, and V. C. Anderson, “Triggerable plasmalogen liposomes: Improvement of system efficiency,” *Biochimica et Biophysica Acta - Biomembranes*, vol. 1279, no. 1, pp. 25–34, 1996.
- [7] P. Shum, J. M. Kim, and D. H. Thompson, “Phototriggering of liposomal drug delivery systems,” *Advanced Drug Delivery Reviews*, vol. 53, no. 3, pp. 273–284, 2001.
- [8] M. B. Yatvin, J. N. Weinstein, W. H. Dennis, and R. Blumenthal, “Design of liposomes for enhanced local release of drugs by hyperthermia,” *Science*, vol. 202, no. 4374, pp. 1290–1293, 1978.
- [9] M. De Cuyper and M. Joniau, “Magnetoliposomes. Formation and structural characterization,” *European biophysics journal : EBJ*, vol. 15, no. 5, pp. 311–9, 1988.
- [10] A. Schroeder *et al.*, “Controlling liposomal drug release with low frequency ultrasound: Mechanism and feasibility,” *Langmuir*, vol. 23, no. 7, pp. 4019–4025, 2007.
- [11] A. Schroeder, J. Kost, and Y. Barenholz, “Ultrasound, liposomes, and drug delivery: principles for using ultrasound to control the release of drugs from liposomes,” *Chemistry and Physics of Lipids*, vol. 162, no. 1–2, pp. 1–16, 2009.
- [12] G. Shim *et al.*, “Light-switchable systems for remotely controlled drug delivery,” *Journal of Controlled Release*, no. August, pp. 0–1, 2017.
- [13] A. Baumschlager, S. K. Aoki, and M. Khammash, “Dynamic Blue Light-Inducible T7 RNA Polymerases (Opto-T7RNAPs) for Precise Spatiotemporal Gene Expression Control,” *ACS Synthetic Biology*, vol. 6, no. 11, pp. 2157–2167, 2017.
- [14] A. Schroeder *et al.*, “Remotely Activated Protein-Producing Nanoparticles,” *Nano Lett*, vol. 12, pp. 2685–2689, 2012.
- [15] V. Chan, S. K. Novakowski, S. Law, C. Klein-Bosgoed, and C. J. Kastrup, “Controlled

- Transcription of Exogenous mRNA in Platelets Using Protocells,” *Angewandte Chemie - International Edition*, vol. 54, no. 46, pp. 13590–13593, 2015.
- [16] M. J. Booth, V. R. Schild, A. D. Graham, S. N. Olof, and H. Bayley, “Light-activated communication in synthetic tissues,” *Science Advances*, vol. 2, no. 4, pp. 1–12, 2016.
- [17] M. Howarth *et al.*, “A monovalent streptavidin with a single femtomolar biotin binding site,” *Nature Methods*, vol. 3, no. 4, pp. 267–273, 2008.
- [18] M. D. Melamed and N. M. Green, “Avidin 2. Purification and Composition,” *Biochemical Journal*, vol. 89, pp. 591–599, 1963.
- [19] N. Krinsky *et al.*, “Synthetic Cells Synthesize Therapeutic Proteins inside Tumors,” *Advanced Healthcare Materials*, vol. 7, no. 9, pp. 1–10, 2018.
- [20] S. Sankaran, S. Zhao, C. Muth, J. Paez, and A. del Campo, “Toward Light-Regulated Living Biomaterials,” *Advanced Science*, vol. 5, no. 8, 2018.
- [21] F. Kawano, H. Suzuki, A. Furuya, and M. Sato, “Engineered pairs of distinct photoswitches for optogenetic control of cellular proteins,” *Nature Communications*, vol. 6, 2015.
- [22] E. Ruggiero, S. Alonso-De Castro, A. Habtemariam, and L. Salassa, “Upconverting nanoparticles for the near infrared photoactivation of transition metal complexes: New opportunities and challenges in medicinal inorganic photochemistry,” *Dalton Transactions*, vol. 45, no. 33, pp. 13012–13020, 2016.
- [23] J. L. B. J. Alvin A. Holder, Lothar Lilge, Wesley R. Browne, Mark A. W. Lawrence, *Ruthenium complexes: Photochemical and biomedical applications*. 2018.
- [24] T. A. Redchuk, E. S. Omelina, K. G. Chernov, and V. V. Verkhusha, “Near-infrared optogenetic pair for protein regulation and spectral multiplexing,” *Nature Chemical Biology*, vol. 13, no. 6, pp. 633–639, 2017.
- [25] K. Müller *et al.*, “A red/far-red light-responsive bi-stable toggle switch to control gene expression in mammalian cells,” *Nucleic Acids Research*, vol. 41, no. 7, 2013.
- [26] T. A. Redchuk, M. M. Karasev, E. S. Omelina, and V. V. Verkhusha, “Near-Infrared Light-Controlled Gene Expression and Protein Targeting in Neurons and Non-neuronal Cells,” *ChemBioChem*, vol. 19, no. 12, pp. 1334–1340, 2018.
- [27] T. A. Redchuk, A. A. Kaberniuk, and V. V. Verkhusha, “Near-infrared light-controlled systems for gene transcription regulation, protein targeting and spectral multiplexing,” *Nature Protocols*, vol. 13, no. 5, pp. 1121–1136, 2018.
- [28] M. H. Ryu and M. Gomelsky, “Near-infrared light responsive synthetic c-di-GMP module for optogenetic applications,” *ACS Synthetic Biology*, vol. 3, no. 11, pp. 802–810, 2014.

- [29] W. Wang *et al.*, *Bacteriophage T7 transcription system: an enabling tool in synthetic biology*. Elsevier Inc, 2018.

4.

A PLATFORM FOR THE PRODUCTION OF THERAPEUTIC shRNA INSIDE CELL-TARGETING VESICLES

Currently, RNA interference-based drugs are the most promising strategy relying on therapeutic RNA, with the first marketed formulation in 2018, and several others on their way. In this study, we explored the potential of fed-vesicle bioreactors described in Chapter 2 for the in-situ production of therapeutic shRNA. We designed DNA templates that generate different shRNA molecules upon in vitro transcription in bulk or directly inside liposomes. The gene silencing efficacy of the shRNA was tested in mammalian cells. The activity of in vitro-transcribed shRNA was demonstrated when conventional transfection methods were used. However, attempts to silence gene expression through liposomal delivery of shRNA failed. To improve delivery, folic acid was incorporated to the surface of liposomes as a ligand targeting cells with high expression levels of folate receptors, like most cancer cells. Although enhanced liposomal uptake by the targeted cells was shown, lysosomal entrapment impeded the successful delivery of shRNA into the cytoplasm. To tackle this problem, the use of the pH-activated melittin peptide to disrupt endosomal membranes was investigated. The lack of evidences for successful production of shRNA in liposomes and for melittin-assisted membrane destabilization prompted us to propose major modifications in the design of a new generation of liposome-based shRNA carriers.

4.1 INTRODUCTION

4.1.1 RNA INTERFERENCE (RNAi)

RNA interference (RNAi) is a cellular process in which non-coding double-stranded RNA (dsRNA) molecules inhibit gene expression [1]. This inhibition allows RNAi to regulate endogenous gene expression and is a mean of innate defense against invading viruses [2]. RNAi occurs naturally in a wide range of organisms, including mammals, plants and fungi [3]. Since its discovery, researchers have intended to harness this process for therapeutic purposes [1]. Theoretically, this process can be harnessed to target any gene of interest [1], providing it an incredibly wide therapeutic utility. Moreover, RNAi allows acting on different targets than conventional drug molecules, such as dysfunctional enzymes [2]. RNAi-based therapeutic applications under pre-clinical and clinical trials include cancer, respiratory diseases, metabolic diseases, viral infections, inherited skin and neurological diseases and ophthalmological disorders [1].

4.1.2 RNAi MECHANISMS

The successful development of RNAi for therapy highly depends on our understanding of the biogenesis pathways of the small RNA molecules that carry out this process. Two main types of RNA molecules, small interfering RNA (siRNAs) and microRNA (miRNA), are directly responsible for gene silencing [1] (Fig. 1).

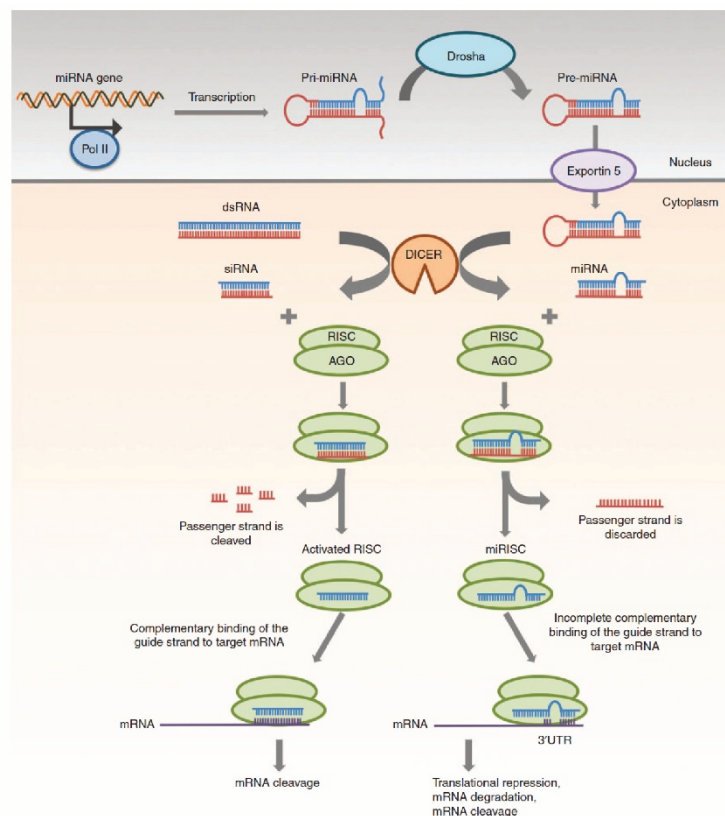


Fig. 1. Simplified scheme of the two main RNAi pathways: siRNA and miRNA. Taken from [2].

siRNAs are short double-stranded RNA molecules, between 21-23 nucleotides in length, with 3' two-nucleotide overhangs. In nature, siRNAs are generated in cells from a long dsRNA molecule originating from infecting pathogens [2]. A ribonuclease (RNase) III enzyme called Dicer is in charge of this process in the cytoplasm. Subsequently, siRNA associates and activates the multiprotein RNA-induced silencing complex (RISC). Then, the endonuclease argonaute 2 (AGO2) present in this complex degrades the passenger strand (sense strand) of the siRNA while the guide strand (antisense strand) remains bound to the RISC. Finally, the guide strand associated to RISC binds to mRNA with full base complementarity (Fig. 2a) and induces mRNA cleavage by AGO2, leading to specific gene silencing. As a result, siRNA induces specific gene silencing through mRNA cleavage [2]. siRNA plays an important role in the innate cellular defense against foreign nucleic acid generally posed by viral infections and in endogenous regulation of gene expression [2].

Conversely, miRNAs originate from endogenous genomic transcription. miRNAs are stem-loop RNA duplexes of 18–25 nucleotides [2]. Like siRNA, miRNA regulates gene expression at the post-transcriptional level. Initially, a primary microRNA (pri-miRNA) is transcribed. pri-miRNA is processed into a precursor microRNA (pre-miRNA) by Drosha, an RNase-III family nuclease. Pre-miRNA is then translocated into the nucleus where it is further processed by Dicer into miRNA. Thus, the conversion of pre-miRNA into miRNA and of long dsRNA into siRNA biogenesis rely on the same cellular machinery [4]. Through its incorporation into the RISC, miRNA triggers mRNA degradation, cleavage or translational repression, depending on the degree of basepair complementarity between both molecules [4, 5]. Differently from siRNA, base pair complementarity between miRNA and their target mRNAs is only partial, relying on a 'seed' region of 2-7 bases with high complementarity (Fig. 2b). miRNAs are mainly involved in the endogenous regulation of gene expression [1].

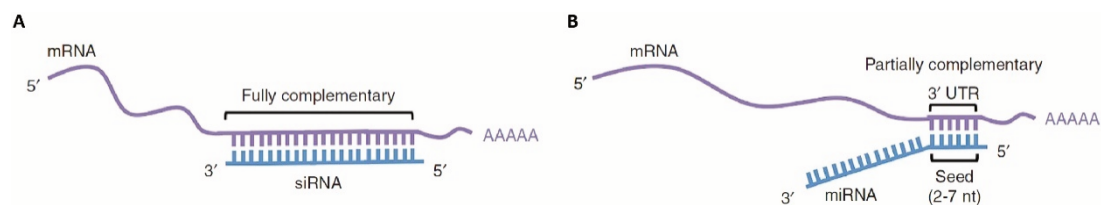


Fig. 2. mRNA sequence recognition and binding in A) siRNA and B) miRNA. Taken from [2].

Though their silencing effects may be different, it is known that the functions of miRNA and siRNA partially overlap. The main functional difference between these molecules is that siRNA silences or regulates the expression of a single specific target mRNA, while miRNA has multiple mRNA targets [2].

4.1.3 HARNESSING THE RNAi NATURAL PROCESS FOR THERAPY

Therapeutically, RNAi has been approached by hacking the natural RNAi-processing machinery at different levels of the process (Fig. 3) [6].

Initially, efforts were focused on the use of long dsRNA (>30 nucleotides). However, the delivery of long dsRNA triggered strong immune responses, inducing the interferon (IFN) pathway [2, 7], as part of the innate defense against viral infection. These undesired responses concluded in nonspecific mRNA degradation and apoptosis [8] and thus impeded the use of long dsRNA molecules for therapy.

Instead, the use of synthetic 21-mer siRNAs has been widely explored [2], since initially it was shown to induce efficient specific gene silencing without triggering IFN responses [9], though later studies showed that siRNA triggered a partial induction of IFN response [10, 11]. However, the induction of IFN responses by siRNA has shown to depend not only on the length of the duplex, but also on the cell type [12]. Additionally, the use of Dicer-substrate siRNAs (DsiRNA), which are synthetic 27mer RNA duplexes, has been explored. DsiRNAs have shown increased RNAi efficacy in comparison with conventional siRNAs [13]. In general, synthetic siRNA has a short lifespan in vivo, lowering its therapeutic power [4]. To overcome this bottleneck, the incorporation of chemical modifications on the backbone of these RNA molecules is introduced.

As an alternative strategy to bypass this bottleneck, short hairpin RNA (shRNA) is used, because it enables the production of siRNA in situ in the cell [14–16]. shRNAs are stem-loop RNAs, that are typically expressed in the nucleus of cells through the delivery of viral DNA vectors. shRNAs can induce specific gene silencing by harnessing the natural RNAi mechanism. After nuclear expression, shRNA is transported to the cytoplasm, where it is processed into siRNA by Dicer and loaded into the RISC for specific gene silencing in the same fashion as long dsRNA [2]. shRNAs can be designed as pre-miRNA-like, pri-miRNA-like or as Ago-shRNA [4]. However, efficient nuclear delivery of DNA has proved challenging through non-viral vectors [17, 18], while viral vectors present safety concerns related to immunogenicity, insertional mutagenesis [19] and long-term effects [20].

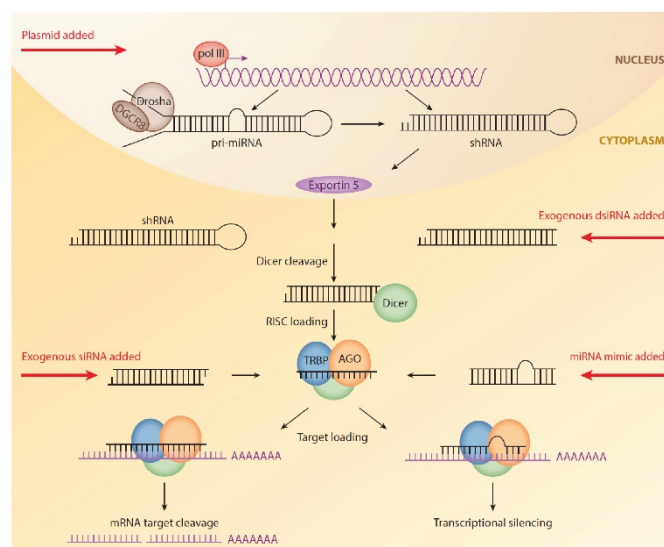


Fig. 3. Main current approaches for RNAi therapeutics. Taken from [6].

4.1.4 FOLATE AS A LIGAND FOR LIPOSOMAL TARGETED DELIVERY

As described on Chapter 2, nuclear delivery is not the only obstacle that non-viral delivery vectors like liposomes need to overcome to achieve gene delivery. Though drug liposomalization can enhance its solubility and stability, and reduce toxicity compared to free drugs, insufficient uptake at target tissues decreases their therapeutic effect. Moreover, their nonspecific association to healthy tissues provokes harmful side effects [21]. Active targeted delivery increases tissue selectivity and thus, decreases side effects. Moreover, it also increases cellular internalization and prolongs the duration of exposure [22].

Folic acid is an interesting ligand for targeted drug delivery because their receptors (FR) are overexpressed on the surface of the cells of a variety of malignant tumors, while minimally distributed in healthy tissues. Consequently, folic acid has been extensively investigated for this purpose. Folic acid is a vitamin essential for the biosynthesis of nucleotide bases [23]. Thus, it is highly consumed by fast growing cells like cancer cells. Normal cells have two folate transporters: a low affinity reduced folate carrier ($K_m \sim 1 \mu\text{M}$) and high affinity folate receptor FR ($K_D \sim 100 \text{ pM}$) [24]. While the reduced folate carrier is found in all cells and represents the primary pathway for the uptake of physiological folates, the FR exhibits a highly limited distribution and is mainly found on activated macrophages and polarized epithelial cells, and preferentially internalize oxidized folates. Additionally, FR is overexpressed on different cancer cells, such as brain, endometrium, kidney, head and neck, mesothelium, ovary or uterus [25]. Probably, this overexpression allows malignant cells to compete for folic acid when the supplies are limited. In addition, FR become accessible to targeted drugs in circulation when epithelial cells undergo malignant transformation, further favoring the tumor-specific targeting properties of this receptor [25]. At the same time, the degree of FR overexpression is positively correlated with a more advance stage and a higher histological grade of the cancer [25]. Additionally, chemotherapy-resistant cancers have been reported to express higher levels of FR [25]. All together, these favorable properties make FR an ideal tumor-specific delivery target.

FR internalizes folic acid into cells via receptor-mediated endocytosis [25]. Folic acid maintains its receptor-binding and endocytosis properties even when covalently linked to a wide range of molecules [26]. The combination of liposomes with folic acid for targeted delivery can potentially allow the delivery of large amounts to specific cells, facilitating the use of drugs with less potency, but higher efficacies due to a better pharmacokinetic behavior [27]. Folate-conjugated lipidic nanocarriers have been shown to increase the tumor accumulation and enhance the antitumor effect of drugs on FR-overexpressing tumors [26, 28, 29]. However, a lipidic composition that favors a prolonged circulation in blood is necessary for these carriers since ligand-modified formulations experience an accelerated clearance from blood. The incorporation of polyethylene glycol (PEG) protects the surface from nanocarriers and reduces their clearance. Note that PEG can be modified with multiple different ligands [30].

Different chemotherapeutic agents have been delivered with liposomes conjugated to the folate ligand via a polyethylene glycol (PEG) spacer [26]. For the creation of folate-targeted liposomes, a folate conjugate called DSPE-PEG-folate can be incorporated into the lipid bilayer during their preparation. In this derivative, folate is covalently attached to a phospholipid via a long PEG linker (see Fig. 4). A study showed that the incorporation of a small molar ratio of DSPE-PEG-Folate (0.03%) with a long PEG chain of molecular weight 5000 Da improves the targeting ability of folate-modified liposomes by more than a 100-fold compared to unmodified liposomes. Results indicate that the delivery efficiency of these vesicles is also influenced by the amount of folate-PEG-lipid included in the liposome formulation, where a higher molar ratio reduces uptake into cells but increases cytotoxicity [31].

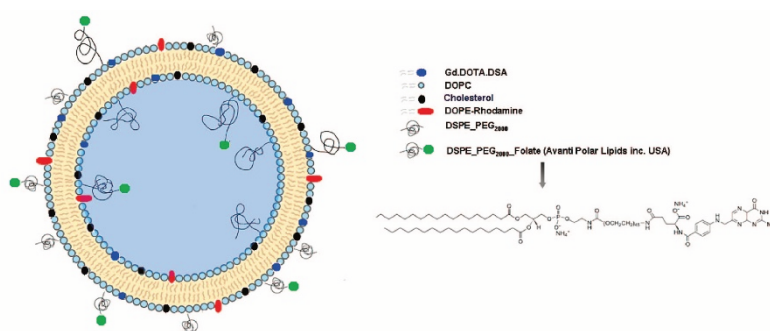


Fig. 4. Example of liposomes labeled with a DSPE-PEG-Folate ligand. Taken from [32].

The human cell lines KB and HeLa have significant FR surface expression levels and are thus used as *in vitro* cell models for the study of the interaction between folate-conjugated drugs and FR expressing cells. However, KB cells have become the standard study model due to their higher FR surface expression which can be more than ten times greater than in HeLa cells due to the higher availability of FR on their membrane [33].

4.1.5 THE LOGISTICS OF THE ENDOSOMAL SYSTEM AND THE ENDOSOMAL ESCAPE PROBLEM

The first step in the delivery of liposomes by active targeted delivery through folate receptor-mediated endocytosis is the bypassing of the plasma membrane barrier by endocytosis via intracellular entrapment inside endosomes. Endocytosis is a basic biological process through which cells internalize biomolecules via the formation of primary-endocytic vesicles or vacuoles by invagination of the plasma membrane followed by membrane fission [34]. Endocytic pathways are energy dependent-processes, since they require exhaustive rearrangements of cellular adaptors and the cytoskeleton [35]. Typically, endocytosis pathways are classified into five major categories (Fig. 5): phagocytosis, micropinocytosis, clathrin and caveole mediated endocytosis, and clathrin- and caveolin- independent pathways [36].

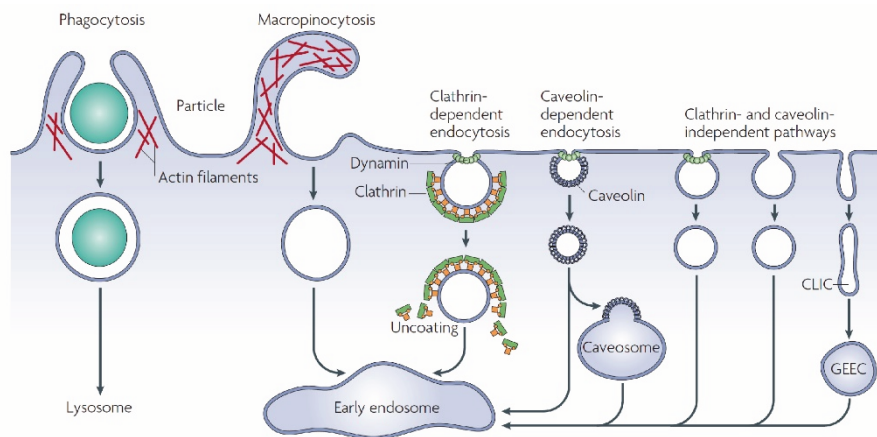


Fig. 5. Cellular entry mechanisms in mammalian cells. Taken from [36].

Large particles ($> 0.5 \mu\text{m}$) are internalized through phagocytosis (endocytosis and exocytosis of nanoparticles in mammalian cells), while fluid uptake is carried out through macropinocytosis. Phagocytosis and micropinocytosis are dependent on the actin-induced rearrangement of the plasma membrane [36].

Except in the case of phagocytosis, in all other endocytic pathways, primary endocytic vesicles deliver their cargoes (ligand and receptor in the case of receptor-mediated endocytosis) and their membrane to early endosomes (pH 6.8-6.1), also called sorting endosomes, in the peripheral cytoplasm (Fig. 6). From early endosomes, cargo can follow different fates. First, it can be recycled back to the plasma membrane through recycling endosomes. Second, it can remain on the early endosomes, that will mature into late endosomes (pH in range 6-4.8) through a pH acidification-dependent process while moving towards the perinuclear area of the cell with the help of microtubules. After continuing the pH-dependent maturation process, late endosomes fuse with lysosomes, where pH can drop to values around 4.5, generating a hybrid organelle called endolysosome, in which the cargo is destroyed through an active process of degradation [34]. Alternatively, some cargoes may be released into the cytosol by formation of intraluminal vesicles (ILVs) inside the endosomes. ILVs induce this delivery through membrane fusion with the endosomal membrane [35].

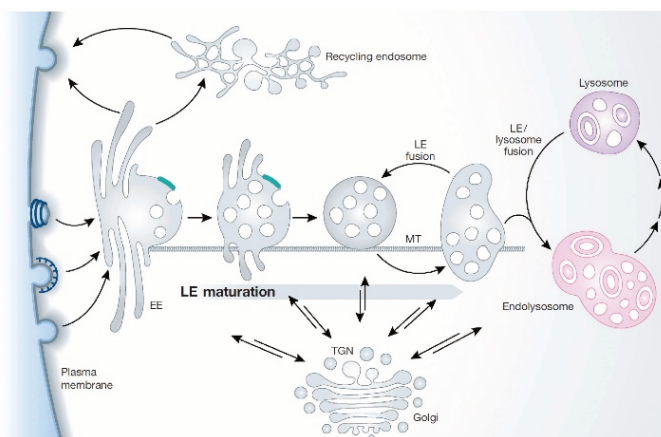


Fig. 6. The endolysosomal system. Taken from [34]. EE: early endosomes; LE: late endosomes; MT: microtubules; TGN: *trans-Golgi network*.

Understanding nanoparticle endocytosis mechanisms is essential to develop effective drug delivery systems [37]. Endosomal entrapment is known to be the major obstacle for intracellular delivery with non-viral nanodelivery systems. Most particles entering cells through endocytosis end up in lysosomes, where they undergo degradation, resulting in limited success from the delivery of therapeutic particles [38]. For successful delivery, it is essential that their cargo is released into the cytoplasm prior to their degradation in the endolysosomal compartment [38–40].


4.1.6 CELL PENETRATING PEPTIDES (CPPS) TO TRIGGER ENDOSOMAL ESCAPE

To overcome this bottleneck, endosomolytic peptides or cell penetrating peptides (CPPs) are commonly coupled to the nanocarrier as an approach to enhance early endosomal escape and release of therapeutic cargos into the cytosol, preventing their degradation in lysosomes [38, 39]. The use of engineered pH-responsive CPPs whose activity is triggered by the endosomal environment (pH 5.5–6.5), but are inactive in the bloodstream (pH 7.4), is of special interest since their use can minimize the toxicity side effects provoked by natural CPPs, as they interact nonspecifically with all biological membranes [39, 41].

Melittin, the major component of bee venom, is a cationic peptide with strong membranolytic activity. Its amphipathic α -helical structure in aqueous solution in combination with its positive charge enable its insertion into the lipid membrane, provoking its destabilization [38]. Like all other natural CPPs, its membranolytic activity is not specific to the endosomal environment. Acid melittin, a modified variant of the melittin peptide, is known to exhibit lower membranolytic activity at physiological pH, but optimal activity at endosomal pH [39, 42]. In this variant, all positively charged amino acids are replaced with glutamic acid to make the peptide pH-responsive through a conformational change induced by the protonation of these residues (see Table 1). Recently, a derivative from acid melittin called azido acid melittin was engineered, that incorporates an azido group at the N-terminus thanks to which the peptide can be chemically conjugated to the surface of liposomes [39]. Acid melittin and azido acid

melittin have shown similar pH-responsive membranolytic activities when assayed as free peptides in calcein leakage assays with SUVs, with up to an 80% higher activity at endosomal pH (5.6) compared to physiological pH (7.4).

Table 1. Melittin peptides. Taken from [39].

Peptide	Sequence and Structural Modifications
Melittin	GIGAVLKVLTTGLPALISWIKRKRQQ
Acid-Melittin	GIGAVLEVLTTGLPALISWIEEEEQQC
Azido-Acid-Melittin	 $\text{N}_3\text{-CH}_2\text{-C(=O)-NH-GIGAVLEVLTTGLPALISWIEEEEQQ}$

4.1.7 VESICLE BIOREACTORS FOR THE EXONUCLEATE PRODUCTION OF THERAPEUTIC shRNA INSIDE MAMMALIAN CELLS

The need of nuclear delivery for the efficacious expression of therapeutic shRNA in mammalian cells could be potentially bypassed through approaches that allow exonucleate transcription inside the cells [18]. The development of artificial intracellular organelles is a potential approach to overcome this and other obstacles in the field of biomedicine [18, 43]. Although liposomes are the most widely studied therapeutic carriers, their potential as intracellular artificial organelles has only recently been shown by Chan et al. [18]. This study demonstrated for the first time that RNA-producing nanoliposomes were capable of producing exogenous mRNA inside anucleate cells (for a detailed description of this study, see Chapter 3).

In this study, we set out to develop an RNA-producing fed-vesicle bioreactor platform that would allow shRNA production inside cells, thus acting as intracellular artificial nano-organelle and avoiding the need for nuclear DNA delivery.

To this end, we designed a standard DNA platform for the production of different shRNA molecules under the control of a T7 RNA promoter. The silencing efficacy of the shRNA produced was tested in vitro with purified components as well as in different mammalian cell types. Bioluminescence assays and RT-qPCR were used as readout of silencing efficacy. The delivery of shRNA entrapped in liposomes with a fed-bioreactor-like composition was explored through silencing assays. Furthermore, folic acid was incorporated to the surface of these liposomes as a ligand to allow targeted delivery of shRNA. The association of liposomes to cells and their final destination within them was explored by confocal microscopy. Moreover, we studied the use of acid-melittin as a potential tool to induce endosomal escape and release shRNA cargo from liposomes through single vesicle assays by confocal microscopy. Finally, we intended to implement the fed-vesicle bioreactor described in Chapter 2 for the production of shRNA (Fig. 7a), and envisioned the further implementation of this system with the future addition of the LA-T7 technology developed in Chapter 3 to provide the system with spatiotemporal control capability. Though we only explored the implementation of this DNA

platform in fed-vesicle bioreactors, non-fed bioreactors (Fig. 7b) could also be developed on the basis of this system.

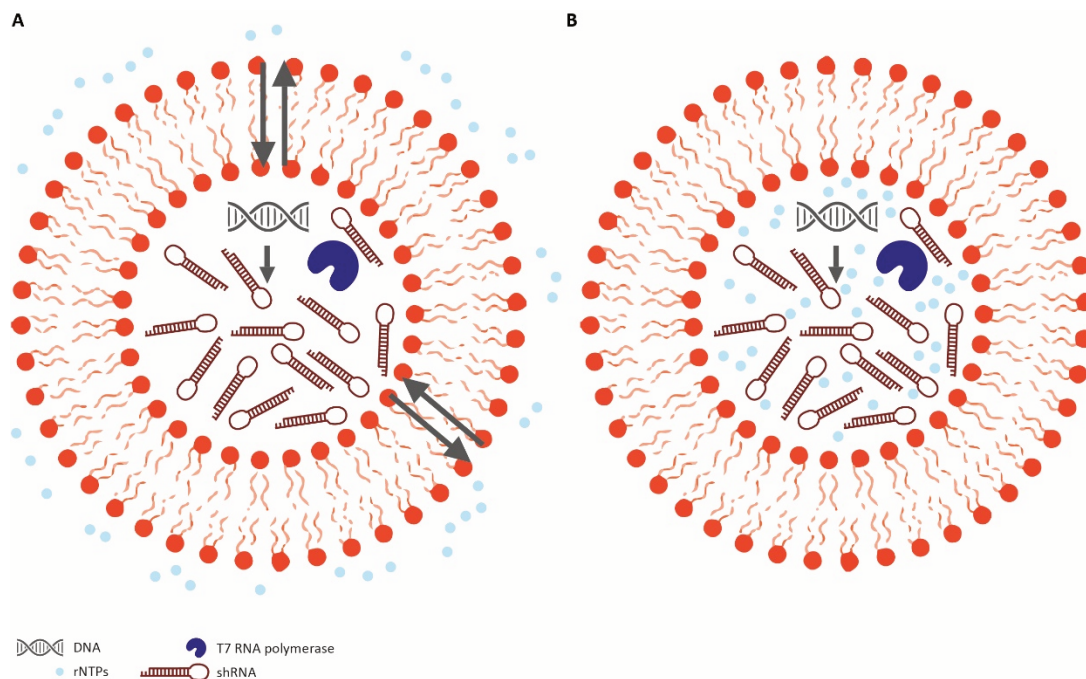


Fig. 7. A) Fed and B) non-fed vesicle shRNA-producing bioreactors.

4.2 MATERIALS AND METHODS

4.2.1 MATERIALS

HeLa cells were kindly provided by Eric P. van der Veer, Leiden University Medical Center, Leiden (The Netherlands). KB cells, a derivative cell line from HeLa, were purchased from DSMZ (ACC 136). 1,2-Dimyristoyl-sn-glycero-3-phosphatidylcholine (DMPC) 10 mg/ml, 1,2-dimyristoyl-sn-glycero-3-phosphoglycerol (DMPG) 10 mg/ml, 1,2-distearoyl-sn-glycero-3-phosphoethanolamine-N-[biotinyl (polyethylene glycol)-2000] (DSPE-PEG (2000) Biotin) 10 mg/ml, Cholesterol 50 mg/ml and 1,2-distearoyl-sn-glycero-3-phosphoethanolamine-N-[folate(polyethylene glycol)-5000] (DSPE-PEG(5000) Folate) 500 μ g were purchased from Avanti Polar Lipids. 1 mg of Texas Red[®] 1,2-dihexadecanoyl-sn-glycero-3-phosphoethanolamine (DHPE-Texas Red) was purchased from ThermoFisher Scientific.

4.2.2 shRNA SEQUENCE DESIGN

shRNA-luc was designed to target a modified version of the luciferase gene from the North American *Firefly* (GenBank Accession No. M15077), *Photinus pyralis*, encoded by the pGL3-control vector (Sigma-Aldrich). The sequence of this shRNA was designed on the basis of a commercially available shRNA-encoding DNA plasmid (SHC007; Sigma-Aldrich), that targets

the positions 159-180 (from ATG) from the coding sequence (CDS) of *Firefly* luciferase carried on the pGL3-Control vector.

shRNA-men1 was designed to target the endogenous human gene MEN1. The sequence of this shRNA was designed on the basis of the commercially available TRCN0000040138 shRNA sequence (Open Biosystems), that targets the sequence 5' CCGAGTACAGTCTGTATCAAAC 3', corresponding to the positions 194 to 216 in the 3' untranslated region (3' UTR) of the human MEN1 gene (GeneBank Accession No. U93236.1).

Scrambled shRNAs were designed as negative controls for both shRNA-luc and shRNA-men1 (named shRNA-scr and shRNA-m-scr, respectively). The sequences of scrambled shRNAs were BLAST searched in the National Center for Biotechnology Information (NCBI) against all human sequences deposited in the GenBank and were not found to have significant homology to any gene (<50%) ensuring no off-target gene silencing in *in vitro* human cell assays.

4.2.3 ssDNA OLIGOS HYBRIDIZATION TO FORM LINEAR dsDNA TEMPLATES FOR shRNA PRODUCTION

DNA constructs encoding the shRNA molecules were assembled by hybridization of two fully complementary ssDNA oligos (see Table 2). Briefly, 6.67 mM of forward oligo and 6.67 mM of reverse oligo were hybridized in T4 DNA Ligase Reaction Buffer (NEB) by an incubation for 5 min at 90 °C in a water bath followed by overnight cooling at room temperature. The hybridization product was analyzed with a 1.2% agarose gel in TAE buffer using a 50-bp DNA ladder (NEB) and further purified with the Wizzard PCR-clean up System (Promega).

Table 2. ssDNA oligos used to assemble shRNA-encoding DNA templates.

ssDNA oligo name	Sequence (5'-3')	Name of shRNA encoded
413ChD (Fw)	GAAATTAATACGACTCACTATA ^a GGCGCTGAGTACTTCGAAATGTC ^b TCTGA ^c GGACATTTCTGAAGTACTCAGCG ^d TTT	shRNA-luc
414ChD (Rv)	AAACGCTGAGTACTTCGAAATGTCCTCGAGGACATTTCTGAAGTACTCAGCGCTATAGTGAGTCGTATTAATTTTC	shRNA-luc
568ChD (Fw)	GAAATTAATACGACTCACTATA ^a GGGCTGCCTCTAACGGGATATTCATCGATGAATATCCCGTTAGAGGCAGCTTT	shRNA-scr
569ChD (Rv)	AAAGCTGCCTCTAACGGGATATTCATCGATGAATATCCCGTTAGAGGCAGCCCTATAGTGAGTCGTATTAATTTTC	shRNA-scr
698ChD (Fw)	GAAATTAATACGACTCACTATA ^a GGGCTGTACCTGAAAGGATCATACTCGAGTATGATCCTTTTCAGGTACAGCCCTATAGTGAGTCGTATTAATTTTC	shRNA-men1
699ChD (Rv)	AAAGCTGTACCTGAAAGGATCATACTCGAGTATGATCCTTTTCAGGTACAGCCCTATAGTGAGTCGTATTAATTTTC	shRNA-men1
726ChD (Fw)	GAAATTAATACGACTCACTATA ^a GGGTAGCTATTCGAAGCACTAGACTCGAGTCTAGTGCTTCGAATAGCTACTTTT	shRNA-m-scr
727ChD (Rv)	AAAGTAGCTATTCGAAGCACTAGACTCGAGTCTAGTGCTTCGAATAGCTACCCTATAGTGAGTCGTATTAATTTTC	shRNA-m-scr

^aT7 promoter

^bSequence encoding shRNA sense strand in coding strand of hybridized DNA template

^cSequence encoding shRNA loop in coding strand of hybridized DNA template

^dSequence encoding shRNA antisense strand in coding strand of hybridized DNA template

4.2.4 BULK shRNA PRODUCTION

1.34 mM dsDNA prepared as described above was transcribed in a mixture containing 10 μ l T7 RNA polymerase, 5 mM ribonucleotide triphosphate (rNTPs) and transcription buffer in a final volume of 100 μ l, by overnight incubation at 37 °C. All components for DNA transcription were obtained from RiboMAX Large Scale RNA production System-T7 (Promega). For the synthesis of fluorescently labelled shRNA, the rNTP composition of the transcription reaction was 200 μ M ATP, 200 μ M CTP, 200 μ M GTP, 160 μ M UTP and 40 μ M of aminoallyl-UTP-ATTO-488 (Jena Bioscience). Following transcription, the DNA template was removed by digestion with 3 μ l of DNase (Q1, Promega) for 30 min at 37 °C. shRNA was subsequently purified with a RNeasy® MinElute® Cleanup Kit (Qiagen) and its concentration and quality were determined with a Nanodrop 2000 UV-Vis Spectrophotometer. The size of the fluorescently labelled shRNA was analyzed by denaturing acrylamide gel electrophoresis.

4.2.5 DENATURING UREA POLYACRYLAMIDE GEL ELECTROPHORESIS (UREA PAGE)

RNA-containing samples were incubated at 65 °C for 5 min in RNA loading buffer (NEB, containing 50% formamide) and the RNA integrity and size were verified by 7 M urea denaturing 12% polyacrylamide gel electrophoresis (120 V, 60 min) followed by gel imaging. When the RNA was not fluorescently labelled, gel imaging was performed after ethidium bromide staining (1×10^{-3} mg/mL in TBE) for 15 min. Gel imaging was performed in a Typhoon Trio (GE Healthcare Life Sciences) with appropriate settings for ethidium bromide and ATTO-488 detection.

4.2.6 CELL CULTURE

HeLa and KB cells were cultured in folate-deficient RPMI-1640 (no folic acid, ThermoFisher) medium supplemented with 10% heat-inactivated FBS (ThermoFisher) with 5% CO₂ at 37 °C. Cells were discarded after 35 passages. HEK 293T cells were cultured in DMEM (ThermoFisher) medium supplemented with 10% heat-inactivated FBS with 5% CO₂ at 37 °C.

4.2.7 CALCIUM PHOSPHATE TRANSFECTION

3×10^5 KB, HeLa or HEK 293T cells were seeded in 6-well plates in 3 ml of growth medium and incubated for 24 h at 37 °C with 5% CO₂ at 37 °C prior to transfection. 0.28 μ g of pGL3 control vector (5256 bp, Promega) harboring the gene encoding the *Firefly* luciferase, was mixed together with 0.019 μ g pRL-SV40 vector (3705 bp, Promega), harboring the gene encoding *Renilla* luciferase at a pGL3:pRL-SV40 ratio of 10:1 (mol:mol). The DNA was added to a solution containing 125 mM CaCl₂ and 1x HEPES buffer saline (HBS), and subsequently added to the cells. After incubation for 5 h (KB, HEK 293T) or 16 h (HeLa), the cells were washed with PBS and fresh growth medium was added.

4.2.8 LIPOFECTAMINE TRANSFECTION

$6 \cdot 10^4$ (or $3 \cdot 10^4$) KB or HeLa cells were seeded in 24-well plates in 600 μ l of growth medium and incubated for 24 h (or 48 h) with 5% CO₂ at 37 °C prior to transfection. For luminescence silencing assays, pRL-SV40 and pGL3 Control plasmid were complexed with cationic lipids using Lipofectamine® 3000 Reagent (ThermoFisher) at a pGL3:pRL-SV40 ratio of 10:1 (mol:mol). 4 μ g of shRNA were transfected using Lipofectamine® 3000 Reagent, 24 h after DNA transfection. When no DNA transfection was required (MEN1 silencing assays), cells were transfected with 4 μ g shRNA using Lipofectamine 3000 Reagent, 24 or 48 h after seeding.

4.2.9 ELECTROPORATION TRANSFECTION

KB cells were suspended in RPMI-1640 (ThermoFisher, containing folic acid) medium or HEPES buffer (20 mM HEPES, 0.7 mM NaPO₄H, 137 mM NaCl, 5 mM KCl and 6 mM Glucose) at a concentration of $2 \cdot 10^6$ cells/ml. 250 μ l of cells were transfected with a total of 5 μ g of pGL3: pRL-SV40 mixed at a ratio of 10:1 (mol:mol). The resulting mix was transferred to an electroporation cuvette (0.2 mm gap width; Bio-Rad) and electroporated with a Bio-Rad MicroPulser set at different voltages and frequency of pulses. Pulse duration was 0.6 ms. After electroporation, the cells were plated on 100 mm x 20 mm poly-lysine coated plates (TC Dish 100, Standard, Sarstedt) and incubated for 24 h at 37 °C and 5% CO₂ before measurements.

4.2.10 DUAL LUCIFERASE ASSAY

All dual luciferase assays were performed using the Dual Luciferase Assay Kit (Promega). 24-h post RNA transfection, cells were washed with PBS and lysed with 1x passive lysis buffer (PLB) and maintained in ice until use according to the manufacturer's instructions. 25 μ l of Luciferase Assay Reagent II (LAR II) were added to 5 μ l of cell lysate in white, flat bottom 96-well Corning plates (3917, Sigma-Aldrich) and the *Firefly* luciferase luminescence was measured immediately for 10 sec. Subsequently, 25 μ l of Stop & Glo reagent was added, and the *Renilla* luciferase intensity measured immediately for 10 sec. All bioluminescence measurements with a CLARIOstar Microplate reader (BMG LABTECH'S) were performed at a focal height of 10 mm and the monochromator set to detect luminescence wavelengths between 520-620 nm. Each sample was measured in triplicate, and the normalized activity intensities of *Firefly* to *Renilla* luciferase (FF/RL) was calculated.

4.2.11 RNA ISOLATION FROM CELLS AND RELATIVE QUANTIFICATION BY RT-QPCR

Total RNA from KB and HeLa cells was isolated using Tri Reagent (Sigma Aldrich) according to the manufacturer's instructions. The resulting RNA pellets were resuspended in nuclease free water and stored at -80 °C until use. RNA concentration and purity was determined using a Nanodrop 2000 UV-Vis Spectrophotometer. RT-qPCR mixtures were prepared using Power SYBR Green RNA-to-Ct 1-Step Kit (Applied Biosystems) following the manufacturer's protocol. Primers were designed to amplify a 269-bp long region of the human MEN1 gene

(FW MEN1, 5'-CAGGGGCCAGACAGTCAATG-3'; RV MEN1, 5'-GGTGGGCTCCAGCTCCTCTA-3', [44]) or a 140-bp long region of the human glyceraldehyde-3-phosphate dehydrogenase gene (GAPDH; FW GAPDH, 5'-GCCACATCGCTCAGACAC-3'; RV GAPDH, 5'-GGCAACAATATCCACTTTACCAG-3'; [45]). An RNA concentration of 52 ng/μl was used. 10-μl RT-qPCR reactions were pipetted on a microplate (Eco Sample Dock, Illumina) and spun for 10 s at 3000 rpm (Eppendorf 5810R centrifuge). All samples were loaded in triplicate. RT-qPCR was performed in a Eco Real-Time PCR system (Illumina). RT-qPCR conditions were as follows: 30 min at 65 °C (for the generation of cDNA), followed by 40 cycles of 30 sec at 63 °C, 45 sec at 72 °C (for PCR amplification of cDNA). Melting curves were generated following RT-qPCR amplification. RT-qPCR amplicon products were analyzed with a 1.2% agarose gel in TAE buffer using the BenchTop 1-kb DNA ladder (Promega).

4.2.12 PREPARATION OF LIPID-COATED BEADS

A mixture of chloroform-dissolved lipids (see Table 3) for a total mass of 1 mg, was assembled in a 25-ml round-bottom glass flask. 0.75 g of 212-300-μm acid-washed glass beads (Sigma-Aldrich) were added to the lipid mixture, and the organic solvent was removed by overnight rotary evaporation at 400 mbar. The dried lipid-coated beads were stored under argon at -20 °C and desiccated for at least 20 min or flushed with argon for 30 sec before use. Each lipid-pipetting tip was washed three times with chloroform, and the washing volumes were added to the mixture.

Table 3. Liposome formulations.

Name	Composition	Molar %
DMPC	DMPC:DMPG:Cholesterol:DSPE-PEG(2000)-biotin:DHPE-TexasRed	66.3:16.6:16.6:0.5:0.2
DMPC-Fol	DMPC:DMPG:Cholesterol:DSPE-PEG(2000)-biotin:DHPE-TexasRed: DSPE-PEG(5000)-Folate	66.2: 16.6:16.6:0.5:0.2:0.1
DOTAP	DMPC:DOTAP:DHPE-TexasRed	98.9:1:0.02

4.2.13 EXTRUSION

Liposome solutions resulting from lipid film swelling were downsized by 13 extrusion passages with a 0.8-μm or a 0.2-μm filter membrane (Avanti Polar Lipids) for the production of large unilamellar vesicles (LUVs) or small unilamellar vesicles (SUVs), respectively, with two mini filter supports (Whatmann) on a mini-extruder (Avanti Polar Lipids). Prior to each extrusion, the assembled extruder was pre-heated to 40-50 °C and pre-washed with sample buffer.

4.2.14 PRODUCTION OF LIPOSOMES

For the production of DMPC liposomes loaded with shRNA-luc for HEK 293T cells transfection, 75 mg of lipid-coated beads of DMPC lipid film were hydrated with 3.5 μg of in vitro transcribed or chemically synthesized shRNA-luc diluted in 200 μl of PBS, by vigorous vortex for 1 min. The resulting liposome was subjected to ten freeze-thaw cycles and extruded to produce SUVs. Unencapsulated shRNA was removed by addition of 0.5 U/μl RNase ONETM Ribonuclease (5-10 U/μl, Promega) followed by an incubation step at 37 °C for 20-30

min. 91 μl of liposome solution were added to HEK 293T cells. DOTAP liposomes encapsulating chemically synthesized shRNA-luc were produced likewise, but the swelling solution contained 0.5 μg of shRNA and 100 μl of SUVs were added to HEK 293T cells instead.

When DMPC-Fol liposomes loaded with shRNA-luc or shRNA-men1 were made, 75 mg of lipid-coated beads were hydrated with 4 μg of in vitro transcribed shRNA diluted in 200 μl of transcription buffer by 2 h incubation at 37 °C and 300 rpm. After extrusion and RNase incubation, 80 μl of shRNA-luc containing liposomes were added to cells for HeLa cell transfection. Empty DMPC-fol and DMPC liposomes were produced likewise, using transcription buffer as swelling solution.

4.2.15 ASSOCIATION OF LIPOSOMES WITH CELLS

3×10^5 HeLa or KB cells were seeded in 3-ml culture medium in glass-bottom microscopy plates (MatTek; 9.5 cm^2) and incubated for 24 h at 37 °C with 5% CO_2 prior to each experiment. Subsequently, 40 μl of empty DMPC-Fol or DMPC liposomes were added to the cells and incubated for 2 h or 18 h after which plates were mounted in a microscope stage maintained at 37 °C and 5% CO_2 for confocal imaging.

4.2.16 COLOCALIZATION OF LIPOSOMES WITH LYSOSOMES

1.5×10^5 HeLa or KB cells were seeded in 3-ml culture medium in glass-bottom microscopy plates (MatTek; 9.5 cm^2) and incubated for 24 h or 72 h at 37 °C with 5% CO_2 , respectively. At this point, cell culture medium was refreshed and cells were transfected with 10 μl or 5 μl of the lysosomal Cell Light® Lysosome-GFP baculovirus solution (ThermoFisher, Bacmam 2.0), and incubated for 16 h following manufacturer's instructions. 80 μl of shRNA-men1 DMPC-Fol liposomes swelled with transcription buffer were added and the plates were mounted in a microscope staged maintained at 37 °C and 5% CO_2 for time-lapse confocal imaging during 60 h.

4.2.17 shRNA RELEASE ASSAY WITH AZIDO ACID MELITTIN (A-A MELITTIN)

A 200- μM stock solution of azido acid melittin was prepared in PBS pH 8.7 to preserve the peptide in inactive state. For the formation of liposomes, 75 mg of DMPC-Fol lipid-coated beads were swelled with a 200- μl solution containing 40 μM free azido acid melittin (A-A melittin, 2981.39 g/mol) peptide, transcription buffer 5x and PBS pH 8.7 overnight at 37 °C. As negative control, transcription buffer 5x and PBS pH 8.7 were used for swelling. Fluorescently labelled shRNA was then externally added to the liposomes at a final concentration of 1 μM and was co-entrapped in the liposomes through ten freeze-thaw cycles. The resulting liposome solutions were downsized by extrusion to produce LUVs or SUVs. After extrusion, the liposome samples were incubated with 2 μl RNase for 30 min at 37 °C, to digest unencapsulated shRNA. Each liposome sample was then split in two and diluted 50x in PBS pH 8.7 or pH 4.5 and incubated for 20 min at 37-40 °C. 7 μl of each liposome-containing sample were immobilized via biotin-neutravidin binding interactions at the bottom of a microscope glass chamber

functionalized with BSA-biotin and neutravidin (see Fig. 6 on Chapter 3), mounted in a stage prewarmed to 37 °C for confocal imaging.

4.2.18 shRNA TRANSCRIPTION IN FED-VESICLE BIOREACTORS

shRNA transcription in fed-vesicle bioreactors was investigated in the presence and absence of Aminoallyl-UTP ATTO-488 in the total rNTP mix. When regular rUTP was used, a 200- μ l pre-transcription reaction consisting of 70 nM DNA templates encoding shRNA-luc or shRNA-men1, 4 μ l of 10-20 U/ μ L T7 RNA Polymerase (Promega) and homemade T7 transcription buffer (that does not contain NTPs) was prepared, and incubated for 20 min at room temperature to induce the formation of DNA-RNA polymerase complexes. Next, 75 mg of DMPC-Fol lipid-coated beads were mixed with the pre-transcription sample for 2 h at 37 °C and gentle manual swirling every 15 min. When Aminoallyl-UTP ATTO-488 was used, the volume of the pre-transcription reaction and mass of lipid-coated beads was halved. The resulting liposome solution was extruded to produce SUVs or LUVs. Unencapsulated DNA was removed by addition of 0.05 U/ μ l DNase (1 U/ μ l, RQ1, Promega) followed by an incubation step for 20 min at 37 °C. When regular rUTP was used, DNA transcription was triggered inside liposomes by addition of 5 mM rNTPs, followed by an incubation step for 3 h at 37 °C. When Aminoallyl-UTP ATTO-488 was used, transcription was triggered by addition of 200 μ M ATP, 200 μ M GTP, 200 μ M CTP, 160 μ M UTP and 40 μ M Aminoallyl-UTP ATTO-488. Control samples without T7 RNA polymerase or DNase were prepared in parallel. The production of non-fluorescent and fluorescently-labelled shRNA inside liposomes was analyzed by denaturing PAGE. The liposome sample in which Aminoallyl-UTP ATTO-488 was used was additionally imaged by confocal microscopy. Briefly, ATTO-488 containing liposomes were diluted 10x in sample buffer and 7 μ l were immobilized in a custom-made imaging chamber functionalized with BSA-biotin and NeutrAvidin (see Fig. 6 on Chapter 3). The sample of immobilized liposomes was imaged by total internal reflection fluorescence microscopy (TIRFM) using a Nikon Tie microscope, with a 100x oil immersion objective, using the 488 nm (ATTO-488) and 561 nm (Texas Red) laser lines with appropriate emission filters.

4.2.19 CONFOCAL MICROSCOPY AND IMAGE ANALYSIS

A Nikon A1+ laser scanning confocal microscope equipped with a 100x oil immersion objective was used in sections 4.2.15, 4.2.16 and 4.1.17. The laser lines 488 nm and 561 nm were used to detect GFP or ATTO-488 and Texas Red dye respectively. Colocalization was quantified by calculating of the Pearson's coefficient with the JaCop plugin for ImageJ [46]. Microscopy images from immobilized liposomes were analyzed with MATLAB (MathWorks).

4.3 RESULTS

4.3.1 DESIGN AND SYNTHESIS OF shRNA FROM A LINEAR DNA TEMPLATE USING T7 RNA POLYMERASE

To enable optimal in vitro shRNA transcription with the T7 RNA polymerase, DNA templates were designed such that transcription would initiate with two GG nucleotides. Moreover, the consensus GAAAT sequence was added at positions -22 through -18. These two features are known to enable efficient RNA transcription [47,48] (Fig. 8a). Thus, all 5' shRNA stems started with GG. Further, shRNA-encoding sequences were designed such that they would yield a 53 basepair (bp) hairpin structure, with a 24 bp stem from which 22 bp were homologous to the nucleotides 159 to 180 of the coding region (CDS) of the target gene *Firefly* luciferase, and a loop composed of the four nucleotides 5' UCGA 3' (Fig. 8b). Loop and gene homologous regions were adapted from an available sequence for shRNA expression from a mammalian vector [49]. The last three nucleotides of the shRNA sequence are three consecutive UUU, to generate a 3' overhang, known to favor Dicer processing [50]. The DNA template encoding the scrambled shRNA was designed by scrambling the 22 bp homologous to the *Firefly* gene sequence, while all other features remain. Transcription templates that were predicted to generate the desired shRNAs were prepared by DNA hybridization of single-stranded complementary DNA oligos (Fig. 8c). A single band on gel around 75 bp was observed, indicating that these shRNA-encoding T7 DNA templates were formed correctly. Next, we tested whether shRNA-luc could be prepared by in vitro transcription with T7 RNA polymerase, and its apparent size was compared to that of the same shRNA produced by chemical synthesis on denaturing conditions. As shown in Fig. 8d, the apparent sizes of both the in vitro transcribed shRNA and the chemically synthesized shRNA were similar, indicating that T7 transcription generates full length shRNA-luc. However, while their theoretical size is 53 bp, their apparent size was considerably lower than expected considering the denaturing conditions of the gel (7.5 M Urea) [51]. Likewise, shRNA-scr showed a similar apparent size to that of both types of shRNA-luc as expected due to their identical length, indicating the successful generation of full-length shRNA-scr. This result was observed in all experimental repeats with these shRNAs and with other tested shRNA sequences (data not shown). These results suggest that, despite the denaturing conditions, the shRNAs remained folded, which influences diffusion in gel. Sometimes, a small fraction of shRNA showed an apparent size matching with the denatured full-length shRNA, but this observation was not consistent over experiments.

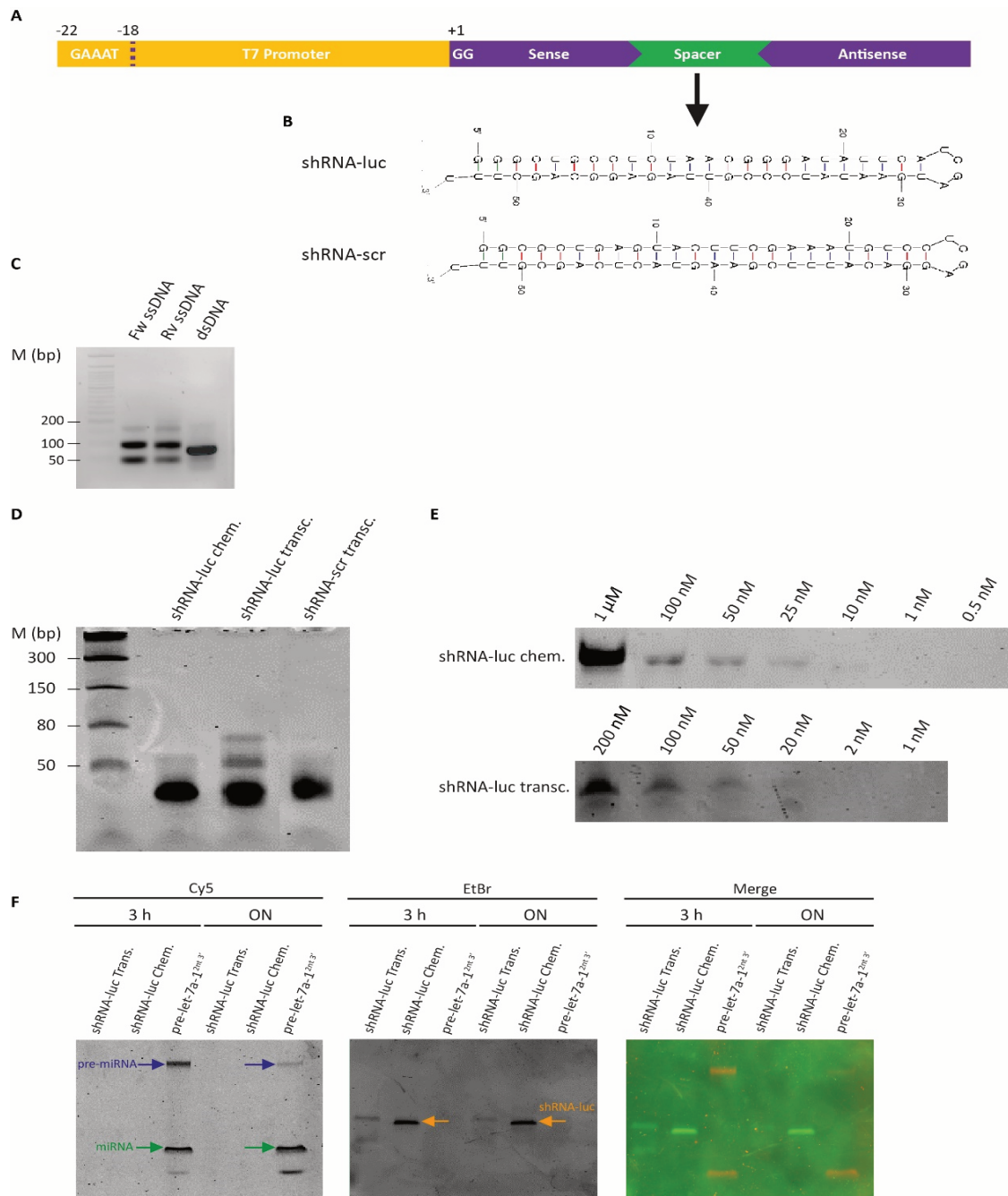


Fig. 8. Design, synthesis and in vitro cleavage of shRNA-luc. A) Design of shRNA-encoding DNA templates for transcription with a T7 RNA polymerase. B) Sequences and predicted secondary structure of representative in vitro T7 transcribed shRNAs. Sequences shRNA-luc and shRNA-scr target the positions 159-180 (from ATG) from the coding sequence (CDS) of *Firefly* luciferase carried on pGL3-Control and the scrambled sequence from shRNA-luc, respectively. C) Hybridization of ssDNA primers to yield an shRNA-encoding DNA template. D) Acrylamide gel visualization of in vitro transcribed shRNA-luc and shRNA-scr compared to chemically synthesized shRNA-luc. E) Titration of chemically synthesized and in vitro transcribed shRNA-luc. F) Analysis of shRNA-luc cleavage by purified human Dicer. The Cy5-labelled pre-let-7a-1^{2nt 3'} was used as a positive control of Dicer activity. The molar concentration of shRNA-luc and pre-let-7a-1^{2nt 3'} were 100 nM and 1 nM, respectively.

4.3.2 IN VITRO STUDY OF shRNA CLEAVAGE WITH PURIFIED HUMAN DICER ENZYME

Prior to studying the efficacy of shRNA-luc as inducer of luciferase gene silencing in mammalian cells, the cleavage of shRNA-luc was assayed *in vitro* with purified human Dicer enzyme [52]. Simulations of Dicer cleavage using the server software PHDcleav [53] predicted the formation of siRNA duplexes with lengths between 21 and 24 bps from shRNA-luc (data not shown). Since the Dicer enzyme concentration available for this assay (1 nM) could only cleave nanomolar RNA concentrations, an RNA titration assay was performed to determine the lowest RNA concentration that could be used for the Dicer cleavage assay without compromising the detectability of the cleavage products, which relied on EtBr staining. As shown in Fig. 8e, nanomolar shRNA-luc concentrations down to 20 nM of *in vitro* transcribed shRNA-luc and 25 nM of chemically synthesized shRNA-luc were detectable on gel. However, to avoid poor RNA detection upon partial shRNA cleavage, 100 nM was selected as optimal final shRNA-luc concentration for the assay, since it is readily detected. In addition, pre-let-7a-1^{3'2nt} (73 nt), a 3' mono-uridylylated form of the human tumor suppressor miRNA precursor (pre-miRNA) pre-let-7a-1 [54–56], was used as a positive control of Dicer activity, since previous studies showed that this pre-miRNA is optimally cleaved *in vitro* by purified human dicer into 22-bp mature let-7a miRNA duplexes [52, 56]. The pre-let-7a-1^{3'2nt} consists of a 21-bp base-paired stem region, a 27-nt terminal loop and a 2-nt 3' overhang. The pre-let-7a-1^{3'2nt} was labelled with a Cy5 fluorophore at the stem region (nt 69), allowing the detection of nanomolar concentrations on gel and, consequently, enabling the use of nanomolar concentrations in Dicer cleavage assays. Detection of shRNA-luc, on the contrary, relied on EtBr staining. Mature siRNA products from all shRNAs were expected to be seen as a band of equal size. As shown in Fig. 8f, as in former studies, Dicer efficiently induced the canonical cleavage of pre-let-7a-1^{3'2nt} pre-miRNA into mature 22-bp miRNA duplexes [52]. While 3 h incubation achieved partial pre-miRNA cleavage (Fig. 8f, middle panel), extending the incubation time overnight achieved the conversion of nearly all pre-miRNA into mature miRNA. Dicer cleavage also produced a minor fraction of a shorter let-7a miRNA isoform, previously observed in a similar study [52], a product of non-canonical cleavage [57]. In agreement with the results obtained for shRNA-luc in the titration assay (Fig. 8e), ethidium bromide staining was not sensitive enough to detect pre-let-7a-1^{2nt 3'} and its cleavage products (Fig. 8f), since the total concentration of RNA in these reactions was 3 nM, i.e. two folds below the ~20-25 nM minimum concentration necessary to detect shRNA-luc. We were unable to detect shRNA-luc Dicer cleavage products. However, the band intensity corresponding to the full length *in vitro* transcribed shRNA-luc was reduced by ~54% after overnight incubation compared to that detected in the sample incubated for 3 h. In contrast, the band density of the full length chemically synthesized counterpart was mildly reduced by ~10% after overnight incubation. Despite these differences, together, these results suggest that some Dicer cleavage took place, but the low concentration of Dicer used in these reactions (1 nM) only generated

concentrations of cleavage products that were below the detection limit using ethidium bromide staining. In combination, these results prompted us to study the silencing efficacy of shRNA-luc in a more direct manner, in mammalian cells, where the readout could be readily detectable through bioluminescence.

4.3.3 shRNA TRANSCRIBED IN VITRO SUPPRESS GENE EXPRESSION IN MAMMALIAN CELLS

The silencing efficacy of shRNA-luc was first assayed in HEK293-T cells, as a model of mammalian cells. As shown in Fig. 9a, co-transfection of *Firefly* and *Renilla* luciferase reporter plasmids with shRNA-luc yielded a ~90% suppression of *Firefly* luciferase without effect on *Renilla* luciferase. Moreover, the performance of the T7-synthesized hairpin closely matched that of the chemically synthesized shRNA with regard to the magnitude of gene expression inhibition. However, when silencing was intended with shRNA-luc encapsulated in DMPC or cationic SUVs (DOTAP), no silencing took place (Fig. 9b). Improved liposome delivery to the cells and shRNA release might be required for more effective silencing.

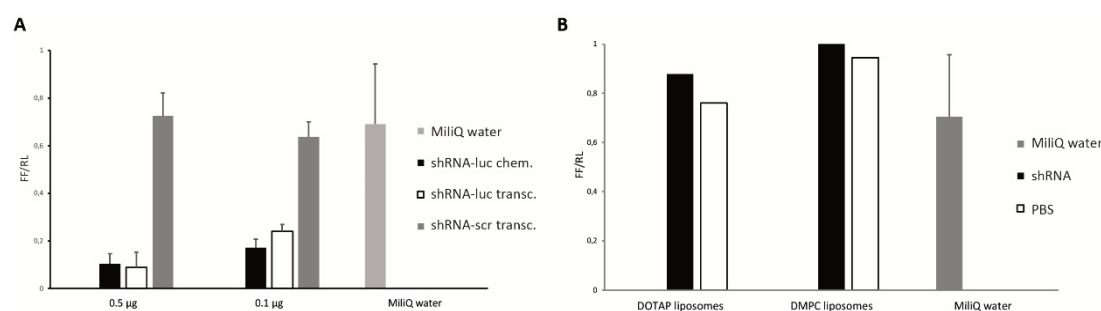


Fig. 9. shRNAs transcribed in vitro suppress gene expression in mammalian cells. A) shRNAs transcribed in vitro suppress expression of the targeted *Firefly* luciferase gene in HEK293T cells. HEK 293T cells overexpressing *Firefly* and *Renilla* luciferase were transfected with shRNA-luc and subjected to dual luciferase assays 48 h post-transfection. The values of *Firefly* luciferase activity are normalized to those of *Renilla* luciferase activity. The average of three independent experiments is shown; error bars indicate standard deviation. B) Normalized *Firefly* luciferase activity on HEK 293T cells transfected with shRNA-luc delivered through cationic (DOTAP) or DMPC SUVs.

4.3.4 FOLATE-TARGETED LIPOSOMES ARE SELECTIVELY UPTAKEN BY KB CELLS

To improve liposome delivery to tumor cells, the surface of DMPC SUVs was conjugated to folic acid. Due to the lack of FR expression of HEK 293T cells [58], the cellular association and uptake of folate-targeted liposomes was qualitatively studied in KB and HeLa cells, two FR-positive (FR+) tumor cell lines expressing distinct FR levels (KB > HeLa) [33, 59]. The uptake of fluorescently labelled folate-targeted liposomes was analyzed by confocal microscopy and compared to that of untargeted liposomes. As seen in Fig. 10a, folate-targeted liposomes showed pronounced binding with cell membranes, internalization and accumulation in the cytosol after 2 h incubation compared to non-targeted liposomes. Red punctuate fluorescence in the periphery of the cell and around the nucleus indicate that folate targeted liposomes selectively bind to KB cells through receptor-mediated endocytosis, as described in former studies [60].

In HeLa cells, the binding and internalization levels of folate-targeted liposomes were similar to those of non-targeted liposomes (Fig. 10b) after 2 h and 18 h incubation, indicating a low level of FR expression. These levels were significantly lower compared to those of targeted-liposomes in KB cells, in agreement with the lower FR expression described in former studies [33, 59].

In contrast, similar levels of internalization were observed in all types of conditions when incubation was extended overnight, indicating that after a certain incubation period, non-receptor mediated liposome endocytosis occurs, and folate-targeted liposomes lose their selective advantage over non-targeted liposomes (Fig. 10a-10b). Liposomes were accumulated in the cytoplasm, with more red punctuated fluorescence around the nuclei. Importantly, no alterations in cell morphology nor increase on apoptosis levels were observed after overnight incubation compared to the start of the incubation (data not shown), suggesting these liposome formulations are not toxic to KB or HeLa cells. Overall, these results were encouraging for the use of folate-targeted liposomes as delivery vehicle for shRNA.

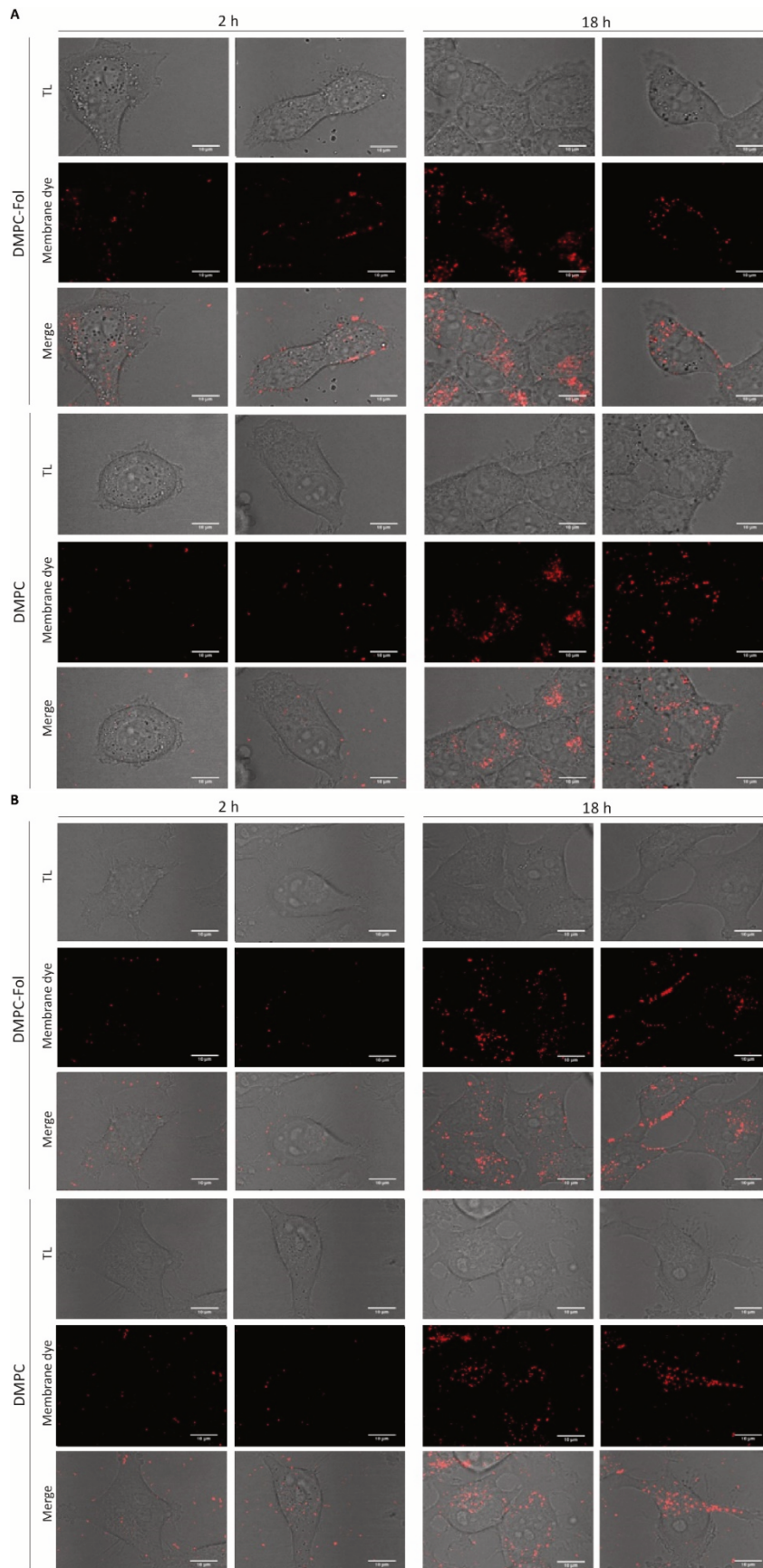


Fig. 10. Cellular association of FR-targeted DMPC SUVs (DMPC-Fol) and non-targeted SUVs (DMPC) to A) KB and B) HeLa cells analyzed by confocal microscopy. KB and HeLa cells were incubated with DMPC-Fol or DMPC liposomes for 18 h and images were acquired after 2 h and 18 h incubation at 37 °C. TL: transmitted light.

4.3.5. IN VITRO TRANSCRIBED shRNA CAN SILENCE LUCIFERASE IN LIPOFECTAMINE TRANSFECTED HELA CELLS, BUT NOT IN KB CELLS

To investigate the silencing efficacy of in vitro transcribed shRNA in HeLa and KB cells, we intended to silence the exogenously expressed luciferase protein in the same manner as for HEK 293T cells, through the consecutive transfections of plasmid DNA and shRNA with calcium phosphate (Fig. 9a). We first tried to optimize a protocol for successful DNA plasmid transfection. However, despite testing different conditions, calcium phosphate plasmid transfection led to excessive cell death and/or undetectable levels of luciferase activity in both cell lines (Table 4).

Table 4. Varying calcium phosphate transfection conditions for the co-transfection of *Firefly* and *Renilla* luciferase-encoding plasmids in HeLa and KB cells.

Total DNA (μg)	[CaCl ₂] (mM)	[HBS] (mM)	Incubation period (h)	HEK 293T	HeLa	KB
0.3	125	125	5	+	-	-
1.5	125	125	5			-
3.0	125	125	5			-
0.3	25	25	5		-	
0.3	12.5	12.5	5		-	
0.3	125	125	16		-	-

Based on a study describing successful transfection of KB cells through electroporation [61], KB cells were electroporated at different transfection conditions. Unfortunately, electroporation did not improve transfection efficiency in KB cells (Table 5).

Table 5. Varying electroporation conditions for the co-transfection of *Firefly* and *Renilla* luciferase-encoding plasmids in KB cells.

Total DNA (μg)	Voltage (V)	Pulses	Medium	<i>Firefly</i>	<i>Renilla</i>
1	370	1	RPMI	-	-
5	750	1	RPMI	-	-
5	1875	1	RPMI	-	-
5	750	1	HEPES	-	-
5	750	2	RPMI	-	-
5	750	5	RPMI	-	-

Lipofectamine transfection of KB and HeLa cells was the most efficient DNA transfection method, showing the highest luciferase expression levels relative to calcium phosphate and electroporation (Fig. 11a). From a range of four different plasmid DNA amounts, transfection of a total plasmid yield of 2.5 μg achieved the highest *Firefly* and *Renilla* luciferase bioluminescence activity. Transfection of 2.5 μg of DNA yielded *Renilla* luciferase activity signals 6.4 and 21.2-fold higher than *Firefly* luciferase in HeLa and KB cells, respectively. However, while *Firefly* activity signal was 16.9-fold higher than that of background signal in HeLa cells, this signal was only 3.7-fold higher than the background signal in KB cells. The latter value was considered too low for the reliable evaluation of silencing efficacy, limiting the use of

luciferase gene expression as a readout of gene silencing in KB cells. Consequently, only HeLa cells were further used to assay silencing of *Firefly* luciferase through lipofectamine transfection.

As shown in Fig. 11b, lipofectamine transfection of in vitro transcribed shRNA-luc yielded a $34 \pm 9\%$ and a $37 \pm 9\%$ suppression of *Firefly* luciferase 24 and 48 h after the start of incubation, respectively, with no effect on *Renilla* luciferase. This result demonstrates the ability of shRNA-luc to silence *Firefly* luciferase in HeLa cells too. Next, we investigated the silencing efficiency of shRNA-encapsulating folate-targeted liposomes in HeLa cells. For this, the liposomes were incubated continuously for 24 and 48 h with HeLa cells to induce maximum cell uptake, at the expense of sacrificing targeting specificity. As seen on Fig. 11c, shRNA-encapsulating folate-targeted liposomes yielded, unfortunately, no significant suppression of *Firefly* luciferase expression compared to empty folate-targeted liposomes, despite the long exposure of the cells to the liposomes.

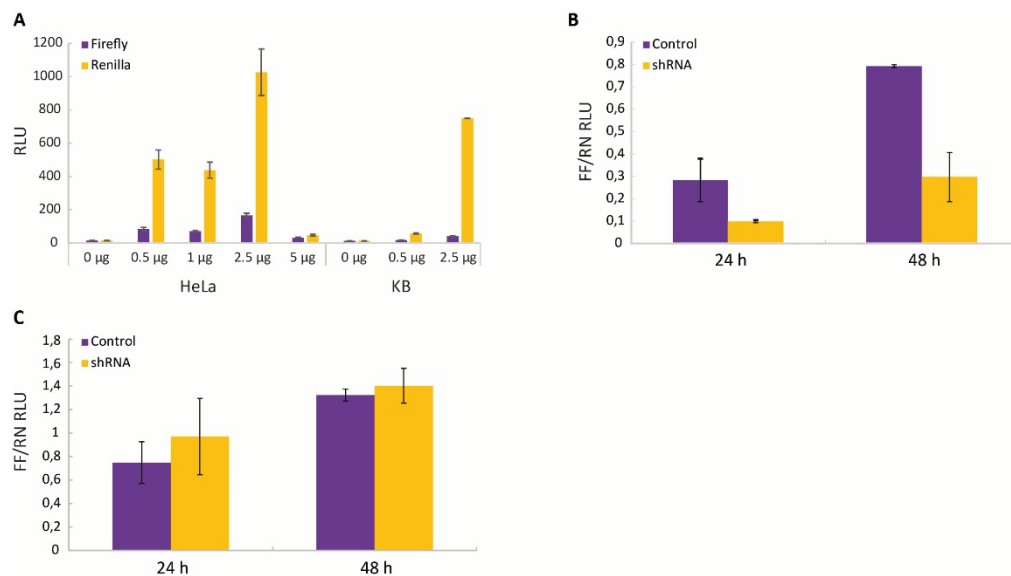


Fig. 11. A) Luminescence signal from *Firefly* (FF) or *Renilla* (RR) luciferase overexpressed in HeLa and KB cells 24 h post-transfection. Error bars represent standard deviation of a technical triplicate. B) Silencing of *Firefly* luciferase expression with in vitro transcribed shRNA-luc in HeLa cells. shRNA-luc was transfected 24 h after the co-transfection of *Firefly* and *Renilla* luciferase-encoding plasmids. Luminescence signals were measured 24 and 48 h post-shRNA transfection. Data represents the mean of the ratio of *Firefly* to *Renilla* luciferase signal. Error bars represent standard deviation of two or three independent experiments. In each experiment, each sample was measured in triplicate. C) Silencing of *Firefly* luciferase expression in HeLa cells with shRNA-luc delivered in DMPC-Fol SUVs. shRNA-luc-loaded liposomes were added to HeLa cells 24 h after the co-transfection of *Firefly* and *Renilla* luciferase-encoding plasmids. Luminescence signals were measured 24 and 48 h post-liposome addition. Error bars represent standard deviation of two independent experiments. Each sample was measured in triplicate. RLU: Relative luminescence units.

4.3.6 POOR MEN1 mRNA EXPRESSION LIMITS ITS USE AS READOUT OF GENE SILENCING

To eliminate possible factors that could negatively influence transfection efficiency, which so far has proven challenging on KB cells, we aimed to silence an endogenously expressed gene instead, thus circumventing the need for DNA transfection. Moreover, we reasoned that avoiding the step of DNA transfection would allow us to have a better control of cell confluency, cell viability and general health of the cells at the time of shRNA transfection. MEN1, a tumor suppressor gene that acts by upregulating genes involved in recombination-directed DNA repair [44], was chosen as silencing target. Prior studies have reported strong MEN1 silencing by siRNAs with no effects on cell viability in HeLa and other mammalian cell types [44, 62]. Despite encoding a tumor suppressor protein, this gene is actively expressed in different well established tumor cell lines such as HeLa or MCF-7 [63]. In particular, shRNA-men1 was designed based on the “human MEN1 shRNA” that was shown to induce ~80% MEN1 silencing through mRNA degradation in primary human melanocytes that targeted the 3' untranslated region (3' UTR) [44]. Moreover, the same features used for successful T7 transcription and the same loop sequence as in shRNA-luc were included in this design. To study MEN1 gene knockdown we intended to report MEN1 mRNA degradation through relative qRT-PCR, using the expression of the widely used housekeeping gene encoding glyceraldehyde-3-phosphate dehydrogenase (GAPDH) as internal reference for comparison of gene expression changes [64].

While the average threshold PCR cycle (C_q) of GAPDH obtained in KB and HeLa was 20.6 ± 0.7 and 21 ± 1 respectively, the one for MEN1 was considerably higher with average C_q values of 36 ± 1 and 36.5 ± 0.4 . These results indicate that the mRNA yields of GAPDH were higher than those of MEN1 in the genomic RNA isolated (Fig. 12a-12c). Amplification products with C_q values above 35 are submitted to greater variability, which can make the measurements unreliable [65]. To validate that these measurements are specific amplification products, all reactions were performed in triplicate and the C_q values obtained were compared to the results from melt curve and agarose gel analysis (Fig. S1). Melting curve analysis revealed one major product of MEN1 and GAPDH amplification, with peaks at ~85 °C and ~82 °C, respectively. Agarose RNA gels confirmed that these major products correspond to the expected RNA fragments, with sizes 259 bp for MEN1 and 140 bp for GAPDH. Unfortunately, RT-qPCR analysis of MEN1 mRNA relative to GAPDH expression showed no significant reduction on MEN1 mRNA levels compared to mock transfected or untransfected cells, meaning that no significant silencing of MEN1 expression in neither KB (Fig. 12a) or HeLa cells (Fig. 12b-12c) occurred, whether shRNA-men1 was transfected with lipofectamine or with folate-targeted SUVs.

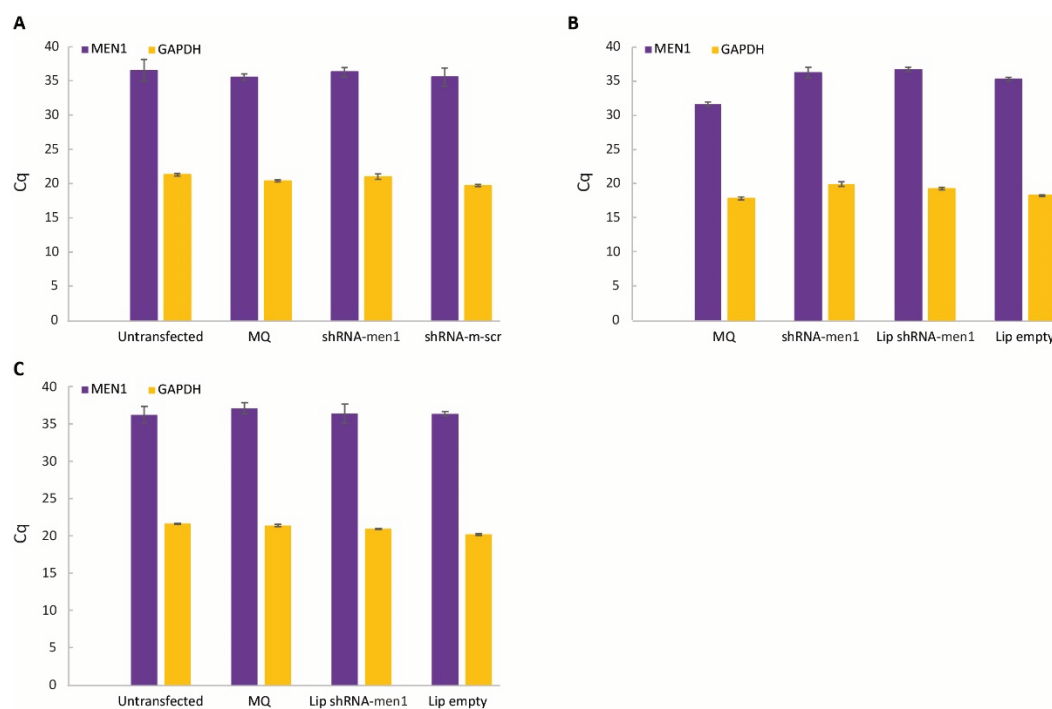


Fig. 12. Analysis of MEN1 gene silencing efficacy by shRNA-men1 in A) KB and B) HeLa cells by RT-qPCR. Values are represented as quantification cycles (Cq), which are inversely proportional to the initial amount of target RNA. Error bars represent standard deviation of a technical triplicate. Lip: Liposomes.

4.3.7 FOLATE-TARGETED LIPOSOMES FOLLOW THE ENDO-LYSOSOMAL PATHWAY AND CONCLUDE TRAPPED IN LYSOSOMES

Studying the intracellular fate of folate-labelled SUVs is essential to address the absence of gene silencing in KB and HeLa cells when delivering shRNA with folate-liposomes (Fig. 10). Although HeLa cells have a poorer expression of folate receptors than KB cells, we showed in Fig. 10 that, after overnight incubation, internalization levels are similar in both cell types. This result suggests that liposome endocytosis does not exclusively take place through a receptor-mediated mechanism. To examine whether liposomes are internalized in lysosomes, we performed time-lapse fluorescence microscopy of live KB and HeLa cells transiently expressing GFP fused to the lysosomal membrane protein Lamp1, serving as lysosomal marker. As can be observed in Fig. 13, lysosome labelling was heterogeneous through the cell population in both KB and HeLa cells, in agreement with the fact that the commercial baculovirus solution does not transfect all cells with equal efficiency [66]. As shown in Fig. 13a, in positively labelled KB cells, most internalized liposomes colocalized with lysosomes after 12 h. A clear increase of colocalization was observed over time and reached a maximum after 48 h, as quantitatively analyzed by calculating the Pearson's coefficient at each time point for the shown fields of view (Fig. 13b). Similar results were observed in HeLa cells (Fig. 13c-13d). However, in contrast to KB cells, a significant fraction of liposomes was located close to the cell membrane even after incubation for 60 h, and the correlation coefficient value decayed from 48 to 60 h, which could suggest that a fraction of liposomes efficiently escaped from endo-lysosomes. On the other

hand, after 60 h incubation the cells became highly confluent and less healthy, specially the HeLa cells that divide faster. All together, these results suggest that after cell internalization in endosomes, a major fraction of liposomes follow the endo-lysosomal pathway and end up trapped in the lysosomes of both KB and HeLa cells. There, active enzymatic degradation processes occur, impeding cargo release into the cytoplasm, as previously described for most targeted non-viral nanoparticulate drug delivery systems [38, 40], from which folate-targeted delivery systems are no exception [67].

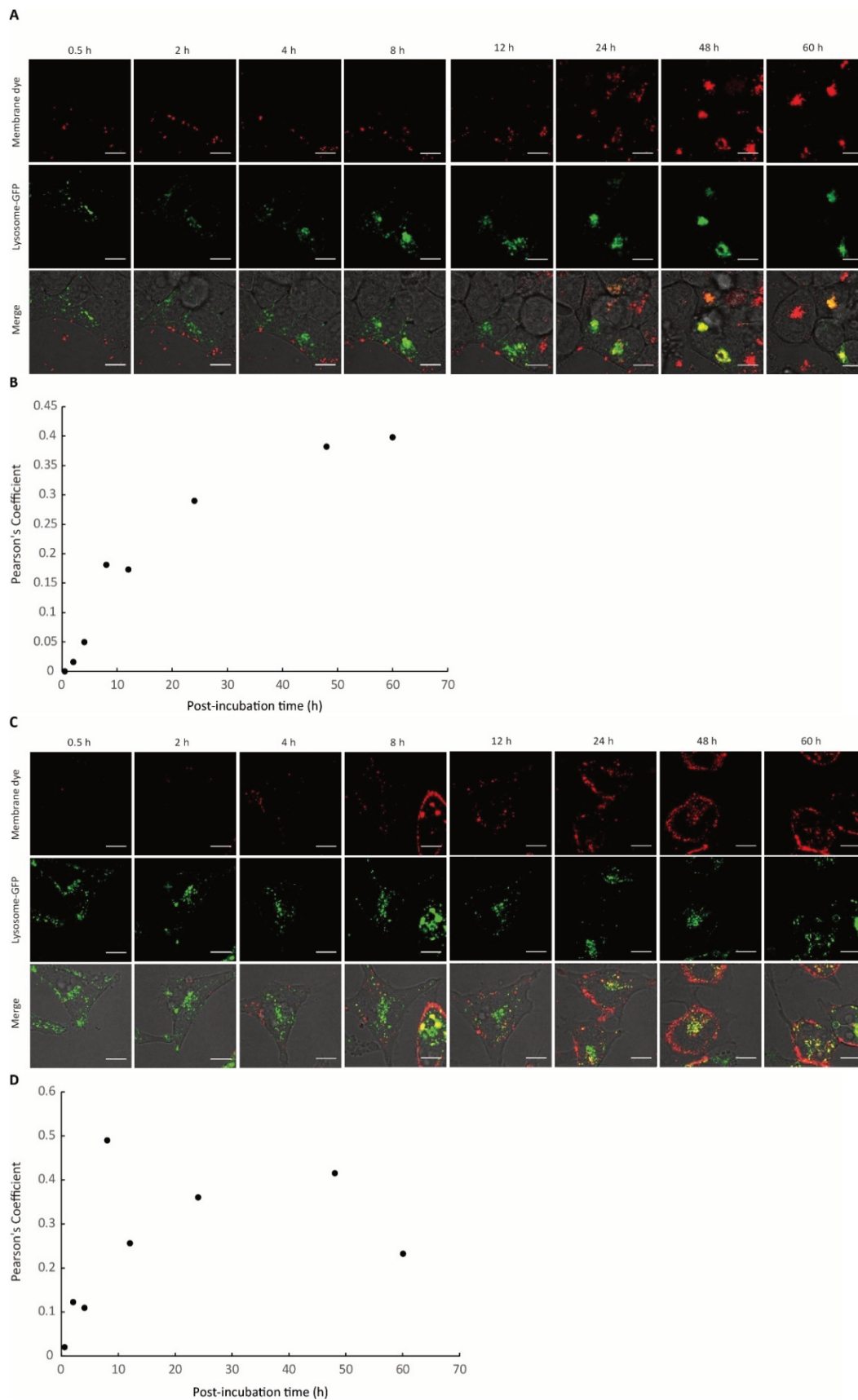


Fig. 13. Association of liposomes with lysosomes in KB (A, B) and HeLa (C, D) cells. A), C) Confocal microscopy of living cells overexpressing Cell Light® Lysosome-GFP incubated with DMPC-Fol SUVs. Scale bar = 10 μm . B), D) Quantitative analysis of lysosome-GFP and membrane dye co-localization with the Pearson coefficient.

4.3.8 FOLATE-LABELLED SUVs ARE NOT SENSITIVE TO AZIDO-ACID MELITTIN (A-A MELITTIN)

In order to implement folate-labelled liposomes with an improved ability for early endosomal escape and shRNA release into the cytosol of cells, we attempted to use the pH-responsive membranolytic peptide azido acid melittin. As a first step, we studied the sensitivity of folate-labelled LUVs and SUVs to azido acid melittin. For this, fluorescently labelled shRNA was produced through the incorporation of a small fraction of Aminoallyl-UTP ATTO-488 in the transcription reaction. As shown in Fig. 14, fluorescently labelled shRNA could be produced by T7 in vitro transcription.

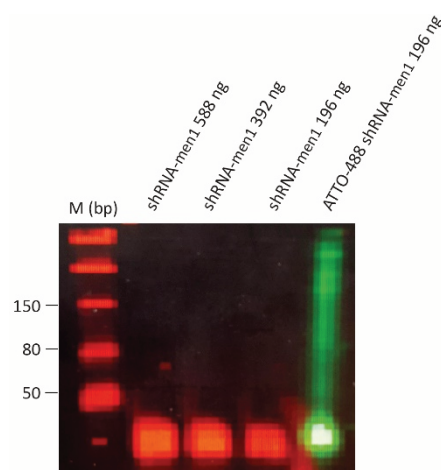


Fig. 14. Denaturing electrophoresis gel analysis of shRNA-men1 transcribed in vitro in the absence (red, EtBr staining) or presence (green, ATTO-488 fluorescence) of Aminoallyl-UTP ATTO-488 in the transcription reaction.

Then, unconjugated azido acid melittin and fluorescently labelled shRNA were co-entrapped in folate-labelled liposomes, and the ability of the peptide to induce complete liposomal collapse or shRNA release through membrane destabilization was monitored by confocal microscopy imaging of immobilized vesicles incubated in-situ at acidic pH (4.5) or basic pH (8.7). At pH 8.7, azido acid melittin should be inactive and liposomes with their content should remain intact. At pH 4.5, azido acid melittin should become active and provoke membrane breakage, allowing the release of shRNA and ultimately liposome collapse. As shown in Fig. 14a-14b, no differences were observed between these two conditions. No signs of liposomal collapse were found, what was expected upon peptide activation at acidic pH, given the high molar ratio of peptide (40 μ M) in the sample over liposomes (2 nM). Moreover, the fluorescence intensity of shRNA trapped in individual liposomes was analyzed. As shown in Fig. 14c-14d, the percentage profile of shRNA intensities at basic pH appeared similar to that obtained at acidic pH for both liposome sizes. However, the average fluorescence intensity in LUVs was 35% lower at acidic pH (258 a.u.) compared to basic pH (397 a.u.), suggesting that some shRNA might be released from liposomes thanks to the activity of azido acid melittin. On the contrary, these values were 99 a.u. and 123 a.u. for pH 8.7 and pH 4.5 in SUVs respectively, suggesting that azido acid melittin did not induce shRNA release in SUVs. However, a liposome size effect is not expected. Therefore, these results show no evidence for shRNA release by azido acid melittin activation.

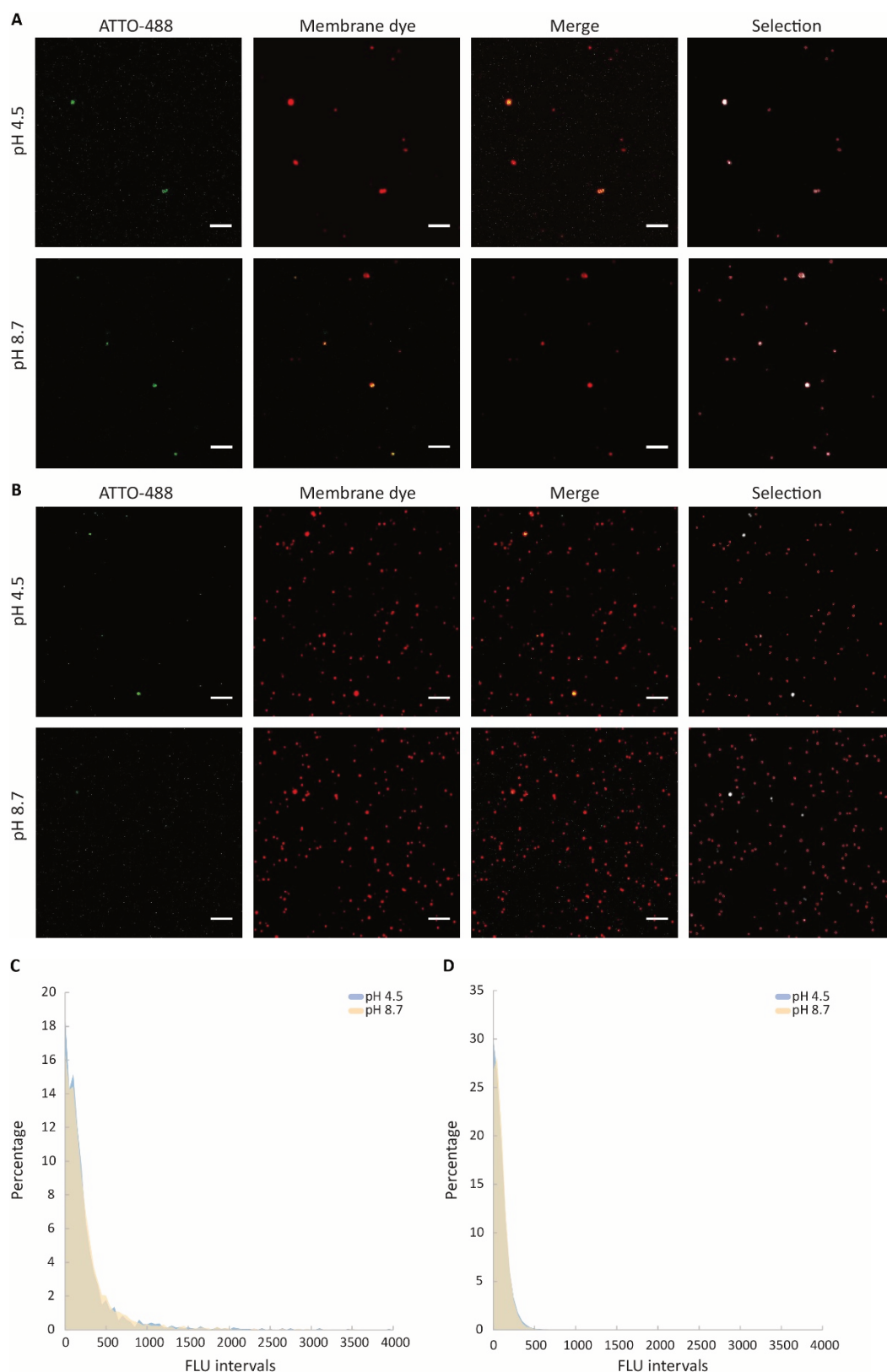


Fig. 15. A) Confocal microscopy and liposome selection of one field of view of LUVs or B) SUVs co-entrapping A-melittin and ATTO-488-labelled shRNA-men1 incubated at pH 4.5 or 8.7. Vesicles were tethered through a biotin-NeutrAvidin linker to a BSA-biotin passivated glass (scale bar: 10 μ m). C) Normalized percentage of ATTO-488 integrated intensities in selected LUVs or D) SUVs.

4.3.9 shRNA PRODUCTION IN FOLATE-LABELLED FED-LIPOSOMES

Despite these results, we found relevant to characterize the potential of the fed-vesicle bioreactors described in Chapter 2, to produce shRNAs with our shRNA-encoding DNA templates. For this, the expression of shRNA-luc and shRNA-men1 inside SUVs was evaluated by gel analysis and confocal microscopy for single-vesicle characterization. In addition, the expression of shRNA in LUVs was characterized by confocal microscopy. As seen in Fig. 16a, the production of shRNA-luc and shRNA-men1 could only be detected in the positive controls, where shRNA production was allowed outside the vesicles. Reasoning that the shRNA yields produced in vesicle were too low to be detected by ethidium bromide staining, we carried out in-vesicle shRNA transcription adding a molar fraction of fluorescently labelled Aminoallyl-UTP ATTO-488, that represented 25% from the total rUTP present in the transcription reaction. However, due to the limited availability of Aminoallyl-UTP ATTO-488, the concentration of all rNTPs was decreased 25 times in order to keep the molar ratio constant between all the rNTPs in the transcription reaction. As shown in Fig. 16b, the detection of shRNA-luc and shRNA-men1 was not possible by ethidium bromide staining. Imaging with 488 settings revealed that only positive controls produced enough shRNA to be detected.

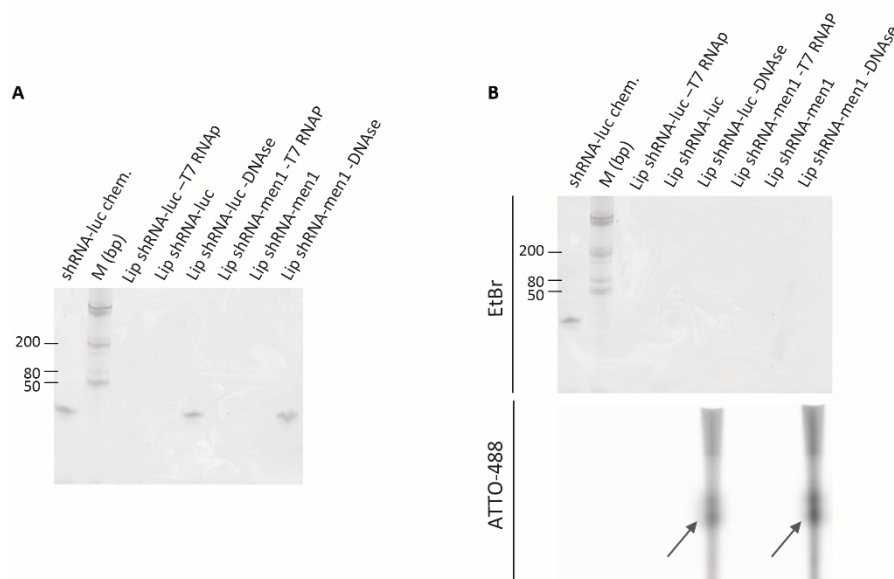


Fig. 16. shRNA production cannot be detected inside SUVs or LUVs. Denaturing electrophoresis gel analysis of in-vesicle (SUVs) production of shRNA-luc and shRNA-men1 transcribed in the A) absence or B) presence of Aminoallyl-UTP ATTO-488 in the transcription reaction.

Analysis of shRNA production at the single-vesicle level by confocal microscopy showed no detectable production of shRNA-luc or shRNA-men1 in individual SUVs (Fig. 17a). Despite their larger size, LUVs did not show detectable expression of shRNA in individual vesicles either (Fig. 17b). Altogether, these results suggest that none of our approaches are sensitive enough to detect the production of shRNA in SUVs or LUVs.

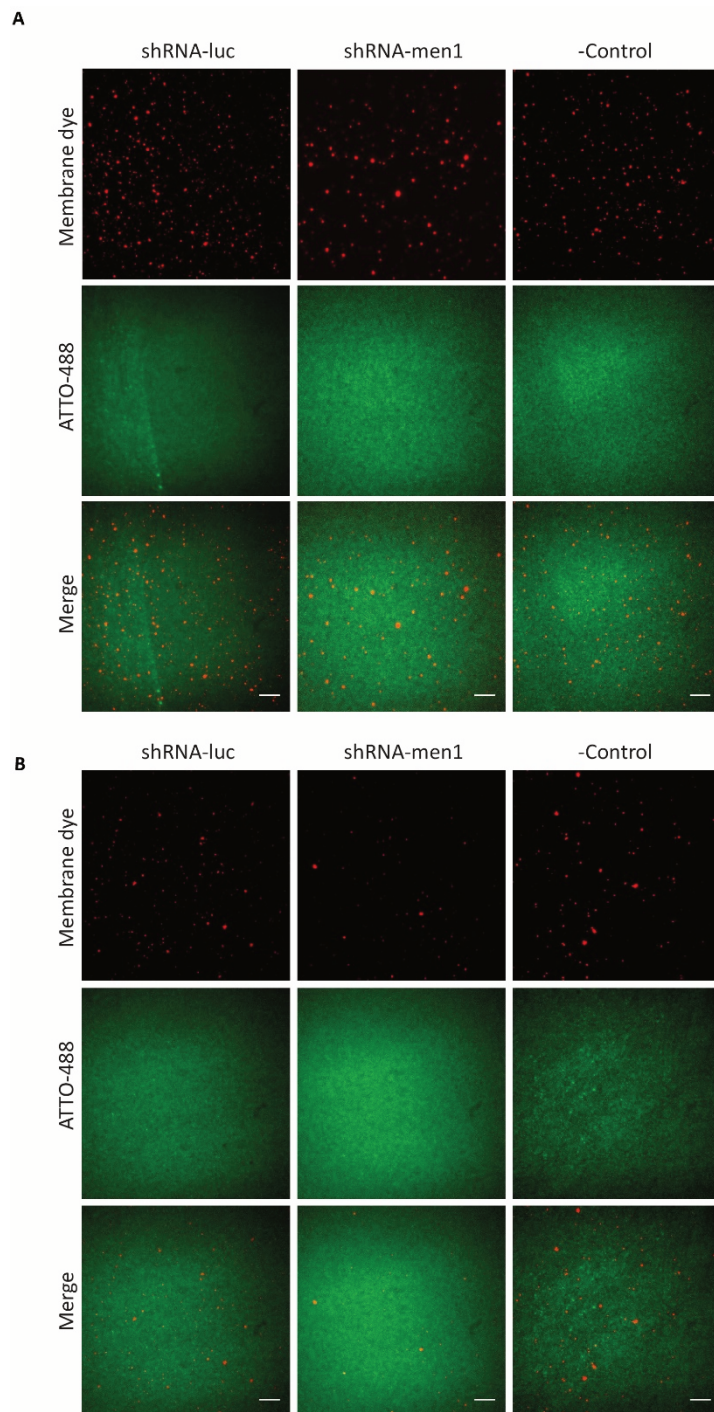


Fig. 17. shRNA production cannot be detected inside SUVs or LUVs. Confocal microscopy images of in-vesicle shRNA production in A) LUVs and B) SUVs. Vesicles were tethered through a biotin-NeutrAvidin linker to a BSA-biotin passivated glass (scale bar: 10 μ m).

4.4 DISCUSSION

4.4.1 POSSIBLE IMPROVEMENTS ON shRNA DESIGN

Secondary structure predictions for the shRNAs used in this study show that these shRNAs contain a 1 nt 3' overhang (Fig. 8b). Although 21 nt RNA duplexes with 1 nt 3' overhang can trigger sequence-specific mRNA degradation, it has been demonstrated that shRNA with 2 nt 3' overhangs are the most efficient silencing inducers [50]. In spite of this, efficient and specific luciferase gene silencing was achieved in mammalian cells in this study (Fig. 9a), demonstrating that, at least, a fraction of shRNA was processed into mature and functional siRNA. In vivo, the protein TUT7, a uridylyl transferase with a key role on controlling the fate of precursor miRNAs through three different uridylation mechanisms, is able to promote miRNA biogenesis by mono-uridylation of pre-miRNAs with 1 nt 3' overhang, such as pre-let-7a-1 [55, 56, 68]. Thus, it is reasonable to hypothesize that, apart from the generation of some functional siRNA through direct Dicer cleavage, a fraction of the shRNA efficiently converted into functional silencing siRNA was subjected to a 3' mono-uridylation step by TUT7 in vivo prior to Dicer cleavage.

In contrast, in vitro cleavage with purified human Dicer enzyme did not yield detectable mature siRNA by EtBr staining on gel (Fig. 8f). The limited amount of purified human Dicer available for these experiments (1 nM final concentration in each cleavage reaction), yielded at most a few nanomolar mature RNA cleavage products, which were undetectable through ethidium bromide staining. In contrast, mature let-7 was readily detectable thanks to its 3' stem cyanine bifunctional label (Cy5), that greatly improves the sensitivity for RNA visualization compared to ethidium bromide. Thus, to succeed in the characterization of shRNA-luc cleavage with purified Dicer in vitro, the creation of a chemically labelled shRNA-luc like in the case of pre-let-7a-1^{3'2nt}, would have been necessary. Even if the low sensitivity of EtBr staining did not allow us to quantify the efficiency of Dicer cleavage in vitro, we predict that some shRNA-luc was cleaved. However, its fraction might be low compared to that yielded in vivo, due to the absence of TUT7 in the cleavage reaction, which might help the efficient conversion of shRNA-luc into mature siRNA-luc. Therefore, though shRNA-luc achieved efficient silencing in HEK 293T cells, the design of the shRNA sequences could be improved to ensure the optimal and direct cleavage of shRNA in vitro and in vivo without the need for intermediate steps.

The newly designed shRNAs should include an extra U base at the 3' of the molecule to harbor a two UU nucleotide 3' overhang. In addition, other modifications can be included, that in combination should further boost the efficiency of shRNA's canonical cleavage, as described by Bofill-De Ros and Gu [4] (Fig. 18). Starting the stem of shRNA with G-C instead of G-U (Fig. 8b) will help to achieve a stable stem. Making the length of the passenger strand exactly 21 base pairs in length, where positions 2-19 have perfect complementarity to the guide strand, in which positions 2-18 have perfect homology with the target mRNA sequence, followed by an arbitrary 2 bp sequence rich in G-C or C-G (positions 31-32) to achieve the desired length and

ensure a clear frontier between stem and loop, can contribute to increase cleavage efficiency. The use of a U nucleotide at the start of the guide strand (position 33) is also recommended, since it favors the incorporation of the guide strand into the Ago protein during the formation of the RISC complex. Last, extending the length of the loop to at least ≥ 6 nt can avoid the possible tension generated close to the stem region when using a short loop (< 5 nt), improving the accessibility of Dicer to the shRNA molecule. The structure of all modified shRNA sequences should be modeled with mFold.

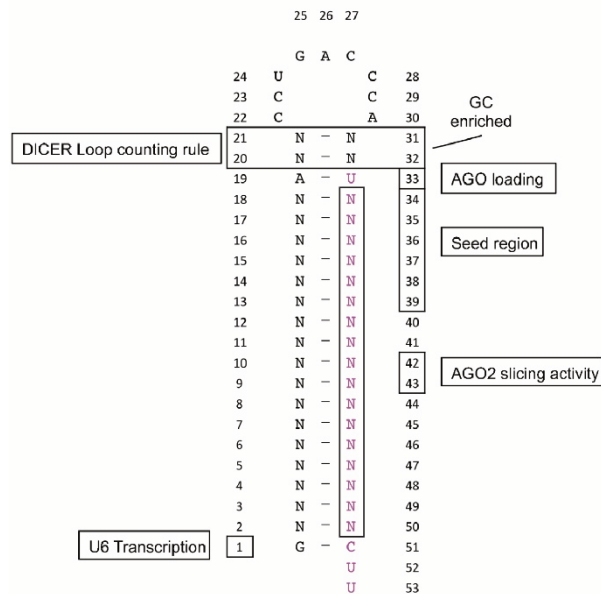


Fig. 18. Compilation of shRNA features involved in correct Dicer processing. Taken from [4].

4.4.2 POSSIBLE IMPROVEMENTS ON THE CHARACTERIZATION OF FOLATE-TARGETED DELIVERY

Aiming to develop a liposome nanofactory that produces therapeutic shRNA in specific targeted tissues, we investigated the selective uptake of our liposome formulation that allows RNA transcription reactions in the vesicle's lumen, when labelled with folic acid moieties, in the folate-receptor expressing cell lines HeLa and KB. Folate receptors are overexpressed in the plasma membranes of a high variety of human tumors [25, 69, 70]. It is known that folate receptor targeted liposomes can improve the antitumor effect of a drug in FR(+) solid tumor models without pronounced unspecific toxicity for the animal [71]. Moreover, different studies have shown that folate receptor targeted non-viral delivery systems improve DNA [72–75], siRNA [76–78] and shRNA [79] therapeutic effects in vitro and in vivo. In this work, the liposomal uptake of a non-targeted and a folate-targeted formulation was compared in cell lines with distinct FR expression levels. Confocal imaging allowed us to determine the localization of liposomes within the cell (Fig. 10). However, to facilitate this evaluation, following studies should include the use of a live cell nuclear staining dye with low inherent toxicity, such as Hoechst 33342, that has previously been successfully employed in similar studies [80, 81].

Selective uptake of folate-targeted liposomes was remarkable for KB cells after 2 h compared to HeLa cells, in agreement with their higher FR expression [82, 83]. However, the amount of internalized liposomes was similar after overnight incubation, indicating that non-receptor mediated endocytosis pathways such as pinocytosis, micropinocytosis or phagocytosis take place [37] in both HeLa and KB cells, once their folate receptors saturated. Such levels of unspecific uptake are not surprising *in vitro* when using fast growing tumor cell lines such as HeLa and KB [84]. Indeed, these cells are extremely metabolically active, and grow as a monolayer, making the surface of most cells widely available for interaction with liposomes. Non-receptor mediated liposomal uptake by KB cells was also described by Chen et al. [82]. The authors found a gradual decrease of the drug efficacy when using folate-targeted liposomes with respect to untargeted liposomes upon extension of the exposure time to cells. A similar effect has been observed as well in KB cells with liposomes labelled with 0.5% DSPE-PEG 5000 Folate, whose uptake reached a plateau after ~2 h, time at which the amount of associated liposomes was 60% higher than with untargeted liposomes. At longer time points, these differences started to vanish, showing a gradual decrease down to ~30% after 5 h incubation [26].

In the future steps following this work, establishing an incubation period that maximizes liposome uptake and avoids unspecific non-receptor mediated endocytosis will be essential. To determine it, flow cytometry can be used as described in previous studies [26], since it allows a more quantitative and straight forward characterization of liposome internalization levels compared to confocal microscopy. Moreover, the folate-receptor deficient lung cancer cell line A549 should be utilized in future studies as a strict negative control of liposome internalization [85].

4.4.3 ALTERNATIVES FOR IMPROVED DNA TRANSFECTION OF KB CELLS

Further, we tried to optimize a DNA transfection protocol in KB and HeLa cells to study the silencing efficacy of shRNA-luc through bioluminescence assays. Attempts to adapt the calcium phosphate-mediated protocol used for HEK 293T cells to transfect HeLa and KB cells failed (Table 4). HeLa cells are known to be efficiently transfected by incubating the precipitate with the cells for 16 h [86]. Thus, we were surprised to observe high cell death in HeLa, even when the incubation time was reduced or the reagent concentrations were lowered. Though the exact reasons remain unknown to us, we hypothesize that inherent properties of the specific HeLa clone used in this study may have caused this unusual intolerance to the transfection reagents. KB cells, in the other hand, did not show high cell death but showed no luciferase activity, suggesting transfection efficiency was low. This result agrees with the fact that no literature was found describing DNA or RNA transfection in KB cells with this method. However, glycerol osmotic shocks following calcium phosphate-mediated transfection have shown enhanced DNA uptake in several cell lines [87] and thus should be tested in future steps prior to continuing the optimization of DNA transfection with electroporation or lipofection onto KB and HeLa cells.

When the DNA plasmids were transfected into KB and HeLa cells using Lipofectamine 3000, the transfection efficiency improved for both cell lines (Fig. 11). Remarkably, *Renilla* luciferase activity was at least 5-fold higher than *Firefly* luciferase in all transfections where the total DNA mass transfected was 0.5-2.5 μg , despite the ten times lower molar fraction of *Renilla* luciferase transfected. This observation has been previously reported in literature [88]. The manufacturers of the Dual-Luciferase assay, however, report similar specific activities for both *Renilla* and *Firefly* luciferase enzymes [89]. Thus, we hypothesize that not the activity of the two enzymes, but distinct expression levels or transfection efficiencies could be the source of this difference, since both genes are expressed from different plasmids with unequal sizes (pRL-SV40: 3.7 kb and pGL3-control: 5.0 kb). Supporting this hypothesis, several studies have demonstrated an inverse correlation between vector size and lipoplexes-mediated transfection efficiency [91–93]. Moreover, while the activities of *Firefly* and *Renilla* luciferase were readily detectable in HeLa cells, the luminescence signal of *Firefly* luciferase activity in KB cells was at most 2-fold higher than the background signal, which prompted us to try a different transfection method.

Electroporation has been successfully employed to transfect a broad spectrum of cell types for which other methods did not work. Based on the physical formation of pores in the plasmatic membrane, it is believed that electroporation is less dependent on cell type compared to other methods [93]. In most of the literature where KB cells were transfected, electroporation was the method of choice for the transfection of DNA plasmids [61, 95, 96], siRNA [96], cDNA [95], RNA nanoparticles [97] and proteins [98]. Unfortunately, in this work, electroporation did not improve the transfection efficiency in KB cells (Table 5), despite the use of similar conditions as in Weecharangsan et al. [61], that showed a 500-fold increase in the transfection efficiency of a \sim 5.4 kb DNA plasmid compared to the non-electroporated cell control. Inherent differences between the KB clones employed in this study and those used in the mentioned studies may have inhibited successful transfection. Perhaps the use of a transfection reagent specifically made for KB cells may improve DNA transfection. In this regard, Altogene Biosystems provides a KB transfection reagent and claims to achieve a 73% siRNA transfection efficiency [99].

Remarkably, in our study, successful transfection and transient expression of GFP fused to Lamp1 was achieved in KB and HeLa cells with a commercial reagent based on the viral baculovirus-mediated gene transfer system (Fig. 13). Baculovirus-mediated gene transfer has been successfully used in diverse types of human cell lines in vitro [100] and has been widely used for the production of recombinant proteins [101]. The Bacmam system, a commercially available technology based on engineered recombinant baculoviruses, allows the delivery of expression vectors for transient protein and shRNA expression in mammalian cells [101]. Thus, this system should be considered as an alternative method to lipofection for transient protein expression in KB cells.

4.4.4 ENDOGENOUS TARGETS HIGH HIGHER mRNA EXPRESSION THAN MEN1 SHOULD BE USED AS MODEL TO REPORT SILENCING VIA RT-QPCR

Despite all the existing possibilities to improve plasmid DNA transfection, simplifying the experimental approach by directly targeting an endogenously produced mRNA may be the best option. In this study, we chose MEN1 mRNA as an example of endogenous target for an in-vitro transcribed shRNA in HeLa cells. Unlike the strong silencing of MEN1 observed in a previous study in melanocytes [44], our results suggest that MEN1 mRNA was not silenced despite targeting the same mRNA sequence (Fig. 12). However, evaluating the successful silencing of this mRNA resulted challenging for us, due to the very low MEN1 mRNA yields found in these HeLa cells. In every condition tested, very high C_q values (C_q>36) or no amplification was obtained by RT-qPCR, giving rise to variability from experiment to experiment. Trizol, an analogue of Tri Reagent, did not enhance the amount of purified RNA (data not shown). A different endogenous mRNA target that yields C_q values in a range closer to that of GAPDH should be chosen in future experiments. Alternatively, the silencing efficacy of shRNA can be determined at the protein expression level by Western blot analysis.

4.4.5 MEMBRANE CONJUGATION OF PH-RESPONSIVE CPPS WILL BE KEY FOR SUCCESSFUL ENDOSOMAL ESCAPE

A significant amount of folate-labelled liposomes entrapped in lysosomes in both HeLa and KB cells was shown (Fig. 13). We attempted to quantify the level of colocalization by calculating the Pearson's coefficient (PC), which measures the linear correlation of the values of fluorescence intensity pixels between the GFP and the membrane dye channels. However, PC is generally used as a rough estimate of colocalization, since it is highly dependent on different parameters. Factors such as noise, bleed-through, variations in fluorescence intensity and the heterogeneity of colocalization events through a sample, have a strong influence on the PC value [46]. In this study, the highly heterogenous cell-to-cell distribution of the lysosomal marker protein in both cell types, and the strong cell-to-cell variability on the levels of internalized liposomes, had a strong influence on the PC. In addition, though to a minor extent, freely diffusing liposomes further influenced this value. Moreover, all the estimated PC values remained in the range between 0 and 0.5, whereas only values ≤ -0.5 or ≥ 0.5 allow drawing firm conclusions [46]. Washing off the medium after a certain incubation period before the start of imaging, optimizing the transfection efficiency of the plasmid encoding lysosomal-GFP, and real-time imaging of liposome internalization events on specific cells, will strongly contribute to a more accurate estimation of colocalization.

Next, we studied the sensitivity of folate-labelled LUVs and SUVs to encapsulated pH-responsive azido acid melittin (Fig. 15). For this, we imaged single vesicles immobilized and analyzed the decrease of shRNA fluorescence intensity in liposomes as a read-out of membranolytic activity. No differences between the samples incubated in acidic pH compared to basic pH were found. Some peptide-induced membrane defects might have been generated.

However, the sole creation of membrane defects might not be enough to induce the release of shRNA with a size around 13 kDa [102].

Several factors can make folate-labelled liposomes insensitive to azido acid melittin. Membrane PEGylation is known to have an inhibiting effect on the ability of melittin to induce membrane leakage [39, 105]. This effect is directly provoked by the interfacial PEG moieties and not by the lipid to which they are conjugated. It is also known that longer PE-PEG-5000 triggers stronger membranolytic inhibition compared to the shorter PE-PEG-2000 [103]. However, the molar percentages of these conjugated polymers for which inhibiting effects were proven (6% and 10%) are considerably higher than those used in the formulation of our folate-labelled liposomes that contain a 0.6% of Pegylated lipids (~0.5% DSPE-PEG2000-Biotin + 0.1% DSPE-PEG5000-Folate).

Moreover, the negative surface charge of the folate-labelled liposomes may also influence melittin's membranolytic activity. Despite the fact that melittin has an increased affinity for membranes containing negatively charged lipids, such membranes seem to be more resistant to its membranolytic activity compared to neutral membranes [105, 106].

In our experimental conditions, melittin's induced leakage might be also influenced by the pH value inside the liposome lumen. Prior in-vesicle transcription experiments in liposomes with a nearly identical lipid composition showed that NTPs are able to cross the lipid bilayer (see Chapter 2), from which we hypothesized that regular buffer components can permeate too. In the case of the membranolytic assay, this would allow the acidification of the liposome lumen upon dilution in acidic buffer. Additionally, membrane tension generated by the liposome immobilization might reduce the peptide ability to lyse the lipid bilayer. Therefore, the membranolytic activity of azido acid melittin could be evaluated using calcein leakage assays [39]. Ultimately, the membrane-destabilizing peptide of choice should be conjugated to the surface of the liposomes as done in previous studies [38, 39, 41].

4.4.6 NON-FED VESICLE BIOREACTORS AS MORE PROMISING SYSTEMS FOR IN SITU RNA PRODUCTION

The production of shRNA inside liposomes could not be detected in either SUVs or LUVs (Fig. 16-17). More sensitive methods should be employed to confirm RNA synthesis in vesicles. Complementary to single liposome techniques, stem-loop primer-based Taqman RT-qPCR can be used for quantification of small RNA like miRNA [107, 108].

Once in the cytoplasm, we predict that the uptake of rNTPs from the cellular environment into the vesicles will be challenging. Therefore, the design of a different liposomal formulation with low permeability in physiological conditions, that allows the co-entrapment of rNTPs together with the other elements required for RNA production, should be considered. Combined with an optogenetic tool such as the LA-T7 promoter (see Chapter 3), RNA production in these bioreactors may be spatiotemporally controlled externally upon arrival into the target tissue

and prior to liposomal disruption by CPPs upon pH acidification in the endolysosomal pathway.

4.5 CONCLUSIONS

In this work, we aimed to develop an shRNA-producing fed-vesicle bioreactor platform that would allow shRNA production *in vivo* once the target tissue or cell is reached. A DNA template encoding functional shRNA molecules under the expression control of a T7 promoter was assembled. The silencing efficacy of one of the *in vitro* transcribed shRNAs was validated in mammalian cells. However, folate-labelled liposomes end up entrapped in lysosomes where their cargo was presumably degraded, impeding the successful delivery of this shRNA to the cytoplasm of cells. To tackle this problem, the use of the pH-dependent CPP azido acid melittin was attempted, unsuccessfully. Additionally, we could not detect the *in-vesicle* production of shRNA, compromising the validation of this platform as a bioreactor for producing therapeutic RNA. We propose major modifications that may help simplifying the overall experimental workflow. Building upon our results, we give strategies to optimize shRNA transcription, delivery and release in targeted cells.

4.6 SUPPLEMENTARY INFORMATION

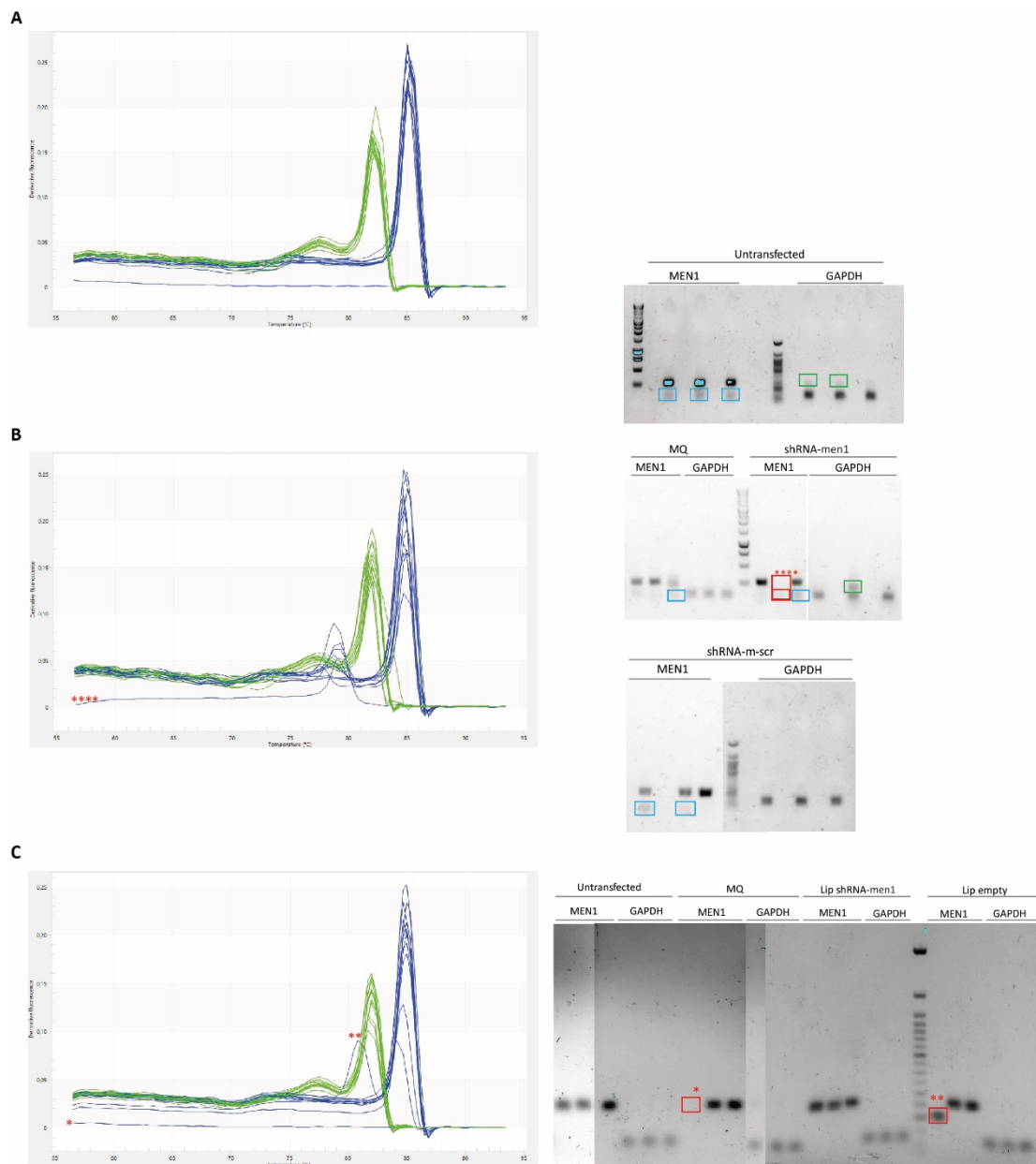


Fig. S1. Melt curves and agarose gel analysis of RT-qPCR amplification from samples corresponding to A) Fig. 11a, B) Fig. 11b and C) Fig. 11c. Blue melt curves correspond to MEN1 amplification (~85 °C). Green melt curves correspond to GAPDH amplification (~82 °C). In B), agarose gel analysis reveals minor amplification products that may be a splice variants from MEN1 (blue frames) and GAPDH (green frames), corresponding to the small peaks observed at ~79 °C and ~77.5 °C in the melt curves, respectively. In the samples labelled with red stars, no amplification took place, or artifact amplification products were obtained.

4.7 ACKNOWLEDGEMENTS

We thank Enrico Mastrobattista for providing us with purified azido acid melittin and for useful scientific discussions. We thank Chirlmin Joo for providing us with Cy5-labelled pre-let-7a-1^{2nt} 3' and purified human Dicer, and for useful discussions. We thank Mohammed Fareh, for the useful discussions and the kind advices regarding siRNA and Dicer. Thanks Mohammed, for teaching me how to perform Dicer cleavage assays. We thank Claudia Oliveira and Denzel Bemelman for their contribution to this project. Thank you Anne, for performing the last experiment. Thank you Sacha, for your help setting the cell culture room in the new building. Thank you Jeremy, for your kind help with confocal microscopy. Thanks Fabrizio and Pauline for the useful discussions and kind advices concerning RNA gels.

4.8 REFERENCES

- [1] B. L. Davidson and P. B. McCray, “Current prospects for RNA interference-based therapies,” *Nature Reviews Genetics*, vol. 12, no. 5, pp. 329–340, 2011.
- [2] J. K. W. Lam, M. Y. T. Chow, Y. Zhang, and S. W. S. Leung, “siRNA versus miRNA as therapeutics for gene silencing,” *Molecular Therapy - Nucleic Acids*, vol. 4, no. 9, p. e252, 2015.
- [3] M. Sioud, “*RNAI Interference: Challenges and therapeutic opportunities*”, 2015.
- [4] X. Bofill-De Ros and S. Gu, “Guidelines for the optimal design of miRNA-based shRNAs,” *Methods*, vol. 103, pp. 157–166, 2016.
- [5] S. W. Eichhorn *et al.*, “mRNA destabilization is the dominant effect of mammalian microRNAs by the time substantial repression ensues,” *Molecular Cell*, vol. 56, no. 1, pp. 104–115, 2015.
- [6] M. L. Bobbin and J. J. Rossi, “RNA Interference (RNAi)-Based Therapeutics: Delivering on the Promise?,” *Annual Review of Pharmacology and Toxicology*, vol. 56, no. 1, pp. 103–122, 2016.
- [7] G. R. Stark, I. M. Kerr, B. R. G. Williams, R. H. Silverman, and R. D. Schreiber, “How Cells Respond To Interferons,” *Annual Review of Biochemistry*, vol. 67, no. 1, pp. 227–264, 1998.
- [8] S. Barik, “Silence of the transcripts: RNA interference in medicine,” *Journal of Molecular Medicine*, vol. 83, no. 10, pp. 764–773, 2005.
- [9] S. M. Elbashir, J. Harborth, W. Lendeckel, A. Yalcin, K. Weber, and T. Tuschl, “Duplexes of 21-nucleotide RNAs mediate RNA interference in cultured mammalian cells,” *Nature*, vol. 411, no. May, pp. 494–498, 2001.
- [10] C. A. Sledz, M. Holko, M. J. De Veer, R. H. Silverman, and B. R. G. Williams, “Activation of the interferon system by short-interfering RNAs,” *Nature Cell Biology*, vol. 5, no. 9, pp. 834–839, 2003.
- [11] A. J. Bridge, S. Pebernard, A. Ducraux, A. L. Nicoulaz, and R. Iggo, “Induction of an interferon response by RNAi vectors in mammalian cells,” *Nature Genetics*, vol. 34, no. 3, pp. 263–264, 2003.
- [12] A. Reynolds *et al.*, “Induction of the interferon response by siRNA is cell type- and duplex length-dependent,” *RNA*, vol. 12, no. 6, pp. 988–993, 2006.
- [13] A. Peek and M. Behlke, “Design of active small interfering RNAs,” *Current opinion in molecular therapeutics*, vol. 9, no. 2, pp. 110–118, 2007.
- [14] P. J. Paddison, A. A. Caudy, E. Bernstein, G. J. Hannon, and D. S. Conklin, “Short hairpin RNAs (shRNAs) induce sequence-specific silencing in mammalian cells,” pp. 948–958, 2002.

- [15] A. P. McCaffrey, L. Meuse, T.-T. T. P. Pham, D. S. Conklin, G. J. Hannon, and M. A. Kay, "RNA interference in adult mice," *Nature*, vol. 418, no. 6893, pp. 38–39, 2002.
- [16] Y. Zeng, E. J. Wagner, and B. R. Cullen, "Both natural and designed micro RNAs can inhibit the expression of cognate mRNAs when expressed in human cells," *Molecular Cell*, vol. 9, no. 6, pp. 1327–1333, 2002.
- [17] H. Yin, R. L. Kanasty, A. a Eltoukhy, A. J. Vegas, J. R. Dorkin, and D. G. Anderson, "Non-viral vectors for gene-based therapy.," *Nature reviews. Genetics*, vol. 15, no. 8, pp. 541–555, Jul. 2014.
- [18] V. Chan, S. K. Novakowski, S. Law, C. Klein-Bosgoed, and C. J. Kastrup, "Controlled Transcription of Exogenous mRNA in Platelets Using Protocells," *Angewandte Chemie - International Edition*, vol. 54, no. 46, pp. 13590–13593, 2015.
- [19] C. L. Hardee, L. M. Arévalo-Soliz, B. D. Hornstein, and L. Zechiedrich, "Advances in non-viral DNA vectors for gene therapy," *Genes*, vol. 8, no. 2, 2017.
- [20] M. A. Kay, "State-of-the-art gene-based therapies: The road ahead," *Nature Reviews Genetics*, vol. 12, no. 5, pp. 316–328, 2011.
- [21] X. Han *et al.*, "9-NC-loaded folate-conjugated polymer micelles as tumor targeted drug delivery system : Preparation and evaluation in vitro," vol. 372, pp. 125–131, 2009.
- [22] H. Bardania, S. Tarvirdipour, and F. Dorkoosh, "Liposome-targeted delivery for highly potent drugs," *Artificial Cells, Nanomedicine and Biotechnology*. 2017.
- [23] J. A. Ledermann, S. Canevari, and T. Thigpen, "Targeting the folate receptor: Diagnostic and therapeutic approaches to personalize cancer treatments," *Annals of Oncology*, vol. 26, no. 10, pp. 2034–2043, 2015.
- [24] A. R. Hilgenbrink and P. S. Low, "Folate receptor-mediated drug targeting: From therapeutics to diagnostics," *Journal of Pharmaceutical Sciences*, vol. 94, no. 10, pp. 2135–2146, 2005.
- [25] Y. Lu and P. S. Low, "Folate-mediated delivery of macromolecular anticancer therapeutic agents," *Advanced Drug Delivery Reviews*, vol. 64, pp. 342–352, 2012.
- [26] A. Yamada, Y. Taniguchi, K. Kawano, T. Honda, Y. Hattori, and Y. Maitani, "Design of folate-linked liposomal doxorubicin to its antitumor effect in mice," *Clinical Cancer Research*, vol. 14, no. 24, pp. 8161–8168, 2008.
- [27] A. Garcia-Bennett, M. Nees, and B. Fadeel, "In search of the Holy Grail: Folate-targeted nanoparticles for cancer therapy," *Biochemical Pharmacology*, 2011.
- [28] A. Gabizon, A. T. Horowitz, D. Goren, D. Tzemach, H. Shmeeda, and S. Zalipsky, "In Vivo Fate of Folate-Targeted Polyethylene-Glycol Liposomes in Tumor-Bearing Mice," *Clinical Cancer Research*, vol. 9, no. 17, pp. 6551–6559, 2003.

- [29] T. Shiokawa *et al.*, “Effect of Polyethylene Glycol Linker Chain Length of Folate-Linked Microemulsions Loading Aclacinomycin A on Targeting Ability and Antitumor Effect In vitro and In vivo,” *Clinical Cancer Research*, vol. 11, no. March 1, pp. 2018–2025, 2005.
- [30] T. Nakamura, K. Kawano, K. Shiraishi, M. Yokoyama, and Y. Maitani, “Folate-Targeted Gadolinium-Lipid-Based Nanoparticles as a Bimodal Contrast Agent for Tumor Fluorescent and Magnetic Resonance Imaging,” *Biological and Pharmaceutical Bulletin*, vol. 37, no. 4, pp. 521–527, 2014.
- [31] K. Kawano and Y. Maitani, “Effects of Polyethylene Glycol Spacer Length and Ligand Density on Folate Receptor Targeting of Liposomal Doxorubicin In Vitro,” *Journal of Drug Delivery*, 2011.
- [32] N. Kamaly, T. Kalber, M. Thanou, J. D. Bell, and A. D. Miller, “Folate Receptor Targeted Bimodal Liposomes for Tumor Magnetic Resonance Imaging,” *Bioconjugate Chemistry*, vol. 20, pp. 648–655, 2009.
- [33] F. Sonvico *et al.*, “Establishment of an in vitro model expressing the folate receptor for the investigation of targeted delivery systems,” *Journal of Drug Delivery Science and Technology*, vol. 15, no. 6, pp. 407–410, 2005.
- [34] J. Huotari and A. Helenius, “Endosome maturation,” *EMBO Journal*, vol. 30, no. 17, pp. 3481–3500, 2011.
- [35] J. C. Lecher, S. J. Nowak, J. L. Mcmurry, and C. Biology, “Breaking in and busting out: Cell-penetrating peptides and the endosomal escape problem,” *Biomol concepts*, vol. 8, pp. 131–141, 2017.
- [36] S. Mayor and R. E. Pagano, “Pathways of clathrin-independent endocytosis,” *Nature Reviews Molecular Cell Biology*, vol. 8, no. 8, pp. 603–612, 2007.
- [37] N. Oh and J. H. Park, “Endocytosis and exocytosis of nanoparticles in mammalian cells,” *International Journal of Nanomedicine*, vol. 9, no. SUPPL.1, pp. 51–63, 2014.
- [38] A. Varkouhi, M. Scholte, G. Storm, and H. Haisma, “Endosomal escape pathways for delivery of biologicals,” *Journal of Controlled Release*, vol. 151, pp. 220–228, 2011.
- [39] E. Oude Blenke, M. Sleszynska, M. J. W. Evers, G. Storm, N. I. Martin, and E. Mastrobattista, “Strategies for the Activation and Release of the Membranolytic Peptide Melittin from Liposomes Using Endosomal pH as a Trigger,” *Bioconjugate Chemistry*, vol. 28, no. 2, pp. 574–582, 2017.
- [40] E. Koren and V. P. Torchilin, “Cell-penetrating peptides: Breaking through to the other side,” *Trends in Molecular Medicine*, vol. 18, no. 7, pp. 385–393, 2012.
- [41] M. Akishiba *et al.*, “Cytosolic antibody delivery by lipid-sensitive endosomolytic peptide,” *Nature Chemistry*, vol. 9, no. 8, pp. 751–761, 2017.
- [42] A. Ahmad, S. Ranjan, W. Zhang, J. Zou, I. Pyykkö, and P. K. J. Kinnunen, “Novel

- endosomolytic peptides for enhancing gene delivery in nanoparticles,” *BBA - Biomembranes*, vol. 1848, no. 2, pp. 544–553, 2015.
- [43] M. Godoy-Gallardo, M. J. York-Duran, and L. Hosta-Rigau, “Recent Progress in Micro/Nanoreactors toward the Creation of Artificial Organelles,” *Advanced Healthcare Materials*, vol. 7, no. 5, pp. 1–35, 2018.
- [44] M. Fang, F. Xia, M. Mahalingam, C.-M. Virbasius, N. Wajapeyee, and M. R. Green, “MEN1 Is a Melanoma Tumor Suppressor That Preserves Genomic Integrity by Stimulating Transcription of Genes That Promote Homologous Recombination-Directed DNA Repair,” *Molecular and Cellular Biology*, vol. 33, no. 13, pp. 2635–2647, 2013.
- [45] E. M. Poursani, B. M. Soltani, and S. J. Mowla, “Differential expression of OCT4 pseudogenes in pluripotent and tumor cell lines,” *Cell Journal*, vol. 18, no. 1, pp. 28–36, 2016.
- [46] S. Bolte and F. P. Cordelières, “A guided tour into subcellular colocalization analysis in light microscopy,” *Journal of Microscopy*, vol. 224, no. December, pp. 213–232, 2006.
- [47] J. F. Milligan, D. R. Groebe, G. W. Witherell, and O. C. Uhlenbeck, “Oligoribonucleotide synthesis using T7 RNA polymerase and synthetic DNA templates,” *Nucleic acids research*, vol. 15, no. 21, pp. 8783–8798, 1987.
- [48] J. J. Dunn, F. W. Studier, and M. Gottesman, “Complete nucleotide sequence of bacteriophage T7 DNA and the locations of T7 genetic elements,” *Journal of Molecular Biology*, vol. 166, no. 4, pp. 477–535, Jun. 1983.
- [49] Sigma-Aldrich, “MISSION shRNA Plasmid DNA Control Vectors,” no. September, pp. 1–12, 2012.
- [50] S. M. Elbashir, J. Martinez, A. Patkaniowska, W. Lendeckel, and T. Tuschl, “Functional anatomy of siRNAs for mediating efficient RNAi in *Drosophila melanogaster* embryo lysate,” *EMBO Journal*, vol. 20, no. 23, pp. 6877–6888, 2001.
- [51] H. Summer, R. Grämer, and P. Dröge, “Denaturing Urea Polyacrylamide Gel Electrophoresis (Urea PAGE),” *Journal of Visualized Experiments*, no. 32, pp. 3–5, 2009.
- [52] M. Fareh, K. H. Yeom, A. C. Haagsma, S. Chauhan, I. Heo, and C. Joo, “TRBP ensures efficient Dicer processing of precursor microRNA in RNA-crowded environments,” *Nature Communications*, vol. 7, pp. 1–11, 2016.
- [53] L. Chen, L. Heikkinen, C. Wang, Y. Yang, H. Sun, and G. Wong, “Trends in the development of miRNA bioinformatics tools,” *Briefings in Bioinformatics*, no. June, pp. 1–17, 2018.
- [54] I. Heo, C. Joo, J. Cho, M. Ha, J. Han, and V. N. Kim, “Lin28 Mediates the Terminal Uridylation of let-7 Precursor MicroRNA,” *Molecular Cell*, vol. 32, no. 2, pp. 276–284, 2008.

- [55] I. Heo *et al.*, “Mono-uridylation of pre-microRNA as a key step in the biogenesis of group II let-7 microRNAs,” *Cell*, vol. 151, no. 3, pp. 521–532, 2012.
- [56] B. Kim *et al.*, “TUT7 controls the fate of precursor microRNAs by using three different uridylation mechanisms,” *The EMBO Journal*, vol. 34, no. 13, pp. 1801–1815, 2015.
- [57] S. Gu *et al.*, “The loop position of shRNAs and pre-miRNAs is critical for the accuracy of dicer processing in vivo,” *Cell*, vol. 151, no. 4, pp. 900–911, 2012.
- [58] Q. Liu, S. Xu, C. Niu, M. Li, D. He, and Z. Lu, “Distinguish cancer cells based on targeting turn-on fluorescence imaging by folate functionalized green emitting carbon dots,” *Biosensors and Bioelectronics*, vol. 64, pp. 119–125, 2015.
- [59] H. Chen, R. Ahn, J. Van den Bossche, D. H. Thompson, and T. V. O’Halloran, “Folate-mediated intracellular drug delivery increases the anticancer efficacy of nanoparticulate formulation of arsenic trioxide,” *Molecular Cancer Therapeutics*, 2009.
- [60] J. Yang, H. Chen, I. R. Vlahov, J.-X. Cheng, and P. S. Low, “Characterization of the pH of folate receptor-containing endosomes and the rate of hydrolysis of internalized acid-labile folate-drug conjugates,” *The Journal of pharmacology and experimental therapeutics*, vol. 321, no. 2, pp. 462–468, 2007.
- [61] W. Weecharangsan, P. Opanasopit, and R. J. Lee, “In vitro gene transfer using cationic vectors, electroporation and their combination,” *Anticancer Research*, vol. 27, no. 1 A, pp. 309–314, 2007.
- [62] P. C. Scacheri *et al.*, “Short interfering RNAs can induce unexpected and divergent changes in the levels of untargeted proteins in mammalian cells,” *Proceedings of the National Academy of Sciences of the United States of America*, vol. 101, no. 7, pp. 1892–1897, 2004.
- [63] F. Ren *et al.*, “Expression and subcellular localization of menin in human cancer cells,” *Experimental and Therapeutic Medicine*, vol. 3, no. 6, pp. 1087–1091, 2012.
- [64] B. Kozera and M. Rapacz, “Reference genes in real-time PCR,” *Journal of Applied Genetics*, vol. 54, no. 4, pp. 391–406, 2013.
- [65] T. Nolan, R. Hands, and S. Bustin, “Quantification of mRNA using real-time RT-PCR,” *Nature Protocols*, vol. 1, no. 3, pp. 1559–1582, 2006.
- [66] Thermo Fisher Scientific, “CellLight Lysosomes-GFP, BacMam 2.0,” 2018. [Online]. Available: <https://www.thermofisher.com/order/catalog/product/C10507>. [Accessed: 03-Dec-2018].
- [67] A. Gabizon, H. Shmeeda, A. T. Horowitz, and S. Zalipsky, “Tumor cell targeting of liposome-entrapped drugs with phospholipid-anchored folic acid-PEG conjugates,” *Advanced Drug Delivery Reviews*, vol. 56, no. 8, pp. 1177–1192, 2004.

- [68] H. Scheer, H. Zuber, C. De Almeida, and D. Gagliardi, "Uridylation Earmarks mRNAs for Degradation... and More," *Trends in Genetics*, vol. 32, no. 10, pp. 607–619, 2016.
- [69] J. Sudimack and R. J. Lee, "Targeted drug delivery via the folate receptor," *Advanced Drug Delivery Reviews*, vol. 41, no. 2, pp. 147–162, 2000.
- [70] C. Lines, J. F. Ross, P. K. Chaudhuri, M. Ratnam, and D. Ph, "Differential Regulation of Folate Receptor Isoforms in Normal and Malignant Tissues In Vivo and in Established," pp. 2432–2443, 1993.
- [71] X. Q. Pan, H. Wang, and R. J. Lee, "Antitumor activity of folate receptor-targeted liposomal doxorubicin in a KB oral carcinoma murine xenograft model," *Pharmaceutical Research*, vol. 20, no. 3, pp. 417–422, 2003.
- [72] J. A. Reddy *et al.*, "Folate-targeted, cationic liposome-mediated gene transfer into disseminated peritoneal tumors," *Gene Therapy*, vol. 9, no. 22, pp. 1542–1560, 2002.
- [73] H. E. J. Hofland *et al.*, "Folate-targeted gene transfer in vivo," *Molecular Therapy*, vol. 5, no. 6, pp. 739–744, 2002.
- [74] E. E. Nelson and A. E. Guyer, "Delivery of calf thymus DNA to tumor by folate receptor targeted cationic liposomes," vol. 1, no. 3, pp. 233–245, 2012.
- [75] G. X. Liu, G. Q. Fang, and W. Xu, "Dual targeting biomimetic liposomes for paclitaxel/DNA combination cancer treatment," *International Journal of Molecular Sciences*, vol. 15, no. 9, pp. 15287–15303, 2014.
- [76] C. Feng *et al.*, "Silencing of the MYCN gene by siRNA delivered by folate receptor-targeted liposomes in LA-N-5 cells," *Pediatric Surgery International*, vol. 26, no. 12, pp. 1185–1191, 2010.
- [77] T. Yang *et al.*, "Co-delivery of doxorubicin and Bmi1 siRNA by folate receptor targeted liposomes exhibits enhanced anti-tumor effects in vitro and in vivo," *Theranostics*, vol. 4, no. 11, pp. 1096–1111, 2014.
- [78] E. Nogueira *et al.*, "Neutral PEGylated liposomal formulation for efficient folate-mediated delivery of MCL1 siRNA to activated macrophages," *Colloids and Surfaces B: Biointerfaces*, vol. 155, pp. 459–465, 2017.
- [79] Z. Y. He *et al.*, "Folate-linked lipoplexes for short hairpin RNA targeting claudin-3 delivery in ovarian cancer xenografts," *Journal of Controlled Release*, vol. 172, no. 3, pp. 679–689, 2013.
- [80] and V. W. Sarathi V. Boddapati, Gerard G. M. D'Souza, Suna Erdogan,† Vladimir P. Torchilin, "Organelle-targeted nanocarriers: specific delivery of liposomal ceramide to mitochondria enhances its cytotoxicity in vitro and in vivo," *Nano Letters*, vol. 8, no. 8, pp. 2559–2563, 2008.

- [81] C. Zhang, N. Tang, X. J. Liu, W. Liang, W. Xu, and V. P. Torchilin, “siRNA-containing liposomes modified with polyarginine effectively silence the targeted gene,” *Journal of Controlled Release*, vol. 112, no. 2, pp. 229–239, 2006.
- [82] H. Chen, R. Ahn, J. Van den Bossche, D. H. Thompson, and T. V O’Halloran, “Folate-mediated intracellular drug delivery increases the anticancer efficacy of nanoparticulate formulation of arsenic trioxide,” *Mol Cancer Ther*, vol. 8, no. 7, pp. 1955–1963, 2009.
- [83] F. Sonvico *et al.*, “Establishment of an in vitro model expressing the folate receptor for the investigation of targeted delivery systems,” vol. 15, no. 6, pp. 407–410, 2005.
- [84] R. A. Robinson, *The healing of osseous tissue*. 1967.
- [85] N. Parker, M. J. Turk, E. Westrick, J. D. Lewis, P. S. Low, and C. P. Leamon, “Folate receptor expression in carcinomas and normal tissues determined by a quantitative radioligand binding assay,” *Analytical Biochemistry*, vol. 338, no. 2, pp. 284–293, 2005.
- [86] ThermoFisher Scientific, “Optimization of plasmid DNA transfection,” 2018. [Online]. Available: <https://www.thermofisher.com/nl/en/home/references/gibco-cell-culture-basics/transfection-basics/guidelines-for-plasmid-dna-transfection/optimizing-plasmid-dna-transfection.html>. [Accessed: 16-Dec-2018].
- [87] H. Kingston, R. E., Chen, C. A., & Okayama, *Calcium phosphate transfection. Current protocols in immunology*. 2001.
- [88] B. W. Dyer, F. A. Ferrer, D. K. Klinedinst, and R. Rodriguez, “A noncommercial dual luciferase enzyme assay system for reporter gene analysis,” *Analytical Biochemistry*, vol. 282, no. 1, pp. 158–161, 2000.
- [89] B. a Sherf, S. L. Navarro, R. R. Hannah, and K. V Wood, “Dual-Luciferase Reporter Assay: An Advanced Co-Reporter Technology Integrating Firefly and Renilla Luciferase Assays,” *Promega Notes*, vol. 57, no. Figure 1, pp. 2–8, 1996.
- [90] S. Ribeiro *et al.*, “Plasmid DNA Size Does Affect Nonviral Gene Delivery Efficiency in Stem Cells,” *Cellular Reprogramming*, vol. 14, no. 2, pp. 130–137, 2012.
- [91] P. Kreiss *et al.*, “Plasmid DNA size does not affect the physicochemical properties of lipoplexes but modulates gene transfer efficiency,” *Nucleic Acids Research*, vol. 27, no. 19, pp. 3792–3798, 1999.
- [92] W. Yin, P. Xiang, and Q. Li, “Investigations of the effect of DNA size in transient transfection assay using dual luciferase system,” *Analytical Biochemistry*, vol. 346, no. 2, pp. 289–294, 2005.
- [93] G. Chu, H. Hayakawa, and P. Berg, “Electroporation for the efficient transfection of mammalian cells with DNA,” *Nucleic Acids Research*, vol. 15, no. 3, pp. 1311–1326, 1987.

- [94] M. Caraglia *et al.*, “EGF activates an inducible survival response via the RAS- Erk-1/2 pathway to counteract interferon- α -mediated apoptosis in epidermoid cancer cells,” *Cell Death and Differentiation*, vol. 10, no. 2, pp. 218–229, 2003.
- [95] M. Haraguchi, T. Furukawa, T. Sumizawa, and S. I. Akiyama, “Sensitivity of Human KB Cells Expressing Platelet-Derived Endothelial Cell Growth Factor to Pyrimidine Antimetabolites,” *Cancer Research*, vol. 53, no. 23, pp. 5680–5682, 1993.
- [96] D. Siegmund, P. Hadwiger, K. Pfizenmaier, H. Vornlocher, and H. Wajant, “Selective inhibition of FLICE-like inhibitory protein expression with small interfering RNA oligonucleotides is sufficient to sensitize tumor cells for TRAIL-induced apoptosis,” *Molecular Medicine*, vol. 8, no. 11, pp. 725–32, 2002.
- [97] R. Reif, F. Haque, and P. Guo, “Fluorogenic RNA Nanoparticles for Monitoring RNA Folding and Degradation in Real Time in Living Cells,” *Nucleic Acid Therapeutics*, vol. 22, no. 6, pp. 428–437, 2012.
- [98] U. Kedjarune-Leggat, C. Supaprutsakul, and W. Chotigeat, “Ultrasound treatment increases transfection efficiency of low molecular weight chitosan in fibroblasts but not in KB cells,” *PLoS ONE*, vol. 9, no. 3, pp. 1–8, 2014.
- [99] Altogen Biosystems, “KB Transfection Reagent (Mouth Epidermal Carcinoma),” 2018. [Online]. Available: <https://altogen.com/product/kb-transfection-reagent-mouth-epidermal-carcinoma/>. [Accessed: 16-Dec-2018].
- [100] K. E. Makkonen, K. Airene, and S. Ylä-Herttulala, “Baculovirus-mediated gene delivery and RNAi applications,” *Viruses*, vol. 7, no. 4, pp. 2099–2125, 2015.
- [101] R. S. Ames, T. A. Kost, and J. P. Condreay, “BacMam technology and its application to drug discovery,” *Expert Opinion on Drug Discovery*, vol. 2, no. 12, pp. 1669–1681, 2007.
- [102] K. A. Whitehead, R. Langer, and D. G. Anderson, “Knocking down barriers: Advances in siRNA delivery,” *Nature Reviews Drug Discovery*, vol. 8, no. 2, pp. 129–138, 2009.
- [103] S. Rex, J. Bian, J. R. Silvius, and M. Lafleur, “The presence of PEG-lipids in liposomes does not reduce melittin binding but decreases melittin-induced leakage,” *Biochimica et Biophysica Acta - Biomembranes*, vol. 1558, no. 2, pp. 211–221, 2002.
- [104] T. Benachir and M. Lafleur, “Study of vesicle leakage induced by melittin,” *BBA - Biomembranes*, vol. 1235, no. 2, pp. 452–460, 1995.
- [105] C. Chen *et al.*, “Real-time quantification of microRNAs by stem-loop RT-PCR,” *Nucleic Acids Research*, vol. 33, no. 20, pp. 1–9, 2005.
- [106] P. Mestdagh *et al.*, “High-throughput stem-loop RT-qPCR miRNA expression profiling using minute amounts of input RNA,” *Nucleic Acids Research*, vol. 36, no. 21, 2008.

5.

DEVELOPMENT AND SINGLE- PARTICLE CHARACTERIZATION OF A LIPOSOMAL DELIVERY SYSTEM FOR THE CHEMOTHERAPEUTIC COMPOUND SN-38

SN-38 is a chemotherapeutic compound with potent antitumor effects. However, its clinical application is currently limited due to its poor solubility and low stability at physiological pH. Liposomes and cyclodextrins have been long studied for the solubilization and delivery of hydrophobic compounds. Aiming to combine the advantages from both systems, we attempted to develop an SN-38-in-cyclodextrin-in-liposome formulation. We found that the encapsulation of SN-38-SBE- β -CD inclusion complexes in the lumen of liposomes was not possible, owing to the disassembly of liposomes and the formation of lipid nanoparticles, as revealed by size exclusion chromatography and single nanoparticle fluorescence microscopy. Interestingly, the retention time of SN-38 inside SN-38-SBE- β -CD-lipid nanoparticles is higher than in liposomes, whereby SN-38 was directly loaded into the lipid film. The toxicity of purified SN-38-SBE- β -CD-lipid nanoparticles was assayed in cultured cancer cells, showing no therapeutic advantage compared to bulk SN-38-SBE- β -CD complexes. Further formulation optimization, in particular an increased concentration of the nanoparticles, will be necessary to obtain cytotoxicity effects. Moreover, the results highlight the value of fluorescence imaging of single, surface-immobilized nanoparticles, in the development of liposomal delivery systems such as drug-in-cyclodextrin-in-liposomes.

5.1 INTRODUCTION

SN-38, 7-ethyl-10-hydroxycamptothecin, is the active metabolite of Irinotecan (CPT-11), a compound approved by the Food and Drug Administration agency for use in the treatment of recurrent metastatic colorectal cancer. SN-38 interferes with the human topoisomerase I, impeding both DNA replication and transcription [1, 2].

The therapeutic activity of CPT-11 depends on its conversion efficiency to SN-38. Upon administration, only 2 to 8% of CPT-11 is metabolized into the active SN-38 through carboxylesterase mediated cleavage in the liver [3, 4]. The conversion rate is relatively dependent on genetic variability, making it variable and unpredictable, posing significant life-threatening risks and complicating clinical management of patients [3, 5]. Unlike its precursor, SN-38 does not require activation in the liver. Moreover, *in vitro* toxicity studies indicate that SN-38 is up to 1,000-fold more potent than CPT-11 against different tumor cell lines [5]. Additionally, the biological half-life of SN-38 is much longer than that of CPT-11 [3]. Thus, SN-38 holds great pharmaceutical advantage over CPT-11 as an anticancer candidate.

Despite its potent activity toward tumor cells *in vitro*, clinical application of SN-38 remains challenging due to its extremely poor solubility in aqueous solutions and other pharmaceutically acceptable solvents [6]. SN-38 exists in two pH-dependent reversible forms: an active lactone ring at acidic pH and an inactive carboxylate form at basic pH (Fig. 1a). The closed lactone moiety is a required feature for the anti-tumor activity of SN-38. Unfortunately, at physiological pH, the active lactone is partially converted into the inactive carboxylate that becomes dominant at equilibrium [3]. In addition, *in vivo*, the carboxylate form tightly binds to human serum albumin with an affinity 150-fold higher than the lactone form, further shifting the lactone-carboxylate equilibrium towards the inactive state [7]. Therefore, the instability of the lactone SN-38 under physiological conditions represents a major challenge towards an effective therapy with SN-38.

In this work, we aimed at developing two types of lipid-based drug delivery systems for SN-38 in order to overcome some of the above challenges: SN-38-loaded liposomes and SN-38-in-cyclodextrin-in liposomes. Liposomal delivery systems can solubilize hydrophobic drugs in their lipid bilayer [8], improve their stability [9] and tumor targeting ability *in vivo* [10], and reduce their systemic toxicity [REF?]. Previous efforts have attempted to incorporate camptothecin derivatives into liposomes [5]. It has been shown that interaction with a lipid bilayer stabilizes the lactone ring moiety of camptothecin drugs by protecting it from hydrolysis [11]. Furthermore, liposomes prevent the complexation of the carboxylate form with human serum albumin [12]. In 2004, Zhang et al. [3] described the development of a non-targeted SN-38 liposomal formulation (LE-SN-38) that improved the pharmacokinetic profile, safety and tolerability of SN-38 in its phase I trial investigation for the treatment of metastatic colorectal cancer [13].

Although liposomalization of drugs can enhance their tumor distribution passively through the enhanced permeability and retention effect [14–16], insufficient uptake at tumor sites and nonspecific association to healthy tissues decrease their therapeutic efficacy and may provoke harmful side effects [17]. Active targeted delivery increases tissue selectivity and thus reduces side effects [18]. Folic acid has been extensively investigated as a ligand for tumor-specific and targeted drug delivery because its receptors (folic acid receptors, FR) are overexpressed on the surface of a variety of malignant tumor cells, while being minimally distributed in healthy tissues [19]. Folate-conjugated lipidic nanocarriers have been shown to increase drug accumulation in FR-overexpressing tumors [20]. Different chemotherapeutic agents have been delivered using liposomes conjugated to the folate ligand via a polyethyleneglycol spacer [21]. Recently, a study has shown that SN-38-loaded, folate-functionalized liposomes can target breast cancer tumors and reduce unspecific SN-38 toxicity *in vivo* [22].

Incorporation of hydrophobic drugs in the lipid bilayer of liposomes is always restricted in terms of the drug-to-lipid mass ratio [23, 24]. Thus, new strategies to further enhance loading efficiency of highly lipophilic camptothecin compounds, like SN-38, into liposomes must be deployed. Cyclodextrins are naturally existing water-soluble cyclic oligosaccharides [25] that form inclusion complexes by sequestering small molecules or moieties of larger molecules inside their hydrophobic cavity [26]. Drugs complexed with cyclodextrins show increased solubility [27], stability [28], dissolution rate and bioavailability [29], leading to enhanced cytotoxicity of several anti-cancer drugs, such as camptothecin, curcumin, doxorubicin, docetaxel and paclitaxel [28]. Sulfobutyl ether- β -cyclodextrin (SBE- β -CD, marketed as Captisol™) is used in various drug formulations. Recently, Vangara et al. [28] found that SN-38 could form stable inclusion complexes with SBE- β -CD, enhancing its solubility by more than 1,000 fold and improving its anticancer potency on ovarian cells. However, the relatively poor affinity of the drug-cyclodextrin complex leads to rapid dissociation and premature clearance of the drug after intravenous injection [30–34].

The entrapment of drug-cyclodextrin complexes in the aqueous phase of liposomes might circumvent the problems associated to the conventional integration of drugs into the lipid phase of liposomes or into the hydrophobic cavity of cyclodextrins. Drug-in-cyclodextrin-in-liposomes could provide an ideal integrative system combining the assets of both approaches. [33, 35]. In this study, we examined the potential of two different lipid-based systems for tumor-targeted delivery of SN-38. First, we prepared a formulation of folate-labeled, SN-38-loaded liposomes (Fig. 1b). To achieve long-term storage of liposome precursors and facilitate laboratory distribution, we prepared SN-38-loaded lipid films coated onto glass beads. Furthermore, we prepared a folate-labeled SN-38-in-cyclodextrin-in-liposome formulation. Particle size distribution, drug retention time and association with human carcinoma FR-overexpressing KB cells were investigated.

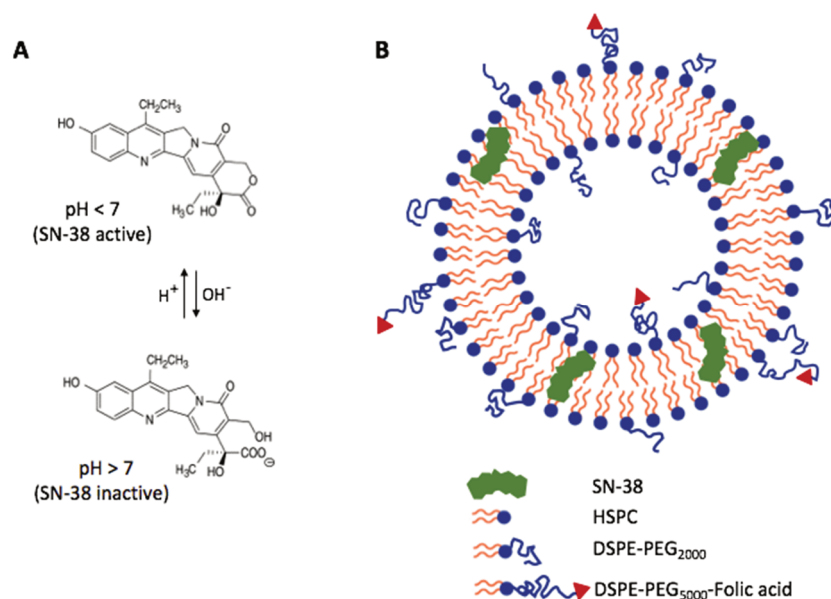


Fig. 1. A) Schematic chemical structure of the lactone and carboxylate forms of SN-38. Adapted from [4]; B) SN-38-loaded folate-targeted liposomes. Note that the folate-conjugated phospholids are very likely present in the inner leaflet of the liposome membrane too.

5.2 MATERIAL AND METHODS

5.2.1 MATERIALS

SN-38 was purchased from Selleckchem (Houston, TX, USA), diluted in DMSO to 50 mM (20 mg/ml), aliquoted and stored at -80°C . CaptisolTM was kindly provided by CyDex Inc. Pharmaceuticals (USA). HeLa cells were kindly provided by Eric P. van der Veer, Leiden University Medical Center, Leiden (The Netherlands). KB cells (ACC 136), a derivative cell line from HeLa, were purchased from DSMZ. Hydrogenated L- α -phosphatidylcholine (Hydro Soy PC, Avanti Polar Lipids) powder was kindly provided by to-BBB Inc (Leiden). 1,2-distearoyl-*sn*-glycero-3-phosphoethanolamine-N-[biotinyl(polyethylene glycol)-2000] (DSPE-PEG (2000) Biotin) 10 mg/ml, cholesterol 50 mg/ml and 1,2-distearoyl-*sn*-glycero-3-phosphoethanolamine-N-[folate(polyethylene glycol)-5000] (DSPE-PEG (5000) Folate) 500 μg were purchased from Avanti Polar lipids. Texas Red[®] 1,2-dihexadecanoyl-*sn*-glycero-3-phosphoethanolamine (DHPE-Texas Red) was purchased from ThermoFisher Scientific.

5.2.2 FORMATION OF SN-38-CONTAINING LIPID FILMS

A 50 mM stock solution of SN-38 in DMSO was diluted in methanol at a final concentration of 10 mM. The sample was further diluted ten times in chloroform and 50 μl were added to a lipid solution composed of 30 μl of Hydro Soy PC (HSPC) 10 mg/ml (stock concentration), 2 μl of cholesterol 50 mg/ml, 10 μl of DSPE-PEG (2000) Biotin (DSPE-PEG-biotin) 10 mg/ml and 5 μl of DHPE-Texas Red (DHPE-TR) 1 mg/ml, all dissolved in chloroform, resulting in a molar ratio HSPC:cholesterol:DSPE-PEG-biotin:DHPE-TR of 56.7:37.8:4.8:0.5 and a total mass of lipids of 0.5 mg. A negative control sample devoid of SN-38 was prepared by mixing 1 μl of

DMSO and 49 μl methanol, and proceeding as described above. The resulting samples were added to 212-300- μm glass beads (Sigma Aldrich) in a round-bottom glass flask at a lipid-to-bead mass ratio 1:760. The solvent was rotary evaporated at room temperature and 500 mbar overnight and the pressure was gradually decreased down to 20 mbar. Then, temperature was increased to 80 $^{\circ}\text{C}$ and rotary evaporation was continued for 3 h at 20 mbar to remove traces of DMSO. Lipid film-coated beads were collected in 2-ml amber glass vials (Sulpeco) and flushed with argon for a few seconds before storage. Vials were closed, sealed with Parafilm and stored at -20°C until use.

5.2.3 FORMATION OF FOLATE-CONTAINING LIPID FILMS

A lipid mixture in chloroform with a molar ratio of HSPC:cholesterol:DSPE-PEG-biotin:DHPE-TR:DSPE-PEG-folate equal to 56.6:37.8:4.8:0.5:0.1 for a total mass of 1 mg was added to 212-300- μm glass beads in a round-bottom glass flask at a lipid-to-bead mass ratio of 0.003:1. The solvent was rotary evaporated at about 40 rpm and 200 mbar overnight and 20 mbar for 10 min. Lipid-coated beads were stored at -20°C and were used within two weeks.

5.2.4 LIPOSOMAL SN-38 PRODUCTION

Lipid-SN-38-coated beads were desiccated for 20 min at room temperature before use. About 50 mg of functionalized beads were poured in a reaction tube and immersed in 200 μl of swelling solution consisting of acidic PBS (pH 5.3). Liposome production was induced by vigorous vortex for 1 min, leading to a final lipid concentration of 0.34 mg/ml and a final SN-38 concentration of 33.3 μM . SN-38-containing liposomes were extruded in a mini-extruder (Avanti Polar Lipids) using a 0.2 μm pore-size polycarbonate membrane (Avanti Polar Lipids) and two 10 mm filter supports (Whatmann) by 11 to 13 extrusion passages. The obtained small unilamellar vesicles (SUVs) were incubated at 4 $^{\circ}\text{C}$ for 48 or 72 h protected from light.

5.2.5 PREPARATION OF FOLATE-LABELED LIPOSOMES

Approximately 50 mg of folate-labeled lipid-coated beads were briefly flashed with argon and immersed in 200 μl of PBS. Liposome production was induced by natural swelling for 2 hours with manual rotation every 15 min at 60 $^{\circ}\text{C}$ (HSPC $T_m = 53^{\circ}\text{C}$). The final lipid concentration was 0.8 mg/ml. Liposomes were downsized by extrusion to obtain small unilamellar vesicles (SUVs) as described above, except that temperature was set to 60 $^{\circ}\text{C}$.

5.2.6 DYNAMIC LIGHT SCATTERING

The size distribution of liposomes was analyzed by dynamic light scattering (DLS). For a typical experiment, 10 μl of the SUV solution was diluted in 90 μl of PBS buffer and placed into a disposable microcuvette (ZEN0040, Malvern). The measurements were carried out on a Zetasizer Nano ZS (Malvern, UK) operating at a scattering angle of 173 $^{\circ}$ at room temperature. For each condition, each run consisted of three measurements of 12-20 acquisitions per sample.

Liposome colloidal stability was studied over time by monitoring their mean size and size distribution every day for 5 days upon storage at 4 °C.

5.2.7 SIZE EXCLUSION CHROMATOGRAPHY

A homemade size exclusion chromatography column was prepared by filling the neck of a 150 mm Pasteur glass pipette with cotton. The cotton was washed with MilliQ water and 1.7 ml or 2 ml of Sepharose beads 4B (45-165 μm bead diameter) were added. Columns were packed overnight at room temperature. Prior to usage, columns were washed three times with a volume equal to that of the beads added. Column washes were done with either sample buffer or ammonium acetate (25 mM, pH 8.6) depending on the experiment. Liposome samples pre-incubated for 0, 48 or 72 h at 4 °C were added when the eluent level reached the top of the gel. Buffer flow was driven by gravity only. The sample was allowed to penetrate the gel entirely prior to adding repetitively small volumes of buffer for continuous elution. A sample volume between 30 and 150 μl was purified in each column, and 30-48 elution samples were collected in microcentrifuge tubes. Two drops of eluate were collected per tube.

5.2.8 FLUORESCENCE SPECTROSCOPY

Elution samples of 10 μl were dispensed in wells of a black 384-well microplate (Greiner Bio One). Fluorescence intensity was measured with a CLARIOstar[®] Microplate reader (BMG LABTECH's) using 379/10 nm excitation and 548/10 nm emission wavelengths for SN-38, and 562/15 nm excitation and 606/10 nm emission wavelengths for the liposome membrane dye (Texas Red). A focal height of 11 mm was set for all measurements. Gains of 1000, 1500, 2000, or 3000 for SN-38 and Texas Red were used depending on the experiment. The emission spectra of SN-38 and Texas Red were measured on a glass-bottom 384-well microplate ($\mu\text{Clear}^{\text{®}}$, non-binding, Greiner Bio One) using excitation wavelengths of 379/10 nm and 562/10 nm, respectively, a gain of 3000 and a focal height of 3 mm.

5.2.9 PREPARATION OF CHAMBERED COVERSLEIPS

Chambered coverslips were fabricated to image liposomes. First, two holes with diameters of 5 and 7 mm were drilled into a coverslide (76 \times 26 mm, Menzel-Gläser) with a Sand Blaster. After a brief washing step with MilliQ water, coverslips were consecutively sonicated in a bath (Branson 1510 ultrasonic cleaner, Ultrasonics) with 2% Hellmanex and MilliQ water for 10 min and with 100% ethanol. Dried coverslips were plasma cleaned in a Harrick Plasma PDC-002. Coverslips (24 \times 60 mm, Menzel-Gläser) were also cleaned following the protocol described above. A drop of Norland optical adhesive (NOA 81, Ultraviolet curing) was applied to the surroundings of the apertures on a single side of the coverslips, and a clean coverslip was immediately sealed on top by 5 min irradiation with a 365-nm light using a Promed UVL 36 lamp. The chambered coverslips were incubated for 48 h at 55 °C, washed as mentioned above, and stored in clean Petri dishes until usage.

5.2.10 FLUORESCENCE CONFOCAL MICROSCOPY

The 5-mm wide well of the chambered coverslip was functionalized with 10 μ l of 1 mg/ml BSA-Biotin (Thermo Fisher Scientific) for 5 min, washed three times with MilliQ water, incubated with 10 μ l of 1 mg/ml NeutrAvidin (Thermo Fisher Scientific) for 5 min at room temperature, washed three times with MilliQ water and finally incubated with 10 μ l PBS. Before imaging, PBS was replaced with 7-10 μ l of the lipid sample (liposomes or nanoparticles). The 7-mm hole was filled with 15 μ l MilliQ water to avoid sample evaporation during imaging. After sample addition, chambered coverslips were sealed with a 1-mm thick silicone spacer (Press-to-seal silicone sheet, Life technologies) and a clean coverslip. Imaging was performed using a laser scanning confocal microscope (A1+, Nikon) equipped with a \times 100 oil immersion objective. The 405 nm and 561 nm laser lines with appropriate dichroic mirrors and emission filters were used to image SN-38 and Texas Red, respectively.

5.2.11 HIGH PERFORMANCE LIQUID CHROMATOGRAPHY

SN-38 detection was performed using a reverse-phase HPLC system (Agilent 1260 Infinity Quaternary LC, Santa Clara, United States) consisting of a quaternary pump, an autosampler module and a fluorescence detector set at 368 nm and 515 nm for excitation and emission wavelengths, respectively. The mobile phase consisted of freshly prepared 25 mM ammonium acetate pH 5.5 (solvent A) and acetonitrile (solvent B) and the column was an Agilent SB-C18 (50 mm \times 2.1 mm, 1.8 μ m). The mobile phase was pumped at a flow rate of 0.5 ml/min in accordance with the following program (time in minute, percent solvent B): 0, 15; 10, 40; 10.01, 100; 11, 100; and 11.01, 15. The total run time was 15 min. The elution times of the SN-38 lactone and carboxylate forms were 6.05 and 1.75 min, respectively. When high amounts of SN-38 were injected, the washing step of the column was extended by one minute and the injection needle was washed with 1:1 (v:v) methanol/water after each injection. Additionally, 10 μ l of acetonitrile were injected between sample runs to clean the column and avoid sample-to-sample contaminations. The flow rate was 0.5 ml/min and the maximum pressure in the column was 600 bar. Samples were loaded into low-volume HPLC vial inserts (250 μ l, Agilent) in 2-ml screw top vials (Agilent) and kept at 4 $^{\circ}$ C until injection. All samples containing liposomes or lipid nanoparticles were pre-diluted ten times in methanol, vortexed for 30 sec and spun down in a tabletop centrifuge for 30-60 sec to remove any precipitates. HPLC samples containing 90% methanol were injected soon after preparation to avoid conversion of carboxylate SN-38 into lactone SN-38. Sample injection volumes were 1 μ l, 2 μ l or 10 μ l depending on the experiment.

5.2.12 PH DEPENDENCE ASSAYS

The 50 mM SN-38 stock solution in DMSO was diluted hundred times in acidic PBS (pH 5.3). This sample was further diluted fifty times in either acidic PBS, neutral PBS (pH 7.4) or in 50 mM sodium phosphate (pH 8.3) leading to a final SN-38 concentration of 10 μ M. Tubes were then sealed, shielded from light and incubated at 37 $^{\circ}$ C overnight. Before HPLC measurements,

samples were spun for 20 min at 13,200 rpm, and 10 μ l were carefully harvested and injected into the HPLC.

For the SN-38 inactivation kinetics study, the SN-38 stock solution was diluted in acidic PBS at 32.5 μ M final concentration. This sample was further diluted twenty times in either acidic PBS or in 50 mM sodium phosphate (pH 8.3), and was incubated at 37 °C in sealed tubes. A 20 μ l aliquot was harvested from each tube at different time points: 1 h, 2 h, 3 h, 4 h, 5 h and 24 h. All samples were diluted ten times in methanol giving a final SN-38 concentration of 1.7 μ M, vortexed for 30 sec, spun for 20 min at 13,200 rpm and 10 μ l were injected into the HPLC.

5.2.13 RELEASE EXPERIMENTS

A 150- μ l sample of SN38-containing SUVs was incubated at 4 °C for 48 h and purified by size exclusion chromatography through a 1.7-ml column pre-washed with acidic PBS. A total of 48 elution samples were collected in microcentrifuge tubes. Fluorescence intensity of SN-38 and Texas Red in each sample was analyzed on a CLARIOstar® spectrofluorometer. The samples containing the highest membrane dye signal (liposome population) were pooled. A 20- μ l aliquot was used for HPLC analysis (time zero), while the remaining volume (195 μ l) was re-purified through a new size exclusion chromatography column with a 20-min lagtime after the first purification. After measuring the SN-38 and Texas Red fluorescence signals from all eluates of the second purification, the fractions corresponding to the liposome population were pooled and 20 μ l were used for a second HPLC inspection.

5.2.14 LIPOSOME-MEDIATED STABILITY ASSAYS

A 10- μ l sample of SN38-containing SUVs was incubated at 4 °C for 72 h, transferred in a new tube and diluted twenty times in ammonium acetate (25 mM, pH 8.6), resulting in 1.6 μ M SN-38 final concentration. A 20- μ l aliquot was used for HPLC analysis (unpurified liposomes, time zero). The remaining solution was incubated for 2 h at 37 °C in sealed tubes shielded from light and a 20- μ l aliquot was harvested for HPLC analysis (unpurified liposomes, time 2 h). SN38-containing SUVs were purified by size exclusion chromatography as described above and 20 μ l of the pooled liposome-containing fractions were analyzed by HPLC (purified liposomes, time zero). The remaining solution was incubated for 2 h at 37 °C in sealed tubes shielded from light and a 20- μ l aliquot was harvested for HPLC analysis (purified liposomes, time 2 h). Negative controls were conducted in the absence of lipids. A sample of 32.5 μ M SN-38 in acidic PBS was prepared as described above and further diluted twenty times in ammonium acetate (25 mM, pH 8.6), resulting in 1.6 μ M SN-38 final concentration. A 20- μ l aliquot was harvested for HPLC analysis (SN-38 bulk, time zero). The remaining solution was incubated for 2 h at 37 °C in sealed tubes shielded from light and a 20- μ l aliquot was harvested for HPLC analysis (SN-38 bulk, time 2 h).

5.2.15 COMPLEXATION OF SN-38 WITH SBE- β -CD

Solubility of SN-38 was studied in the presence of varying amounts of SBE- β -CD in 1 ml final volume of acidic PBS. First, a 200-mM SBE- β -CD solution was prepared by dissolving 0.215 g of SBE- β -CD (CyDex Inc. Pharmaceuticals, USA) in 500 μ l of acidic PBS. Samples of 800 μ M, 10 mM, 48 mM, 100 mM and 150 mM SBE- β -CD were prepared by serial dilutions in the same buffer. All tubes were vortexed and incubated at 37 °C until all SBE- β -CD was dissolved. Next, SN-38 was added to a final concentration of 100 μ M in each tube, resulting in samples with the following SN-38 to SBE- β -CD molar ratios: 1:8, 1:100, 1:480, 1:1000 and 1:1500. Samples were sonicated for 15 min in a bath sonicator, tumbled overnight at room temperature to form SN-38-SBE- β -CD complexes, centrifuged for 5 min at 13,200 rpm, and 900 μ l were carefully transferred to new tubes in order to remove undissolved precipitates. Quantitation of SN-38 solubilization was carried out by measuring SN-38 fluorescence intensity by HPLC (1- μ l sample injection) and by spectrofluorometry using a plate reader, as described above. For each technique, a solubility curve was generated by plotting the measured fluorescence intensity values (plate reader) or the chromatogram peak areas (HPLC) against the molar excess of cyclodextrin used in each condition.

We also prepared samples with lower ratios of SN-38 to SBE- β -CD, namely 1.25:1 and 1:8, and varying absolute amounts of both molecules. All samples were sonicated for 15 min and rotated at 20 rpm overnight at room temperature. Aliquots of 600 μ l from each sample were filtered with a 0.45- μ m filter to remove undissolved SN-38 and 2 μ l were injected for HPLC analysis. Moreover, the protective effect of SBE- β -CD on the lactone SN-38 was investigated in samples containing 25 μ M SN-38 and 10.2 mM SBE- β -CD (or none in negative controls, the equivalent volume was substituted with MilliQ water) in 50 mM sodium phosphate buffer (pH 8.3). Sample preparation was as described above for the solubility study. Preparation of SN-38-SBE- β -CD complexes for cell viability assays was performed as described above, except that final concentrations of 1 mM SN-38 and 8 mM SBE- β -CD in acidic PBS were used.

5.2.16 QUANTITATION OF SN-38

Ten standards consisting of 100, 50, 25, 5, 2, 1, 0.5, 0.1, 0.05 and 0.01 μ M of SN-38 in acidic PBS supplemented with a molar excess of SBE- β -CD were prepared. A minimum molar ratio of SN-38:SBE- β -CD of 1:1000 was used by adding 100 mM SBE- β -CD to ensure complete SN-38 solubilization. First, 200 mM SBE- β -CD stock solution was prepared in PBS by dissolving 1.72 g in 4 ml of acidic PBS. The tube was vortexed and incubated at 37 °C until SBE- β -CD was dissolved, and the appropriate volume was added to the ten SN-38 standard samples, each having a final volume of 500 μ l. All samples were sonicated for 15 min in a bath sonicator, tumbled overnight at room temperature in sealed tubes protected from light, spun for 5 min at 13,200 rpm and 400 μ l were carefully transferred to new tubes. SN-38 fluorescence signal was measured by spectrofluorometry and HPLC as described above. Two calibration curves were generated by plotting the measured SN-38 fluorescence intensity values and chromatogram

peak areas for each standard against their predetermined amounts. The standard curves were then used to calculate the concentration of SN-38 added to cells in cytotoxicity assays.

5.2.17 PREPARATION OF SN-38-SBE- β -CD-LIPID NANOPARTICLES

Folate-labeled lipid-coated beads were briefly flashed with argon and about 50 mg were immersed in 200 μ l of swelling solution consisting of either 8 mM SBE- β -CD or 1 mM SN-38 complexed with 8 mM SBE- β -CD in acidic PBS. Liposome production was carried out by natural swelling for 2 h at 60 °C with gentle manual rotation of the tube every 15 min. Final lipid concentration was 0.8 mg/ml in the two samples. Liposomes were extruded as described above, except that temperature was set to 60 °C. Right after extrusion, the resulting SUV solutions were directly purified by size exclusion chromatography through freshly prepared columns (see above). The column was washed six times with 1 ml neutral PBS (pH 7.12) prior addition of 125 μ l of an SUV solution. A total of 48 eluates per sample were collected in microcentrifuge tubes. The SN-38 and membrane dye fluorescence was measured as previously described.

5.2.18 CELL CULTURE

HeLa and KB cells were cultured in folate-deficient RPMI-1640 medium (ThermoFisher) supplemented with 10% heat-inactivated fetal bovine serum (ThermoFisher) with 5% CO₂ at 37 °C. Cells were discarded after 35 passages.

5.2.19 FLUORESCENCE IMAGING OF KB CELLS

3×10^5 KB cells were seeded on glass-bottom microscopy plates (MatTek; 9.5 cm²) and incubated for 24 h at 37 °C with 5% CO₂ prior to imaging. Then, 40 μ l of either the folate-decorated HSPC-liposomes or the SN-38-SBE- β -CD lipid nanoparticles were added to the monolayers of KB cells. To assay the selective binding of the folate-decorated HSPC-liposomes with KB cells, a control experiment was performed, in which the cell medium was supplemented with 5 mM soluble folic acid during incubation with the SUVs. After 2-h incubation, the microscopy plates were mounted on the stage of a confocal microscope (see above for details) equipped with an environment control chamber set to 37 °C and 5% CO₂. When indicated, time-lapse imaging was carried out during 2 h.

5.2.20 CELL VIABILITY ASSAY

100- μ l cell suspensions with a density of 10 cells/ μ l were seeded on a white flat-bottom opaque walled 96-well plate (Sigma Aldrich) and cultured in RPMI-1640 medium supplemented with 10% heat-inactivated fetal bovine serum and penicillin/streptomycin (ThermoFisher) at 37 °C and 5% CO₂ overnight. A volume of 12 to 15 μ l of purified SN-38-SBE- β -CD-lipid nanoparticles was added to KB and HeLa cells. In a series of controls, the SN-38-SBE- β -CD-lipid nanoparticles solution was substituted with either PBS pH 7.4, a bulk SN-38-SBE- β -CD solution with an SN-38 concentration adjusted to that of the elution pool of SN-38-SBE- β -CD,

purified SBE- β -CD-lipid nanoparticles with a lipid concentration adjusted to that of the purified SN-38-SBE- β -CD-lipid nanoparticles, an SN-38-SBE- β -CD bulk solution with 1 mM SN-38 and 8 mM SBE- β -CD, or a solution with 8 mM SBE- β -CD. All conditions were assayed in triplicate. Cell viability was performed after 72 h incubation according to the CellTiter-Glo[®] protocol (Promega). Luminescence was measured with a CLARIOstar[®] Microplate Reader (BMG LABTECH's) with a monochromator set to detect light with wavelength between 520 nm and 620 nm, and a focal height of 11 mm.

5.3 RESULTS

5.3.1 LIPOSOME PRODUCTION BY SWELLING OF SN-38-LOADED LIPID FILMS SUPPORTED ON GLASS BEADS

SN-38-containing liposomes were prepared by lipid film hydration. A lipid composition mimicking that of Doxil[®] was supplemented with three types of functionalized phospholipids conjugated to either folate as a cell targeting agent, Texas Red as a fluorescent membrane reporter and to biotin through a polyethylene glycol linker for enhanced immobilization during imaging (Fig. 1b). To facilitate storage, handling and distribution of lipid mixtures, while increasing the solubilization of SN-38, we prepared lipid-coated glass beads with SN-38 incorporated in the lipid film. Upon rehydration, multilamellar vesicles are produced as precursors of 200-nm unilamellar vesicles prepared by extrusion. Formulation of lipid-SN-38-coated beads as precursors of SN-38-containing small unilamellar vesicles is particularly suited because large batches can be prepared at once and be easily distributed across laboratories in the form of solvent-free aliquots. The functionalized beads could be stored for more than 6 months at -20 °C without noticeable conversion of SN-38 from the lactone to the carboxylate form or liposome stability.

Liposomes were prepared in acidic PBS (pH 5.3) to maintain SN-38 in its active state. SN-38-doped HSPC-liposomes were immobilized on a glass coverslip and imaged by fluorescence microscopy. The SUVs were localized through their membrane dye. They appear as discrete diffraction-limited spots with a width <1 μ m (Fig. 2a). The population-wide liposome size distribution was determined by light scattering. Both SN-38-loaded SUVs and control SUVs had a similar average diameter of 225 and 216 nm, respectively, 7 days after liposome production (Fig. 2b, Fig. S1). These results indicate that the inclusion of SN-38 does not influence vesicle size, aggregation state or stability.

The ability of folate-modified HSPC-liposomes to target living cells was investigated in the absence of SN-38 using cultured KB cells. The specific role of the folate ligand in cellular interaction was evaluated by performing a competitive binding assay in which 5 mM of free folic acid was added to the medium to saturate the cell-surface folate receptors. Fluorescence imaging up to 2 h after incubating liposomes with the cells revealed that SUVs interact with the plasma membrane of KB cells mostly in the absence of free folate (Fig. 2c), demonstrating that

folate ligand promotes liposome binding. Moreover, several vesicles clearly localized on the inner side of the plasma membrane (Fig. 2c) suggesting internalization during endocytosis of the folate receptors. These results prompted us to study the potential of folate-conjugated HSPC-liposomes for the targeted delivery of SN-38.

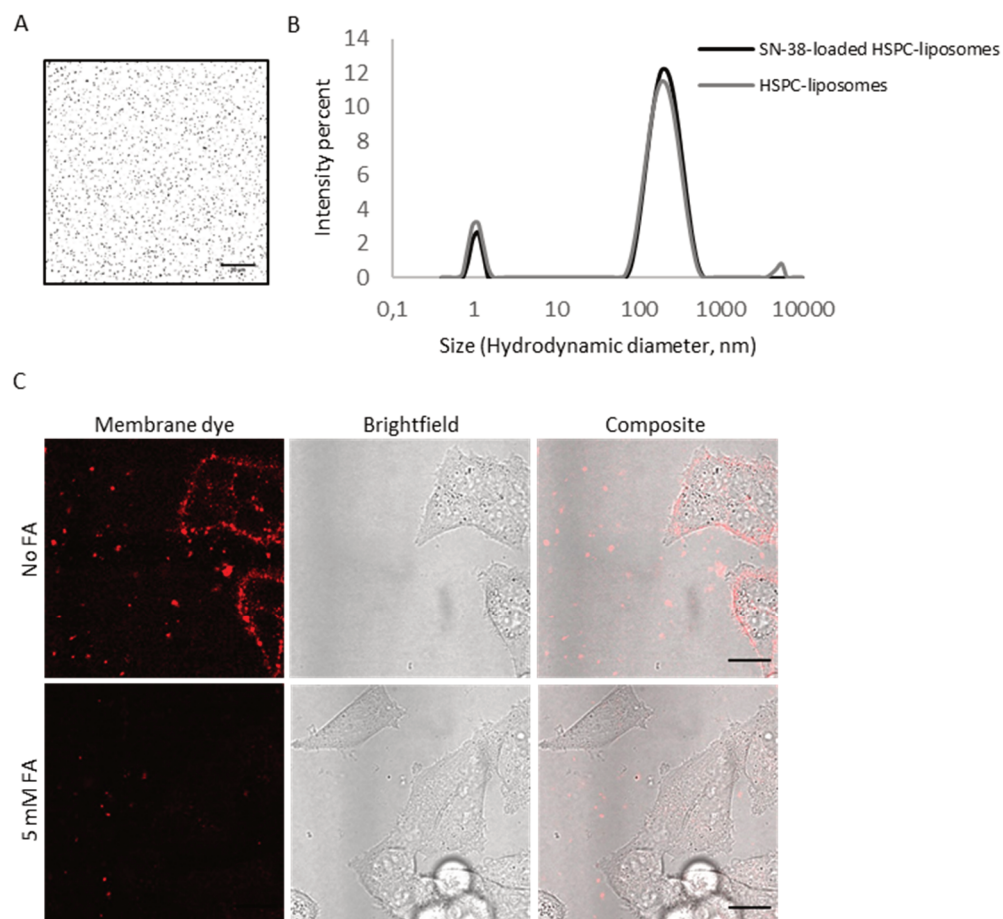


Fig. 2. A) Fluorescence confocal image of SN-38-doped HSPC-liposomes tethered on a glass coverslip. The Texas Red membrane dye channel is shown. Single liposomes correspond to diffraction-limited spots. Scale bar is 20 μm . B) Liposome size distribution as measured by dynamic light scattering. The SN-38-doped HSPC-SUV and HSPC-SUV samples were analyzed after 7 days at 4 $^{\circ}\text{C}$. C) Fluorescence and brightfield confocal images of cultured KB cells in the presence of folate-labeled HSPC-liposomes incubated for 2 h at 37 $^{\circ}\text{C}$. In a control sample, 5 mM folic acid (FA) was supplemented during incubation with the vesicles. Scale bars are 20 μm .

5.3.2 SN-38 IS RAPIDLY RELEASED FROM FOLATE-HSCP LIPOSOMES

The stability of SN38 in the liposome membrane was investigated by size exclusion chromatography to quantify the amounts of free and liposome-loaded SN-38 molecules. The spectrally separated SN-38 and membrane dye fluorescence signals allowed us to monitor their respective levels in the course of elution. The corresponding intensity profiles are shown in Fig. 3a, b. Folate-modified HSPC-liposomes were identified as a single peak spanning across eight fractions, both in the presence and absence of SN-38. SN-38 mostly eluted as one peak after fraction 20, representing the free drug that has been released from the SUVs. Interestingly, a fraction of SN-38 co-eluted with liposomes when the sample was left to pre-incubate for 48 h

prior column purification (Fig. 3b). Although the underlying mechanism requires clarification, we decided to quantify the rate of release under this condition and to determine the amounts of active (lactone) and inactive (carboxylate) SN-38.

SN-38 was incubated in buffers with different pH values to populate the solution with a single or the two species. The lactone and carboxylate SN-38 forms can clearly be distinguished as two baseline-separated peaks by HPLC (Fig. 3c). The peaks eluting at 1.8–2.0 min and 6.2–6.3 min correspond to the inactive and the active forms of SN-38, respectively. At pH 5.3, approximately ~100% of SN-38 remained in the lactone state. At pH 7.4, ~69% of SN-38 was converted to the carboxylate form, whereas ~95% underwent conversion at pH 8.3. In acidic PBS, SN-38 remained active for several weeks (data not shown). Maximum conversion of the lactone SN-38 to the carboxylate form in the inactivating sodium phosphate buffer (pH 8.3) was reached after 2 h (Fig. 3d).

Next, we set out to determine whether the liposomes exerted a protective effect on SN-38 against pH inactivation. We diluted free lactone SN-38, unpurified SN-38-loaded HSPC-liposomes and purified SN-38-loaded HSPC-liposomes in an inactivating basic buffer. The remaining fraction of active SN-38 present in each sample was quantified by HPLC. No significant difference was found between the three conditions after 2 h incubation (Fig. 3e), suggesting that SN-38 is released from the membrane and undergo conversion in the bulk solution. Alternatively, SN-38 interacting with, or entrapped in liposomes would get inactivated. To discriminate between these two scenarios, the SN-38 release rate from HSPC-liposomes was studied by a two-step column purification. All liposome-containing fractions in the first chromatography (indicated with parentheses in Fig. 3f) were pooled and subjected to a second purification after 20 min. Less than 10% of the SN-38 that had co-eluted with liposomes in the first purification step was recovered (Fig. 3f). This result shows that SN-38 is rapidly released from the HSPC liposomes into the outside solution, where it can be converted into the carboxylate form under basic conditions.

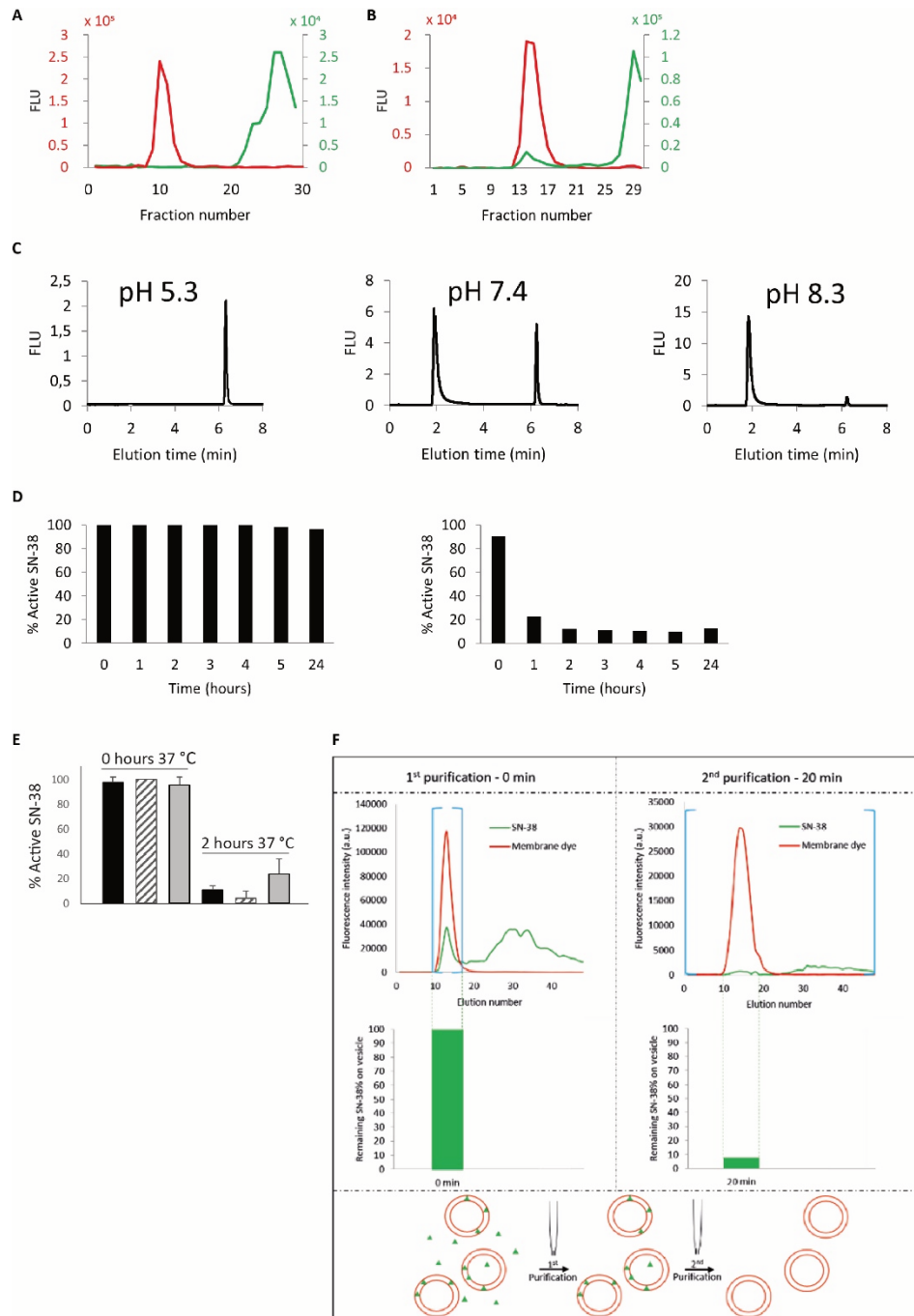


Fig. 3. A) Elution profiles of SN-38 (green) and liposome (red) fluorescence intensity in size exclusion chromatography experiments with SN-38-loaded HSPC-liposomes. The sample was directly transferred to the purification column (A) or was incubated for 48 h at 4 °C prior to purification (B). C) HPLC chromatograms of SN-38 (10 μ M) incubated overnight at 37 °C in acidic PBS (pH 5.3), neutral PBS (pH 7.4) or 50 mM sodium phosphate (pH 8.3). D) Percentage of remaining active SN-38 (1.7 μ M total concentration) at different incubation time points in acidic PBS (left panel) and sodium phosphate buffer (right panel) at 37 °C. E) Percentage of active SN-38 in bulk (dashed bars), unpurified SN-38-loaded HSPC-liposomes (grey bars) and purified SN-38-loaded HSPC-liposomes (black bars) after dilution in basic buffer, and 0 and 2 h incubation at 37 °C. F) Assay of SN-38 release from HSPC-liposomes. SN-38-containing liposomes were subjected to a two-step purification and the fraction of remaining SN-38 was calculated. The elution profiles of SN-38 (green) and liposome (red) fluorescence intensity are shown for the two chromatography steps. The percentages of remaining SN-38 after the first (left)

and second (right) purification are displayed. A schematic of the two-step liposome purification assay is shown at the bottom. SN-38 molecules are represented as green triangles.

5.3.3 COMPLEXATION OF SN-38 WITH SBE- β -CD INCREASES THE DRUG SOLUBILITY

To avoid premature release of SN-38 from HSPC vesicles, we aimed to create an SN-38-in-cyclodextrin-in-liposome system as a novel strategy for liposomal SN-38 delivery (Fig. 4a). First, we addressed the ability of SBE- β -CD to solubilize SN-38 without affecting its conversion rate. We verified that complexation with SBE- β -CD does not influence the elution profile of the lactone SN-38 by HPLC (Fig. S2). An SN-38 solubility curve was plotted by measuring the amount of solubilized drug (100 μ M input concentration) as a function of SBE- β -CD concentration (Fig. 4b). The solubility of SN-38 increased linearly with respect to cyclodextrin concentration until a molar excess of SBE- β -CD to SN-38 of 1,000 was reached, after which the curve plateaued. A good agreement was found between the plate reader and HPLC methods. Maximum SN-38 solubilization is observed at a 1,000-fold molar excess of SBE- β -CD for concentrations of SN-38 \leq 100 μ M. SN-38 solubility increases by more than 70-fold compared to a molar ratio 1:8. Fluorescence-based calibration curves were constructed to enable SN-38 quantification in liposome samples from HPLC and plate reader measurements. As shown in Fig. 4c, the obtained curves were linear across four orders of magnitude of SN-38 concentrations.

The solubilization profile of SN-38 was further examined at lower relative amounts of SBE- β -CD, specifically at 1.25:1 and 1:8 SN-38 to SBE- β -CD molar ratios. The absolute concentrations of the drug and of SBE- β -CD were varied, while maintaining constant the ratio values, and the concentration of soluble SN-38 was determined by HPLC after discarding the insoluble fraction. Complexation with 64.9 μ M of SBE- β -CD enhances SN-38 solubility by about 1.5 and 10 times at a 1.25:1 and 1:8 molar ratio, respectively (Fig. 4d).

We assayed whether inclusion of SN-38 in the SBE- β -CD binding cavity confers stability of the lactone ring against an inactivating surrounding buffer. The lactone SN-38 was mixed with a large excess of cyclodextrin and incubated in a basic buffer. As shown in Fig. 4e, the fraction of lactone SN-38 was almost 5 times higher after complexation with SBE- β -CD and 90 h incubation. This result demonstrates that docking of the lactone SN-38 into SBE- β -CD improves its stability, which is consistent with previous observations [28].

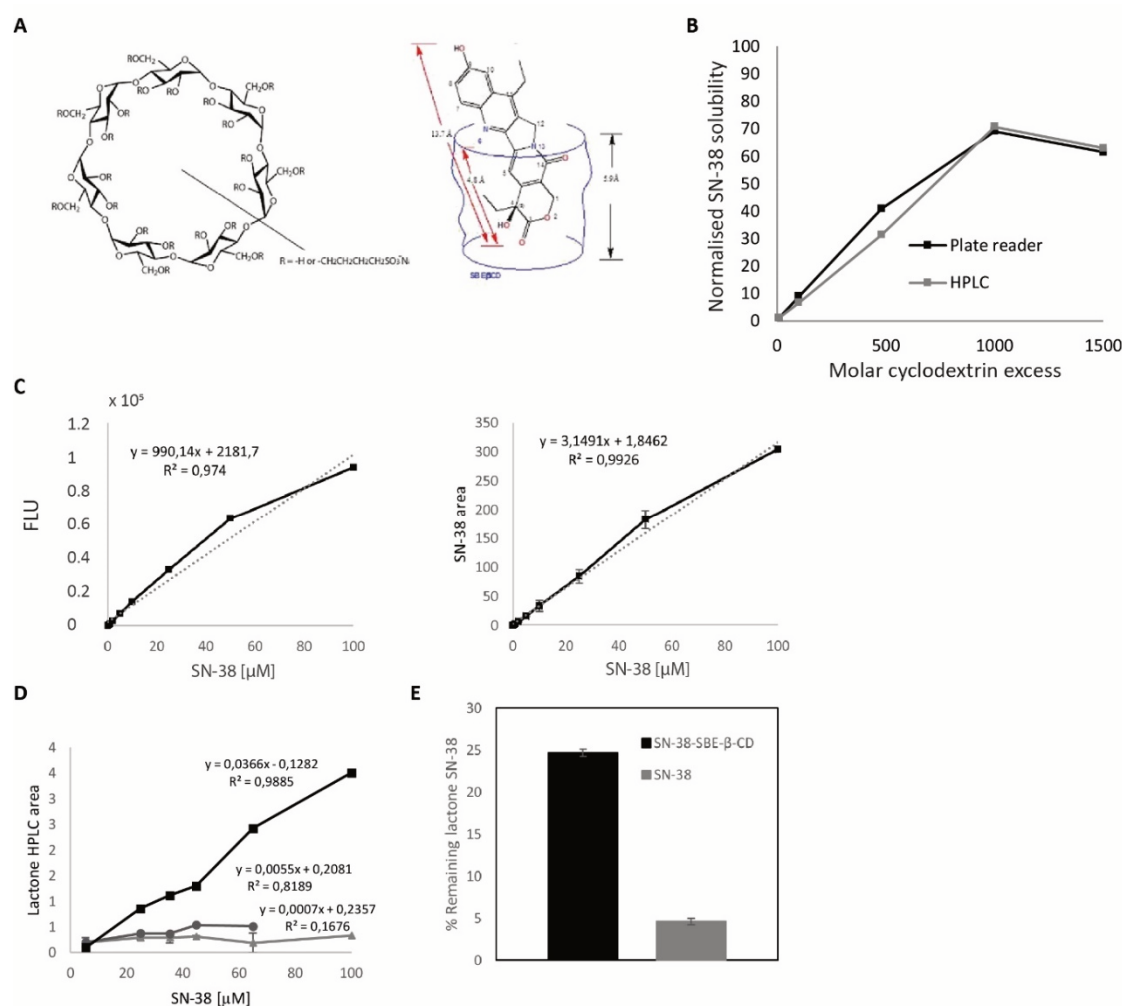


Fig. 4. A) Chemical structures of Captisol (left, adapted from [36]) and of an SN-38-SBE-β-CD inclusion complex (right, adapted from [28]). B) Solubilization curves of 100 μM SN-38 by varying amounts of SBE-β-CD as measured by HPLC and on a plate reader. C) Calibration curves for quantification of SN-38 on a plate reader (left) and by HPLC (right). Eleven different SN-38 concentrations ranging from 0.01 to 100 μM were solubilized with 100 mM SBE-β-CD. The SN-38 fluorescence intensity (FLU) and chromatogram peak area were measured and plotted as a function of the SN-38 concentration. The appended dotted lines represent a linear regression across the data. D) The SN-38 fluorescence peak area was measured at different SBE-β-CD concentrations by HPLC. Samples consisted of SN-38 (light grey), 1.25:1 SN-38 to SBE-β-CD molar ratio (dark grey) or a 1:8 SN-38 to SBE-β-CD ratio (black). E) Percentage of lactone SN-38 in samples with or without an excess of SBE-β-CD after 90 h incubation at room temperature in 50 mM sodium phosphate (pH 8.3). The percentage of active lactone SN-38 was calculated based on the integrated peak areas of the lactone and carboxylate species in the HPLC chromatogram. Error bars in B-E indicate mean values ± s.e.m. from three independent experiments.

5.3.4 ENTRAPMENT OF SN-38-SBE-β-CD COMPLEXES INTO LIPOSOMES LEADS TO THE FORMATION OF STABLE SN-38-SBE-β-CD-LIPID NANOPARTICLES

Next, we aimed to encapsulate pre-formed SN-38-SBE-β-CD inclusion complexes inside the lumen of folate-conjugated HSPC-liposomes. Because SBE-β-CD can deplete lipids [37], we anticipated that liposomes may not be stable in the presence of high concentration of either SBE-β-CD or SN-38-SBE-β-CD complexes. We first verified that the conditions to swell the

lipid film did not inactivate SN-38 (Fig. S3). Then, liposomes were produced by lipid film hydration with an aqueous solution containing pre-incubated SN-38 (44 μM) and SBE- β -CD at a 1:8 molar ratio. The sample was analysed by size exclusion chromatography. As shown in Fig. 5a, the membrane dye signal was split in two distinct populations, in contrast to the single-peak profile obtained in the absence of SBE- β -CD (Fig. 3a-3b). The earlier population corresponds to the typical profile of liposomes, while the later may support the presence of smaller lipid nanoparticles resulting from partly solubilized liposomes by cyclodextrin. A similar characteristic elution profile was observed when the lipid film was rehydrated with SBE- β -CD only (Fig. 5b, middle panel). We found that SN-38-SBE- β -CD inclusion complexes co-eluted with the lipid nanoparticle fractions but not with the vesicles. No changes of the co-elution profile were observed when swelling duration was extended from 2 h to overnight (Fig. S4) or when freeze-thaw cycles were applied to increase the encapsulation efficiency (Fig. 5c). Moreover, preparing lipid particles of bigger diameter (extruded across a membrane with 400-nm pores) to better accommodate SBE- β -CD-SN-38 complexes in the lumen of vesicles failed to enhance encapsulation.

Based on these results, we hypothesized that the late-eluting particles are composed of water soluble lipid-cyclodextrin-SN-38 complexes as a product of lipid depletion and complexation by SBE- β -CD. We examined the elution profile of SN-38-SBE- β -CD inclusion complexes in the absence of lipids and found that it matches with the one observed in the presence of HSPC liposomes (Fig. 5b, right panel). Therefore, it is not possible to unambiguously conclude from these chromatography data that the SN-38-SBE- β -CD and lipid-SBE- β -CD inclusion complexes directly interact or assemble into mixed supramolecular structures. To further study the nature of these molecular complexes, we prepared lipid-SN-38-SBE- β -CD samples and attempted to characterize the purified fractions corresponding to the second population by fluorescence confocal microscopy. Lipid particles were immobilized on the glass surface through their biotin linker and imaged with the Texas Red dye. SN-38 fluorescence was also imaged and its localization analysed. Larger and brighter lipid particles were found to also exhibit SN-38 fluorescence, unlike the more abundant smaller and dimer structures (Fig. 5e). Increasing the concentration of SBE- β -CD from 800 μM to 8 mM (the concentration of SN-38 was also increased 10 times to keep the same molar ratio) did not affect the apparent size of the lipid aggregates (Fig. 5e). These results of visualization of single particles suggest direct interaction between SN-38-SBE- β -CD and lipid-SBE- β -CD inclusion complexes, at least for the bigger structures. The fact that these lipid-SN-38-SBE- β -CD aggregates retained a fraction of SN-38 even 24 h after dilution in physiological buffer (PBS pH 7.4) through size exclusion chromatography prompted us to explore their antitumor effect in vitro.

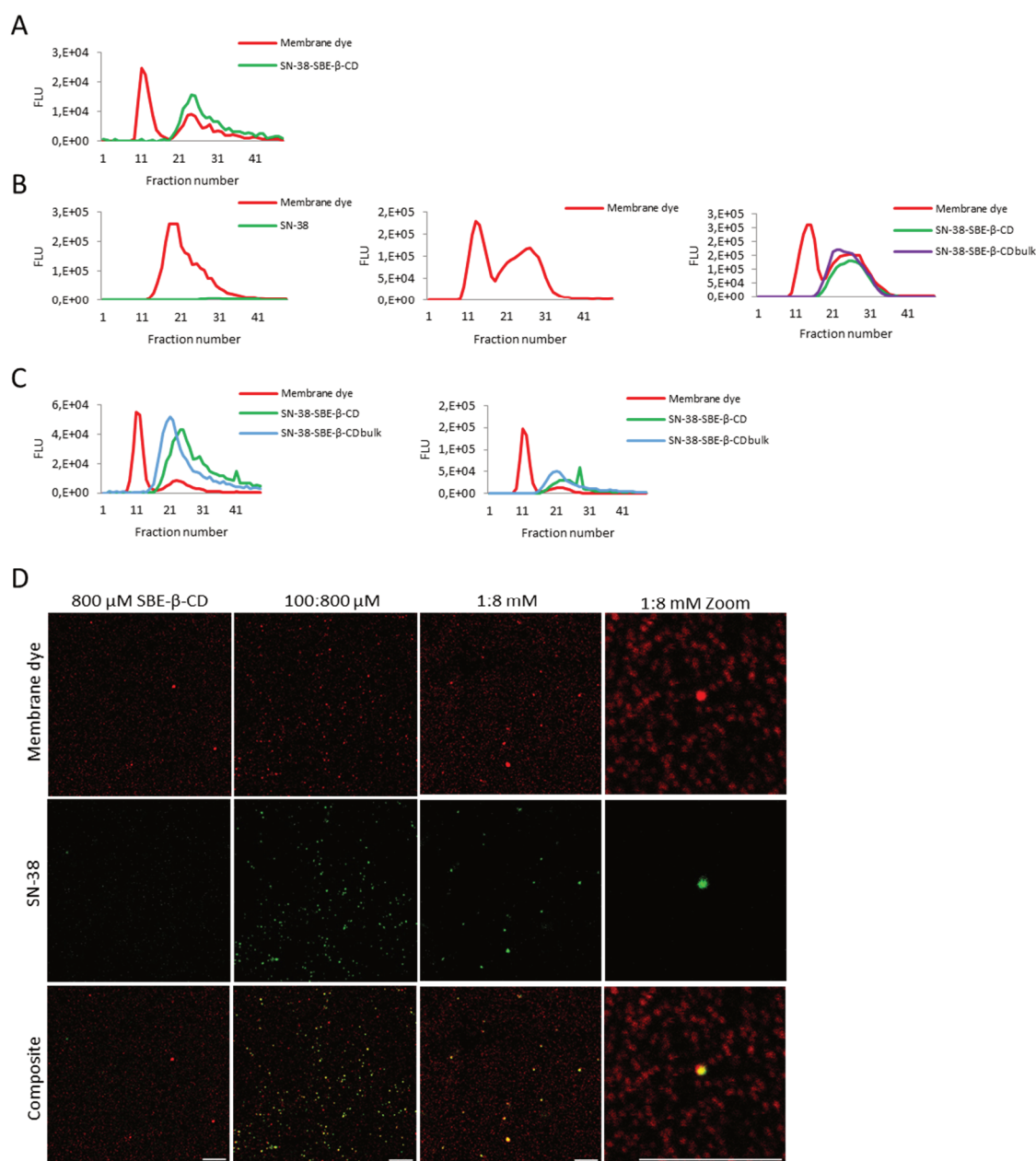


Fig. 5. A) Elution profiles of SN-38-SBE- β -CD-loaded HSPC-liposomes after 2 h swelling (SN-38 was 44 μ M, SBE- β -CD was 357.6 μ M, corresponding to a 1:8 molar ratio). Fluorescence signals of Texas Red membrane dye (red) and SN-38 (green) are displayed. B) Comparison of the elution profiles with only SN-38 (left), only SBE- β -CD (middle) and with SN-38-SBE- β -CD (right). Lipid film swelling occurred for 72 h at room temperature. C) Liposomes were exposed to freeze-thaw cycles after swelling in the presence of SN-38-SBE- β -CD. Lipid particles were extruded across a 200-nm (left) or 400-nm (right) cutoff membrane. D) Confocal microscopy images of single immobilized nanoparticles from the second population of HSPC-nanoparticles entrapping 100 μ M SN-38 + 800 μ M SBE- β -CD, only 800 μ M SBE- β -CD, or 1 mM SN-38 + 8 mM SBE- β -CD. Scale bars are 10 μ m.

5.3.5 SN-38-SBE- β -CD-LIPID NANOPARTICLES CAN INTERACT WITH CANCER CELLS

The first step in the antitumor mechanism of a therapeutic lipid nanoparticle is the interaction with the plasma membrane and subsequent internalization. Thus, we investigated the

interaction of SN-38-SBE- β -CD lipid nanoparticles with cultured KB cells. Purified lipid nanoparticles from the second population obtained by size exclusion chromatography were incubated with plated living cells in a growth medium for up to 2 h. Though the yield of nanoparticles was very low due to the loss of material during column purification, the interaction of a few SN-38-SBE- β -CD-lipid nanoparticles with KB cells was observed by time-lapse confocal microscopy (Fig. 6a). The fluorescence signal of SN-38 was too low to be measured in cells.

To evaluate the *in vitro* toxicity of SN-38 as an SN-38-SBE- β -CD-lipid nanoparticle formulation, the purified particles were incubated for 24 h with KB and HeLa cells. Control experiments were performed with SN-38-SBE- β -CD inclusion complexes. Fig. 6b and 6c show the results from three independent experiments. The toxicity effects on KB cells in the third experiment significantly differed from the other two. Nevertheless, the antitumor effect of SN-38-SBE- β -CD-lipid nanoparticles was similar to that of the SN-38-SBE- β -CD complexes in both cell types for all experiments. Importantly, SBE- β -CD-lipid nanoparticles (no SN-38) did not induce cytotoxicity, strongly suggesting that this range of cyclodextrin concentrations (up to 8 mM) is safe for drug delivery and will not lead to unspecific effects. In addition, HeLa cells were on average less sensitive to the effect of SN-38 than KB cells. Altogether, we attribute the lack of toxicity to the low concentration of SN-38-SBE- β -CD-lipid nanoparticles used in these experiments, a consequence of the large dilution during size exclusion chromatography.

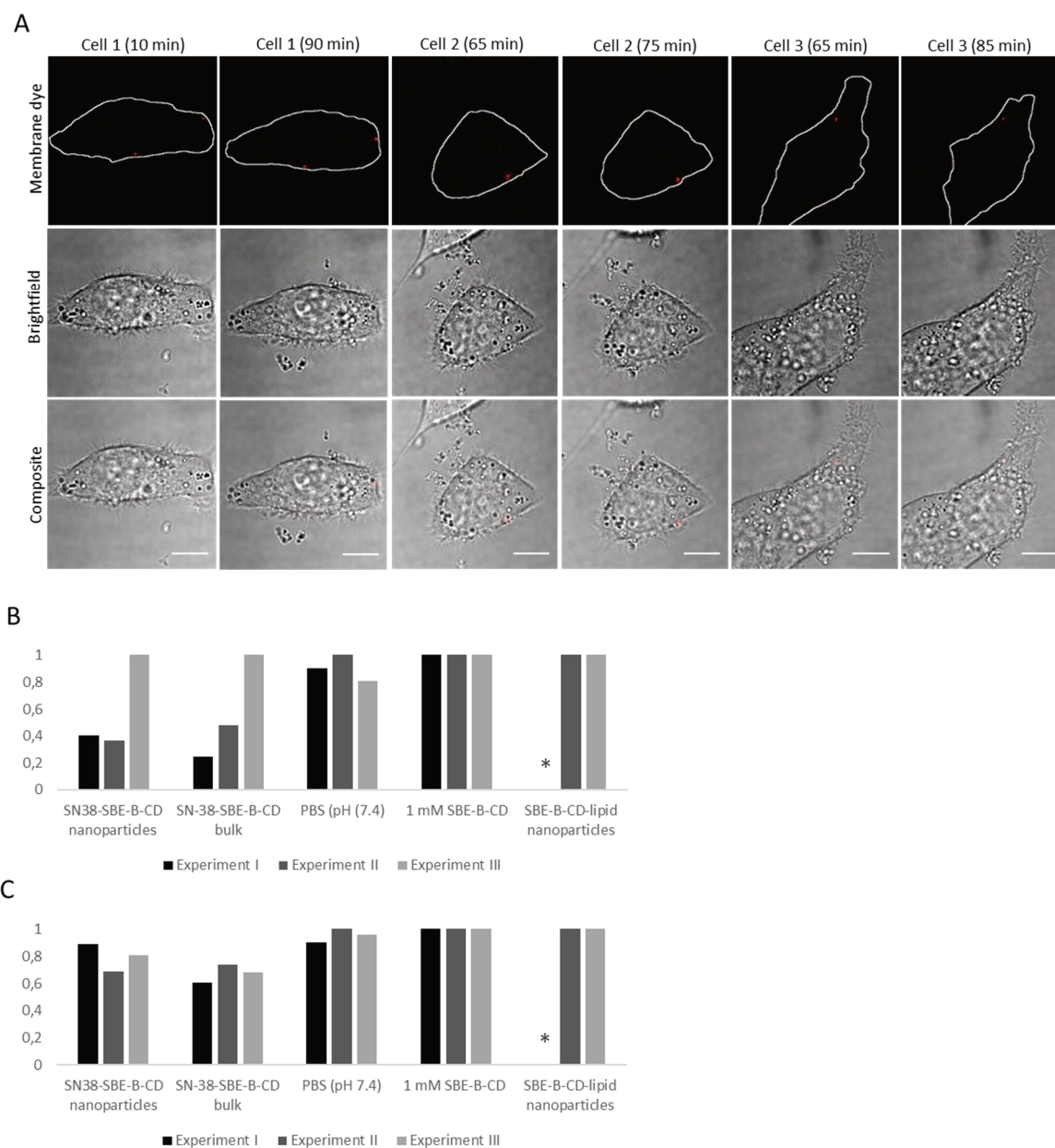


Fig. 6. A) Confocal images of SN-38-SBE- β -CD-lipid nanoparticles interacting with KB cells at different time points. Scale bars are 10 μ m. B,C) Normalized cell viability of B) KB and C) HeLa cells after 72 h incubation with either SN-38-SBE- β -CD-nanoparticles, bulk SN-38-SBE- β -CD, SBE- β -CD-lipid nanoparticles, 1 mM SBE- β -CD or PBS pH 7.4. The asterisk indicates that this experimental condition was not conducted. Three independent experiments were performed.

5.4 DISCUSSION

In spite of its efficacious activity against tumor cells *in vitro*, the clinical use of SN-38 (and other hydrophobic compounds) for chemotherapy remains limited due to its limited solubility and instability at physiological pH. To solve these problems, a variety of liposomal formulations have been developed [6]. In recent years, drug-in-cyclodextrin-in-liposomes have been designed to further improve the delivery properties [38]. Complexation of SN-38 with SBE- β -

CD greatly increases its solubility [28]. In the present study, the development of SN-38-in-cyclodextrin-in-liposomes has been explored. We have attempted to equip this system with folic acid as a ligand for targeted delivery and with polyethylene glycol to manage highly stable, long-circulating lipid particles.

With the ultimate goal of developing liposomes that selectively deliver SN-38 to tumor cells, we developed a formulation of folic acid-labelled liposomes. For more than two decades, folate receptors have been intensively studied as tumor-specific drug delivery targets [38–40]. Here, we demonstrated selective uptake of folate-labelled HSPC-liposomes by cultured cells expressing folate receptors (Fig. 2b). In vivo, this would translate into an increased tumor accumulation of liposomes compared to non-targeted liposomes. However, the degree of increase is highly variable and in vivo studies would be required to evaluate the tumor targeting potential of this liposome formulation to folate receptor-overexpressing tumors [42].

As a first approach to solubilize and protect SN-38, we developed a formulation of SN-38-loaded-HSPC liposomes. The production of lipid-coated beads enabled the optimal storage of the SN-38-lipid formulation for months and presumably leads the achievement of a higher concentration of liposomes and an enhanced drug-encapsulation efficiency thanks to the increased surface area provided by the glass beads compared to ordinary methods [42, 43]. Preliminary liposome characterization by fluorescence microscopy and dynamic light scattering demonstrated that the presence of SN-38 did not interfere with the formation or stability of these lipid vesicles (Fig. 2b-2c). This was an important verification considering that some lipophilic drugs are known to interfere with bilayer formation and stability upon entrapment [23, 24]. The observed variability on the fractions at which liposomes eluted during size exclusion chromatography can be attributed to inherent differences between the purification columns (e.g. resin packing, amount of resin), as they were handmade for each sample (Fig. 3a-3b). Successful entrapment of some SN-38 molecules in HSPC-liposomes was demonstrated and a larger fraction of SN-38 was shown to interact if the sample is incubated prior to purification (Fig. 3b). Since the buffer used to generate the liposomes was acidic, all SN-38 molecules were in the closed lactone ring conformation. Due to the high hydrophobicity of the lactone SN-38, the drug is expected to be buried in the lipid bilayer [3]. In particular, the long 18-carbon acyl chains of HSPC could favor the entrapment of SN-38 into the membrane. A different formulation of SN-38-loaded liposomes, named LE-SN-38, has previously been created and SN-38 was found to localize in the outer leaflet of the liposome bilayer, at the water interface [3]. In our study, the rapid release of SN-38 from HSPC liposomes indicates a weak interaction (Fig. 3f). Moreover, the non-significant difference in the fraction of active SN-38 between purified liposomes, non-purified liposomes and bulk SN-38, all incubated in an inactivating alkaline buffer, further indicates that HSPC-liposomes do not protect SN-38 from external protons (Fig. 3e). Hence, SN-38 might not be stably buried in the core of the lipid bilayer, but may instead interact near the liposome surface, as shown for LE-SN-38 (Fig. 3f).

To circumvent the short retention time of SN-38 by liposomes, we aimed to develop a drug-in-cyclodextrin-in-liposome system that would encapsulate drug-cyclodextrin complexes within the lumen of the vesicle. Consistent with previous results [28], the solubility and stability of SN-38 increased upon formation of inclusion complexes with SBE- β -CD (Fig. 4a-4b, Fig. 4d). Current marketed Captisol-enabled drug formulations have molar cyclodextrin excesses between 1.4 and 4.3 [45]. Cyclodextrins have the ability to interact with and extract cholesterol [46] and other membrane lipids [36], altering the properties of cellular membranes and inducing cytotoxic effects [37]. Mindful that large amounts of cyclodextrin could be lethal to cells, we first characterized the solubilization of SN-38 at low SBE- β -CD to drug molar ratios, and found that a value of 1:8 offered a good compromise between effective solubilization of SN-38 and absolute cyclodextrin concentration for further cytotoxicity assays (Fig. 4c).

Though the concept of drug-in-cyclodextrin-in-liposomes as drug delivery system was first proposed more than two decades ago [24], cyclodextrin-drug complexation competes with liposomal membrane assembly, tempering the potential benefit of complexation in prolonging hydrophobic drug retention [47]. Earlier studies on the effect of different cyclodextrins on the integrity of liposomes reported that vesicles can collapse due to cyclodextrin-induced extraction of lipids, causing the formation of water soluble lipid-cyclodextrin complexes. Moreover, this effect depends on the cyclodextrin type, and the length of the lipid fatty acid chain [46, 48, 49]. Herein, we showed that SN-38-in-SBE- β -CD-in-liposomes fail to self-assemble at 1:8 drug to cyclodextrin molar ratio (Fig. 5). Instead, size exclusion chromatography and fluorescence confocal microscopy revealed that SN-38 is trapped in lipid nanoparticles, likely arising from a cyclodextrin-induced lipid extraction mechanism (Fig. 5d). Under certain conditions, cyclodextrin molecules and their ligands can form non-inclusion aggregates with a size ranging from 20 to 100 nm in diameter [50]. We hypothesized that the observed nano-aggregates comprise SN-38-SBE- β -CD and lipid-SBE- β -CD inclusion complexes. Their nearly identical elution profiles suggest that both types of particles have similar sizes (Fig. 5c). It is known that the aggregation propensity and the size of the aggregates increase with increasing cyclodextrin concentration [50]. The optical microscopy experiments performed here should be complemented with transmission electron microscopy measurements to determine the size, morphology and exact molecular structure of these nanoparticles.

Liposomes are intrinsically highly heterogeneous assemblies, exhibiting different physical and chemical properties (e.g. size, lipid composition, encapsulation efficiency) even within a same batch [51]. Therefore, successful implementation of liposome-based drug delivery systems requires characterization of those properties at the single nanoparticle level. Transmission electron microscopy is a powerful technique to characterize the size, morphology and lamellarity of individual liposomes [51] and can be used as well for examining the heterogeneity of drug encapsulation yield in vesicles [52–54]. However, this technique necessitates laborious sample preparation and allows the analysis of only a small fraction of the sample. Fluorescence microscopy of immobilized liposomes or nanoparticles does not provide accurate information

about the size or morphology of molecular assemblies with dimensions lower than about 200 nm. However, it enables high-throughput evaluation of the drug loading heterogeneity between individual liposomes provided the drug has fluorescent properties, as demonstrated in this study for SN-38 (Fig. 5e). The use of fluorescence microscopy of surface-immobilized vesicles in the field of liposomal drug delivery development has already been proposed [55, 51], but had not been applied yet.

Due to the low concentration of purified SN-38-SBE- β -CD-lipid nanoparticles, we were unable to reliably assay their interaction dynamics with cultured KB cells and to visualize the fate of SN-38 after binding to the plasma membrane. Although we primarily attribute the lack of enhanced cytotoxicity of SN-38-SBE- β -CD-lipid nanoparticles compared to non-lipidic formulations of SN-38 to their low concentration, we cannot exclude that other factors may contribute too, such as poor nanoparticle uptake due to low folic acid ligand availability on their surface, poor endosomal escape and release of SN-38 in the cytoplasm, and SN-38 inactivation.

5.5 CONCLUSIONS

Together, our results provide clear directions for further nanoparticle characterization and physico-chemical optimization of the formulation. Electron microscopy will be an essential tool to understand the molecular nature and size of these nano-aggregates. Furthermore, increasing the amount of HSPC-liposomes relative to that of SN-38-SBE- β -CD complexes might lessen the lipid bilayer depletion effect and facilitate the successful production of drug-in-cyclodextrin-in-liposomes. Alternatively, the lipid-extraction effect of other SN-38 solubilizing β -cyclodextrins such as randomly methylated β -cyclodextrin (RM β CD, Trappasol) or methylated β -cyclodextrin (M β CD) [28] should be explored. Finally, increasing the concentration of purified SN-38-SBE- β -CD-lipid nanoparticles, currently a bottleneck for cellular cytotoxicity, might be achieved by scaling up the production and by concentrating the particles by ultracentrifugation or solvent evaporation.

5.6 SUPPLEMENTARY INFORMATION

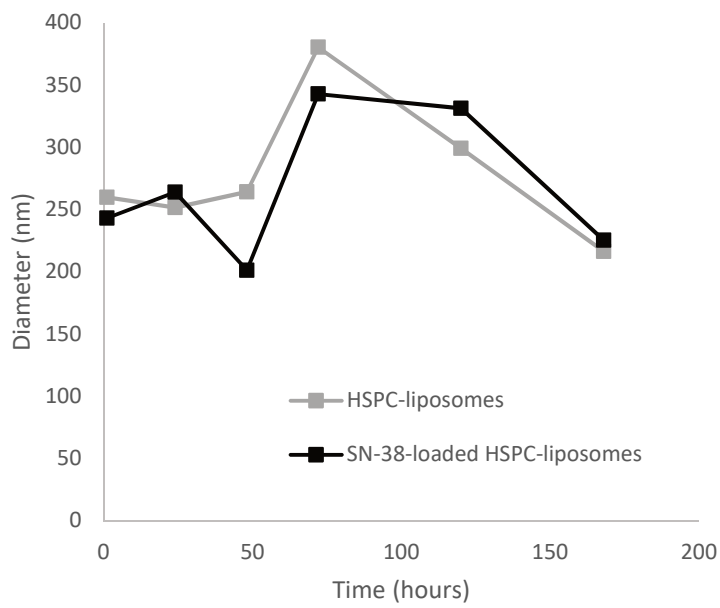
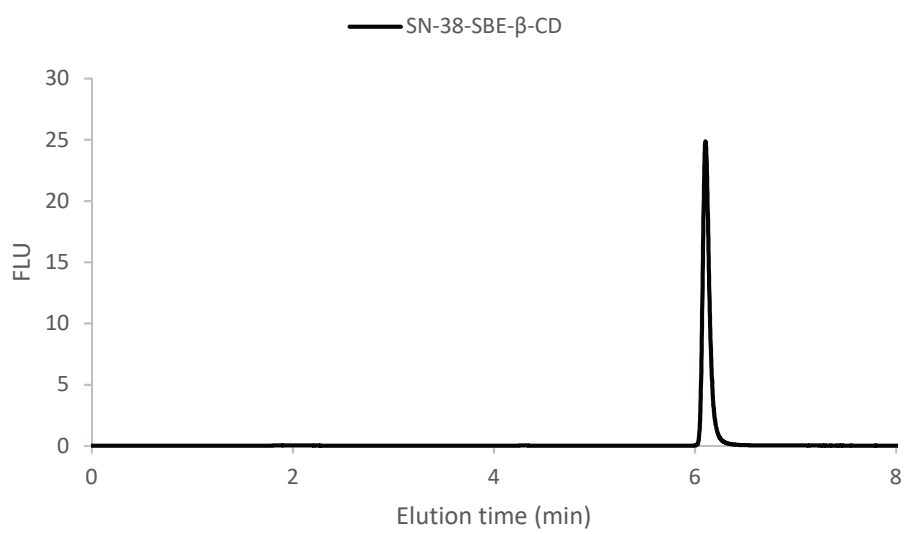


Fig. S1. Liposome size distribution of SN-38-loaded HSPC-liposomes vs HSPC-liposomes over time.



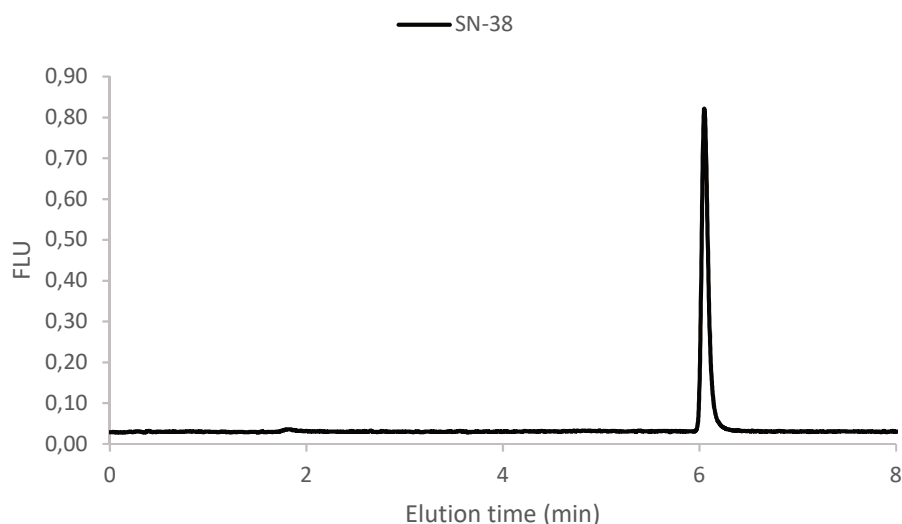
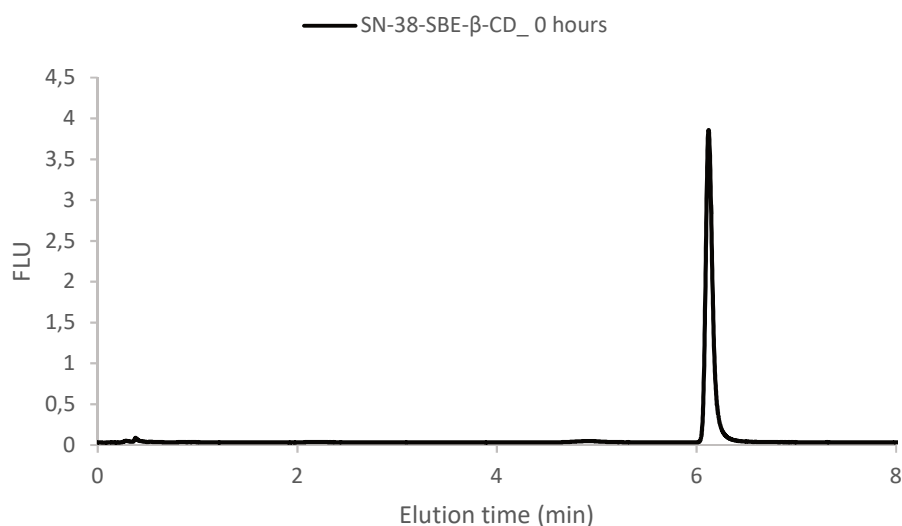


Fig. S2. HPLC chromatograms of SN-38- SBE- β -CD (top) and SN-38 (bottom).

To discard a possible influence of SBE- β -CD complexation on the elution profile of SN-38, we incubated SN-38 (25 μ M) at room temperature overnight in the presence or absence of a large excess of SBE- β -CD (4.8 mM, 1:192 molar ratio) and the resulting elution time and shape of the lactone SN-38 peak was analyzed by HPLC. As expected, due to the non-covalent interaction between SN-38 and SBE- β -CD, the elution time of lactone SN-38 remained constant in the sample containing SBE- β -CD compared to that of SN-38 alone.



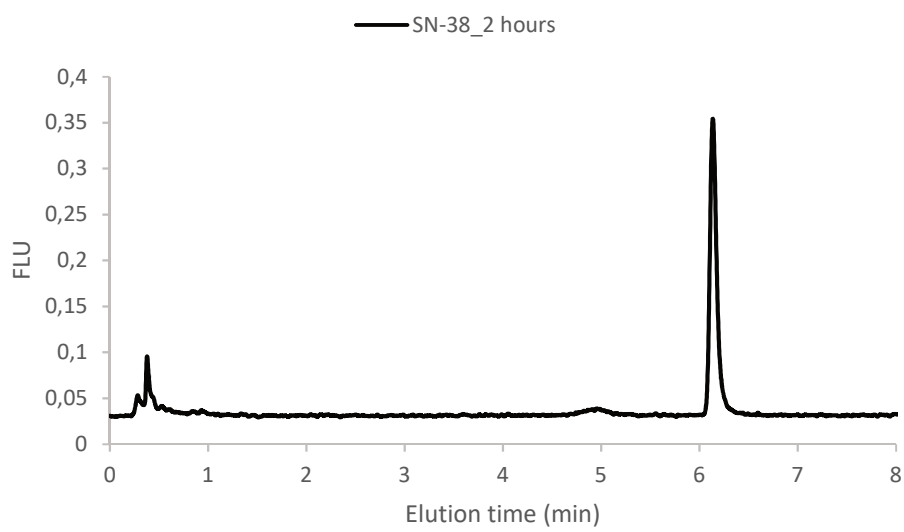
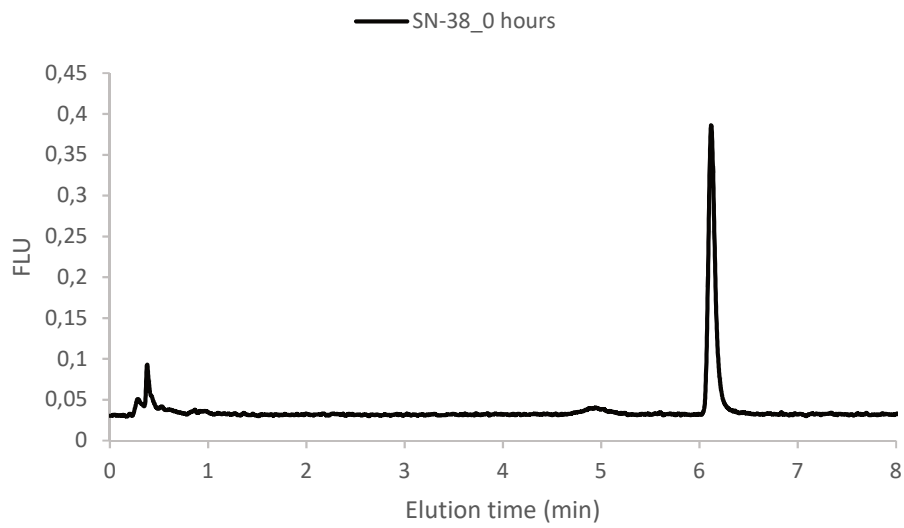
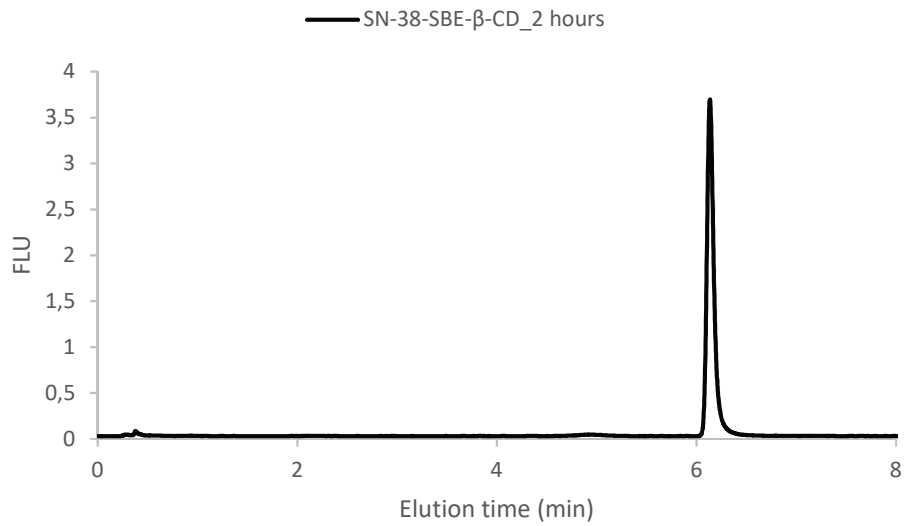


Fig. S3. Stability of SN-38 at 60 °C in the presence or absence of SBE- β -CD. HPLC chromatograms of SN-38-SBE- β -CD after A) 0 and B) 2 hours incubation at 60 °C and SN-38 after C) 0 and D) 2 h incubation at 60 °C. Concentrations of SN-38 and SBE- β -CD in solution were 100 μ M and 800 μ M, respectively.

A solution containing 100 μ M and 800 μ M of SN-38 and SBE- β -CD respectively and a solution containing 100 μ M SN-38 were prepared in acidic PBS (pH 5.3). The tubes were then sonicated for 15 min and incubated with tumbling at room temperature overnight and filtrated through a 0.45- μ m filter. The tubes were then sealed with Parafilm to avoid moisture loss and incubated at 60 °C for 2 h in a shaker at 250 rpm. 10 μ l were injected into the HPLC and analyzed for the amount of lactone and carboxylate. 10 μ l of acetonitrile were injected between sample runs to prevent sample-to-sample contaminations. As shown, complexed and non-complexed SN-38 remained in the lactone form after 2 h incubation at 60 °C. Moreover, the shape of lactone SN-38 peaks after incubation was as sharp as at time point 0, confirming that this condition does not harm the structure of SN-38. Consequently, swelling for up to 2 h at temperatures equal or lower than 60 °C does not affect the structure of SN-38.

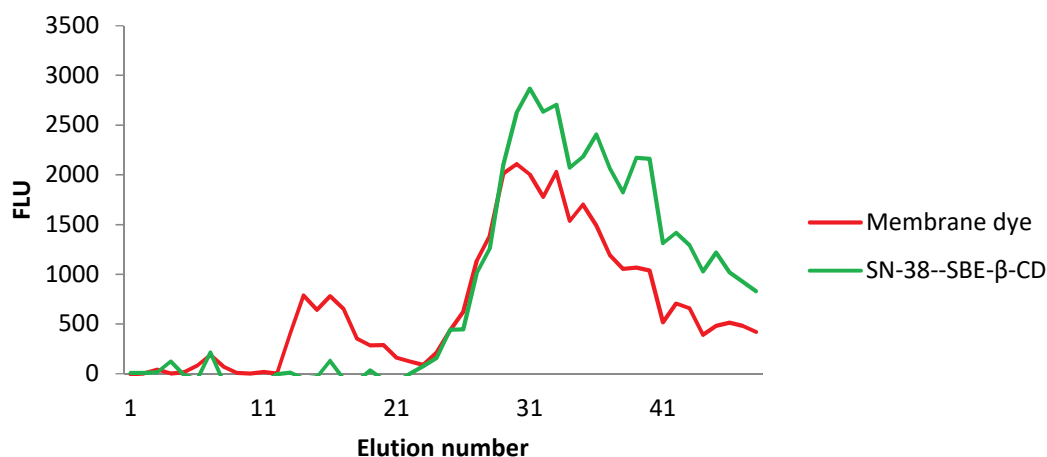


Fig. S4. Elution profile of SN-38-SBE- β -CD-loaded HSPC-liposomes after overnight welling (SN-38 44 μ M, SBE- β -CD 357.6 μ M, 1:8 molar ratio).

5.7 ACKNOWLEDGEMENTS

We thank Esther Hulleman, Sewing Lot, and Dennis Metselaar for providing us with SN-38 and for useful scientific discussions. Dennis, thank you for testing our nanoparticles on DIPG primary cells. We thank Niels van Den Broek for his help with the implementation of an HPLC method to detect SN-38. Thanks Gabriella Tany and Jasper van Lopik for their help with the first liposome purifications. Thanks Fabai for your feedback on the paper.

5.8 REFERENCES

- [1] Y. Kawato, M. Aonuma, Y. Hirota, H. Kuga, and K. Sato, "Intracellular Roles of SN-38, a Metabolite of the Camptothecin Derivative CPT-11, in the Antitumor Effect of CPT-11," *Cancer Research*, vol. 51, no. 16, pp. 4187–4191, 1991.
- [2] D. S. Yves Pommier, Philippe Pourquier, Yi Fan, "Mechanism of action of eukaryotic topoisomerase I and drugs targeted to the enzyme," *Biochimica et Biophysica Acta - Gene Structure and Expression*, vol. 1400, no. 1–3, pp. 139–154, 1998.
- [3] J. A. Zhang *et al.*, "Development and characterization of a novel liposome-based formulation of SN-38," *International Journal of Pharmaceutics*, vol. 270, no. 1–2, pp. 93–107, 2004.
- [4] P. Ebrahimnejad, R. Dinarvand, A. Sajadi, M. R. Jafari, F. Movaghari, and F. Atyabi, "Development and validation of an ion-pair HPLC chromatography for simultaneous determination of lactone and carboxylate forms of SN-38 in nanoparticles," *Journal of Food and Drug Analysis*, vol. 17, no. 4, 2009.
- [5] A. Pal *et al.*, "Preclinical safety, pharmacokinetics and antitumor efficacy profile of liposome-entrapped SN-38 formulation," *Anticancer Research*, vol. 25, no. 1 A, pp. 331–341, 2005.
- [6] V. Bala, S. Rao, B. J. Boyd, and C. a. Prestidge, "Prodrug and nanomedicine approaches for the delivery of the camptothecin analogue SN38," *Journal of Controlled Release*, vol. 172, no. 1, pp. 48–61, 2013.
- [7] Z. Mi and T. G. Burke, "Differential Interactions of Camptothecin Lactone and Carboxylate Forms with Human Blood Components," *Biochemistry*, vol. 33, no. 34, pp. 10325–10336, 1994.
- [8] G. T. Noble, J. F. Stefanick, J. D. Ashley, T. Kiziltepe, and B. Bilgicer, "Ligand-targeted liposome design: Challenges and fundamental considerations," *Trends in Biotechnology*, vol. 32, no. 1, pp. 32–45, 2014.
- [9] G. A. Koning and G. Storm, "Targeted drug delivery systems for the intracellular delivery of macromolecular drugs," *Drug Discovery Today*, vol. 8, no. 11, pp. 482–483, 2003.
- [10] R. Bai, X. Deng, Q. Wu, X. Cao, T. Ye, and S. Wang, "Liposome-loaded thermo-sensitive hydrogel for stabilization of SN-38 via intratumoral injection: optimization, characterization, and antitumor activity," *Pharmaceutical Development and Technology*, vol. 0, no. 0, pp. 1–10, 2017.
- [11] T. G. Burke, a K. Mishra, M. C. Wani, and M. E. Wall, "Lipid bilayer partitioning and stability of camptothecin drugs," *Biochemistry*, vol. 32, no. 20, pp. 5352–64, 1993.
- [12] G. E. Flaten, T. T. Chang, W. T. Phillips, M. Brandl, A. Bao, and B. Goins, "Liposomal formulations of poorly soluble camptothecin: Drug retention and biodistribution," *Journal of Liposome Research*, 2013.
- [13] U. Bulbake, S. Doppalapudi, N. Kommineni, and W. Khan, "Liposomal formulations in clinical use: An updated review," *Pharmaceutics*, vol. 9, no. 2, pp. 1–33, 2017.
- [14] N. Z. Wu *et al.*, "Increased Microvascular Permeability Contributes to Preferential Accumulation of Stealth Liposomes in Tumor Tissue Increased Microvascular Permeability Contributes to Preferential Accumulation of," *Cancer Research*, vol. 53, no. 0, pp. 3765–3770, 1993.
- [15] F. Yuan *et al.*, "Vascular Permeability in a Human Tumor Xenograft: Molecular Size Dependence and Cutoff Size," *Cancer Research*, no. 55, pp. 3752–3757, 1995.
- [16] Y. Matsumura and H. Maeda, "A new concept for macromolecular therapeutics in cancer chemotherapy: mechanism of tumorotropic accumulation of proteins and the antitumor agents Smancs," *Cancer research*, vol. 46, no. 12 Pt 1, pp. 6387–6392, 1986.
- [17] Z. Zhang and J. Yao, "Preparation of Irinotecan-Loaded Folate-Targeted Liposome for Tumor Targeting Delivery and Its Antitumor Activity," *AAPS PharmSciTech*, vol. 13, no. 3, pp. 802–810, 2012.

- [18] H. Bardania, S. Tarvirdipour, and F. Dorkoosh, "Liposome-targeted delivery for highly potent drugs," *Artificial Cells, Nanomedicine and Biotechnology*. 2017.
- [19] Y. Lu and P. S. Low, "Folate-mediated delivery of macromolecular anticancer therapeutic agents," *Advanced Drug Delivery Reviews*, vol. 54, pp. 675–693, 2002.
- [20] A. Garcia-Bennett, M. Nees, and B. Fadeel, "In search of the Holy Grail: Folate-targeted nanoparticles for cancer therapy," *Biochemical Pharmacology*, 2011.
- [21] A. Yamada, Y. Taniguchi, K. Kawano, T. Honda, Y. Hattori, and Y. Maitani, "Design of folate-linked liposomal doxorubicin to its antitumor effect in mice," *Clinical Cancer Research*, vol. 14, no. 24, pp. 8161–8168, 2008.
- [22] Y. P. Fang, C. H. Chuang, Y. J. Wu, H. C. Lin, and Y. C. Lu, "SN38-loaded <100 nm targeted liposomes for improving poor solubility and minimizing burst release and toxicity: In vitro and in vivo study," *International Journal of Nanomedicine*, 2018.
- [23] G. Gregoriadis, N. Garcon, H. da Silva, and B. Sternberg, "Coupling of ligands to liposomes independently of solute entrapment: observations on the formed vesicles," *BBA - Biomembranes*, vol. 1147, no. 2, pp. 185–193, 1993.
- [24] B. McCormack and G. Gregoriadis, "Drugs-in-cyclodextrins-in liposomes: a novel concept in drug delivery," *International Journal of Pharmaceutics*, vol. 112, no. 3, pp. 249–258, 1994.
- [25] M. M. & T. J. Thorsteinn Loftsson, Pekka Jarho and To, "Cyclodextrins in drug delivery system," *Expert Opinion on Drug Delivery*, vol. 36, no. 1, pp. 1–2, 2005.
- [26] T. Loftsson, "Drug solubilization by complexation," *International Journal of Pharmaceutics*, vol. 531, no. 1, pp. 276–280, 2017.
- [27] M. Cirri, M. Bragagni, N. Mennini, and P. Mura, "Development of a new delivery system consisting in 'drug - In cyclodextrin - In nanostructured lipid carriers' for ketoprofen topical delivery," *European Journal of Pharmaceutics and Biopharmaceutics*, vol. 80, no. 1, pp. 46–53, 2012.
- [28] K. K. Vangara, H. I. Ali, D. Lu, J. L. Liu, S. Kolluru, and S. Palakurthi, "SN-38-cyclodextrin complexation and its influence on the solubility, stability, and in vitro anticancer activity against ovarian cancer.," *AAPS PharmSciTech*, vol. 15, no. 2, pp. 472–82, 2014.
- [29] H. Chen, J. Gao, F. Wang, and W. Liang, "Preparation, characterization and pharmacokinetics of liposomes-encapsulated cyclodextrins inclusion complexes for hydrophobic drugs.," *Drug delivery*, vol. 14, no. 4, pp. 201–208, 2007.
- [30] K. F. and J. P. OHTANI, Yoshiro, Tetsumi IRIE, Kaneto UEKAMA, "Differential effects of α -, β - and γ -cyclodextrins on human erythrocytes," vol. 22, pp. 17–22, 1989.
- [31] T. Kiss *et al.*, "Evaluation of the cytotoxicity of β -cyclodextrin derivatives: Evidence for the role of cholesterol extraction," *European Journal of Pharmaceutical Sciences*, vol. 40, no. 4, pp. 376–380, 2010.
- [32] Y. Hiasa, M. Ohshima, Y. Kitahori, N. Konishi, T. Fujita, and T. Yuasa, "B-Cyclodextrin: promoting effect on the development of renal tubular cell tumors in rats treated with N-ethyl-N-hydroxyethylnitrosamine," *Journal of the National Cancer Institute*, vol. 69, no. 4, pp. 963–967, 1982.
- [33] L. Zhang *et al.*, "Drug-in-cyclodextrin-in-liposomes: A novel drug delivery system for flurbiprofen," *International Journal of Pharmaceutics*, vol. 492, no. 1–2, pp. 40–45, 2015.
- [34] J. Chen, "Drug-in-cyclodextrin-in-liposomes: a promising delivery system for hydrophobic drugs," *Expert Opinion on Drug Delivery*, vol. 11, no. 4, pp. 565–577, 2014.

- [35] R. Gharib, H. Greige-gerges, S. Fourmentin, C. Charcosset, and L. Auezova, "Liposomes incorporating cyclodextrin – drug inclusion complexes : Current state of knowledge," *Carbohydrate Polymers*, vol. 129, pp. 175–186, 2015.
- [36] Captisol, "What is Captisol?" (2018). [Online]. Available: <https://pdfs.semanticscholar.org/b4e1/70cf0e2063d409d9eff7302cac66dd099fb1.pdf>.
- [37] G. Piel, M. Piette, V. Barillaro, D. Castagne, B. Evrard, and L. Delattre, "Study of the relationship between lipid binding properties of cyclodextrins and their effect on the integrity of liposomes," *International Journal of Pharmaceutics*, vol. 338, no. 1–2, pp. 35–42, 2007.
- [38] L. Zhang *et al.*, "Drug-in-cyclodextrin-in-liposomes: A novel drug delivery system for flurbiprofen," *International Journal of Pharmaceutics*, 2015.
- [39] R. J. Lee and P. S. Low, "Folate-mediated tumor cell targeting of liposome-entrapped doxorubicin in vitro," *BBA - Biomembranes*, vol. 1233, no. 2, pp. 134–144, 1995.
- [40] A. R. Hilgenbrink and P. S. Low, "Folate receptor-mediated drug targeting: From therapeutics to diagnostics," *Journal of Pharmaceutical Sciences*, vol. 94, no. 10, pp. 2135–2146, 2005.
- [41] M. Fernández, F. Javaid, and V. Chudasama, "Advances in targeting the folate receptor in the treatment/imaging of cancers," *Chemical Science*, vol. 9, no. 4, pp. 790–810, 2018.
- [42] X. Q. Pan *et al.*, "Boron-containing folate receptor-targeted liposomes as potential delivery agents for neutron capture therapy," *Bioconjugate Chemistry*, vol. 13, no. 3, pp. 435–442, 2002.
- [43] Z. Nourian, W. Roelofsen, and C. Danelon, "Triggered Gene Expression in Fed-Vesicle Microreactors with a Multifunctional Membrane," *Angew. Chem. Int. Ed.*, vol. 51, pp. 3114–3118, Jan. 2012.
- [44] K. Yamabe, Y. Kato, H. Onishi, and Y. Machida, "In vitro characteristics of liposomes and double liposomes prepared using a novel glass beads method," *Journal of Controlled Release*, vol. 90, no. 1, pp. 71–79, 2003.
- [45] Captisol, "How much Captisol is needed in an injectable formulation?," 2018. [Online]. Available: <https://www.captisol.com/faqs/category/669/how-much-captisol>.
- [46] P. G. Yancey *et al.*, "Cellular Cholesterol Efflux Mediated by Cyclodextrins.pdf," *The Journal of biological chemistry*, vol. 270, no. 29, pp. 17250–6, 1996.
- [47] B. McCormack and G. Gregoriadis, "Comparative studies of the fate of free and liposome-entrapped hydroxypropyl-beta-cyclodextrin/drug complexes after intravenous injection into rats: Implications in drug delivery," *Biochimica Et Biophysica Acta-General Subjects*, vol. 1291, no. 3, pp. 237–244, 1996.
- [48] J. Nishijo, S. Shiota, K. Mazima, Y. Inoue, H. Mizuno, and J. Yoshida, "Interactions of cyclodextrins with dipalmitoyl, distearoyl, and dimyristoyl phosphatidyl choline liposomes. A study by leakage of carboxyfluorescein in inner aqueous phase of unilamellar liposomes.," *Chemical & pharmaceutical bulletin*, vol. 48, no. 1, pp. 48–52, 2000.
- [49] R. Gharib, S. Fourmentin, C. Charcosset, and H. Greige-Gerges, "Effect of hydroxypropyl- β -cyclodextrin on lipid membrane fluidity, stability and freeze-drying of liposomes," *Journal of Drug Delivery Science and Technology*, vol. 44, pp. 101–107, 2018.
- [50] Throrsteinn Loftsson & Marcus E. Brewster, "Cyclodextrins as functional excipients: Methods to enhance complexation efficiency," *International Journal of Drug Development and Research*, vol. 3, no. 2, pp. 26–33, 2012.
- [51] C. Chen, S. Zhu, T. Huang, S. Wang, and X. Yan, "Analytical techniques for single-liposome characterization," *Analytical Methods*. 2013.

- [52] P. L. Luisi, M. Allegretti, T. P. De Souza, F. Steiniger, A. Fahr, and P. Stano, "Spontaneous protein crowding in liposomes: A new vista for the origin of cellular metabolism," *ChemBioChem*, vol. 11, no. 14, pp. 1989–1992, 2010.
- [53] T. Pereira de Souza, F. Steiniger, P. Stano, A. Fahr, and P. L. Luisi, "Spontaneous crowding of ribosomes and proteins inside vesicles: A possible mechanism for the origin of cell metabolism," *ChemBioChem*, vol. 12, no. 15, pp. 2325–2330, 2011.
- [54] T. P. de Souza, A. Fahr, P. L. Luisi, and P. Stano, "Spontaneous Encapsulation and Concentration of Biological Macromolecules in Liposomes: An Intriguing Phenomenon and Its Relevance in Origins of Life.," *Journal of molecular evolution*, pp. 179–192, Nov. 2014.
- [55] B. Lohse, P. Y. Bolinger, and D. Stamou, "Encapsulation efficiency measured on single small unilamellar vesicles," *Journal of the American Chemical Society*, vol. 130, no. 44, pp. 14372–14373, 2008.

SUMMARY

Synthetic biology is an emerging and rapidly expanding field of research focused on the assembly of novel biological systems with new functionalities tailored for different applications. Genetic circuits have been re-wired or constructed with elements from different organisms, and metabolic pathways have been engineered to endow cells with non-natural capabilities. One of the most exciting goals of synthetic biology is bringing solutions to biomedical challenges. Though this research area is still in its infancy, translational medicine is already witnessing the first steps towards the development of therapies based on synthetic biology.

Cell-free synthetic biology (or *in vitro* synthetic biology), a branch of synthetic biology, makes use of cell-free gene expression systems to create biological networks that operate outside the chassis of a living cell. More than a decade ago, the convergence of synthetic biology, cell-free gene expression systems and liposome technology gave rise to the creation of artificial vesicle bioreactors that can synthesize genetically-encoded molecules. Though the primary motivation of these studies was the assembly of a semi-synthetic cell, the application of such technologies for different therapeutic purposes has been envisioned. Examples of this are the creation of antigen-producing liposomes as novel vaccination systems, the development of bioreactor liposomes suited for remotely controlled in-situ mRNA or protein production, and the assembly of a PCR-based nanofactory for gene delivery.

Liposomes are the most successful drug delivery scaffolds ever developed with more than fifteen liposome-based drugs approved. Liposomes have long been investigated in the field of gene therapy as delivery vehicles for nucleic acids to overcome the barriers encountered by these molecules *in vivo*. In particular, the field of RNA interference-based drugs is very promising, with the first marketed formulation in 2018, and several others on their way.

However, despite their long history of investigation, most of the structural and functional properties of the liposome-based drug delivery systems are inferred from bulk measurements. Therefore, the level of heterogeneity regarding, e.g. encapsulation efficiency, lipid composition, remains largely unknown within liposome preparations, which complicates the development of new formulations with improved therapeutic efficiency. Another important limitation is the observed membrane leakiness and premature drug release upon administration. Controlling the bio-distribution of a therapeutic drug is essential to minimize toxic side effects and enhance the efficiency of the treatment. To tackle this problem, the creation of targeting delivery systems with stimuli-responsive ability can improve the biodistribution profile of a drug and allow its delivery on demand.

This work contributes to the convergence of the fields of synthetic biology, single-liposome biophysics and biomedicine, presenting different possible applications of vesicle bioreactors for the improvement of current RNA-based gene delivery systems.

In **Chapter 1**, we provide a general overview about synthetic biology in therapeutics, gene therapy and liposomal delivery systems. At the end of this chapter, we include a thesis outline where a brief introduction to the content from the rest of the chapters in this thesis is given.

In **Chapter 2**, we established a method for the high-throughput characterization of RNA encapsulation in liposome preparations at the single vesicle level. An RNA aptamer-fluorogen complex called Spinach, was used as a model system to report on liposomal RNA content by fluorescence microscopy. The loading potential of fed-vesicle bioreactors, where RNA is internally produced from a DNA template, was compared to that of conventional RNA encapsulation in liposomes. The results from this study show that direct entrapment of pre-synthesized RNA provides a higher fraction of RNA-loaded liposomes. Additionally, we show for the first time how biotin-based vesicle immobilization can be conveniently applied to study liposomal gene delivery systems by high-throughput fluorescence imaging of single vesicles. Although we did not achieve the implementation of a highly RNA-producing fed-vesicle bioreactor, we propose several recommendations to improve our technology and achieve this goal.

In **Chapter 3**, we intended to implement a light sensitive switch for remote spatiotemporal control of gene expression in liposomes. For this, the assembly of a light-inducible RNA-producing vesicle bioreactor was attempted. A light-activated T7 promoter (LA-T7) that inhibits the binding of T7 RNA polymerase in the off state was prepared, characterized and incorporated into a Spinach-encoding DNA template. Though light-inducible Spinach RNA production was demonstrated in bulk, leaky expression in the off state impeded the achievement of light-activated Spinach RNA production in vesicle bioreactors. Importantly, the remaining steps for the assembly of a fully repressed LA-Spinach are described in this work. Moreover, the potential of alternative optogenetic systems that allow spatiotemporally controlled production and delivery of therapeutic RNA molecules is discussed.

In **Chapter 4**, we created a platform for the *in vitro* production of shRNA inside vesicle bioreactors. We designed DNA templates that generate different shRNA molecules upon *in vitro* transcription in bulk or directly inside liposomes. The gene silencing efficacy of the shRNA was tested in mammalian cells. The activity of *in vitro*-transcribed shRNA was demonstrated when conventional transfection methods were used. However, attempts to silence gene expression through liposomal delivery of shRNA failed. To improve delivery, folic acid was incorporated to the surface of liposomes as a ligand targeting cells with high expression levels of folate receptors, like most cancer cells. Although enhanced liposomal uptake by the targeted cells was shown, lysosomal entrapment impaired the successful delivery of shRNA into the cytoplasm. To tackle this problem, the use of the pH-activated melittin peptide to disrupt

endosomal membranes was investigated. The lack of evidences for successful production of shRNA in liposomes and for melittin-assisted membrane destabilization prompted us to propose major modifications in the design of a new generation of liposome-based shRNA carriers.

In **Chapter 5**, we developed a new liposomal drug delivery system for the chemotherapeutic molecule SN-38. SN-38 is a compound with potent antitumor effects but it has limited clinical application due to its poor solubility and low stability at physiological pH. Liposomes and cyclodextrins have long been studied for the solubilization and delivery of hydrophobic compounds. Aiming to combine the advantages of both systems, the development of SN-38-in-cyclodextrin-in-liposomes was explored. We found that the encapsulation of SN-38-SBE- β -cyclodextrin in the lumen of liposomes was not possible, owing to the disassembly of liposomes and the formation of SN-38-SBE- β -CD-lipid nanoparticles. Interestingly, the retention time of SN-38 inside SN-38-SBE- β -CD-lipid nanoparticles is higher than in liposomes whereby SN-38 was directly loaded in the lipid film. The toxicity of SN-38-SBE- β -CD-lipid nanoparticles was assayed in cancer cells, showing no therapeutic advantage compared to bulk SN-38-SBE- β -CD complexes *in vitro*. Though a possible therapeutic advantage of SN-38-SBE- β -CD nanoparticles *in vivo* should not be discarded, further characterization of this system and formulation optimization may allow the development of SN-38-in-cyclodextrin-in-liposomes.

In summary, this thesis presents original efforts towards the development of better characterized liposomal gene delivery systems. Moreover, this work sets up the first stages for the construction of liposome delivery systems that act as spatiotemporally controlled RNA-producing nanofactories. As a whole, this thesis highlights the value of high-throughput single vesicle analysis for the characterization of drug delivery systems.

SAMENVATTING

Synthetische biologie is een opkomende en snel groeiende onderzoeksdiscipline die zich bezig houdt met het assembleren van innovatieve biologische systemen met nieuwe functionaliteiten, op maat gemaakt voor verschillende applicaties. Genetische netwerken zijn opnieuw aangelegd of samengesteld met elementen uit verschillende organismes en metabole routes zijn gemanipuleerd om cellen te voorzien van onnatuurlijke capaciteiten. Een van de meest enerverende doestellingen van de synthetische biologie is het vinden van oplossingen voor ingewikkelde biomedische vraagstukken. Hoewel dit onderzoek nog in de kinderschoenen staat, zijn in de translationele geneeskunde inmiddels de eerste stappen gezet om behandelingen te ontwikkelen die gebaseerd zijn op synthetische biologie.

Cel-vrije synthetische biologie (of *in vitro* synthetische biologie), een tak van synthetische biologie, maakt gebruik van cel-vrije genexpressiesystemen om biologische netwerken te creëren die functioneren buiten het chassis van een levende cel. Meer dan een decennium geleden zorgde de samensmelting van synthetische biologie, cel-vrije genexpressiesystemen en liposomentechnologie voor de ontwikkeling van artificiële blaasjes die dienen als bioreactor om genetische gecodeerde moleculen te synthetiseren. Hoewel de primaire motivatie van deze studies het assembleren van een semi-synthetische cel was, heeft men inmiddels de toepassing van deze technologieën voor diverse therapeutische doeleinden voor ogen. Voorbeelden hiervoor zijn het ontwerpen van liposomen die antilichamen produceren voor nieuwe vaccinatiesystemen, de ontwikkeling van liposomen als bioreactor die, op afstand bediend, *in-situ* mRNA of eiwitten kunnen produceren en het samenstellen van een op PCR gebaseerde nanofabriek voor genafgifte.

Liposomen zijn het meest succesvolle chassis voor de afgifte van medicijnen dat ooit ontwikkeld is, met meer dan vijftien goedgekeurde medicijnen die op liposomen gebaseerd zijn. Binnen de genterapie wetenschap worden liposomen al langere tijd onderzocht om als koerier te dienen voor de aflevering van nucleïnezuren om de barrières die deze moleculen *in vivo* ondervinden te omzeilen. In het bijzonder is de op RNA-interferentie gebaseerde medicatie veelbelovend; de eerste formulering is 2018 op de markt gekomen en enkele anderen zullen volgen.

Ondanks de lange onderzoekshistorie zijn de meeste structurele and functionele eigenschappen van op liposomen gebaseerde medicijnen afgeleid uit bulkmetingen. De mate van heterogeniteit ten op zichte van b.v. de inkapselingsefficiëntie en samenstelling van de lipiden blijft daarom grotendeels onbekend binnen de liposoompreparaten en dat maakt de ontwikkeling van nieuwe formuleringen met een verbeterde therapeutische efficiëntie lastig. Een andere belangrijke

limitatie is dat er bij toediening vervroegd afgifte van het medicijn plaatsvindt doordat het membraan kleine lekkages vertoont. Het beheersen van de bio-distributie van een therapeutisch medicijn is van essentieel belang om de toxische neveneffecten te minimaliseren en de efficiëntie van de behandeling te verhogen. Om dit probleem te ondervangen zou een systeem ontwikkeld moeten worden met stimuli-responsieve eigenschappen dat wordt afgeleverd bij een specifiek doelwit om het bio-distributieprofiel van een medicijn te verbeteren en het op aanvraag vrij te maken.

Dit werk draagt bij aan de convergentie van de vakgebieden synthetische biologie, individuele-liposoom biofysica en bio medicatie, en presenteert diverse mogelijke applicaties voor bioreactorblaasjes ter verbetering van de bestaande RNA-gebaseerde genafleversystemen.

In **Hoofdstuk 1** geven we een algemeen overzicht met betrekking tot synthetische biologie in therapeutische behandelingen, gentherapie en liposomale afleversystemen. Aan het eind van dit hoofdstuk geven we een korte introductie over de inhoud van de overige hoofdstukken van de scriptie.

In **Hoofdstuk 2** hebben we een methode opgezet voor “high-throughput” karakterisatie van inkapseling van RNA in liposoompreparaten op het niveau van individuele blaasjes. Een RNA aptameer-fluorogeen complex, genaamd “Spinach”, is gebruikt als model systeem om de liposomale RNA inhoud te detecteren met behulp van fluorescentiemicroscopie. De laadcapaciteit van gevoede bioreactorblaasjes waarin RNA geproduceerd wordt vanaf een DNA-molecuul is vergeleken met die van conventionele RNA-inkapseling in liposomen. De resultaten van deze studie laten zien dat inkapseling van vooraf gesynthetiseerd RNA een hogere fractie van gevulde liposomen oplevert. Daarnaast laten we voor het eerst zien hoe door biotine geïmmobiliseerde blaasjes op een handige manier kunnen worden gebruikt om liposomale genafleversystemen te bestuderen met “high-throughput” fluorescentiemicroscopie van individuele blaasjes. Hoewel we er niet geslaagd zijn om bioreactorblaasjes te maken die een grote hoeveelheid RNA produceren, hebben we wel een aantal aanbevelingen om onze technologie te verbeteren.

In **Hoofdstuk 3** hebben we beoogd om een lichtgevoelige schakel te implementeren om tijdruimtelijke controle van genexpressie in liposomen te bewerkstelligen. Hiervoor is geprobeerd om een RNA-producerend bioreactorblaasje te maken dat geactiveerd kan worden met licht. Een met licht activeerbare T7-promoter (LA-T7) die de binding van T7RNA polymerase in de “uit”-modus remt is ontworpen, gekarakteriseerd en ingebouwd in een DNA molecuul coderend voor Spinach. Productie van LA-Spinach RNA is aangetoond in een bulkexperiment, maar door onvolledige inhibitie van genexpressie in de “uit”-modus wordt de productie van LA-Spinach RNA in de bioreactorblaasjes belemmert. De vervolgstappen voor het assembleren van een volledig gerepasseerd LA-Spinach worden beschreven in dit werk. Bovendien wordt de potentie van alternatieve optogenetica-systemen die geschikt zijn voor het tijdsruimelijk reguleren van productie en de afgifte van therapeutisch RNA bediscussieerd.

In **Hoofdstuk 4** hebben we een platform opgezet voor de *in vitro* productie van shRNA binnenin de bioreactorblaasjes. We hebben DNA moleculen ontworpen die verschillende shRNA-moleculen generen door middel van *in vitro* transcriptie in bulk of direct in de liposomen. De efficiëntie van ‘gene silencing’ door shRNA is getest in zoogdiercellen. Wanneer conventionele transfectiemethodes gebruikt werden kon de activiteit van *in vitro* getranscribeerd shRNA aangetoond worden. Pogingen om genexpressie stil te leggen met shRNA via afgifte met liposomen zijn mislukt. Om de afgifte te optimaliseren werd aan de oppervlakte van de liposomen folinezuur ingebouwd, dat fungeert als een ligand dat bindt aan cellen met grote hoeveelheden folinereceptoren, zoals de meeste kanker cellen. De cellen met receptoren vertoonden een verbeterde opname van de liposomen, maar lysosomale insluiting verminderde de succesvolle aflevering van shRNA in het cytoplasma. Om dit probleem aan te pakken werd het gebruik onderzocht van de pH-geactiveerde melittin-peptide om endosomale membranen te ontwrichten. Het gebrek aan bewijs voor succesvolle productie van shRNA in liposomen en destabilisatie van membranen door melittin heeft er toe geleid dat we grote aanpassingen voorstellen om in het ontwerp van een nieuwe generatie op liposomen gebaseerde shRNA-dragers.

In **Hoofdstuk 5** hebben we een nieuw liposomaal afgiftesysteem voor het chemotherapeutisch molecuul SN-38 ontwikkeld. SN-38 is een stof met een krachtig antitumoreffect, maar door lage oplosbaarheid en stabiliteit bij fysiologische pH zijn er beperkingen in klinische toepassingen. Liposomen en cyclodextrines zijn al lange tijd onderzocht om te gebruiken voor oplossen en afleveren van hydrofobe stoffen. Met als doel om de voordelen van beide systemen te combineren, is de ontwikkeling van SN-38-in-cyclodextrine-in-liposomen verkend. De inkapseling van SN-38-SBE- β -cyclodextrine in het lumen van liposomen bleek niet mogelijk vanwege het uit elkaar vallen van de liposomen en de formatie van SN-38-SBE- β -CD-lipid nanodeeltjes. Interessant genoeg was de retentietijd van SN-38 binnenin de SN-38-SBE- β -CD-lipid nanodeeltjes hoger dan in liposomen waarbij SN-38 direct geladen werd in de lipidefilm. De toxiciteit van SN-38-SBE- β -CD-lipid nanodeeltjes is getest in kankercellen, maar er was geen therapeutisch voordeel ten opzichte van niet-gekapselde SN-38-SBE- β -CD-complexen *in vitro*. Desondanks moet een mogelijk therapeutisch voordeel van SN-38-SBE- β -CD nanodeeltjes *in vivo* niet worden uitgesloten. Verdere karakterisatie van dit systeem en optimalisatie van de formulering zou de ontwikkeling van SN-38-in-cyclodextrin-in-liposomen mogelijk kunnen maken.

Samengevat laat dit proefschrift vernieuwend werk zien naar de ontwikkeling van beter gekarakteriseerde liposomale genafgifte systemen. Bovendien zet dit werk de eerste stappen in de richting van de constructie van liposomale genafgifte systemen die dienen als tijdruimtelijk gecontroleerde RNA-producerende nanofabriekjes. Als geheel laat dit proefschrift de belangrijke waarde van “high-throughput” analyse van individuele blaasjes voor de karakterisering van medicinale afgiftesystemen zien.

ACKNOWLEDGEMENTS

I would like to dedicate the first words of gratitude to my supervisor Christophe Danelon. Christophe, thank you so much for your precious guidance and continuous support through this long journey. Thank you for always having your door open for me, ready to discuss science at any time. You are a role model of what solid scientific rigor is, and I admire you for that.

Jonasín, Johannes, thank you for all your support, always there in the good and in the bad times. Thank you for sharing the toughest period of my PhD with a great deal of good sense of humor. You are both great friends and amazing people. I am honored to have you as paranymphs. Raquelona, you are an incredible friend. Thank you for always being there for me. I am so grateful for all the time and experiences we have shared together during the last decade, you are family to me.

To my Dirty Nerdy crew, Nicole, Mehran, Jo, what an amazing and genuine team you are. Whether we are in a Swedish cabin with an exciting composting toilet, running a Mud Master without prior training, or just around the corner for a quick dinner, I truly enjoy our time together. Thank you for your continuous support through good and bad times. I love the connection we have, over normal and weird things.

To my E1.420 friends, David, Duco, Jonas, Jo. I will never stop missing the great time I have had with you guys at the office. The uncountable laughs, the daily frusbol breaks, the many spontaneous beers and dinners, and your always supportive attitude, where no problem is a problem with a good round of expired Martini shots and a couple of witty jokes. To Elisa, thanks for joining our mentally dysfunctional environment with enthusiasm.

To my former mates, thank you for the fun working environment, your help and advice. Pauline, Andrew, you are fascinating people. Thank you for your friendship and the great times together. Ilja, what can I say, you rock! I am so glad you are back at BN, you are a pillar to the Danelon lab! Fab, you are missed! Anne, thank you for your help with the last experiments. Huong, you are the sweetest.

To my students Claudia, Denzelo, Gaby, Robin, working with you was great fun. Microscope time in your absence is still wonderful, but far less entertaining. Thank you for your contribution to the projects. To other great temporary lab members: Ilias, Gabriel, Sophie, Roy, Celine, etc., thank you for your cheerfulness in and out the lab.

To Zohreh, thank you for your kind supervision during my internship at the lab. Mona, Just, thank you for the nice times during my internship. It was a real pleasure to start my time at TUDelft sitting next to you.

Vanessica, thank you for being a great friend from the very start living at Leegwaterstraat. Thanks for your great Portuguese gastronomical influence. Your red-wine marinades are now part of my regular cooking. Nuno, thank you for the nice times we shared and for being my IT technical support. Fabai, you are a fabulous friend. I am very grateful for the many great experiences we have shared together. Eve, what can I say, you are awesome! You are my acting muse! I hope that soon we can spend more time together in Leiden.

Sophie, thank you for your generous friendship. I hope you give me a second chance as skying student, I promise not to sit on my skis! Siddharth, your positivism and enthusiasm are contagious. I hope soon we can both find time to meet more often.

Louis, thank you for teaching me to knit, how to make jams, to pickle things. You are a truly inspiring person. Patrick, before you know it we will be celebrating your graduation! Essie, thank you for encouraging me to run! To Niels, Jeremy, Sacha, infinite thanks for your friendly support with every kind of technical struggle. Mohammed, thank your kindness and your very useful scientific advices. I am sure you are rocking it in Australia! Luuk, thank you for all the nice chats at the BN corridors, I wish you all the best in your academic future, you are awesome! To Becca, Laura, Mathia, Viktorija, Helena, Lisa, thank you for the nice BN girl evenings, I hope we can repeat soon. To Victor, Dominik, Da, Hirad, Fede, Francesca, Adi, Kuba, Mahipal, Daniel, Benjamin, Carlsten, Alessio, Fayeze, Yoones, Anthony, Sebastian, Afshin, Magnus, David, Sam, Misha, Maurits, Jacob, Vladimir, Jochem, Pawel, Stephanie, Stanley, Michela, Jetty, thank you for the good times at BN.

To my current ProQR mates, Janne, Lenka, Lissanne, Cherie, Tess, thank you for receiving me with enthusiasm and thank you for your flexibility throughout the end phase of my writing. Blanca, Heleni, I am so grateful to have such a first class “Mediterranean corner” around!

To my Lindy friends, with whom I have shared so many Lindy-related and unrelated adventures during the last three years. Thank you, Maria, Kelly, Raj, Giullia, Astrid, Aaron, Eva, Oisin, Gene, Jeanette, Catherine, Sabrina, Adje, Ana, Elke, Pieter, Praveen, Yara and Dolinde. Thank you also Sanne and Hakon, for welcoming us into Team Amsterdam, providing us with a unique opportunity to improve our dancing skills. We were happy Oompa Loompas.

To Janeto and Gioladika, thank you for your warm friendship and the unforgettable Wageningen times. I look forward to our reunion in November. Delyan, thank you for all the good times we have shared and counting. Surya, how many nice moments together. Still hoping you will move back one day! Elenilla, looking forward to the next river race! This time I am wearing water wings. Ariadna, prepare the couch! Alex, thank you for coming from Slovenia to enjoy my panicking face on stage. You are a great friend, and an amazing baker. To the rest of the Alien crew: Remco, Fabienne, Julia, Roel and Koen, thank you for the fun times during our biotech studies.

Marc, Susanne, Anton, Karo, my Swedish crew and “accidental” English school. Thank you all for welcoming me into your lives when I couldn’t put two sentences together. Karo, I still dream of spaghetti with NOTHING and our forest-guard rescue in Åre.

To my lifelong friends Olgui, Cafu and Ali, who love me and support me no matter how long and how far we live from each other. Thank you for your unconditional love. Your friendship is priceless and precious to me. To Marquitos, you are a wonderful person and I am honored to be your friend. Thank you for the nice times we share together whenever we have the opportunity.

To my Biology and Biology-derived/related friends. I am so infinitely grateful that back in September 2005 I had to register for the afternoon shift. Without knowing it, fate or fortune brought me truly fantastic lifelong friends and perhaps what I now consider the best years of my life. Thank you Gelili, Mariolito, Merisula, Lore, Ale, Pablo, Meri Peque, Martita, Rebe, Miguel, Nacho, Marcos, Jorge, Gema, Alvarito, Juanqui, Ángel, Ramonchu, Victor, Harry and Jorba. Claudia, Hakuna Matata!

To Hisse, and the rest of the 221-lab crew, it was my time with you what made my love for research grow. Thank you so much!

To Willem, Bernadette, Marius, Bastian, thank you for welcoming me into your family with open arms!

My acknowledgement would be incomplete without thanking the biggest source of my strength, my family. To my extraordinary mom, or how Paco would wisely say, “Luisita, the one and only”, thank you for being my lifelong greatest and absolute supporter. Thank you for having nurtured not only a mother-to-daughter relationship, but also a big friendship between the two of us. It might sound like a cheesy Hollywood movie, but I truly owe you everything I have achieved. Thank you for transmitting me your curiosity and passion for learning. Papá, you are always in my thoughts and in my heart.

To my amazing grandparents, Yayi & Lolo. Thank you for your unconditional love and generosity. I am so lucky to have you, I have learned so much from you both. Yayi, thank you for being the kindest and showing all of us how to be better persons each day. Also, thank you for trying to make me a more organized person, a continuous work in progress. Lolo, thank you for transmitting me your passion for cinema and science. I can still remember our phone calls where I would dictate you equations I couldn’t solve, and you would call me twenty minutes later to explain to me how to do them. I cannot imagine better grandparents than you.

To María, my fabulous sister, thank you for being there for me during the ups and downs, no matter the distance. I cannot live without your absolutely unique sense of humor. Juan, Fernando, you are hilarious, and exhausting, but I miss you every day! Rubén, thank you for

being a great brother in law, I hope you are looking forward to the Soler Sister Night 2019 edition.

To my cousin Pato, thank you for being the sweetest, I wish I could have a cloned version of you to squeeze each day. I often think back of the super happy times we had living together in Delft. I hope I can bring you back to NL one day! To the rest of my loving family, Luigy, Rosa Mari, Tio Ino, Nuria, Javier, little ponies Mario and Daniel, thank you for the support and affection you have always given me and for the quality time we spend together whenever we have the opportunity.

To Paco, thank you for being the greatest friend to my parents. You are one more member of our family.

To Roland, I am so grateful for these amazing four years. I am a very happy person by your side! Thank you for always believing in me, you are the greatest possible personal coach. Thank you for making me laugh each day. I truly enjoy our shared absurd sense of humor.

To anybody that I might have forgotten, thanks you for making these years a great journey!

CURRICULUM VITÆ

Alicia SOLER CANTÓN

02-03-1987 Born in Xàtiva, Spain

EDUCATION

- 1999-2005 Secondary Education
Instituto de Enseñanza Pública Pintor Antonio López, Tres Cantos, Spain
- 2005-2011 B. Sc + M. Sc. Biology
Autonomous University of Madrid, Madrid, Spain
- 2009-2010 Erasmus exchange study and internship
Lund University, Lund, Sweden
- 2011-2013 M. Sc. Molecular Biotechnology
Wageningen University & Research, Wageningen, The Netherlands
- 2013-2019 Ph. D. research
Department of Bionanoscience, Delft University of Technology, Delft,
The Netherlands
Thesis: Synthetic biology meets liposome-based drug delivery
Supervisor: Dr. C. J. A. Danelon
Promotor: Dr. C. J. A. Danelon
Co-Promotor: Prof. dr. M. Dogterom

LIST OF PUBLICATIONS

A. Soler Cantón, Niels J. F. van den Broek, and C. Danelon, Development and single-particle characterization of a liposomal delivery system for the chemotherapeutic compound SN-38, submitted.

N. Chakrova, A. Soler Cantón, C. Danelon, S. Stallinga, and B. Rieger. Adaptive illumination reduces photobleaching in structured illumination microscopy. *Biomed. Opt. Express* 7(10), 4263-4274 (2016).

P. van Nies, A. Soler Cantón, Z. Nourian and C. Danelon, Monitoring mRNA and Protein Levels in Bulk and in Model Vesicle-Based Artificial Cells, *Methods in Enzymology*, Volume 550: 197-214 (2015).